الجمهورية الجزائرية الديمقراطية الشعبية
People's Democratic Republic of Algeria
وزارة التعليم العالي والبحث العلمي
Ministry of Higher Education and Scientific Research

Mohamed Khider University – Biskra
Faculty of Science and Technology
Department: Civil and Hydraulic Engineering
Reference:……..

جـــامعة محمـــد خـيضر بـــسكرة
كـلية الـعلـــوم و التكـــنولوجـيا
قسم: الهنـدسـة المـدنيـة و الـــري
المرجع: ……..……

Thesis presented with a view to obtaining

LMD Doctorate in Civil Engineering

Option: Numerical modelling in civil engineering

Contribution to the numerical analysis of the effect of movements induced by underground structures on nearby foundations

Contribution à l'analyse numérique de l'effet des mouvements induits par les ouvrages souterrains sur les fondations des structures à proximité

Presented by:

AMARI Tamir

Publicly supported on:

Before the jury composed of:

Pr. BENMEBAREK Sadok	**Professor**	**Chair**	**University of Biskra**
Pr. HOUHOU Mohamed Nabil	**Professor**	**Supervisor**	**University of Biskra**
Pr. REMADNA Mohamed Saddek	**Professor**	**Examiner**	**University of Biskra**
Pr. ABBECHE Khelifa	**Professor**	**Examiner**	**University of Batna 2**

ACKNOWLEDGEMENTS

First of all, all praise is due to “Allah” almighty, owner of many graces for enabling me to execute this research and complete this work.

I would like to sincerely thank my supervisor Pr. HOUHOU Mohamed Nabil from the University of Biskra for providing the scientific supervision, guidance and support throughout the preparation of this thesis. His availability, his experience, and his thoroughness allowed this thesis to succeed. It was also a great pleasure for me to work under his direction.

I would also like to thank Pr. BENMEBAREK Sadok from the University of Biskra for having done me a great honor by accepting to chair the jury of this thesis. I thank him for the advice and the encouragement during my doctoral studies. It was an honor for me to be one of MN2I2S laboratory members that he directs professionally.

I also thank Pr. REMADNA Mohamed Saddek (University of Biskra) and Pr. ABBECHE Khelifa (University of Batna 2), first of all for doing me honor by agreeing to participate in the jury of this thesis, and also for the time and the interest that they brought to this research by agreeing to examine this work.

I want to thank those in charge of External Relations & Cooperation Mr. Moummi Mohammed and Pr. Debabeche Mahmoud (University of Biskra) and Mrs. Güler Aysel (Yildiz Technical University Istanbul-Turkey) for their support and guidance during the framework of the Student Mobility Program "Erasmus+ KA107" Funded by the Erasmus+ Programme of the European Union. A special thanks to Pr. Berilgen Mehmet Muhit from Yildiz Technical University who supervising me during the 04 months I spent in Istanbul. I thank also friends who helping and encouraging me during this grant.

I would like to extend my gratitude to my family members for their never-ending love, support, tolerance and sacrifice in encouraging me to complete this research: my dear parents, my sisters and their sons, and my wife. Without them, this would not have been possible. This thesis is dedicated to my dear son Sadjed.

I would also like to thank all members and PhD students of the MN2I2S laboratory at Biskra University for their encouragement.

Last but not least, to the remaining people whom I am unable to list down, who encouraged me to complete this thesis, please accept my sincere appreciation and thanks.

Abstract

The rapid development of dense urban areas leads to an increased demand for underground constructions which often conducted at a close distance from nearby pile foundations of existing buildings. Therefore, ground movements caused by excavation will potentially affect the performance of nearby pile foundations. The issue of estimating the damage caused by the construction of underground works is of paramount importance because, if the problems of adjacent damage and disturbance are not correctly assessed, the basic concept of the design will be faulty and no amount of precision thereafter can make up for the initial errors in judgment. In this context, the present thesis focuses on the numerical analysis of the effect of ground movements induced by the construction of underground works on nearby pile foundations in soft clay overlying dense sand using the explicit finite element codes PLAXIS 2D & 3D. The validation of the proposed numerical modeling approach is based on the results of centrifuge tests found in the literature.

The various contributions made in this research consist of numerical modeling to investigate the additional responses of the adjacent piles due to tunneling- and excavation-induced ground movements. The numerical modeling of the problem includes four main aspects: construction phasing, three-dimensional effects, hydromechanical coupling and soil-pile-structure interactions. The numerical analyses mainly focus on both vertical and horizontal single pile responses (settlements, deflections, moments, shears, and axial forces).

To better understand the single pile behaviour, a thorough parametric study was carried out to investigate the effect of some key parameters such as construction phasing, the size and depth of the structural elements, pile location, the behavior of the soil mass, and the stiffness of the various elements constituting the problem. To provide supplementary comprehensions concerning the response of pile group system, several configurations of pile group were considered including two, three, four and six single piles. Each configuration has been tested for two different pile head condition cases, namely free and capped.

The 3D numerical analysis results showed that tunneling- and excavation-induced ground movements have the potential to cause additional forces, moments and deflections in nearby piles. The 2D plane strain modelling could give conservative results.

The construction of underground works must be potentially controlled because the induced ground movements and hence the induced bending moments due to excavation may be sufficient to cause structural failure of the piles near uncontrolled excavation works, especially concrete piles, as they are generally not designed to withstand large lateral loads. The results also reveal that group effects are generally beneficial.

Assessment of ground movement effects is critical for many urban infrastructure developments below and adjacent to existing structures. For a preliminary design, this numerical study can serve as a practical basis for similar projects.

Keywords: Tunnel, deep excavation, pile foundations, numerical modelling, soil-structure interaction, bearing capacity, volume loss, diaphragm wall, strut.

Résumé

Le développement rapide des zones urbaines denses entraîne une demande accrue de constructions souterraines qui sont souvent réalisées à une distance proche des fondations sur pieux des bâtiments existants. Par conséquent, les mouvements de terrain causés par l'excavation affecteront potentiellement la performance des fondations sur pieux à proximité. Le sujet de l'estimation des dommages causés par la construction d'ouvrages souterrains est d'une importance primordiale car, si les problèmes de dommages et de perturbations adjacents ne sont pas correctement évalués, le concept de base de la conception sera erroné et aucune précision ultérieure ne pourra compenser les erreurs de jugement initiales. Dans ce contexte, la présente thèse de doctorat porte sur l'analyse numérique de l'effet des mouvements de terrain induits par la construction d'ouvrages souterrains sur des fondations à proximité en pieux dans de l'argile molle recouvrant du sable dense en utilisant les codes d'éléments finis explicites PLAXIS 2D & 3D. La validation de l'approche numérique proposée est basée sur les résultats d'essais en centrifugeuse trouvés dans la littérature.

Les différentes contributions apportées dans cette recherche consistent à la modélisation numérique pour étudier les réponses supplémentaires des pieux adjacents dues aux mouvements de terrain induits par le creusement de tunnels et excavations profondes. La modélisation numérique du problème regroupe quatre aspects principaux : le phasage de la construction, les effets tridimensionnels, le couplage hydromécanique et les interactions sol-pieu-structure. Les analyses numériques se concentrent principalement sur les réponses verticales et horizontales des pieux isolés (tassements, déflections, moments, cisaillements et efforts normaux).

Pour mieux comprendre le comportement du pieu isolé, une étude paramétrique approfondie a été réalisée pour étudier l'effet de certains paramètres clés tels que le phasage de la construction, la taille et la profondeur des éléments structuraux, la position du pieu, le comportement du sol, et la rigidité des différents éléments constituant le problème. Pour mieux comprendre la réponse du système de groupe de pieux, plusieurs configurations ont été considérées. Chaque configuration a été testée pour deux cas différents de condition de tête de pieu, à savoir libre et fixe.

Les résultats de l'analyse numérique 3D montrent que les mouvements de terrain induits par le creusement de tunnels et excavations profondes ont le potentiel de provoquer des forces, des moments et des déflections supplémentaires dans les pieux voisins. La modélisation 2D en déformations planes pourrait donner des résultats conservateurs. La construction d'ouvrages souterrains doit être potentiellement maîtrisée car les mouvements de terrain induits et donc les moments de flexion induits dus à l'excavation peuvent être suffisants pour provoquer une rupture structurelle des pieux à proximité des travaux d'excavation non contrôlés, notamment des pieux en béton, car ils ne sont généralement pas conçus pour résister à des fortes charges latérales. Les résultats révèlent également que les effets de groupe sont généralement bénéfiques.

Pour un avant-projet, cette étude numérique peut servir de base pratique pour des projets similaires.

Mots Clés : Tunnel, excavation profonde, modélisation numérique, interaction sol-structure, capacité portante, pieu, perte de volume, paroi moulée, buton.

ملخص

يؤدي التطور السريع للمناطق الحضرية الكثيفة إلى زيادة الطلب على الإنشاءات تحت الأرض والتي تتم غالبًا على مسافة قريبة من أساسات الخوازيق (الركائز) القريبة للمباني القائمة. لذلك من المحتمل أن تؤثر حركات الأرض الناتجة عن الحفريات على أداء أساسات الخوازيق القريبة. تعتبر مسألة تقدير الضرر الناجم عن إنشاء الأعمال تحت الأرض ذات أهمية قصوى لأنه إذا لم يتم تقييم مشاكل الأضرار والاضطرابات المجاورة بشكل صحيح ، فإن المفهوم الأساسي للتصميم سيكون خاطئًا ولن يكون هناك قدر من الدقة بعد ذلك يمكن أن يعوض عن الأخطاء الأولية في الحكم. في هذا السياق، تركز أطروحة الدكتوراه الحالية على التحليل العددي لتأثير حركات الأرض الناتجة عن إنشاء أعمال تحت الأرض على أساسات خوازيق قريبة في الطين الناعم الذي يغطي الرمل الكثيف باستخدام برنامج PLAXIS الرقمي ثنائي الأبعاد وثلاثي الأبعاد. يعتمد التحقق من صحة نهج النمذجة العددية المقترحة على نتائج اختبارات أجهزة الطرد المركزي الموجودة في بعض المنشورات العلمية.

تتمثل المساهمات المختلفة التي تم إجراؤها في هذا البحث في النمذجة العددية للتحقيق في الاستجابات الإضافية للركائز المجاورة بسبب الحركات الأرضية الناتجة عن حفر الأنفاق والحفر العميقة. تشتمل النمذجة العددية للموضوع على أربعة جوانب رئيسية: مراحل الإنشاء، التأثيرات ثلاثية الأبعاد، الاقتران الهيدروميكانيكي، والتفاعلات ركيزة-تربة. تركز التحليلات العددية بشكل أساسي على كل من الاستجابات الرأسية والأفقية للركيزة الفردية (الهبوط، الانحرافات، عزم الانحناء، والقوى المحورية).

لفهم سلوك الركيزة المفردة بشكل أفضل، تم إجراء دراسة بارامترية شاملة للتحقق من تأثير بعض المعلمات الرئيسية مثل مراحل الإنشاء، حجم العناصر الهيكلية وعمقها، موقع الركيزة، سلوك التربة، وصلابة العناصر المختلفة التي تشكل المشروع. لتوفير مزيد من الفهم فيما يتعلق باستجابة نظام مجموعة الركائز، تم النظر في العديد من التكوينات لمجموعة الركائز بما في ذلك اثنين، ثلاثة، أربعة وستة ركائز مفردة. تم اختبار كل تكوين لحالتين مختلفتين لحالة رأس الركيزة، وهما الحران والمغلفان.

أظهرت نتائج التحليل العددي ثلاثي الأبعاد أن الحركات الأرضية التي يسببها الأنفاق والحفر العميقة لديها القدرة على إحداث قوى و عزوم انحناء وانحرافات إضافية في الركائز القريبة. النمذجة ثنائية الأبعاد يمكن أن تعطي نتائج متحفظة.

يجب التحكم جيدا في إنشاء الأعمال تحت الأرض لأن حركات الأرض الناتجة وبالتالي عزوم الانحناء الناتجة بسبب الحفر قد تكون كافية للتسبب في تمزق هيكلي للركائز بالقرب من أعمال الحفر غير الخاضعة للرقابة، وخاصة الركائز الخرسانية، لأنها عمومًا غير مصممة لتحمل أحمال عرضية كبيرة. تكشف النتائج أيضًا أن تأثيرات مجموعة الركائز مفيدة بشكل عام.

يعد تقييم تأثيرات حركة الأرض أمرًا ضروريًا للعديد من عمليات تطوير البنية التحتية الحضرية أسفل الهياكل القائمة وبجانبها. بالنسبة لمشروع أولي ، يمكن أن تكون هذه الدراسة الرقمية بمثابة أساس عملي لمشاريع مماثلة.

كلمات مفتاحية: نفق، حفر عميق، نمذجة عددية، تفاعل هياكل - تربة ، قدرة التحمل، ركيزة، فقدان الحجم، جدار الحجاب الحاجز، دعامة.

Table of Contents

First Part: Bibliographic Study

Chapter 1: Tunnelling-Induced Ground Movements

Chapter 2: Tunnel-Soil-Pile Interactions

Chapter 3: Deep Excavation-Induced Ground Movements

Chapter 4: Excavation-Soil-Pile Interactions

Second Part: Numerical Modelling

Chapter 5: 3D Numerical Analysis of the Effects of Tunnelling-Induced Ground Movements on Nearby Piles

List of Figures

CHAPTER 01

CHAPTER 02

CHAPTER 03

CHAPTER 04

CHAPTER 05

CHAPTER 06

List of Tables

CHAPTER 03

CHAPTER 05

CHAPTER 06

List of Symbols

Symbols related to the pile

Symbol	Description	Unity
$\mathbf{X_p}$	Pile (front pile) location from: tunnel centreline/ excavation face	[m]
X	Lateral direction	[m]
Y	Longitudinal direction	[m]
Z	Vertical direction	[m]
$\mathbf{d_p}$, **d**	Pile diameter	[m]
$\mathbf{L_p}$	Pile length	[m]
$\mathbf{A_p}$	Cross-sectional area of the pile	$[m^2]$
$\mathbf{P_h}$	Pile head load	[kN]
$\mathbf{E_p}$	Young's modulus of the pile shaft	$[kN/m^2]$
$\mathbf{E_l}$	Young's modulus of the concrete tunnel lining	$[kN/m^2]$
$\mathbf{S_p}$	Center-to-center spacing between piles	[m]
s	Centre-to-Centre pile spacing between 2 piles in the plane strain direction.	[m]
$\mathbf{Z_p}$	Certain depth of pile (from pile head)	[m]
$\mathbf{E_P A_P}$	Pile axial rigidity	[kN]
$\mathbf{E_P I_P}$	Pile bending rigidity	$[kNm^2]$
$\mathbf{I_p}$	Moment of inertia of the pile	$[m^4]$
Myy	Pile bending moment in the lateral direction	[kNm]
Mxx	Pile bending moment in the longitudinal direction	[kNm]
$\mathbf{U_x}$	Pile lateral displacement in the lateral direction	[mm]
$\mathbf{U_y}$	Pile lateral displacement in the longitudinal direction	[mm]
$\mathbf{U_z}$	Pile settlement	[mm]
$\mathbf{U_{z,i}}$	Pile head settlement due to the working load prior to tunnelling	[mm]
$\mathbf{U_{z,net}}$	Net increase in the pile head settlement due to tunnelling only	[mm]
$\boldsymbol{\delta_{ph,max}}$	Maximum pile head settlement corresponding pile ultimate capacity	[mm]
P	Axial force at a certain depth of pile	[kN]
$\mathbf{P_w}$	Working load applied on the pile head prior to tunnelling	[kN]
$\mathbf{Q_u}$	Bearing capacity of the pile	[kN]
$\mathbf{N_{pile}}$	Total pile bearing capacity	[kN]
$\mathbf{Q_p}$	Base resistance	[kN]
$\mathbf{F_{max}}$	Base resistance	[kN]
$\mathbf{Q_s}$	Skin friction resistance	[kN]
T	Skin friction resistance	[kN/m]
$\mathbf{T_{top,max}}$	Maximum skin resistance at the pile head	[kN/m]
$\mathbf{T_{bot,max}}$	Maximum skin resistance at the pile bottom	[kN/m]
$\mathbf{T_{max}}$	Maximum skin resistance	[kN/m]
$\mathbf{q_p}$	Unit base resistance	$[kN/m^2]$
$\mathbf{f_s}$	Unit skin friction resistance	$[kN/m^2]$
$\mathbf{N_q}$ **and** $\mathbf{N_c}$	Bearing capacity factors	[-]
D	Embedded length of pile in each layer	[m]
$\mathbf{A_s}$	Embedded surface area of the pile	$[m^2]$
P	Perimeter of the pile section	[m]
Δ**l**	Embedded length for each layer	[m]

σ'_0	Vertical effective pressure	$[kN/m^2]$
β	Parameter used for β-Methods	[-]
n	Number of piles in the plane strain direction	[-]

Symbols related to the tunnel

Symbol	Description	Unity
D_t	Tunnel diameter	[m]
R	Tunnel radius	[m]
H_t; z_0; z_t	Tunnel horizontal axis position (Tunnel depth)	[m]
C	Cover above the tunnel crown	[m]
C/D_t	Cover-to-diameter ratio of the tunnel	[-]
t_l	Thickness of concrete tunnel lining	[m]
t_r	Thickness of pile cap (raft foundation)	[m]
E_l	Young's modulus of concrete tunnel lining	$[kNm^2]$
C_{ref}	Linear contraction reference value	[%]
$C_{inc,axial}$	Contraction increment	[%/m]
α_{dec}	Ratio of stress release (unloading level)	[-]
L_{dec}	Length of the unlined zone	[m]
σ_s	Surface surcharge pressure	$[kN/m^2]$
σ_t	Tunnel support pressure	$[kN/m^2]$
i, i_x	Trough width parameter	[m]
K	Trough width factor (empirical parameter)	[-]
S_{max}	Maximum settlement above the tunnel axis	[mm]
$S_{c,max}$	Maximum vertical displacement at the tunnel crown	[mm]
S; S_v; $S_{z=0}$	Vertical settlement trough at transverse distance X	[mm]
S_x; S_h	Surface horizontal displacement (Lateral soil movement)	[mm]
S_z	Subsurface settlement	[mm]
V_t	Volume to be excavated	$[m^3]$
V_s	Volume of settlement trough	$[m^3]$
V_l; ε_0	Volume loss (Ground loss ratio)	[-]
N	Tunnel/ Excavation stability factor	[-]
N_c	Tunnel/ Excavation critical stability factor	[-]
X	Lateral distance from the tunnel centerline	[m]

Symbols related to the retaining wall

Symbol	Description	Unity
H	Wall height	[m]
H_e	Final excavation depth	[m]
E_w	Young's modulus of the wall	$[kN/m^2]$
I_w	Moment of inertia of the wall	$[m^4]$
EI_w	Wall flexural stiffness	$[kNm^2]$
S	System stiffness factor	[-]
B	Excavation width	[m]
h_{uns}	Unsupported excavation depth	[m]
h_{avg}	Average vertical props/struts space	[m]
L_s	Out of plane space of anchors structural elements	[m]

$\mathbf{z}$	Depth below ground surface	[m]
$\mathbf{a_d}$	Area of the lateral wall deflection	[m^2]
$\mathbf{l_x}$	Distance from a point at a distance from the wall	[m]
$\boldsymbol{\delta_v}$	Ground surface settlement (Settlement at the distance of l_x)	[mm]
$\boldsymbol{\delta_{vm}}$	Maximum ground surface settlement	[mm]
$\boldsymbol{\delta_{hm}}$	Maximum wall displacement	[mm]
$\mathbf{D}$	Influence range of ground settlement	[m]

Symbols related to the soil properties

Symbol	Description	Unity
$\mathbf{E_{50}^{ref}}$	Reference secant stiffness	[kN/m^2]
$\mathbf{E_{oed}^{ref}}$	Reference tangent stiffness	[kN/m^2]
$\mathbf{E_{ur}^{ref}}$	Reference unloading-reloading stiffness	[kN/m^2]
$\mathbf{P^{ref}}$	Reference stress for stiffness	[kN/m^2]
$\mathbf{G_0^{ref}}$	Reference shear modulus at very small strains	[kN/m^2]
$\mathbf{m}$	Power for stress dependent stiffness	[-]
$\boldsymbol{\gamma_{0.7}}$	Shear strain	[-]
$\mathbf{K_0^{nc}}$	Coefficient of earth pressure for normal consolidation	[-]
$\mathbf{K_0}$	Coefficient of earth pressure at rest	[-]
$\mathbf{RD;\ D_r}$	Relative density of the sand	[%]
$\mathbf{G_s}$	Specific gravity of soil particles	[kN/m^2]
$\mathbf{C_c}$	Compression index for HSs model	[-]
$\mathbf{C_s}$	Swelling index for HSs model	[-]
$\mathbf{C_v}$	Coefficient of consolidation	[m^2/year]
$\mathbf{C_u}$	Undrained shear strength	[kN/m^2]
$\mathbf{C_{ref};\ c'}$	Effective cohesion	[kN/m^2]
$\boldsymbol{\nu}$	Poisson's ratio	[-]
$\boldsymbol{\nu_{ur}}$	Poisson's ratio for unloading-reloading	[-]
$\mathbf{k}$	Coefficient of permeability	[m/s]
$\mathbf{e}$	Current void ratio	[-]
$\mathbf{e_{init}}$	Initial void ratio	[-]
$\mathbf{e_{max};\ e_{min}}$	Sand maximum and minimum void ratio, respectively	[-]
$\boldsymbol{\varphi'}$	Effective internal friction angle	[°]
$\boldsymbol{\psi}$	Dilatancy angle	[°]
$\boldsymbol{\gamma}$	Unit weight	[kN/m^3]
$\boldsymbol{\gamma_w}$	Unit weight of water	[kN/m^3]
$\boldsymbol{\lambda}$	Compression index for Modified Cam Clay model	[-]
$\boldsymbol{\kappa}$	Swelling index for Modified Cam Clay model	[-]
$\mathbf{M}$	Tangent of the critical state line for Modified Cam Clay model	[-]
$\mathbf{R_{inter}}$	Interface strength reduction factor	[-]
$\boldsymbol{\gamma'}$	Effective soil unit weight	[kN/m^3]
$\boldsymbol{\delta}$	Soil-pile friction angle	[°]
$\mathbf{OCR}$	Over Consolidation Ratio	[-]

List of Abbreviations

Abbreviations	Its meaning
AVPULL	Analysis of Vertical Piles Under Lateral Loading (FE program)
ALPC	Apparent Loss of Pile Capacity
BM	Bending Moment
BEM	Boundary Element Method
CGC	Cambridge Geotechnical Centrifuge
CTRL	Channel Tunnel Rail Link
DCM	Displacement Control Model
EWM	Elastic Winkler Method
EPB	Earth Pressure Balance
F	Axial forces / shear forces
FOS	Factor Of Safety
FEA	Finite Element Analysis
FDM	Finite Difference Method
FLAC	Fast Lagrangian Analysis of Continua (finite difference code)
HS	Hardening Soil model
HSs	Hardening Soil model with small-strain stiffness
HKU	Hong Kong University
LVDTs	Linear Variable Differential Transducers
LL	Liquid Limit
MCC	Modified Cam Clay model
MC	Mohr-Coulomb model
MRT	Mass Rapid Transit
NATM	New Austrian Tunnelling Method
NUS	National University of Singapore
OCR	Over Consolidation Ratio
PLAXIS	PLastic and AXISymmetry (finite element program)
PRAB	Piled Raft Analysis with Batter piles
PALLAS	Piles And Lateral Loading Analysis (boundary element program)
PI	Plasticity Index
PL	Plastic Limit
PIZ	Primary Influence Zone
RD	Relative Density
SCL	Sprayed Concrete Lining method
SEM	Sequential Excavation Method
SPB	Slurry Pressure Balance
SIZ	Secondary Influence Zone
TSAM	Two-Stage Analysis Method
TBM	Tunnel Boring Machine
TPI	Tunnel Pile Interaction
TSI	Tunnel-Structure Interaction
TPSI	Tunnel-Pile-Structure Interaction
TTM	Tokyo Tech Mark
UCL	University College London

General Introduction

1. Problematic

Due to the growth of urban cities, the demand for underground infrastructure such as tunnels, basements of high-rise buildings, underground car parks or subway stations, has been greatly increased. Such structures are often carried out at a close distance from the neighboring pile foundations of existing buildings.

The release of in situ soil stresses caused by the excavation of underground workings in soft ground can lead to excessive vertical and lateral ground movements. As a result, it is very likely that the performance of adjacent pile foundations will be potentially affected (Poulos and Chen, 1997; Goh et al. 2003; Leung et al. 2006; Huang and Mu, 2012; Shi et al. 2019; Sohaei et al. 2020; Ng et al. 2021). There have been several examples where pile foundations have been affected or damaged by excavation induced ground movements. For example, but not limited to, we mention the disasters that befell: The Leaning Tower of Shanghai, July, 2003; Nicol Highway Collapse of Singapore, 2004; Pinheiros Station of Sao Paulo, 2007; Historic Archive of Cologne, 2009.

The issue of estimating the damage caused by the construction of underground works is of paramount importance because, if the problems of adjacent damage and disturbance are not correctly assessed, the basic concept of the design will be faulty and no amount of precision thereafter can make up for the initial errors in judgment. Therefore, it is necessary to have a thorough understanding of excavation-induced ground movements, which are often considered more critical for nearby pile foundations, especially concrete piles, as they are generally not designed to support large lateral loads. Thus, the accurate prediction of the effects of underground structures (tunnels or deep excavations) on existing pile foundations constitutes a major challenge during design and practice in urban geotechnical environments.

Due to the overlap of many factors, the accurate assessment of additional settlements and lateral deflections as well as additional axial forces and bending moments in existing neighboring piles induced by the construction process of underground structures has been, and continues to be, the topic of much research.

As a first approach, the analysis is generally based on field monitoring (Kaalberg et al. 2005; Selemetas et al. 2005; Coutts and Wang, 2017), model tests (Chen et al. 1997; Lee and Bassett, 2007; Sohaei et al. 2017), and centrifuge modeling technique (Loganathan et al. 2000; Leung et al. 2000; Leung et al. 2003; Jacobsz et al. 2004a, 2004b; Ong et al. 2006a; Leung et al. 2006; Lee and Chiang, 2007; Ong, 2009; Ong et al. 2009; Zheng et al. 2012; Ng et al. 2013; Hong et al. 2015a, 2015b; Ng et al. 2017; Soomro et al. 2017, 2018a; Shi et al. 2019; Leung et al. 2019). These tests reveal some basic characteristics of the problem. However, for the preliminary design, the experimental methods can be time-consuming and expensive.

Otherwise, several researchers investigated the pile performances due to tunneling-induced ground movements by analytical methods (Chen et al. 1999; Loganathan et al. 2001; Huang et al. 2009; Zhang et al. 2011a; Huang and Mu, 2012; Basile, 2014; Marshall and Haji, 2015; Franza et al. 2017; Zhang et al. 2018). Current analytical studies have mainly employed the plane strain analysis and do not take into account the multiple interactions between the different elements constituting the problem.

The additional responses of piles subjected to ground movements induced by tunneling or deep excavation were also evaluated using simplified methods known as two-stage analysis methods (TSAM). First: excavation-induced Greenfield ground movements are estimated using empirical methods and also analytical closed-form solutions (Peck, 1969; Clough and Schmidt, 1981; Mair et al. 1993; Loganathan and Polous, 1998; Chen et al. 1999). In the second step, these soil movements are imposed on the pile using simplified boundary element method (BEM) to compute the pile responses. It should be mentioned that this approach assumes the soil mass as a homogeneous linear elastic material under plane strain conditions, which makes its extension to nonlinear problems and multilayered soils problematic unsuitable. The numerical analysis is rather a viable choice for a number of studies which have the ability to take into account and simulate parameters neglected from analytical and experimental methods. Therefore numerical analysis using finite differences or finite element method has become indispensable.

The analyses of the induced soil movements and the response of the piles due to the construction process of underground works (tunnels or deep excavations) have been studied by various researchers using numerical methods by decoupled loadings in the plane strain model. However, experimental studies have highlighted the limitations of the 2D approach, due to the restricted assumptions on which the formulations are based, and have confirmed that the problem is clearly three-dimensional. Thus, a full three-dimensional coupled numerical analysis of the problem, which takes into account complex geometries and the multiple interactions between the different components of the problem, has become an important contribution to a thorough understanding of the observed phenomena (Mroueh and Shahrour, 2002; Kitiyodom et al. 2005; Cheng et al. 2007; Yang et al. 2011; Lee, 2012a, 2013; Zidan and Ramadan, 2015; Soomro et al. 2015; Lee et al. 2016; Liyanapathirana and Nishanthan, 2016; Nishanthan et al. 2017; Shakeel and Ng 2018; Al-Omari et al. 2019; Soomro et al. 2020b; Ng et al. 2021; Zhang et al. 2021).

2. Objective and Scope of the Study

Despite the numerous developments of specific numerical codes conducted to date and their encouraging results, discrepancies are still observed during comparison of numerical simulation of such structures with monitored sites and laboratory tests. The reason is due partly to the difficulty of taking into account the actual conditions of the construction process of the underground structures and also the difficulties of estimating the evolution of lateral stresses of the surrounding soil (due to the anisotropic small-strain nonlinear behavior of the soil).

The results obtained from previous studies show that ground movements induced by tunneling and deep excavations have the potential to cause additional axial forces, bending moments and deflections in adjacent foundation piles. This is related to a complex phenomenon of soil-structure-piles interaction which involves the geological conditions, the geometry of the tunnel, the rigidity of the walls, the support system, the distance between the pile and the tunnel centreline (excavation face), volume loss, pile diameter, pile length, and the method of excavation, etc. Thereby, advance research studies are required to develop more insight on the mechanical behaviour of the pile foundation system subjected to soil movements induced by the excavation process of underground structures.

In this context, the present research theme focuses on the numerical analysis of the effect of ground movements induced by the construction process of underground works on nearby pile foundations of existing buildings. The objective of this research work is to investigate the additional responses of the neighbouring single pile and group of piles due to tunnelling-and deep excavations-induced ground movements in bilayer soil (soft clay overlying dense sand) using the explicit finite element code PLAXIS 3D. To model the small-strain nonlinear behaviour of the soil, the Hardening soil model with small-strain stiffness (HSs), implemented in PLAXIS, was used in this analysis**.** The validation of the proposed numerical modeling approach is based on the results of centrifuge tests found in the literature. The relevance of the 3D model is also judged by comparison with the 2D plane strain model using the PLAXIS 2D code.

The numerical modeling of the problem includes four main aspects: construction phasing, three-dimensional effects, hydromechanical coupling and soil-pile-structure interactions. The numerical analyses mainly focus on both vertical and horizontal single pile responses (settlements, deflections, bending moments, shears, axial forces and pile bearing capacity).

To better understand the single pile behavior, an in-depth parametric study in 3D was carried out to investigate the effect of some key parameters such as construction phasing, the size and depth of the structural elements, pile location, the behavior of the soil mass, and the stiffness of the various elements constituting the problem. To provide supplementary comprehensions concerning the response of pile group system, several configurations of group of piles were considered including two, three, four and six single piles. Each configuration has been tested for two different pile head condition cases, namely free and capped.

For a preliminary design, this numerical study can serve as a practical basis for similar projects.

3. Organisation of Thesis

This thesis consists of two main parts: The first part is devoted to a bibliographic study comprising four chapters. The second part, which includes two chapters, is the subject of the various contributions made in this research. In total this thesis consists of six chapters, and the contents of each chapter are briefly described as follows:

Chapter 1 presents a literature review on soil movements due to tunnel excavation. This chapter briefly discusses the features of various methods developed by researchers to predict tunnelling induced ground movements. In this chapter soil movements due to tunnelling in sands and clays are discussed separately.

Chapter 2 reviews the main studies that address the problem of the effects of tunneling on piles and piled structures in different types of soil (sand or clay). A variety of methods for the analysis of pile-soil-tunnel interaction problems have been developed and briefly reviewed in this chapter. The analysis of the response of neighboring piles due to tunneling effect has been based on field monitoring, model and centrifuge tests, analytical and numerical methods.

Chapter 3 introduces the types of ground movements induced by an adjacent deep excavation. This chapter also exhibits the various popular methods available for predicting ground movements due to deep excavation and the limitations associated with each method.

Chapter 4 provides a summary and assessment of the literature related to the wall-soil-pile interaction problem. This chapter highlights the various existing methods to investigate piles responses due to ground movements induced by adjacent deep excavation. The analysis summarizes field observations, analytical methods, laboratory tests, and numerical methods.

Chapter 5 is dedicated to a full 3D numerical analysis, using the explicit finite element code PLAXIS 3D, to study the additional responses of nearby single piles due to tunneling-induced ground movements in soft clay overlying dense sand. The Slurry Pressure Balance (SPB) technique is used in this numerical analysis to simulate the construction process of the tunnel. The numerical analyses mainly focus on both vertical and horizontal single pile responses. The numerical model is validated on the basis of the results of a centrifuge test. The relevance of the 3D model is also judged by comparison with the 2D plane strain numerical model. From a 3D numerical reference model, an extensive parametric study was conducted to investigate the effect of some key parameters such as tunnel advancement, volume loss, pile location, pile length, pile diameter, tunnel diameter, over consolidation ratio of the clay (OCR), and tunnel depth. To give supplementary comprehensions concerning groups of piles, a 2×2 pile group with two different pile head conditions (free and capped) was considered.

Chapter 6 focuses on a full three-dimensional numerical analysis to investigate single pile and pile group responses due to deep braced excavation-induced soil movements in bilayer soil (soft clay overlying dense sand). The explicit finite element numerical code PLAXIS 3D is used to model the various phases of excavation in the presence of piles. To better understand the single pile behaviour near deep strutted excavations, a thorough parametric study was carried out using 3D numerical model. It focuses on the effects of excavation depth, pile location, sand density, support system rigidity, pile stiffness, head conditions, and pile length. In order to provide further insights about the response of pile group system, several configurations of pile group were considered including two, three, four and six single piles. Each configuration has been tested for two different pile head condition cases, namely free and capped.

First Part

Bibliographic Study

CHAPTER 1
Tunnelling-Induced Ground Movements

CHAPTER 1

Tunnelling-Induced Ground Movements

1.1 Introduction

The construction of tunnels inevitably causes substantial ground movements due to the relaxation of in-situ ground stresses. This can be a great concern in the urban environment due to the effects of soil movements on adjacent buildings, other tunnels and services. The prediction of ground movements and the assessment of potential effects on infrastructure are therefore essential aspects of the design and construction of a tunnelling project in the urban environment. Ground movements 'Greenfield' are taken as those occurring without interaction from nearby structures or foundations (i.e. only ground deformations caused by tunnel construction are considered) and these movements which are most commonly used in both design and analysis. Typical Greenfield ground movements associated with tunnelling are shown in Figure 1.1 (Attewell et al. 1986). In this chapter soil movements due to tunnelling in sands and clays are discussed separately. Clay behaviour can be modelled in the short term as undrained with constant volume, as this is the time period in which the majority of the case study data is taken from and when the risk of damage due to differential settlements are greatest. Sand always behaves in a drained and contractile/dilatant manner and hence is more difficult to model simply.

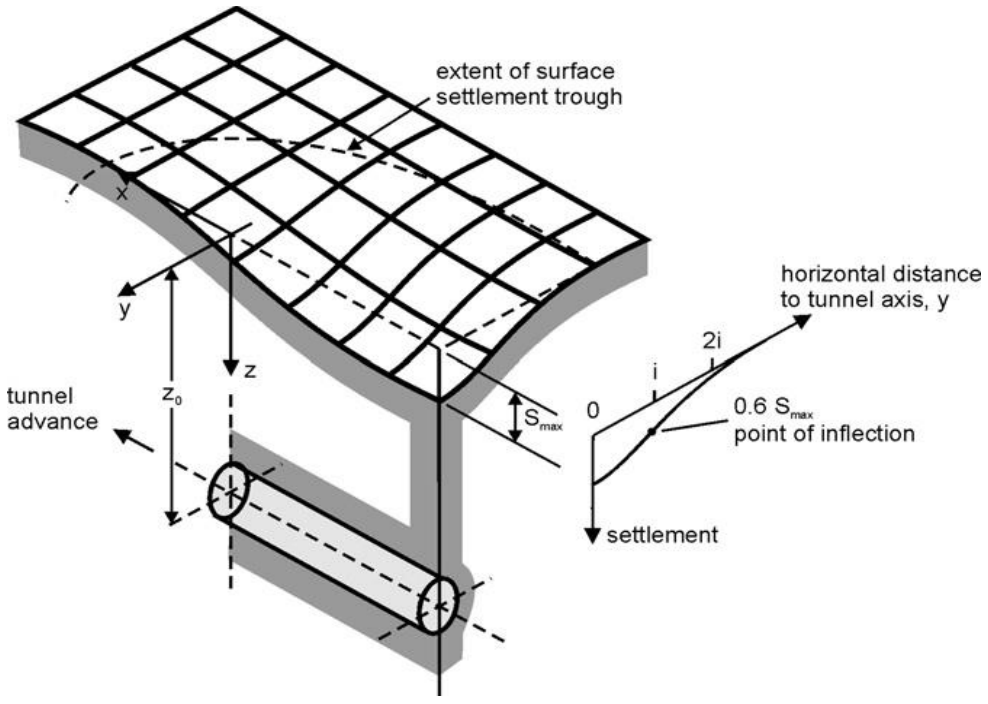

Figure 1.1 Ground movements associated with tunnel construction (Attewell et al. 1986), with transverse Gaussian settlement profile

1.2 Tunnelling induced ground movements

In practice, tunnelling is obviously a 3D problem and the tunnelling process is associated with ground surface movements, subsurface movements, and lateral deformations.

1.2.1 Surface movement

1.2.1.1 Vertical transverse settlement

1.2.1.1.1 Clays

For clay soils, the vertical transverse movements during tunnel excavation are generally considered to form a Gaussian settlement trough as shown in Figure 1.2 (Peck, 1969), and as given in Eq. (1.1). Loganathan & Poulos (1998) proposed a closed-form analytical solution to predict the vertical surface settlements trough as given in Eq. (1.2).

$$S = S_{max} \exp\left(-\frac{X^2}{2i^2}\right) \tag{1.1}$$

$$S_{z=0} = 4\varepsilon_0(1-\nu)R^2 \frac{H}{H^2+x^2} \exp\left(-\frac{1.38x^2}{(H+R)^2}\right) \tag{1.2}$$

Where: $S = S_v = S_{z=0}$ = vertical settlement trough at transverse distance X/ S_{max} = maximum settlement above the tunnel axis/ x = lateral distance from the tunnel centerline/ i = distance from the tunnel centreline to the point of inflection of the settlement trough (trough width parameter)/ $z_0 = H$ = tunnel depth/ R= tunnel radius/ ν = soil poisson ratio.

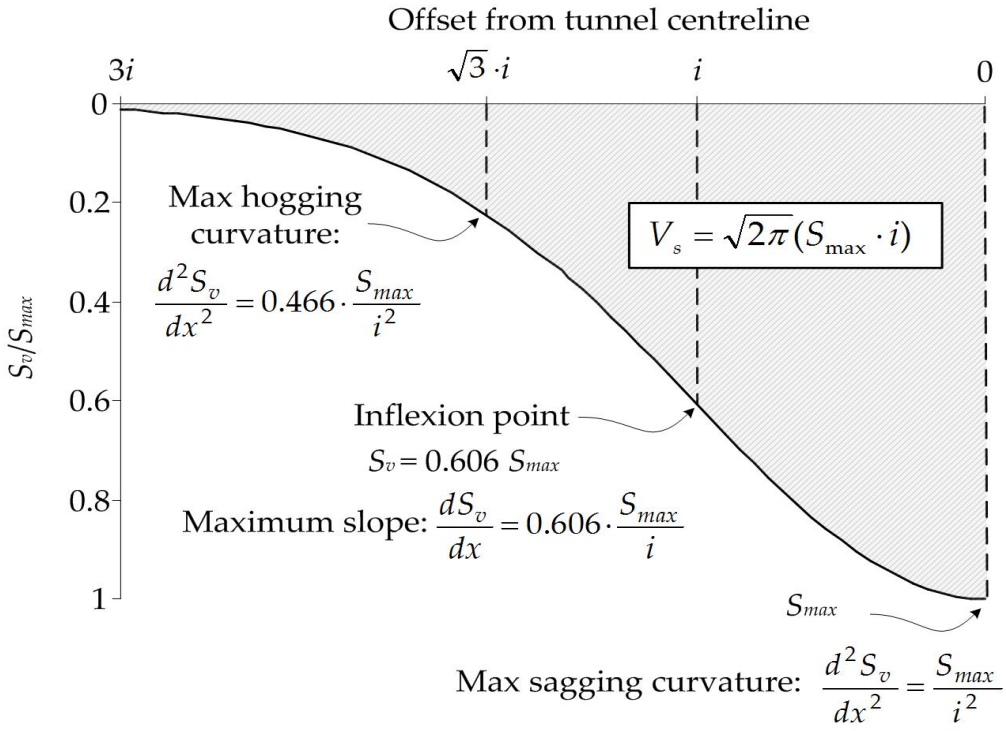

Figure 1.2 Settlement trough described by Gaussian distribution curve

The Gaussian trough was first proposed by Martos (1958) and subsequently shown by Schmidt (1969) and Peck (1969) to provide an approximation to the transverse vertical settlement profile immediately following the excavation of a tunnel.

1.2.1.1.2 Sands

The settlement trough has been shown to be much narrower for sands than in clays, and hence Celestino et al. (2000) and Jacobsz (2002) showed that some modification to the Gaussian was appropriate. Vorster et al. (2005) proposed the modified Gaussian settlement trough as given in Eq. (1.3) which has been shown by Marshall (2009) and Farrell (2010) to provide a better approximation to tunnelling in sands both for centrifuge and case study data.

$$S = S_{max} \frac{n}{(n-1)+\exp\left[\alpha_{MG}\left(\frac{x}{i_x}\right)^2\right]} \tag{1.3}$$

$$n = e^{\alpha_{MG}} \frac{2\alpha_{MG}-1}{2\alpha_{MG}+1} + 1 \tag{1.4}$$

Where n is the shape function parameter controlling the width of the profile and α_{MG} is controlled such that i remains constant for any variation in n and α_{MG}.

It is best described in Figure 1.3 where increasing or decreasing n has the effect of moving the point of inflection vertically up or down respectively and increasing or decreasing i results in moving the point inflection to the right or to the left respectively for positive x/i (where x/i is normalised distance from tunnel centreline).

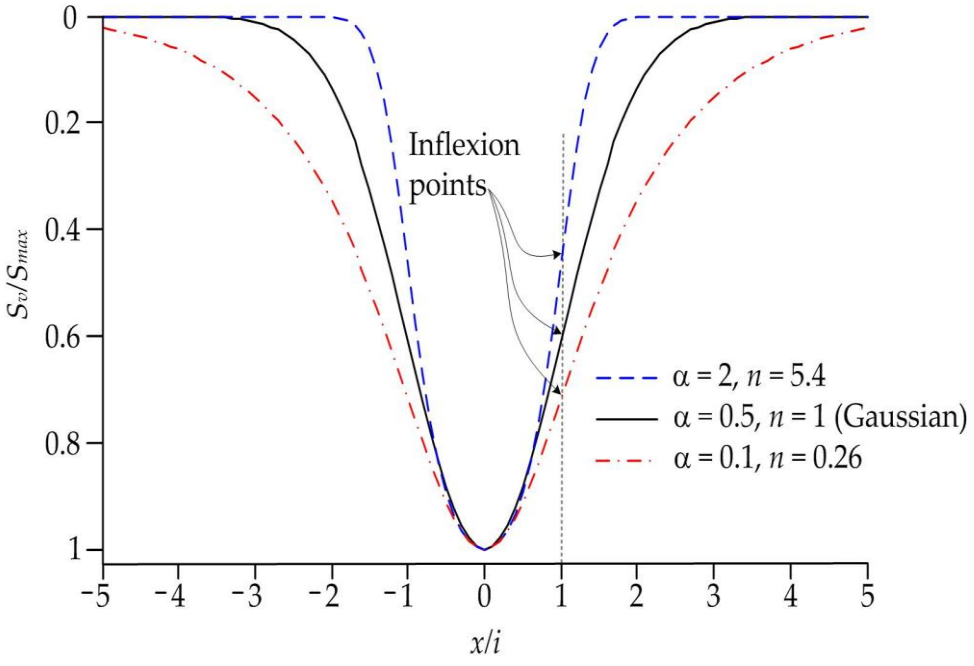

Figure 1.3 Modified Gaussian settlement troughs after (Vorster et al. 2005)

1.2.1.2 Longitudinal settlement

1.2.1.2.1 Clays

In urban environment, structures close to or directly above the tunnel axis may experience some damage from the progressive longitudinal settlement trough generated ahead of the tunnel face. New and O'Reilly (1991) proposed that the longitudinal profile should have the form of a cumulative probability curve, assuming that the transverse settlement profile has a Gaussian shape and all ground deformations take place at constant volume (Feng, 2004). This is applicable to tunnelling in clays. Attewell and Woodman (1982) also showed the cumulative probability curve to be reasonably valid for the longitudinal settlement trough (Figure 1.4). They found that the surface settlement directly above the tunnel face generally corresponds to about 0.5 S_{max} for tunnels constructed in stiff clays without face support (open-faced tunnelling techniques). However, for tunnels constructed in soft clays with face support provided by compressed air, the surface settlement directly above the tunnel face is less than 0.5 S_{max} (S_v= 0.2-0.3 S_{max}).

1.2.1.2.2 Sands

Ata (1996) observed the surface settlements above a 9.48-m diameter EBP shield made tunnel in Cairo at a depth of about 16 m in medium to dense sands overlain by a clay layer, and found the settlement above the tunnel face was in the range of 0.25 to 0.3 S_{max} (Figure 1.5). Overall, the longitudinal settlement trough having the form of the cumulative probability curve illustrated in Figure 1.4 is generally reasonable but it has only been validated for tunnels in clays.

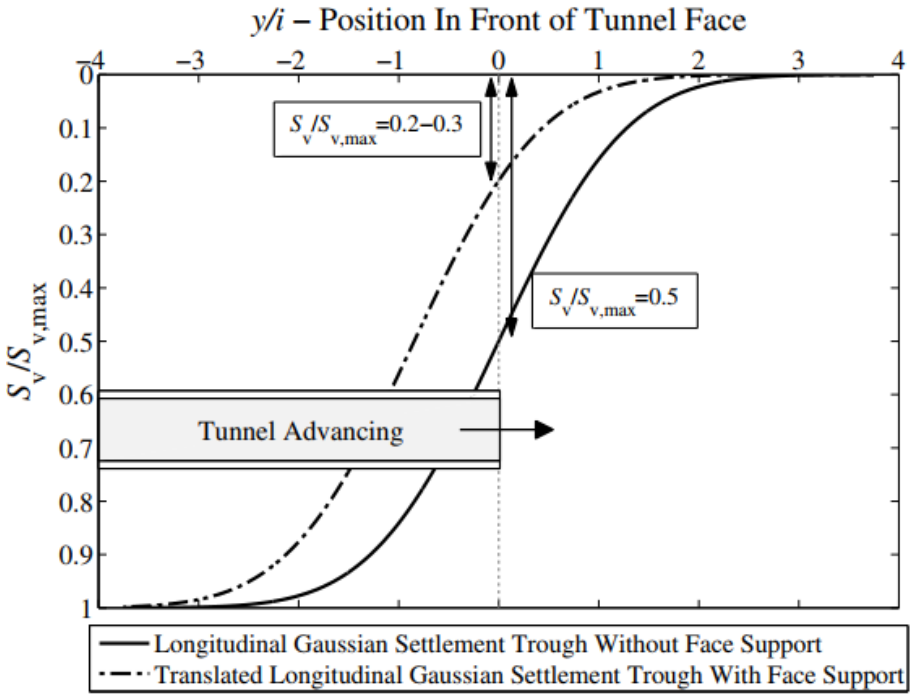

Figure 1.4 Longitudinal settlement trough after (Attewell and Woodman, 1982)

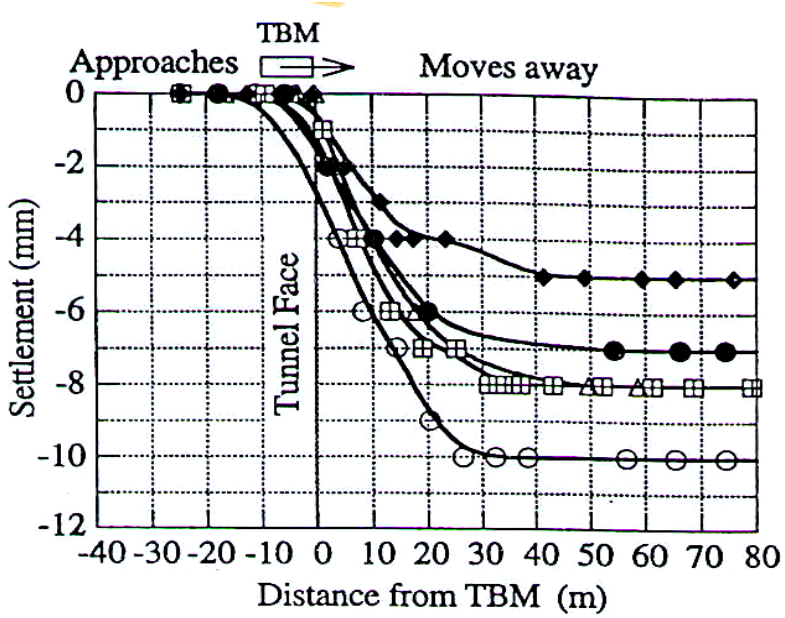

Figure 1.5 Settlements above EPB shield in sands in Cairo (Ata, 1996)

1.2.1.3 Horizontal transverse movements (lateral soil movements)

1.2.1.3.1 Clays

Horizontal surface movements (lateral soil movements) can cause damage to structures in urban environment. It is important to know clearly her magnitude due to tunnelling. Horizontal surface movement generally assumed to act in proportion to the vertical movement with the ground movement vectors all directed towards a single point. O'Reilly and New (1982) proposed that in cohesive soils (undrained and constant volume conditions) the ground movement vectors pointed towards the tunnel axis, with the magnitude given by Eq. (1.5) and shown in Figure 1.6.

$$S_x = -\frac{x*S}{z_0} \tag{1.5}$$

This assumption leads to the distribution of surface horizontal ground movements given by:

$$S_x = \frac{1.65*x*S_{x,max}}{i} \exp\left(-\frac{x^2}{2i^2}\right) \tag{1.6}$$

Loganathan and Poulos (1998) presented a closed-form solution to predict the surface lateral soil movements, as follow:

$$S_x = -\varepsilon_0 R^2 x \left(\frac{1}{x^2+(H-z)^2} + \frac{3-4\nu}{x^2+(H+z)^2} - \frac{4z(z-H)}{(x^2+(H+z)^2)^2}\right) \exp\left[-\left(\frac{1.38x^2}{(H+R)^2} + \frac{0.69z^2}{H^2}\right)\right] \tag{1.7}$$

Where $S_x = S_h =$ is lateral soil movement (the horizontal surface displacement)/ S_v vertical settlement trough at distance x/ z = depth below ground surface/ $z_0 = H =$ tunnel depth.

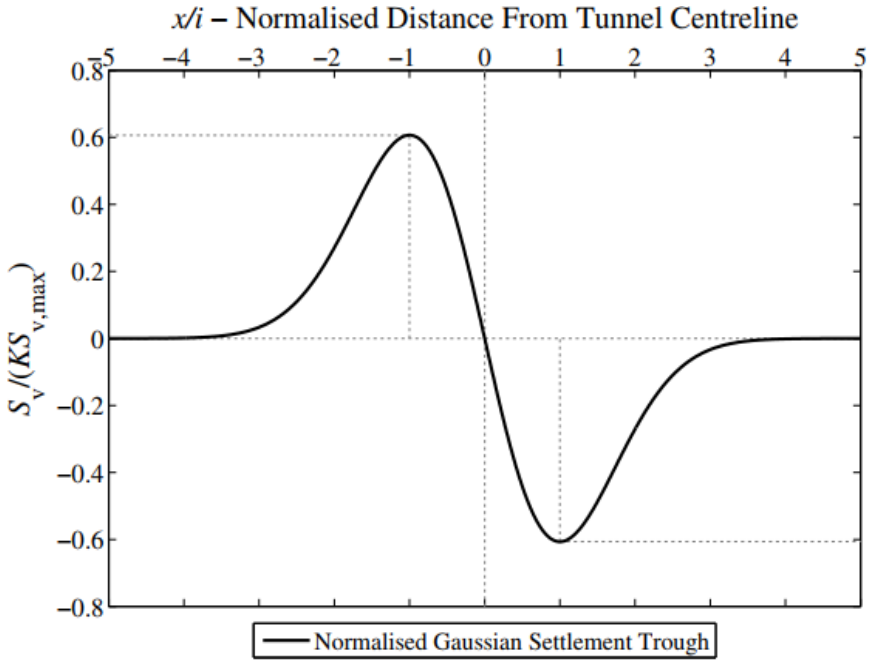

Figure 1.6 Horizontal surface movements after (O'Reilly and New, 1982)

Loganathan et al. 2000 compares the lateral soil movements predicted from Eq. (1.7) with the measured values from centrifuge tests at a lateral distance x =5.5 m, for a ground loss of 1%. This comparison reveals that the predictions agree reasonably well with both the magnitude and distribution of the lateral movements measured in centrifuge tests.

1.2.1.3.2 Sands

Horizontal movements in sand are often underestimated by Eq. (1.5) at the edge of the settlement trough as noted in Cording (1991) and Hong and Bae (1995). However, given the magnitude of these horizontal movements at this distance from the tunnel centreline they are generally considered of little significance.

1.2.1.4 Trough width

1.2.1.4.1 Uniform soil

1.2.1.4.1.1 Clays

For the Gaussian movement model in clays, the settlement trough width is defined as the distance to the point of inflexion. Several authors have proposed relationships linking this parameter to either the tunnel depth and/or the tunnel diameter including Peck (1969), Attewell (1977), and O'Reilly and New (1982). Clough and Schmidt (1981) proposed a relationship which non-dimensionalises the parameters by the tunnel diameter, D_t, as given in Eq. (1.8).

$$i = \left(\frac{D_t}{2}\right)\left(\frac{z_0}{D_t}\right)^{0.8} \tag{1.8}$$

Many researchers made the hypothesis that the width of the settlement trough can be estimated by an empirical parameter K (trough width factor) for a uniform soil (one layer). The most commonly used relationship is that proposed by O'Reilly and New (1982) as given in Eq. (1.9) for tunnels in cohesive soils (clay, silt) with a value of K = 0,5.

$$i = K z_0 \quad (1.9)$$

The authors suggested a range of K from 0.4 for stiff clays to 0.7 for soft and silty clays. Mair and Taylor (1999) updated the work of O'Reilly and New (1982) and showed that the value of K for surface settlement troughs is typically 0.5 and 0.35 for tunnels in clays and sands, respectively.

1.2.1.4.1.2 Sands

The mechanisms associated with tunnelling movements in sands are somewhat different to clays. At low volume losses the soil behaves in a very stiff and elastic manner resulting in very wide and shallow settlement troughs. At higher volume losses as shear bands propagate up from the tunnel the mechanism narrows greatly and is referred to as the 'chimney' mechanism owing to its narrow, near vertical movement of the soil body directly above the tunnel (Williamson, 2014). For shallower tunnels this chimney mechanism occurs at much lower volume losses, whereas for deeper tunnels it occurs at larger volume losses. Based on a review of surface settlement data from various tunnelling projects, the authors suggested a range of K from 0.2 to 0.3 for granular materials above the water table based on Eq. (1.9). O'Reilly and New (1982) proposed a value of K for sands and gravels of 0.25. This low value is consistent with the steep 'chimney' mechanism shown in sands by Atkinson and Potts (1977) at higher volume losses.

1.2.1.4.2 Multi-layered soils (Clays and sands)

Tunnels are often constructed in layered soil strata comprising both clay and granular soils. New and O'Reilly (1991) suggested that the equations for tunnels in clays and in sands can be combined by taking account of the thicknesses of the different strata (multi-layered soils), such that for a two-layered system:

$$i = K_1 z_1 + K_2 z_2 \quad (1.10)$$

Where K_1 is the empirical parameter (trough width factor) for the soil type in layer 1 of thickness z_1, and K_2 is the empirical parameter for the soil type in layer 2 of thickness z_2.

Field observations of surface settlement profiles above stratified soils where the tunnel is in sands overlain by clay layers indicated wider profiles than would be obtained if the tunnels were only in sands. There is less evidence, however, of cohesionless layers overlying tunnels in clays causing a narrowing of the surface settlement profile, as implied by Eq. (1.10).

Centrifuge model studies by Grant and Taylor (1996) indicated that in case of tunnelling in soft clay overlain by sand, the surface settlement profile is wider than in the case of tunnelling only in soft clay (Feng, 2004). This is probably because the overlying sand layer being significantly stiffer that the soft clay, and also the reduced influence of movements in the sand resembling a chimney failure mechanism, which can affect the overall settlement trough (Mair, 1996).

1.2.2 Subsurface movements

1.2.2.1 Vertical transverse subsurface settlements

1.2.2.1.1 Clays

In urban environment, new tunnels are often constructed close to existing tunnels and deep foundations. It is thus becoming increasingly important to predict how subsurface settlement profiles develop and how they relate to surface settlement troughs. Available field data for subsurface settlements are limited, however, subsurface settlements are known to exhibit different characteristics to those of surface settlements. O'Reilly and New (1982) proposed the use of a Gaussian subsurface trough, based on the plane strain, undrained and constant volume condition of the surface Gaussian settlement trough, and this has been subsequently verified by field and centrifuge data for clays (Williamson, 2014). Mair et al. (1993) analysed subsurface data from various tunnel projects in stiff and soft clays, together with centrifuge model test results in soft clays. They showed that subsurface settlement profiles can be reasonably approximated in the form of Gaussian distribution in the same way as surface settlement profiles. Mair et al. (1993), presented an empirical method to estimate the subsurface settlement S_z at any depth z, given by:

$$S_z = S_{z,max} * \exp\left(-\frac{x^2}{2*k^2*(z_0-z)^2}\right) \tag{1.11}$$

$$S_{z,max} = \left(\frac{1.25*V_l}{0.175+(0.325*(1-z/z_0))} * \frac{R^2}{z_0}\right) \tag{1.12}$$

$$K = \frac{0.175+(0.325*(1-z/z_0))}{(1-z/z_0)} \tag{1.13}$$

Loganathan & Poulos (1998) presented a closed-form solution to estimate subsurface settlement as:

$$S_z = \varepsilon_0 R^2 \left(-\frac{(z-H)}{x^2+(z-H)^2} + \frac{(3-4\nu)(z+H)}{x^2+(z+H)^2} - \frac{2z\left[x^2-(z+H)^2\right]}{[x^2+(z+H)^2]^2}\right) \exp\left[-\left(\frac{1.38x^2}{(H+R)^2} + \frac{0.69z^2}{H^2}\right)\right] \tag{1.14}$$

Where ν is Poisson's ratio of soil above the tunnel, ε_0 is the ground loss (ratio), H is the tunnel depth, R is the tunnel radius, z is the depth below ground surface and x is the horizontal distance from the tunnel centreline.

Figure 1.7 shows comparisons of the subsurface settlement measured in the centrifuge tests along tunnel centreline with measured settlement profiles estimated from Mair et al. (1993) and Loganathan & Poulos (1998), for a ground loss value of 1%. The predictions using Eq. (1.14) reveal a slightly better agreement with measured values from the centrifuge tests than the empirical approach of Mair et al. (1993). Mair et al. (1993) proposed a modification to Eq. (1.9) as given in Eq. (1.15), to account for the effect of depth combined with a new proposed relationship for K varying with depth as given in Eq. (1.16).

$$i = K * (z_0 - z) \tag{1.15}$$

$$K = \frac{0.175+(0.325*(1-z/z_0))}{(1-z/z_0)} \tag{1.16}$$

Where z_0 is the depth to tunnel axis, and z is the depth below ground surface.

In clays, Grant and Taylor (2000) showed that varying the volume loss from 2 to 20 % had no effect on the settlement trough width, but that as described by Mair et al. (1993) it was shown to vary significantly with depth. Grant and Taylor (2000) showed that the use of Eq. (1.16) breaks down within $0.5D_t$ of the tunnel crown, and hence should not be used to evaluate deformations this close to the tunnel crown. This is not considered an issue for very deep tunnels, however for shallow tunnels the use of the equation may lead to significant errors (Williamson, 2014).

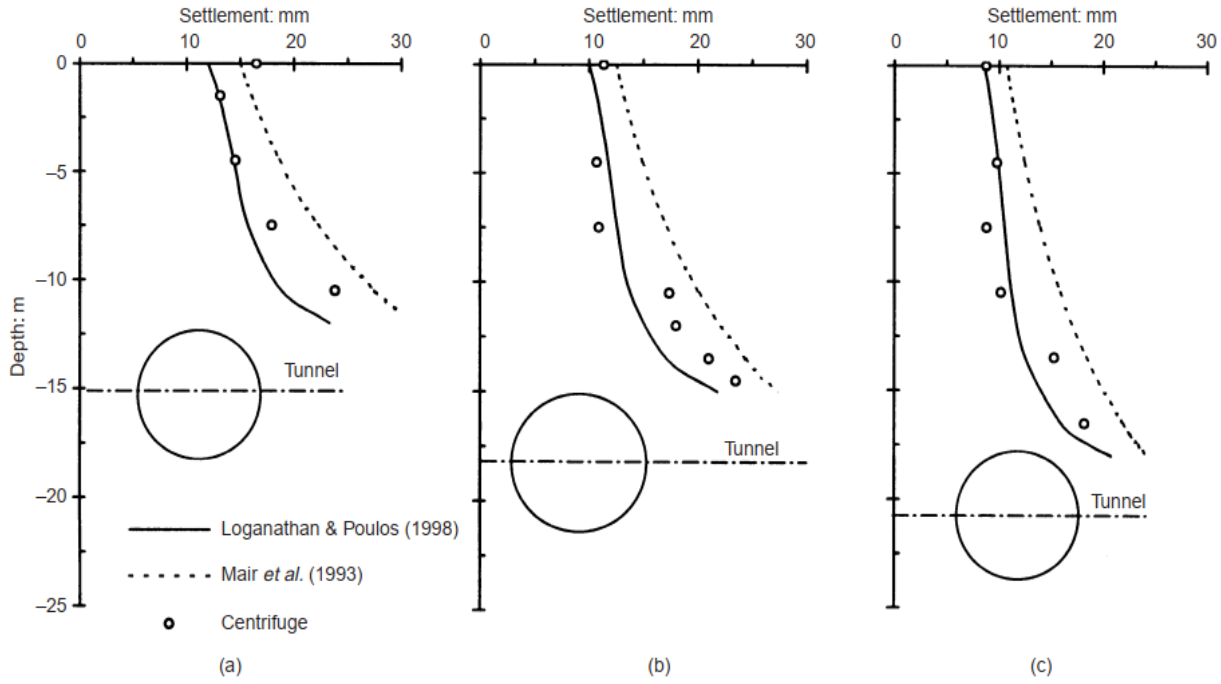

Figure 1.7 Comparison of subsurface profiles (a) tunnel depth 15 m, (b) tunnel depth 18 m and (c) tunnel depth 21 m (Loganathan et al. 2000)

1.2.2.1.2 Sands

Moh et al. (1996) analysed subsurface settlement data from the Taipei Mass Transit system where the ground conditions consisted of very silty sands. Moh et al. (1996) proposed the relationship given in Eq. (1.17) based on the work of Clough and Schmidt (1981).

$$i = \left(\frac{D_t}{2}\right)\left(\frac{z_0}{D_t}\right)^{0.8}(z_0 - z/z_0)^m \tag{1.17}$$

Values of m = 0,8 and m = 0,4 were proposed for silty clays and silty sands respectively.

Dyer et al. (1996) analysed subsurface settlements above a pipe-jacked sewer in sand which showed a widening of the settlement trough width, K, with depth. This general trend of increase in trough width with increasing depth is in agreement with both Moh et al. (1996) and Mair et al. (1993) as shown in Figure 1.8 for tunnel diameter of D_t = 4,65 m and tunnel depth of $z_t = z_0 =$ 20,625 m (Williamson, 2014).

Marshall et al. (2012) studied centrifuge data for tunnels of different C/D_t ratios (where C is the tunnel cover), and showed that the C/D_t ratio is a significant factor in the trough width at depth. The data also showed that at higher volume losses the trough width narrows as the chimney mechanism occurs; this is in agreement with previous centrifuge data. Marshall et al. (2012) suggested a new model for trough widths which is based on Mair et al. (1993) using the Modified Gaussian curve and accounting for the C/D_t ratio and tunnel volume loss; this is given in Eqs. (1.18) and (1.19). It is difficult to compare trough width parameters from the Gaussian and Modified Gaussian calculations but x^* and K^* are slightly comparable with the standard values of i and K. x^* is the point at which:

$S/S_{max} = 1/\sqrt{e}$ and for a Gaussian curve, i,e when $\alpha_{MG} = 0.5$, $x^* = i$ and $K = K^*$.

$$K^* = x^*(z_0 - z) = \frac{(K_s^* + \partial x^*)/(\partial z\,(z/z_0))}{(1 - z/z_0)} \tag{1.18}$$

$$K_s^* = K_{s,C/D_t}^{intercept} + K_{s,C/D_t}^{slope}(C/D_t) + K_{s,V_l}^{slope}(V_l) \tag{1.19}$$

Though the formulation of Marshall et al. (2012) is significantly more complex, it is able to predict the data better than both Mair et al. (1993) and Moh et al. (1996). This is most apparent at higher volumes losses when K^* reduces with depth when compared with the analysed PIV data from centrifuge test GS2 as reported in Williamson (2010). As discussed previously a constant value of K with depth is often used in practice and this is clearly not suitable for lower volume losses as shown in Figure 1.8; at 5% volume loss the value of K^* is nearly constant with depth. Marshall et al. (2012) show that K^* is approximately constant at lower volume losses for shallower tunnels indicating that the chimney mechanism propagates to the surface much faster.

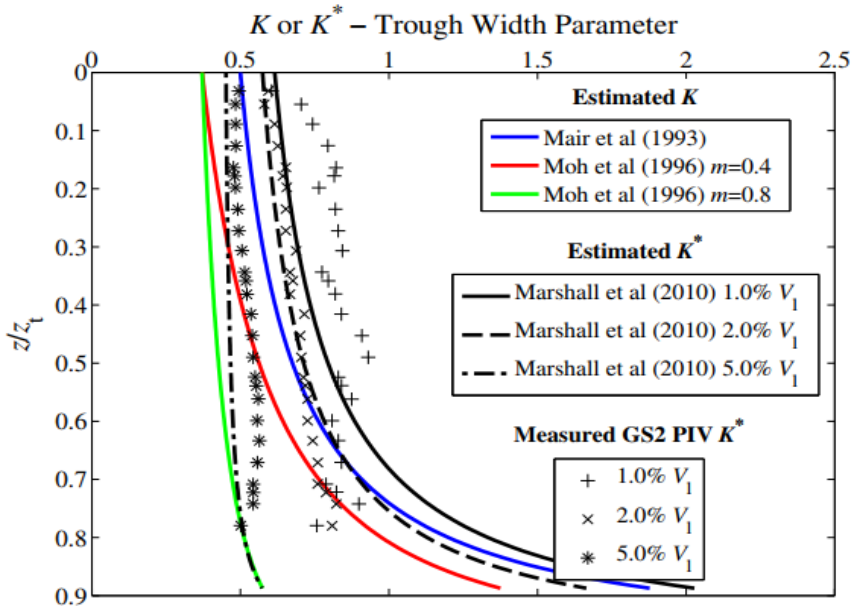

Figure 1.8 Comparison of subsurface K and K* calculation values

1.2.2.2 Horizontal Transverse Movements

1.2.2.2.1 Clays

As discussed in Section 1.2.1.3, it is often assumed that the horizontal surface movements correspond to vectored movements of the soil towards the tunnel axis. If K is assumed to be constant with depth, then to ensure the compatibility of strains in undrained conditions, subsurface movements would also point to the tunnel axis. However, Eq. (1.16) shows this is not the case and that for the K profile given in Eq. (1.16) the vectors should point at a position (0,175/0,325) z_0 below the the tunnel centreline as derived by Taylor (1994) based on constant volume conditions and a single horizontal horizon having the same vector direction. The lower vector focus results in a reduction in the magnitude of all horizontal subsurface movements to only 65% of those focussed on the tunnel axis (Williamson, 2014). Others have shown that the vector focus of the tunnel movements are at a point between the tunnel axis and the invert, e.g. New and Bowers (1994) using the ribbon sink method. There is also a cases where the tunnel vectors point towards a position above the tunnel axis (Standing and Selemetas, 2013), and those which vary with depth (Grant, 1998).

1.2.2.2.2 Sands

Case studies in sands are very limited, though as stated in Section 1.2.1.3 the horizontal movements close to the surface are generally underestimated using the above methods at the surface settlement edges. Marshall (2009) presents centrifuge data for subsurface movements, showing predominantly vertical movements at the subsurface for low volume losses, moving towards a vector focus point of 1.1 z_0 to 1.4 z_0 below the ground surface at higher volume losses (Williamson, 2014).

As described in Section 1.2.2.1.2, the trough width factor K or K^* is shown to vary with depth, C/D_t and volume loss for sands. Results from a number of centrifuge tests in sands (Hergarden et al. 1996; Jacobsz, 2002; Vorster, 2005; and Marshall, 2009) have shown the trough width factor K in its various forms reducing with increasing volume loss both at the surface and at depth, independent of the form of the settlement trough chosen.

1.3 Conclusion

This chapter briefly discusses the features of various methods developed by researchers to predict tunnelling induced ground movements. The prediction of ground movements is necessary and important to prevent potential damage to pre-existing structures, foundations and services in the form of serviceability (displacements) or ultimate limit states (stress). The engineer responsible for design and construction of the tunnel should be able to predict these movements to a reasonable degree of accuracy with the aid of numerous methods that are available to him. The selection of method would largely depend on the complexity and severity of the tunnel-soil-structure interaction anticipated from the tunnel excavation project and the resources available to the engineer.

Various methods are available to the engineer to predict soil deformation due to tunnel excavation. These methods can be generally categorized as; (i) empirical, (ii) analytical and (iii) numerical to which each has its merits and limitations.

Empirical methods are limited to Greenfield conditions and hence unable to account for tunnel-soil-pile interaction. Analytical and experimental methods still face the deficiencies (soil models and difficulty of simulation the three-dimensional problem such as tunnel advancement) in predicting accurate tunnelling induced soil movement. Therefore, numerical methods are deemed to be an alternative attractive to understand ground deformations due to tunnel construction, the tunnel-soil-pile interaction mechanisms and provide preliminary assessment of loads and deformations induced on adjacent piles due to tunnelling which is the main object of the thesis.

CHAPTER 2

Tunnel-Soil-Pile Interactions

CHAPTER 2

Tunnel-Soil-Pile Interactions

2.1 Introduction

In general, the construction of new tunnels in the proximity of deep foundations raises concerns related to pile failure and associated structural damage (in both the superstructures and the foundation). Additionally, because of uncertainties related to excavation-induced effects on piles, significant project costs are committed to structural protection measures according to a conservative approach. To reduce uncertainties in the design of tunnel route/depth and the provision of preventative actions, it is required to achieve an understanding of the global soil-pile-structure interaction and the way it may affect/damage the superstructure. The first step towards the global understanding is the study of the response of piles and pile groups to tunnelling when the effects of protective measures or other construction activities are not present. In this chapter, an overview of the main studies that address the problem of the effects of tunnelling on piles and piled structures in different types of soil, both soft soils and stiff soils, which can be categorised into: (1) Field Observations, (2) Centrifuge and Laboratory Studies, (3) Numerical Methods, (4) Analytical and Simplified Numerical Methods.

2.2 Field Observations

Relatively little work available that investigate the effect of tunnelling on piled foundations through field observations, which are limited in various aspects of measurements, due to deficiencies in instrumentation planning or difficulties in collecting field data.

2.2.1 Second Heinenoord Tunnel

Tunnelling for the new North/South line in Amsterdam is to take place close to and in some cases beneath piled foundations (timber and concrete square piles). The field trials were conducted in strata consisting of a layer of 4 m of soft clay underlain by fine sand. The tunnels were 8.3 m outside diameter twin bore tunnels constructed using a slurry tunnel boring machine (TBM). The piles were loaded to give factors of safety of 1.5 and 2.0 on the timber and concrete piles respectively. The results showed that pile settlements took place rapidly following the TBM passage, while the time-dependent deformation is accounting for almost 10-20% of the final settlement. Also the tunnel settlement trough was much steeper than expected. By comparing the resulting pile settlements with the ground surface settlements it was possible to identify three distinctive zones of influence around a tunnel in which pile settlements were correlated to surface settlements (see Figure 2.1). Piles with their bases located in zone (A) settled more than the surface, piles located in zone (B) settled almost by the same amount as the surface, whereas piles located in zone (C) settled less than the surface settlement.

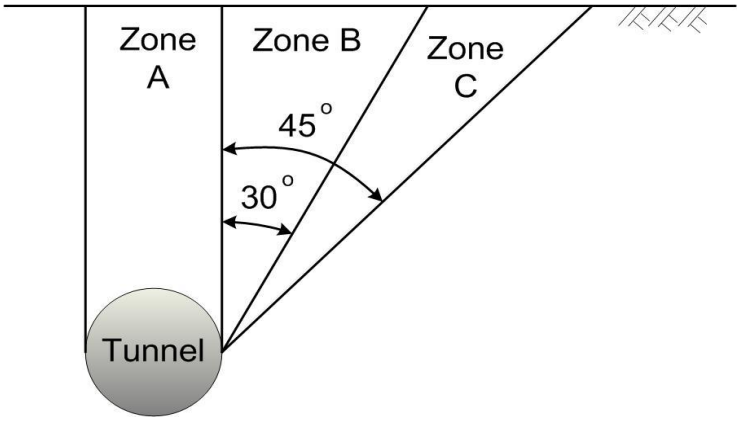

Figure 2.1 Zones of influence for tunnels constructed beneath piles (Kaalberg et al. 2005)

2.2.2 Channel Tunnel Rail Link (CTRL)

Selemetas (2005) presented the results of a full-scale trial investigating the effects of construction of twin tunnels using EPB machines on piles. The field study took place in Channel Tunnel Rail Link (CTRL) Contract 250, in Dagenham, Essex, UK. The study involved the installation, loading and monitoring of four instrumented piles along the route of the twin tunnels (two were friction piles and two were end-bearing piles). The piles were loaded to 50% of their ultimate design capacity. A comparison was made between the resulting pile head settlements due to tunnelling with the ground surface movements. The results identified three zones of influence in which the pile settlements were correlated to the ground surface settlements (see Figure 2.2):

1. Piles in Zone A settled 2-4 mm more than the ground surface.
2. Piles in Zone B settled by the same amount as the ground surface.
3. Piles in Zone C settled less than the ground surface.

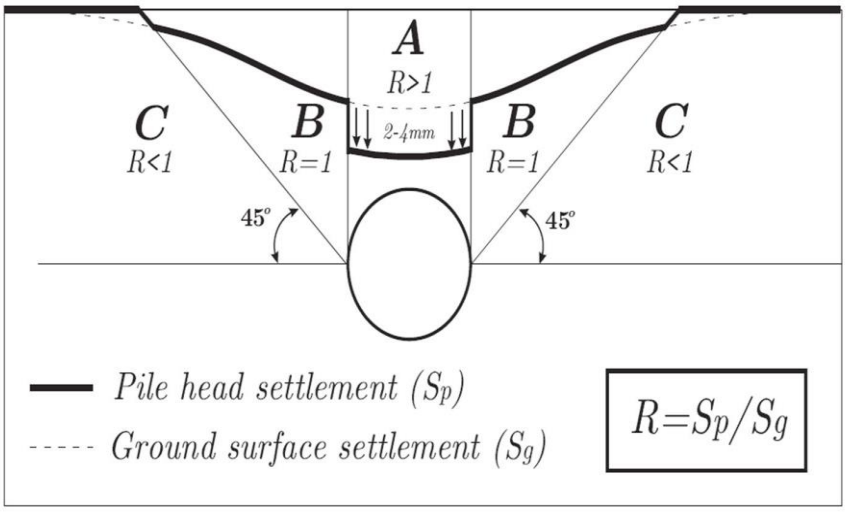

Figure 2.2 Zones of influence for EPBM tunnels constructed beneath piles (Selemetas, 2005)

2.2.3 Singapore MRT North East Line

The North East Line of the Singapore Mass Rapid Transit (MRT) encompassed the construction of a new piered viaduct supported by 4 or 6 pile groups consisting of 25 m to 65 m long, 1.2 m diameter bored piles, and the excavation of long bored twin tunnels of 6.5 m diameter using two Earth Pressure Balance machines (EPB), both under the same contract, C704. The details of the project are described in Coutts and Wang (2017), Pang et al. (2005a) and Pang et al. (2005b). The piles were instrumented with a series of strain gauges to determine the axial loads and bending moments in transverse and longitudinal directions. In general the results indicate that the piles closer to the tunnel showed significantly higher induced axial loads and bending moments due to tunnelling than the piles further away from the tunnel. The bending moment and axial load were shown to have a near linear relationship to the volume loss as the tunnel face passed the pile group. The surface settlement profile due to tunnelling follows a Gaussian form with a maximum value of about 18 mm.

2.3 Centrifuge and Laboratory Studies

A number of centrifuge and laboratory models have been described in this section to investigate the effect of tunnelling on piles and piled structures in both in sands and clays.

2.3.1 Centrifuge Models

2.3.1.1 Loganathan et al. (2000)

Loganathan et al. (2000) performed a series of three centrifuge tests under an acceleration of 100g at the University of Western Australia (UWA) to investigate the effects of tunnelling on a single pile and 2×2 pile group in kaolin clay. The depth of the tunnel was varied in the three tests (15, 18 and 21 m) in relation to the pile position as shown in Figure 2.3. Strain gauges used to measure the induced axial load and bending moment in the piles. The piles were loaded to a service load corresponding to 50% of the ultimate load (i.e. safety factor FOS= 2). The tunnel excavation is simulated by gradually reducing the volume of liquid contained in the latex membrane (silicone oil) simulating a volume loss of 1%.

This experimental study has shown that tunnel excavation generates displacements of the piles as well as axial load and bending moments inside the piles. A linear relationship was found between the volume loss and the maximum transverse bending moment. Induced bending moment profiles in the single pile and the front piles are almost the same except for a small difference near the pile cap, while, the rear piles experience the maximum value at pile head (effects of head fixity in the group piles). The maximum axial load was found to occur in Test 3 (the pile is subjected to negative skin friction). The vertical displacement of the piles relative to the surface and subsurface settlements are measured. Also single pile and pile group deflection are presented. The results shows that the effect of pile group was generally reduced settlement and the induced loads (positive group effect), indicating that a single pile may considered as the worst case scenario for assessing the effects of tunnelling on piles.

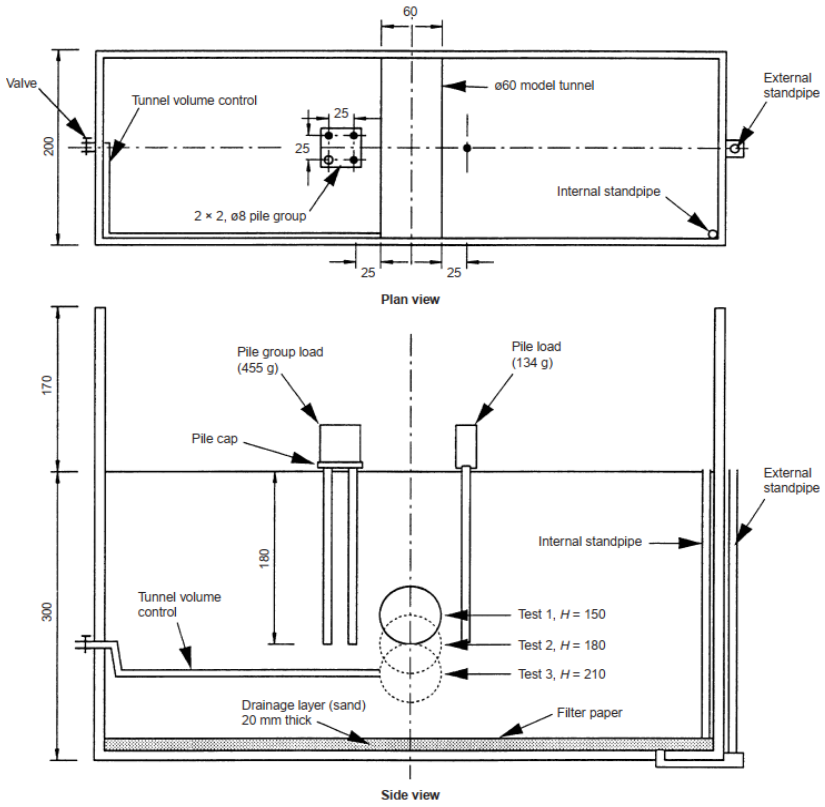

Figure 2.3 Layout of UWA centrifuge tests (Loganathan et al. 2000)

2.3.1.2 Feng (2003)

Feng (2003) performed a series of centrifuge tests to investigate the pile responses associated with a lined tunnel in dry sand. All the centrifuge model tests were conducted at 100g on the National University of Singapore (NUS) Geotechnical Centrifuge. Two piles were used in the test, one is for axial load, and the other is for bending moment. The simulation method of tunnel excavation proposed by Sharma et al. (2001) using polystyrene foam (dissolved by an organic solvent to simulate the process of tunnel excavation) was adopted and the tunnel deformation is oval shape. The results showed that the induced pile bending moment demonstrates an opposite behaviour as most practical cases. The results showed also that both the maximum induced bending moment and maximum axial load of the pile occurs at the depth of tunnel horizontal axis.

2.3.1.3 Jacobsz (2002, 2004)

Jacobsz (2002) and Jacobsz et al. (2004a) investigated, with centrifuge tests, on the Cambridge Geotechnical Centrifuge, the problem of tunnelling beneath single piles installed in dense dry sands with different horizontal offsets with respect to the tunnel centreline. The tests were carried out under an acceleration of 75g. Tunnel excavation was simulated by extracting water in a controlled manner from the annulus between the tunnel and the membrane to induce volume loss. The experimental setup is shown in Figure 2.4a.

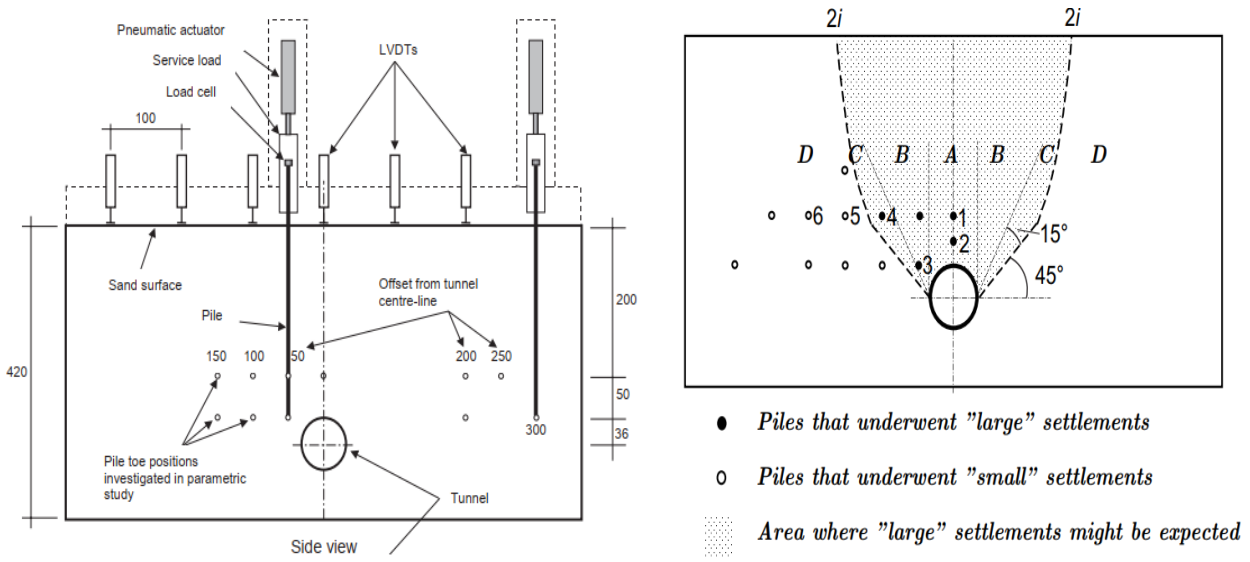

(a) **(b)**

Figure 2.4 Jacobsz (2002) study (a) Centrifuge layout (b) Influence zone around a tunnel

The authors defined an influence zones and then, they partitioned the area above the tunnel in four influence zones (A, B, C, and D) to describe the ratio of pile head settlement to ground surface movement depending on the pile base location as shown in Figure 2.4b. Pile settlement is greater than surface soil settlement for zones A and B, similar to surface soil movements in zones C, and less than the surface soil settlement in zone D.

2.3.1.4 Ran (2004)

Ran (2004), carried out a series of experiments for unloaded piles in the National University of Singapore (NUS) centrifuge in soft Kaolin Clay to investigate the effects of pile-to-tunnel distance, pile length, and volume loss effect. The volume losses were carried out using a model tunnel with a brass cylinder with lap joint and foam inner, with the foam dissolved in flight to simulate volume loss.

The effects of volume loss on Tests 1, 6 and 7 was non-linear in terms of bending moment and lateral pile head deflection. However the maximum axial load, pile head settlement and pile base load all appeared to vary in a more linear fashion. The low strength of the soft clay and hence the likelihood of the soil behaving in a plastic manner may explain this variation in behaviour with increasing volume loss. The results showed that the effect of increasing X_p from the tunnel in Tests 1, 2 and 3 reduces the maximum axial force, pile head settlement and pile base load. The effect of pile tip location, on vertical pile head displacement is shown in Figure 2.5a for Test 5. Based on the results of this and Tests 1, 4 and 5 the diagram in Figure 2.5b is proposed. With Zone (A) described as producing slightly greater settlements than Zone (B). From the studies, it is demonstrated that the pile responses in clay are time-dependent.

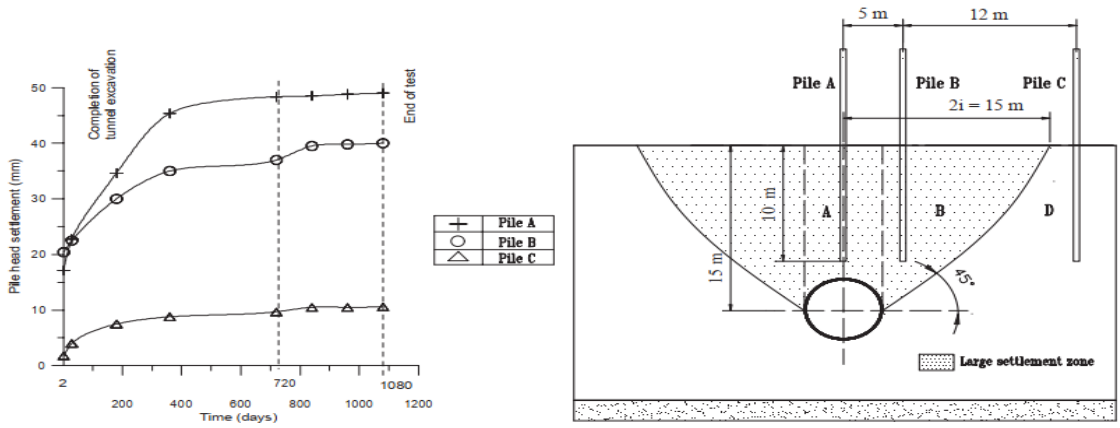

(a) Variation in Vertical Pile Displacement Due to Volume Loss with Time

(b) Zones of Vertical Pile Displacement

Figure 2.5 Results of Ran (2004) centrifuge tests (a) pile head movement (b) influence zone

2.3.1.5 Lee and Chiang (2007)

Lee and Chiang (2007) report a series of centrifuge tests carried out at the National Central University (NCU) in Taiwan to analysis of tunnel-bored pile interaction in saturated quartz sand. The tunnels of 6 m diameter were embedded at depths with various cover-to-diameter ratios. The instrumented axial and bending piles constructed from aluminium tubing and placed either side of the tunnel. The maximum bearing capacity of the pile is defined as the load corresponding to a settlement of the pile head equal to 10% of the pile diameter.

The measurements of pile settlements and forces indicated that only the tunnel-pile depth ratio influences the bending moment distribution, but both the pile-tunnel depth ratio and the working load on the pile determine the axial force profile along the pile. Interestingly, the more the pile is loaded, the more the pile is expected to settle. Furthermore, the authors identified the main causes of pile settlements: loss of skin friction for tunnelling adjacent to piles and the reduction of end bearing capacity during tunnelling at the pile base depth. To sum up, the author represented the qualitative variation of axial load (load transfer mechanism), skin friction and bending moment.

2.3.1.6 Marshall (2009)

Analysing the results of two centrifuge tests, Marshall (2009), Marshall and Mair (2011) and Marshall (2012) evaluated the main aspects of tunnelling movements conducted under plane strain conditions beneath pile group in dense sands, with applied constant head loads during tunnelling. The series of centrifuge tests are conducted under an acceleration of 75g in the Cambridge Geotechnical Centrifuge. The layout of the experiments is shown in Figure 2.6. Prior to volume loss modelling, the driving force was reduced to a lower service load giving a safety factor FOS= 1.6. The first test consisted of a pile immediately above the tunnel centreline and another pile at an offset of 2.1 tunnel diameters, whereas the second test had two offset piles at a distance of approximately one tunnel diameter from the tunnel.

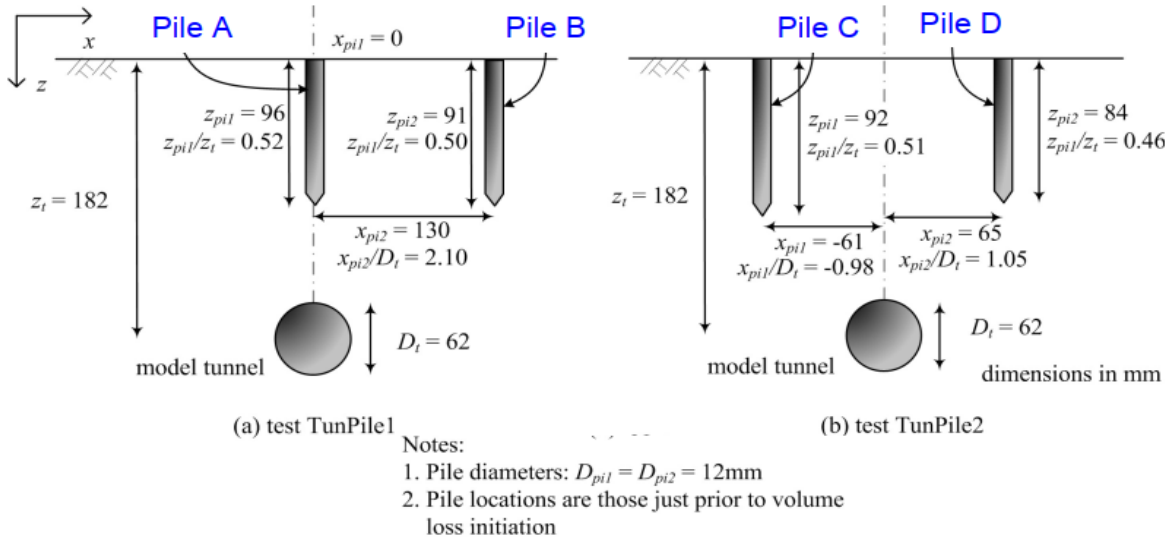

Figure 2.6 Position of piles in relation to the tunnel (Marshall and Mair, 2011)

The results show that pile 'A' showed displacements up to approximately 1% volume loss which were much less than the Greenfield surface settlement. Pile 'B' showed very little movement at all volume losses, much less than the Greenfield settlement. Pile 'C' and Pile 'D' both showed similar pile movements up to 1.74% volume loss which was much less than the Greenfield movement, at which point the displacement of Pile 'C' accelerated and failed at approximately 2.5% whilst Pile 'D' continued to displace at a similar rate, moving at approximately the same amount at the greenfield settlement.

2.3.1.7 Ong (2009)

Ong (2009) describes a series of centrifuge experiments to investigate the effect of tunnel construction on adjacent piles in soft Kaolin clay overlying Toyoura dense sand using the Geotechnical Centrifuge facility on the National University of Singapore. The centrifuge tests were conducted at an acceleration field of 100g. The model was prepared and tested in a plane strain strongbox. Figure 2.7a shows the centrifuge model setup. The position of the pile bases relative to the tunnels for the single pile tests are shown in Figure 2.7b.

The tunnelling movement were found to be Gaussian in the short term, but in the long term settlement profiles was relatively more uniform with distance from the tunnel centreline. Maximum bending moments and axial loads were seen close to the tunnel horizontal axis (except test 7 and 8). Socketing the piles into the sand was seen to induce greater axial load in the piles, with free headed piles (Test 10) showing the greatest overall load. The fixed headed pile showed the greatest bending moment at the pile head, but the free headed was greatest at depth. The effect of pile length showed shorter piles exhibiting much lower induced axial loads and bending moments, but much greater head settlements and lateral head movements than longer piles. The effect of pile distance (X_p) showed that, settlement, bending moments and axial loads reduced nearly linearly with distance from the tunnel centreline.

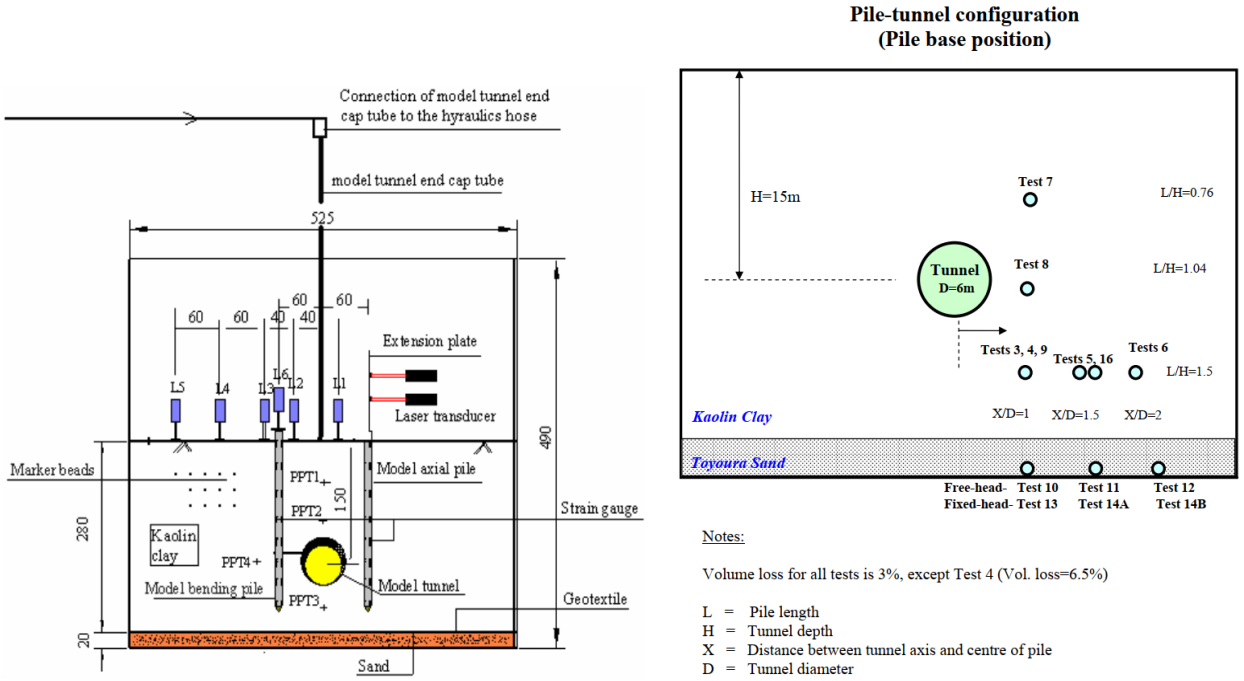

(a) **(b)**

Figure 2.7 Ong (2009) study (a) centrifuge model setup (b) Layout of single pile cases

2.3.1.8 Ng et al. (2013)

A series of three-dimensional centrifuge model tests were performed by Ng et al. (2013) to investigate the behaviour of a bored single pile due to the construction of twin tunnels one after the other in dry sand at the Hong Kong University of Science and Technology Tests. All of the centrifuge tests were carried out at an acceleration of 40g. Four centrifuge model tests were carried out (test L, T, TT, and SS) with different cover-to-diameter ratios (C/D). To obtain the capacity of the pile, a pile load test was carried out without tunnelling effects (Test L). Test T (C/D= 2.7) is designed to investigate the behaviour of a single pile due to a single tunnel constructed near pile toe. Test TT (C/D= 2.7) was designed to study the effects on the pile induced by the construction of twin tunnels near the pile toe. Finally, test SS (C/D= 1.5) was designed to investigate pile responses induced by the construction of twin tunnels near the mid-depth of pile shaft.

The effects of the 3D tunnel excavation were simulated in-flight by draining away a controlled quantity of water (filled inside rubber bags) equivalent to a volume loss of 1.0% in each stage of excavation of each tunnel. A single tunnel model was constructed using three cylindrical rubber bags for test (T) and in the case of twin tunnel models, each tunnel consisted of five rubber bags (Test TT and Test SS). A rigid aluminum divider was installed between each two rubber bags in order to stop any possible soil movement towards tunnel face and to control the water. Figure 2.8 is a schematic view of Ng et al. (2013) study.

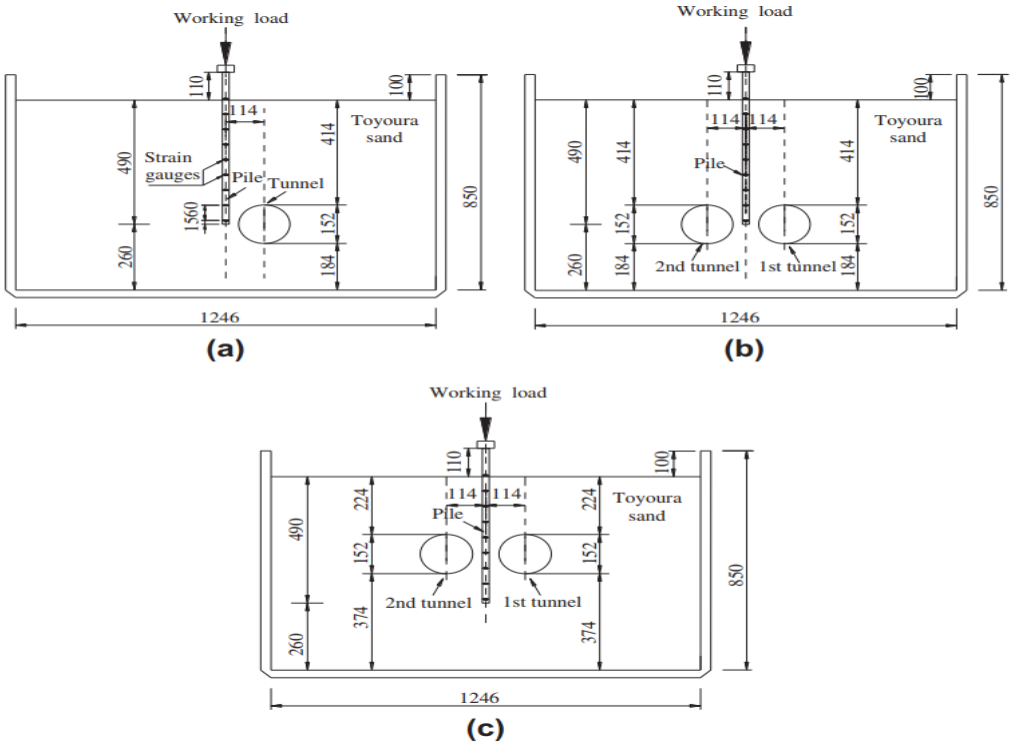

Figure 2.8 Elevation view of centrifuge model tests conducted by (Ng et al. 2013)

The results reveal that when the tunnels were excavated below the pile toe, most settlement and significant loss of the pile capacity resulted. It was also reported that the effects of the construction of the second tunnel on pile settlement were smaller than that of the first tunnel (Sohaei et al. 2020). The pile settlement occurred by the twin tunnelling excavation is mainly depend to C/D ratios (cover-to-diameter ratio) of tunnels and the relative position of a tunnel to the pile. The results showed that the axial force of the single pile was increased for twin tunnel construction near the mid-depth of the pile compared with near the toe and below the toe. The results demonstrates that the largest bending moment was induced after the first tunnel was constructed near the pile toe resulted with the pile tilting. In other words, research of Ng et al. (2013) revealed a favourable effect on the bending moment along the piles after the construction of the second tunnel completed.

2.3.1.9 Williamson (2014)

Williamson (2014) performed a series of centrifuge tests of tunnelling beneath non-displacement piles in sand and stiff clay with a constant service load. Parts of the results were discussed by Mair and Williamson (2014). The test plan investigated the effects of pile horizontal offset to the tunnel centreline, pile load condition and soil stiffness/strength. The trends of the pile settlements confirmed previous research showing that piles directly above and adjacent to the tunnel settle, respectively, more and less than the greenfield surface settlement trough. Additionally, there was a remarkable influence of the external head load on pile displacements due to a given volume loss (the higher load the greater pile settlement).

Regarding pile failure, it should not be expected, even at high tunnel volume loss, for non-displacement piles in clays (Franza, 2017). This is due to the tunnelling-induced soil degradation at the pile shaft and base being balanced by additional pile settlements relative to the soil (that mobilise positive shaft friction).

2.3.1.10 Boonsiri and Takemura (2015)

Boonsiri and Takemura (2015) carried out a fairly exhaustive parametric study of the influence of the excavation of a tunnel on groups of piles in dry Toyoura sand. These tests were carried out on the Tokyo Tech Mark (III) centrifuge under an acceleration of 100g considering plane strain conditions (2D). The tunnelling process was simulated by reducing the diameter of the model tunnel. The test cases were conducted at two different tunnel cover depth and diameter ratios (C/D= 1.5 and 2.5) and three different horizontal distances between the pile groups and the tunnel. In this study, the ultimate load is defined as the load causing group settlement equal to 10% of the pile diameter.

The results showed that the mechanical behaviour of the group of piles was strongly dependent on the relative position between the tunnel and the group of piles. For pile groups shallower than the tunnel, the axial force increase in the piles closer to the tunnel and decrease in the piles farther away. When piles and tunnel were at the same depth, there was an increase in the axial force in both piles. The results reveal that the pile group induced more soil surface settlement in the area above the tunnel crown. This trend is more significant for cases with small C/D (= 1.5) ratios, small horizontal distances between the pile group and the tunnel, and large ground loss ratios. However, the induced soil settlement is negligible for the cases with C/D= 2.5 and small ground loss ratios. Also the results shows that the settlement profiles could be represented by the Gaussian distribution curve at small and large ground loss ratios. In this study, a zone of influence was adopted for the model of C/D= 2.5 and 1.5 as shown in Figure 2.9 (Boonsiri and Takemura, 2015).

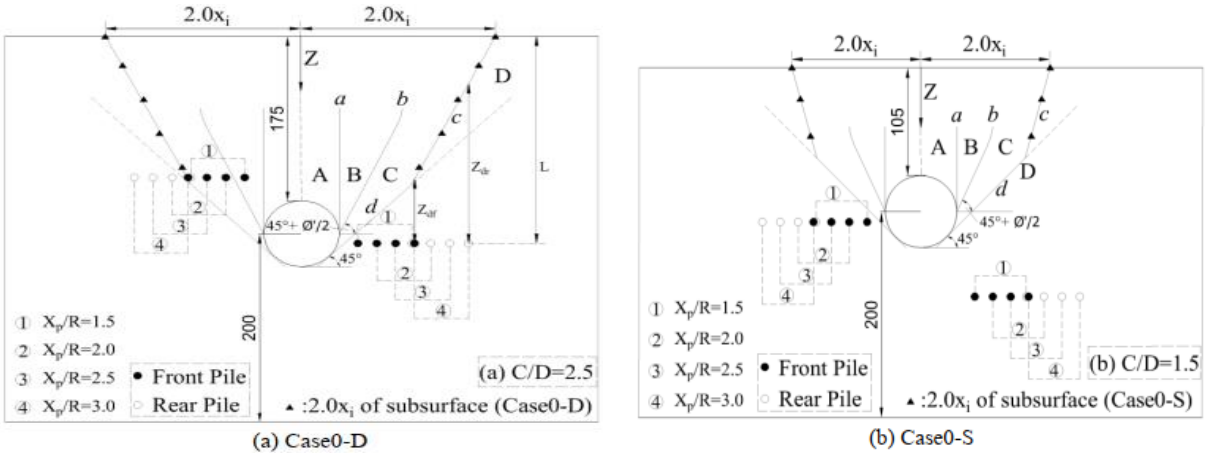

Figure 2.9 The adopted zones of influence, the pile base positions (short and long piles), different (X_p), for C/D= 2.5 and 1.5 (Boonsiri and Takemura, 2015)

2.3.1.11 Franza and Marshall (2018)

Franza and Marshall (2018) performed a series of geotechnical centrifuge experiments to simulate the effect of excavating a tunnel beneath piled structures in a uniform dry fine silica sand. The experiments were performed at 80 times normal gravity (80g) using the University of Nottingham geotechnical centrifuge. The centrifuge package includes the centrifuge strong box, soil, model tunnel, and tunnel volume control system. The model layouts are shown in Figure 2.10. The inside plan dimensions of the strong box are 640×260 mm and the maximum elevation of soil within the box is 500 mm. Uniform dry fine silica sand was used for testing. The model tunnel diameter is 90 mm which buried at a depth of 225 mm. A tunnel volume control system comprising an actuator connected to a hydraulic cylinder was used to control the volume of fluid within the tunnel. Piles diameter is 9 mm and the embedment depth is 135 mm.

The results showed that piled foundations change the global tunnel-pile-structure interaction with respect to shallow foundations, producing a greater potential for damage of flexible structures. The relationship between structure stiffness and weight, as well as the safety factor of the piles control the structure settlements. Generally, an assessment of the post tunnelling pile safety factor should be carried out, by considering pile head load redistribution and that pile capacity may be reduced by tunnel volume loss.

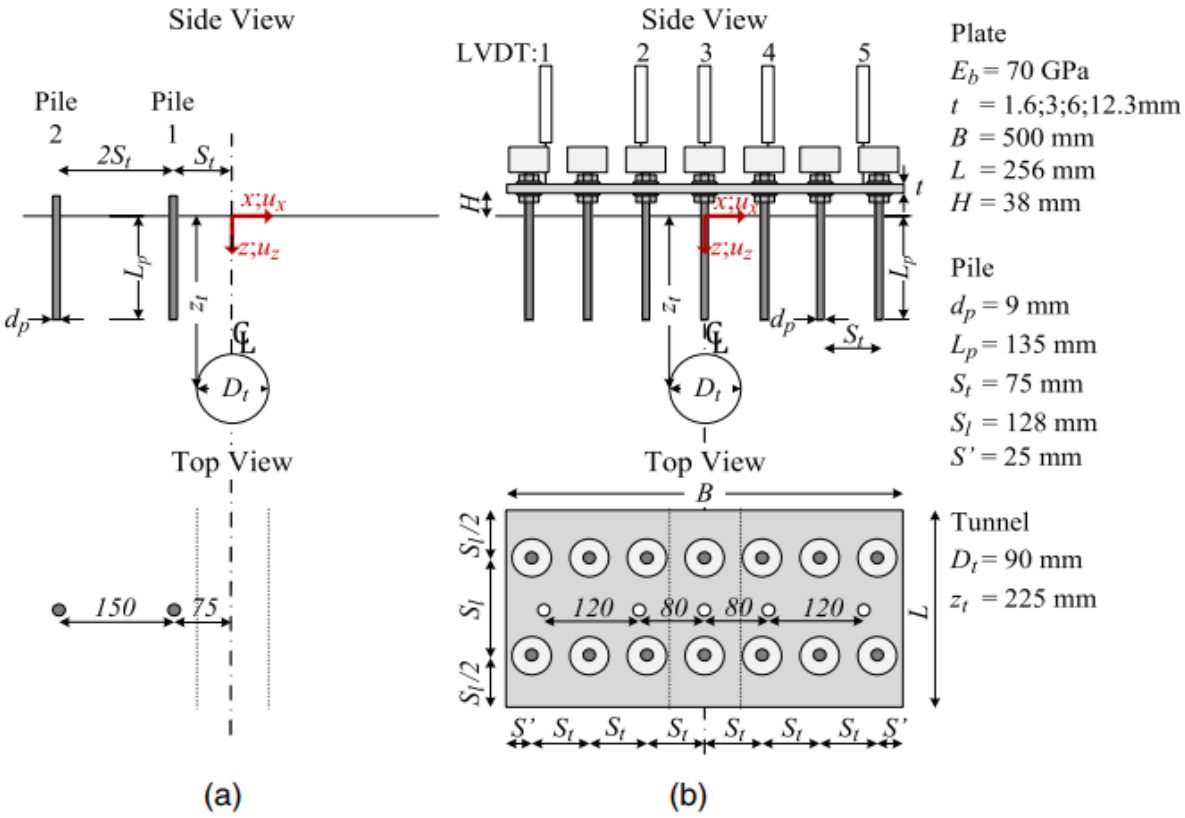

Figure 2.10 Test layout (in model scale): (a) loading tests (b) tunnelling beneath piled plate (Franza and Marshall, 2018)

2.3.1.12 Soomro et al. (2018a)

A series of 3D centrifuge model tests were performed by Soomro et al. (2018a) to investigate the lateral responses of an existing 2×2 pile group to advancement of side-by-side twin tunnels in dry sand. The 3D centrifuge experiments were conducted under an acceleration of 40g at the Geotechnical Centrifuge Facility at the Hong Kong University. Pile load test was performed first in greenfield conditions to find the ultimate capacity of the pile group. Three centrifuge tests were carried out (test SS, TT, and BB) at various depths of the twin tunnels relative to the pile shaft. Both the tunnels were located near mid-depth of the pile shaft in test (SS) with cover-to-diameter ratios (C/D= 1.5), next to the pile shaft (test TT) with (C/D= 2.7) and below the toe (test BB) with (C/D= 3.7. The 3D tunnel advancement was modelled by the same way used in Ng et al. (2013) study. The centrifuge tests were back-analysed by a three-dimensional finite element study.

The results showed that the most significant lateral movement of the pile cap induced after the completion of the first tunnel in each test. The three tests indicate that the largest and the smallest lateral movement of the pile cap obtained from tunnelling below the pile toe (i.e. test TT) and near mid-depth of the pile shaft (i.e. test SS), respectively. From test TT, the induced bending moment and pile deflection can be critical when first tunnelling advanced adjacent to pile toe. However, the induced bending moment decreased significantly owing to the excavation of the second tunnel in each case (caused a stress release on the opposite side of the pile). The results show also that shearing forces induced in piles during twin tunnelling and induced as a reaction of pile deflection in tests TT and BB (Soomro et al. 2018a).

2.3.2 Laboratory Models

This section reviews some published work carried out to investigate the effects of tunnels on piles using simple 1g testing and other lab-floor techniques.

2.3.2.1 Morton and King (1979)

One of the first studies of the tunnel-deep foundation interaction using an experimental model was conducted by Morton & King in 1979, where they describe 1g tests conducted on model wooden piles in medium dense sands. The loaded piles are installed at various locations from the tunnel and placed at various depths above the tunnel. The tunnel was simulated using an advancing steel tube and cutting head. Based on the test results the authors suggested the existence of a limiting pile failure zone whereby piles with their bases within this zone are likely to experience considerable settlements even at small ground loss values. Figure 2.11 shows the various positions at which pile bases where installed with reference to the model tunnel and the limits of pile failure zone (shown by the red dotted curves). The shape of this critical zone was approximated by a line drawn from the tunnel spring line to the surface (shown by the blue solid lines). The authors also observed that piles located further than ($1.75D_t$) did not experience significant settlements.

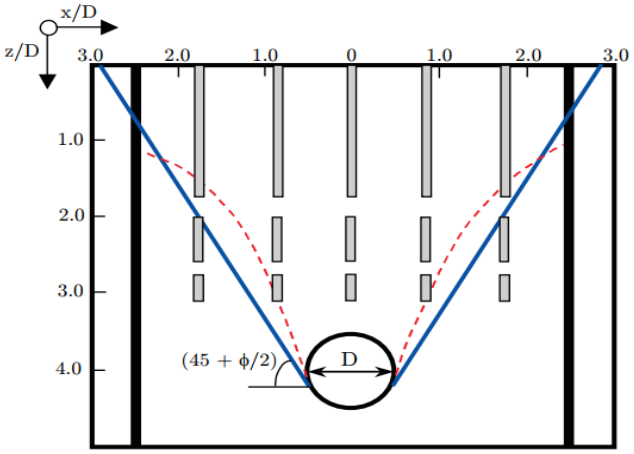

Figure 2.11 Limiting pile failure zone after (Morton and King, 1979)

2.3.2.2 Lee and Bassett (2007)

Lee and Bassett (2007) performed some interesting 1g model experiments relating to the problem of tunnelling near piles. The experiments conducted at University College London (UCL). The authors describe the use of multi-sized aluminium rods to model the plane-strain behaviour of sand. The model test has a total of 21 cases, i.e. five different tunnel positions (2, 1, 0, +1, +2) with respect to four different pile tip locations (A, B, C, D). Experimental layout and pile toe positions are shown in Figure 2.12a and Figure 2.12b, respectively. The authors provide their own 'map' of influence zones based on experimental and numerical modelling results, illustrated in Figure 2.12c. It's evident that the proposed influence zones are relatively wider and deeper than those proposed by previous studies both centrifuge modelling and field trials. However, the influence zones are dependent on the pile tip location, 2D volume loss, soil condition, working load, pile geometry, dilation effect of the granular material, and tunnel dimension (Sohaei et al. 2020).

2.3.2.3 Sohaei et al. (2017)

Sohaei et al. (2017) established a micropiles method to control the ground surface settlement, settlement and lateral movement of the existing pile due to tunnelling. For this purpose, a series of three-dimensional (3D) physical modelling tests in dry sand were carried out under single gravity (1g condition). A single pile (hollow aluminum tube) was placed at a horizontal distance of a tunnel diameter (1D) from the tunnel vertical axis. A row of micropiles (rigid circular steel rod) was later placed in between the pile and the tunnel. The results showed that the shallow tunnelling close to an existing pile has significant influences on the pile such as settlement, lateral movement, bending moments, and the axial force. The pile settlements were found to be nearly the same as the ground settlement (1.10%D) in all cases. The results of the apparent loss of pile capacity (ALPC) showed only 1.4% of the pile diameter compared to 6% of tunnelling without micropiles (i.e., positive effect of micropiles method and pile capacity is improved significantly).

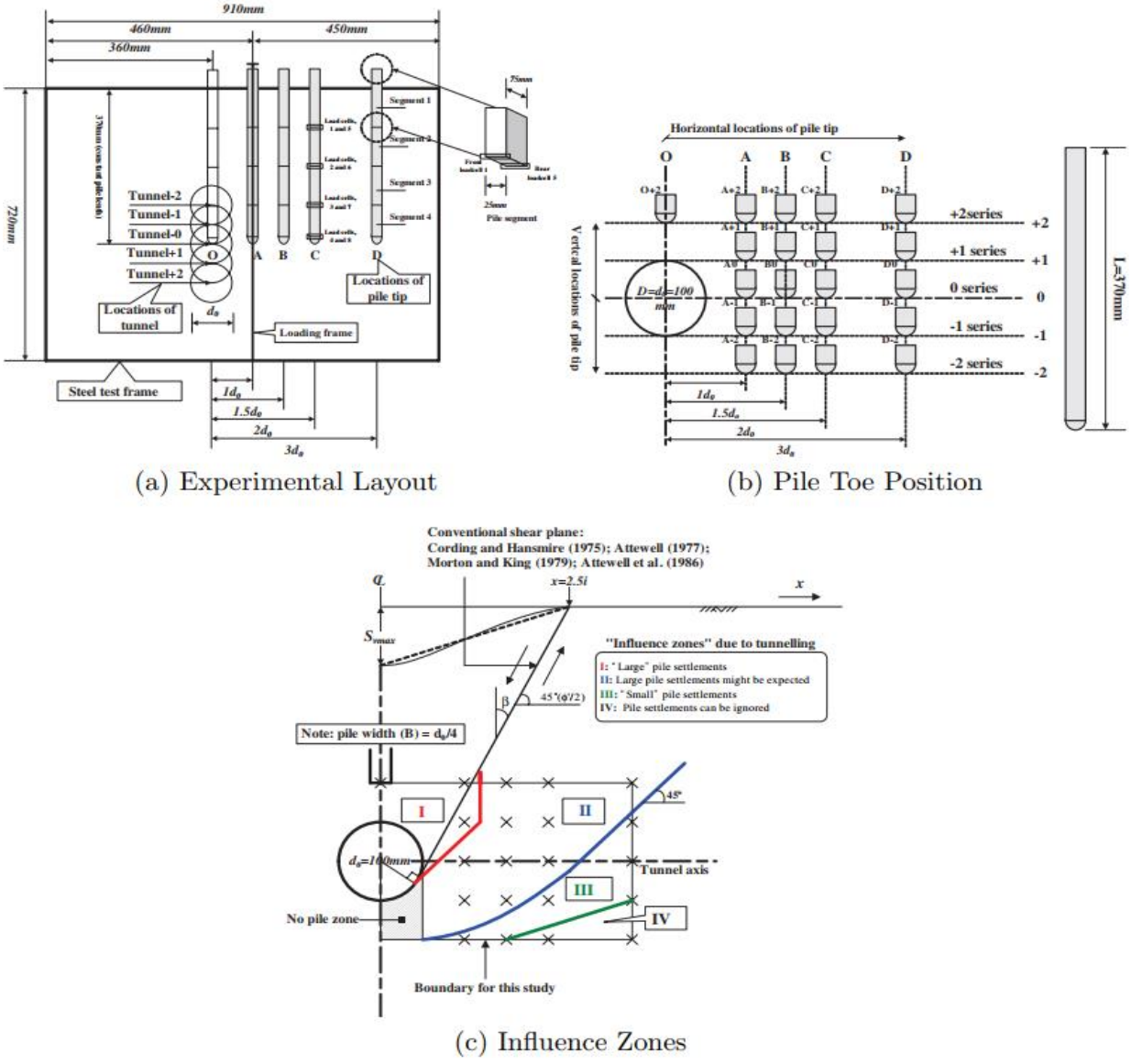

(a) Experimental Layout (b) Pile Toe Position

(c) Influence Zones

Figure 2.12 Layout, pile toe position and influence zones of (Lee and Bassett, 2007) tests

2.4 Numerical Methods

A number of numerical studies have been undertaken investigating the effects of tunnelling on pile foundation, a review of those of significance is given below.

2.4.1 Mroueh and Shahrour (2002)

Mroueh and Shahrour (2002) investigated single piles and groups of piles response to tunnelling through a full 3D analysis using the finite element program PECPLAS. Numerical simulations were performed in two stages: (a) application of an axial load about 50% of pile capacity and (b) the construction of the tunnel, which was performed using the parameters α_{dec} and L_{dec} (which stand for the ratio of stress release and the length of the unlined zone, respectively). Figure 2.13 shows the 3D finite element mesh used in the study.

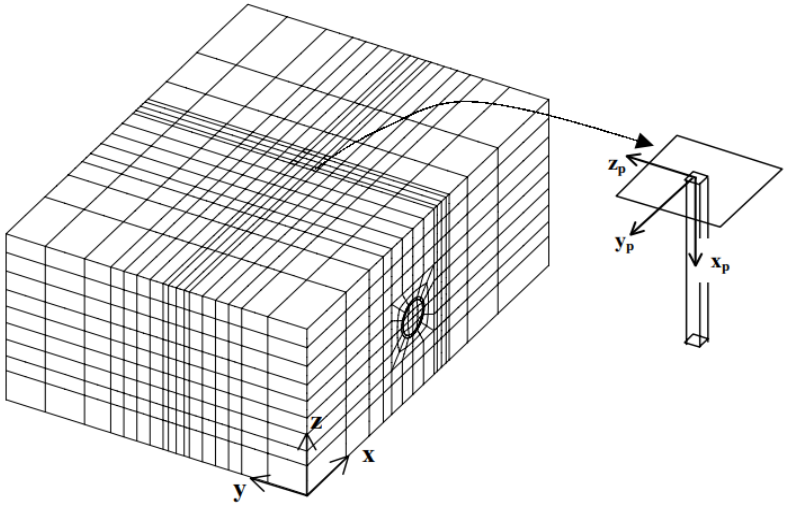

Figure 2.13 3D finite element mesh used in (Mroueh and Shahrour, 2002) study

Analysis of the soil movement in the lateral and longitudinal directions showed that pile responses in lateral direction were reached after passage of the tunnel face, while in the longitudinal directions were reached when the tunnel face was directly in line with the pile. From the parametric study, the results reveals that when the pile tip is above the tunnel axis level there is a continuous increase of axial force with depth (which results from the downward movement of the soil adjacent to the pile), whereas when the pile tip is located below the tunnel axis the results show an increase of the axial force up to a maximum value followed by a decrease (results from the upward movement of the soil below the tunnel horizontal axis). In the first case where the pile tip is located above the tunnel axis, tunnelling induces low bending moments relative to the second case. The increase of the distance between the pile axis and the tunnel centre-line from 1D to 1.5D causes a significant reduction in the magnitude of axial force and bending moment along the pile shaft.

Pile group response investigation showed that the group of piles were less affected by axial load and bending moment than a single pile, even when they were not connected. The presence of the additional pile would increase the stiffness of the ground around the group of piles, and the effect of a pile cap was shown to have little effect on the bending and axial load.

2.4.2 Cheng et al. (2003, 2004, 2007)

Cheng et al. (2004) present the results of a series of a 3D finite element analysis of the effects of tunnelling on piled foundations. A novel kinematic technique known as the Displacement Control Model (DCM) was used in the finite element program ABAQUS to simulate non-uniform soil convergence around the excavated tunnel boundary and obtain the soil displacement field around the deforming tunnel. The soil-pile interface behaviour was modelled using zero thickness interface elements assigned with the Coulomb frictional failure criterion. Various pile positions were simulated including different piles length and at various offsets from the tunnel centre-line.

The results showed that tunnel excavation creates a zone of large soil displacements around the tunnel (zone of influence). The envelope of this zone is defined by symmetrical boundaries extending upwards at an angle of 45° to the horizontal from the tunnel spring-line to the ground surface. The results shows that the pile settlement is tend to decrease with increasing pile length. In general, the induced pile axial forces and bending moments were shown to depend on the position of the pile tip relative to the zone of large displacements, the pile-soil stiffness ratio, and the magnitude of volume loss. Tunnel case histories were back analysed using the DCM by Cheng et al. (2007), and the analysis results found to be consistent with the results of field measurements and centrifuge test.

The pile failure mechanisms induced by tunnelling in three different pile locations with respect to the tunnel axis level is shown in Figure 2.14 (Cheng, 2003). In case (I) in which the pile toe is below the tunnel axis level, the damage of the structure is induced due to a combination of excessive bending moment and excess of the pile compressive strength. In case (II) it is shown that the pile toe is above the tunnel axis level without pile restraint. In case (III), the pile toe is located in large deformation zone and the pile head is restraint with high vertical resistance. Negative skin friction of the soil drags downward the pile, but the vertical restraints on the pile head resist the pile head movements (Sohaei et al. 2020).

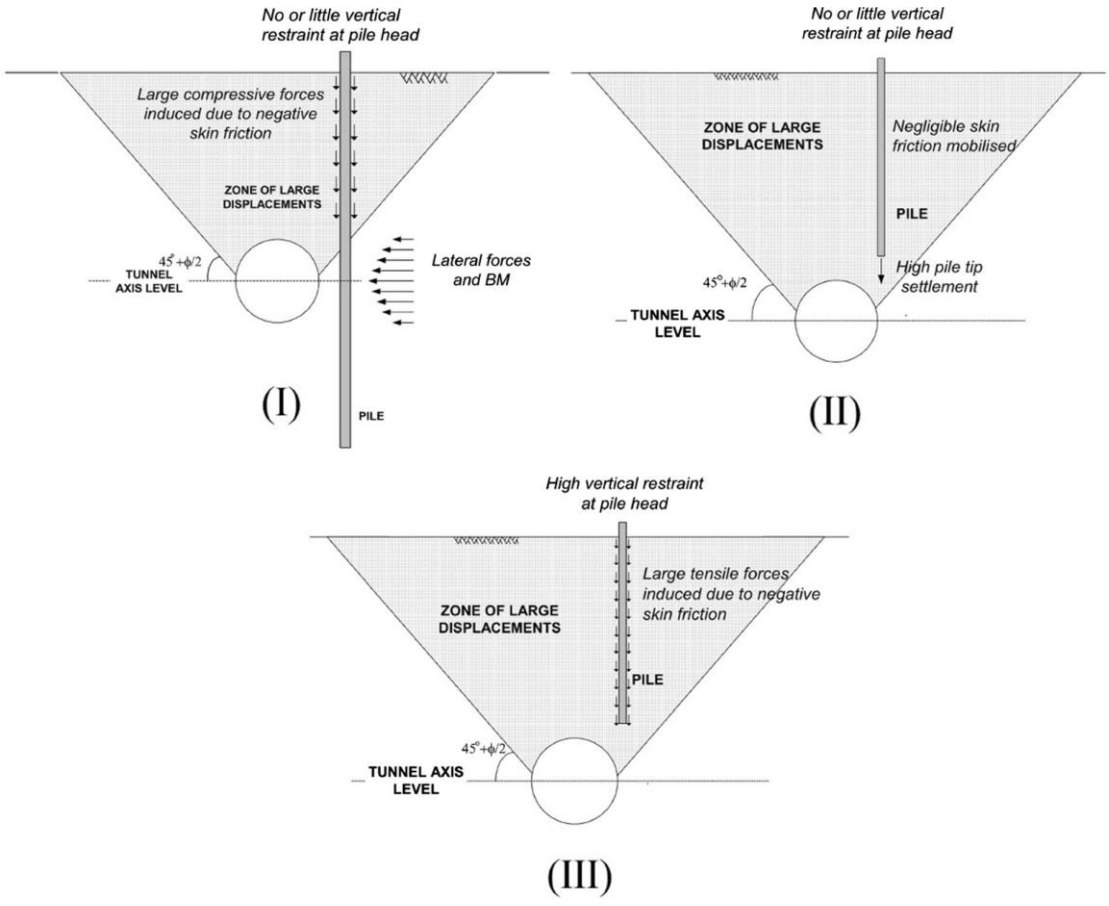

Figure 2.14 Pile failure mechanisms induced by tunnelling (Cheng, 2003)

2.4.3 Yang et al. (2011)

Yang et al. (2011) present the results of a 3D finite element simulation to investigate the effects of tunnel construction on nearby pile foundation using the finite element program PLAXIS 3D. The displacement controlled model (DCM) proposed by Cheng et al. (2007) was used to simulate the tunnelling-induced volume loss effects. The numerical model was verified based on the results of a centrifuge test (Ong et al. 2007a). The volume loss was 3.3% according to the test. Figure 2.15 shows the 3D finite element mesh and pile toe positions used in the numerical analyses. The Hardening-Soil model implemented in PLAXIS was adopted to model the non-linear stress-strain soil behaviour.

The results showed that there is a line separates two different zones: the zone of influence and support zone. The zone of influence extends from tunnel spring-line to the ground surface forming an angle of 45°. Regarding the pile tip position to the tunnel horizontal axis level, if the pile base located in the zone of influence, the pile settlement is greater or equal to soil surface settlement, whereas if pile base located outside the zone of influence the pile settlement is less than the soil surface settlement.

Due to tunnelling, both the compressive and tensile forces can be induced in pile, according to the pile base location. The results indicate the axial force increases when pile length, and volume loss increases, and when the pile becomes closer to the tunnel. Generally, the pile moves in the same direction when pile base located in the zone of influence, and the pile head moves laterally more than the pile tip, with the pile base outside the zone of influence. The numerical analyses show that when the pile base located outside the zone of influence, the bending moment is greater compared with the pile base located within the zone of influence. A positive group effect noticed compared to single pile case.

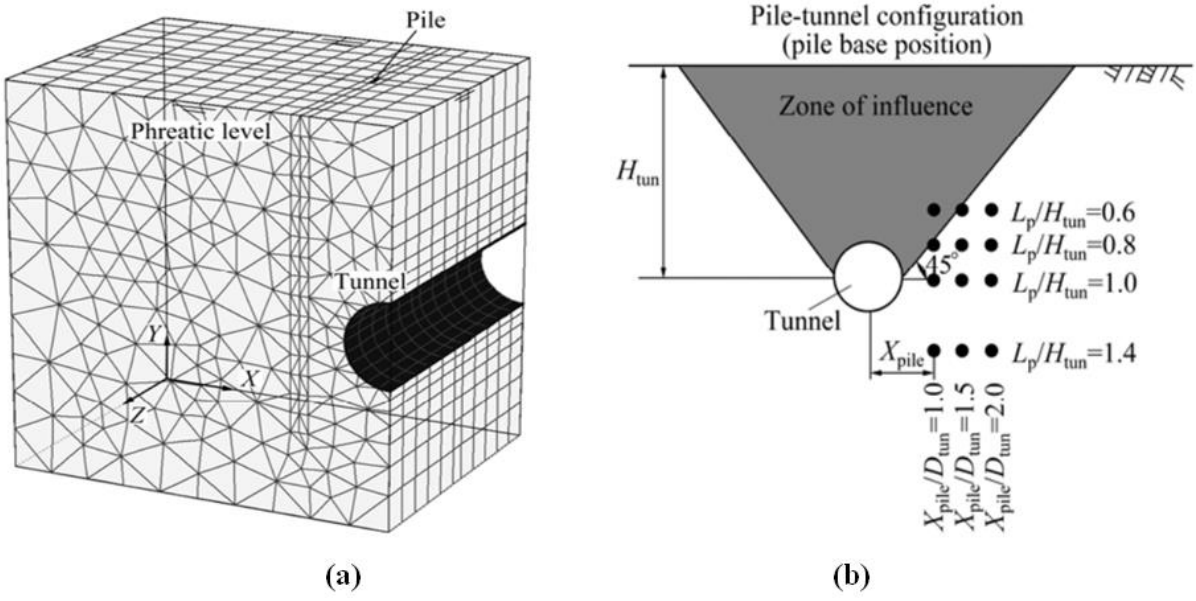

Figure 2.15 Yang et al. (2011) study (a) 3D finite element mesh (b) pile base position

2.4.4 Lee (2013)

Using the numerical code PLAXIS 3D, Lee (2013) carried out a series of (3D) finite element effective coupled consolidation analysis to study the behaviour of a single pile and a free-headed isolated piles in 3×3 and 5×5 pile groups during open face tunnelling in London stiff clay adopting the sprayed concrete lining (SCL) method. Figure 2.16 shows the 3D finite element mesh used in the numerical analyses and the problem geometry. The effects of pile installation not included and the pile is wished-in-place (similar to a bored pile). The Mohr-Coulomb model governed by non-associated flow rules with an isotropic elastic modulus was used to simulate soil behaviour. The numerical modelling involved three steps: initial geostatic equilibrium, application of an axial load, and tunnel excavation.

The results showed that tunnelling can induce significant increases in pile settlement compared to the pile settlement induced from the working load prior to tunnelling. Due to tunnelling a substantial changes in axial pile force distributions, causing tensile pile forces. The pile groups are more significantly affected than single piles in terms of serviceability (higher pile settlements and smaller tensile axial forces inside groups). The computed results indicate that the pile head settlement was higher than the free-field soil surface settlement. It was found that the influence zone for the pile head settlement involves a distance of -2D behind piles and +1.5D in front of piles in the longitudinal direction. Lee (2013) suggests that an equation may be necessary to estimate the ground settlement trough when there are pre-existing piles (especially for the pile group's case). A significant decrease in the factor of safety is anticipated because the apparent pile capacity decreased substantially. With tunnel progress, significant changes noticed in the distributions of the relative shear displacement and stress components along the pile due to tunnelling.

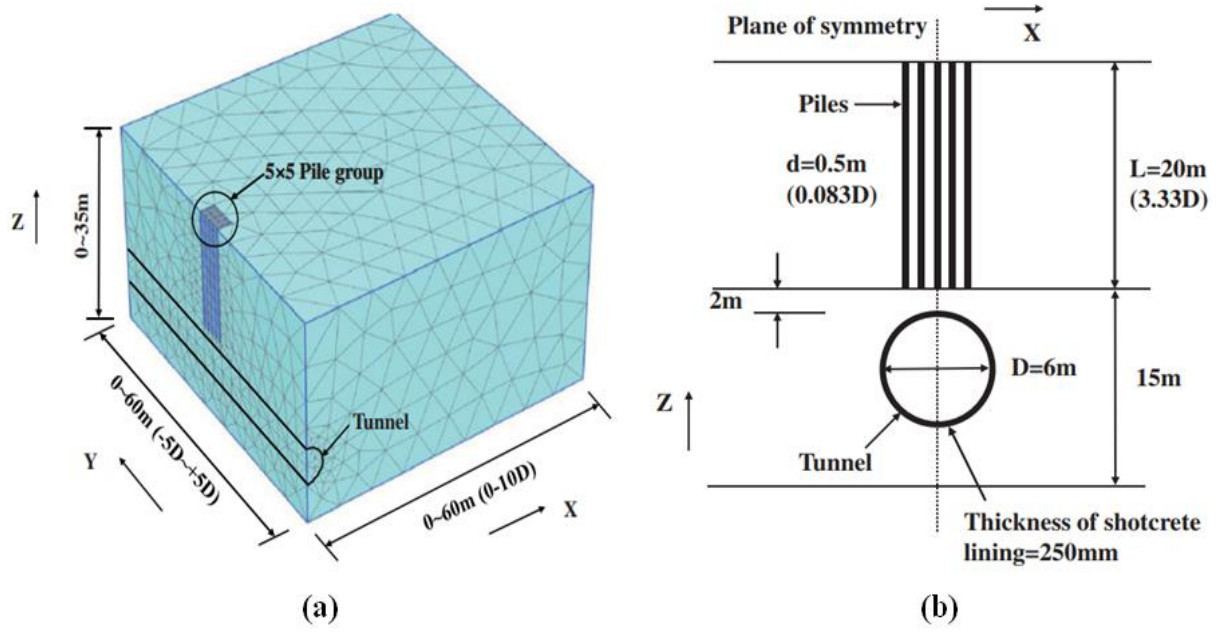

Figure 2.16 Pile group (5×5 case) (a) 3D finite element mesh (b) geometry (Lee, 2013)

2.4.5 Jongpradist et al. (2013)

Three-dimensional elasto-plastic numerical analyses are conducted by Jongpradist et al. (2013) to investigate the influences of tunnel excavation on existing loaded piles using the finite element program PLAXIS 3D in a stiff clay layer of typical Bangkok subsoil (undrained condition). A 2×2 pile group and three single piles with pile diameters of 0.25, 0.5 and 1.0 m are investigated. Different pile tip positions and clear distances from the tunnel are considered. The analysis is performed in 2 stages: application of axial load on pile head, and tunnel excavation. The tunnel construction is modelled by consecutively deactivating the soil elements, activating the concrete lining, then application of pressure on the tunnel face to stabilize the excavation face.

An influence zones are suggested based on the analysed data with consideration of various influence factors (obtained by combining those coming from consideration of the normalized pile settlement and those of the maximum pile bending moment). Jongpradist et al. (2013) suggests the critical line lies at 1D clearance from pile, because the maximum bending moment is considered when the pile tip position compared to the tunnel horizontal axis is below -1D, and because the bending moment in all cases significantly decreases when the clearance exceeds 1D. Figure 17a show that in zone I and zone II, the piles are tend to settle more than the ground due to the reduction in their base load. In zone III, no reduction of the pile base load is expected as the pile settlement is smaller than the ground surface settlement. Figure 2.17b compares the proposed influence zone in this study with those of previous studies.

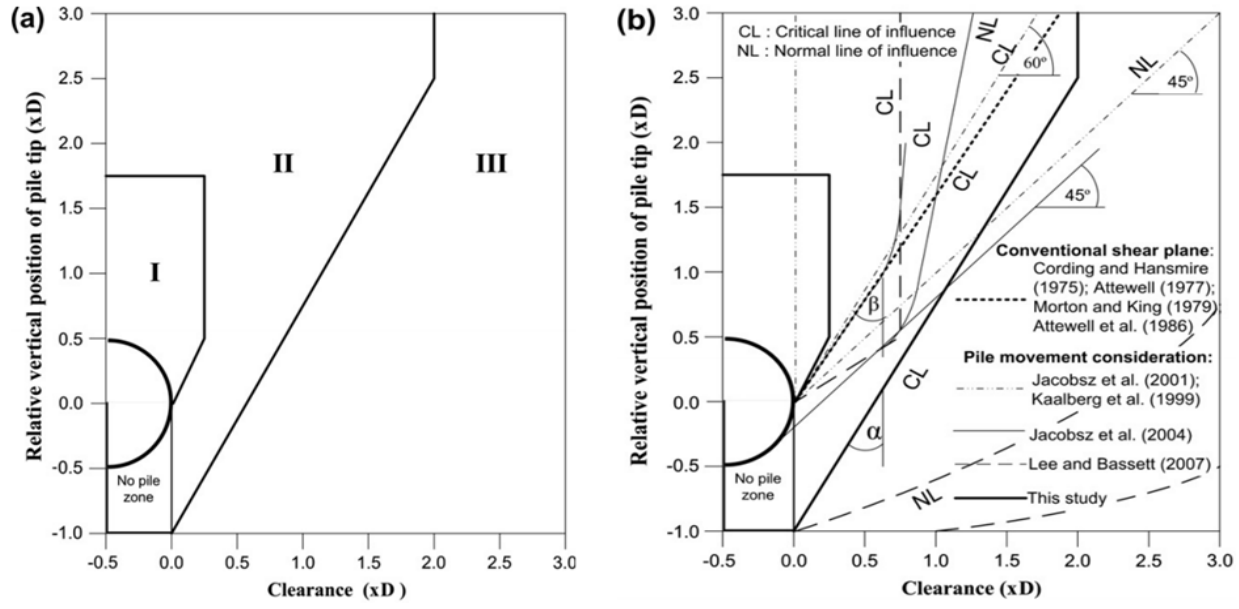

(a) **(b)**

Figure 2.17 Lines of influence suggested (a) with defined influence zones, and (b) compared with those proposed from previous studies (Jongpradist et al. 2013)

2.4.6 Soomro et al. (2015)

Three-dimensional coupled-consolidation finite element analyses are conducted by Soomro et al. (2015) to investigate the effects of open face tunnelling on wished-in-place existing 2×2 pile group using the finite element programme ABAQUS. Three distinct tunnels were excavated close to the pile group at different cover depths of 9 m (near the pile shaft), 15 m (at the toes of the piles) and 21 m (below the toes of the piles), thus the cover-to-diameter (C/D) ratios were 1.5, 2.5 and 3.5, respectively. Figure 2.18 shows both the 3D mesh and the geometry of the problem. An elasto-plastic soil model with the Drucker-Prager failure criterion with a non-associated flow rule was used to model the behaviour of stiff clay similar to London Clay. The analysis is performed in 3 stages: establish the initial stress conditions, application of the working load on pile head, tunnelling using an advancing rate of 1.5 m/day.

The computed results showed that the most critical stage for settlement, tilting and induced bending moment of pile group due to tunnelling is when the tunnel face is near to the pile group rather than at the end of tunnel excavation. Tunnel depth relative to the pile group can affect the settlement, tilting of pile group and the load transfer mechanism between piles in pile group due to tunnelling. Tunnelling near the mid-depth of the pile group (i.e. C/D= 1.5) induces the largest bending moment in the piles, but the settlement and tilting of the pile group are relatively small. Based on a settlement criterion, apparent loss of capacity of the pile group is 14% and 23% for tunnels constructed at depths of C/D= 1.5 and at both C/D= 2.5 and 3.5, respectively. The largest load redistribution between the front and rear piles in the group and the largest tilting of the pile cap towards the tunnel occurs when tunnel excavated at C/D= 2.5 (Soomro et al. 2015).

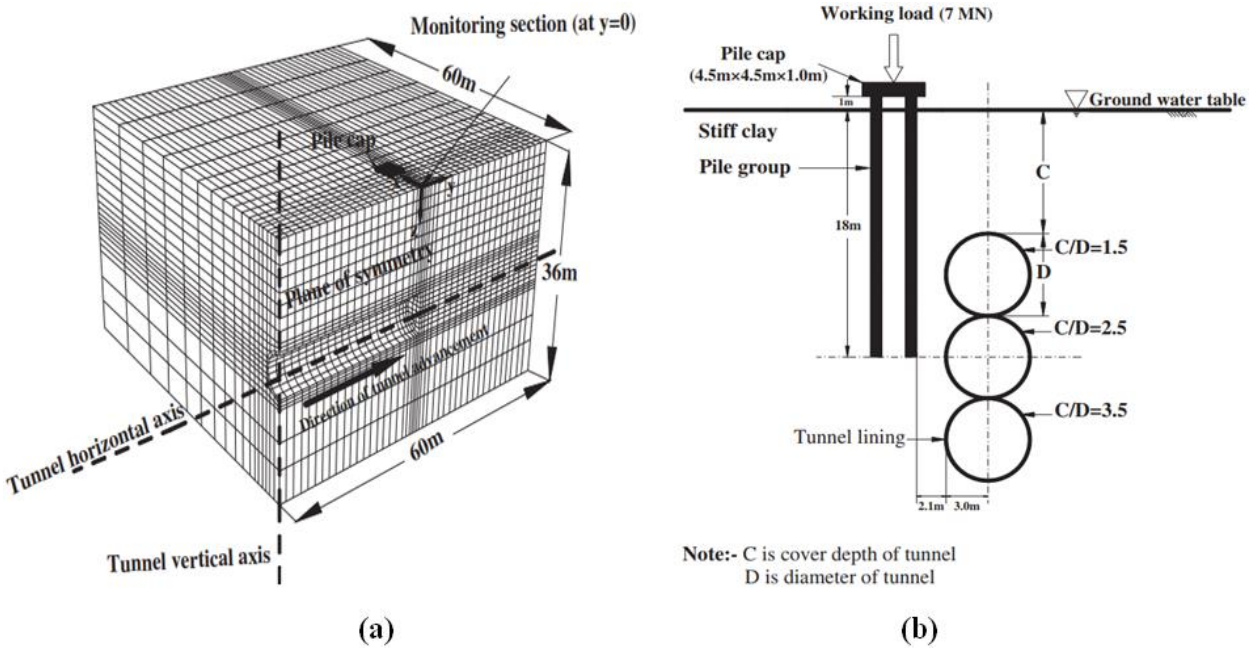

Figure 2.18 Soomro et al. (2015) study (a) 3D mesh (C/D= 2.5) (b) geometry of the problem

2.4.7 Al-Omari et al. (2019)

A three dimensional finite element analysis using PLAXIS 3D was performed by Al-Omari et al. (2019) to study the behaviour of a single pile and 3×3 piles group during the advancement of shield tunnelling (TBM) in sandy ground. The Hardening Soil (HS) model was used to simulate the soil behaviour. The numerical modelling composed of three stages: initial geostatic equilibrium, application of an axial load on the single pile head and on the pile cap for the pile group, and tunnel excavation. The results showed that the pile head settlement is higher than that for ground surface settlement and increases with tunnel advancement but becomes negligible at a distance equal to 5D beyond the pile. The maximum pile head settlement of the single pile and the centre pile of the group due to tunnelling is 1.27 and 1.42 times larger than that computed from the Greenfield condition (only tunnelling), respectively. According to the presented results, a zone of influence was deduced involves a distance of ± 2D from the pile in the longitudinal direction, a distance of ± 2D from both sides of the pile in the lateral direction, and 2D vertically below the pile tip.

2.5 Analytical and Simplified Numerical Methods

Despite the non-linear behaviour of the soil and the complex mechanisms that rule the interactions, analytical solutions have been developed for tunnel-pile interaction system.

2.5.1 Two-stage analysis method (TSAM)

Various studies for tunnel-pile interaction system have been reported using the two-stage procedure: (1) through closed-form expressions, or numerical software, the free-field soil movements due to tunnelling are estimated analytically or empirically; (2) the analysis of the full system, including soil, foundation and superstructure, external loads. The most representative embodiment of "TSAM" is the boundary element method "BEM".

2.5.1.1 Boundary Element Methods

Boundary Element Methods (BEM) are used as a benchmark to the other models with the case shown in Figure 2.19 used as the reference conditions for single and pile groups. Chen et al. (1999) presented a TSAM using the Loganathan and Poulos (1998) closed-form analytical solution to calculate the greenfield movements, these were then applied to an uncoupled BEM using the software programs. Chen et al. (1999) carried out a thorough parametric study and developed a set of design charts to estimate the maximum pile responses due to tunnelling. Corrections for soil undrained shear strength, pile diameter, and pile length were considered. The method was described by the authors as a conservative approach. Surjadinata et al. (2006) combine the use of FEM for the Greenfield movements with the above boundary element analysis (Williamson, 2014). Loganathan et al. (2001) and Xu and Poulos (2001) analysed single piles and pile groups. They used the 3D elastic BEM proposed by Xu and Poulos (2000) for pile-soil interaction with fully coupled axial, lateral and torsional behaviour of the pile and no slippage or soil plastic behaviour at the pile-soil interface.

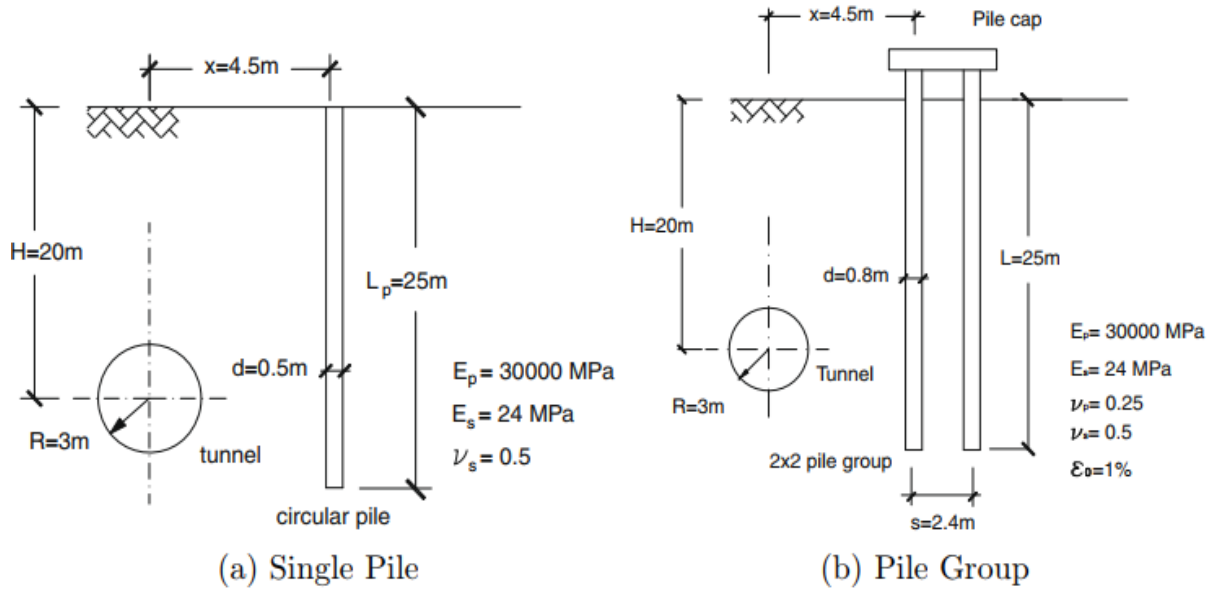

Figure 2.19 Boundary Element Method (BEM) benchmark after (Loganathan et al. 2001)

Basile (2014) extended previous works on BEMs to include the non-linear and plastic soil behaviour at the soil-pile interface. The author limited the maximum normal and tangential stress at the pile-soil interfaces (shaft and base) and implemented a soil stiffness degradation curve with the pile-soil interface stress according to a hyperbolic stress-strain law (see Figure 2.20). The comparison of this BEM model outcome with previously published results was satisfactory. It was confirmed that the group effect is beneficial because it decreases foundation displacements and internal pile forces compared to isolated piles. Furthermore, the work of Basile (2014) indicated that soil non-linearity leads to a remarkable reduction of axial forces within the piles at high volume loss (Franza, 2017).

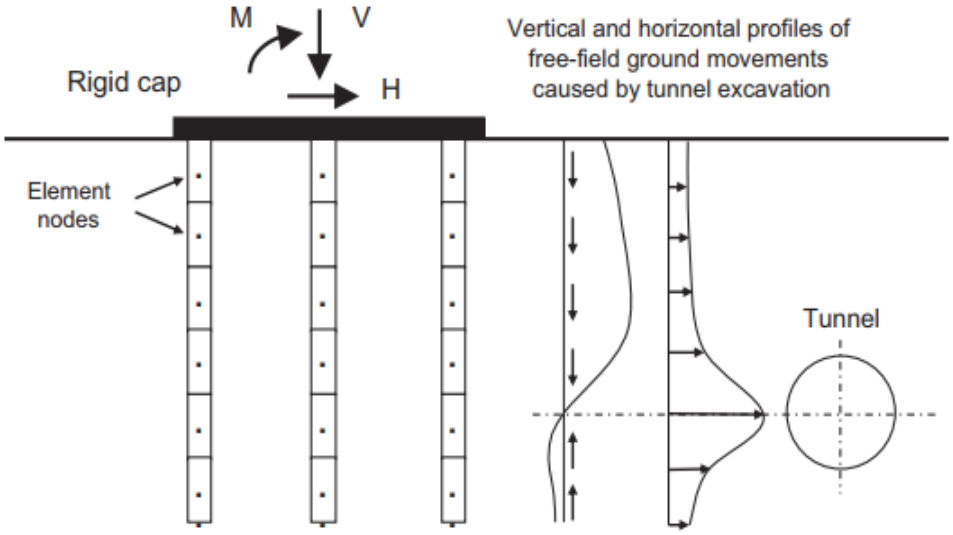

Figure 2.20 Boundary Element Method (BEM) schematisation of the problem (Basile, 2014)

2.5.1.2 Elastic Winkler Methods

Several authors considered a beam on a Winkler elastic foundation to investigate the problem of tunnel-pile group interaction, confirming the beneficial effects of pile-soil-pile interaction. Kitiyodom et al. (2005) used the FEM computer programme PRAB (Piled Raft Analysis with Batter piles) to study the considered problem, implementing as free-field input the tunnelling-induced movements predicted by Loganathan and Poulos (1998). The problem consists of a piled flexible raft and the ground modelled with a plate, elastic beams and interactive springs (see Figure 2.21). The interactions between structural members (pile-soil-pile, pile-soil-raft and raft-soil-raft interactions) were modelled based on Mindlin's solutions for both vertical and lateral forces, whereas the integral method was adopted for the definition of the springs stiffness and to consider the interaction between the nodes of the same pile.

Huang et al. (2009) proposed to solve the problem of tunnel-pile group interaction with the use of a fully elastic Winkler-based model implemented with a FDM (finite difference method) with no gap and slippage at the soil-pile interface. Firstly, the problem of tunnel-single pile interaction is solved with the theory of a beam on a Winkler elastic foundation. Secondly, the difference in displacement between the Greenfield and the single pile displacement is computed and propagated to the other piles, resulting in additional forces to the receiver pile, to account for the shielding effect within a pile group (using a logarithmic attenuation function and Mindlin's solution in vertical and horizontal solution, respectively).

Zhang et al. (2011a) and Zhang et al. (2013) improved the Winkler-based soil model to account for soil non-linearities, unloading and reloading curves, and pile-soil interface characteristics following the FDM approach used by Huang et al. (2009). When considering the response of a pile group, to account for the pile-pile interaction (numerically implemented with an iterative process), it was assumed that only the elastic contribution of the tunnel-single pile interaction propagates to other piles (with a logarithmic attenuation function), whereas the plastic behaviour is limited at the pile shaft (attenuation function is null).

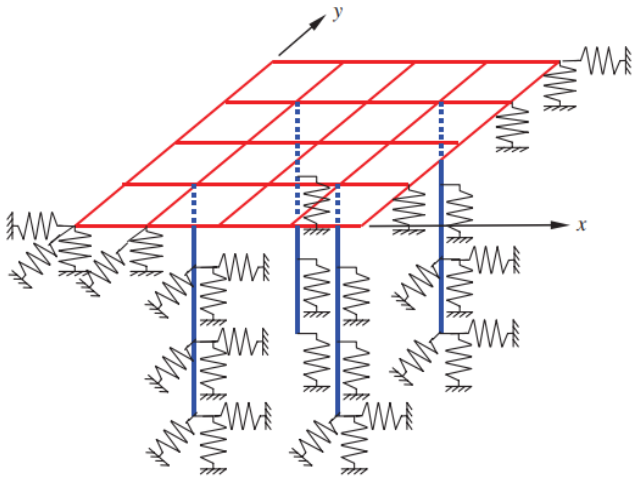

Figure 2.21 Plate-beam-spring model of a piled raft foundation (Kitiyodom et al. 2005)

2.5.2 Simplified methods used in practice

In practice, simplified tools are used to assess the effects of tunnelling on piles. Devriendt and Williamson (2011) describe the methods used in currently in practice prior to the use of 3D FEM. These are (I) Assumed Depth Method**;** this method uses Greenfield settlements at a given depth along the pile for simple first stage analysis. (II) Neutral Axis Method**,** this method adopting Greenfield settlements and an analytical solution with elastic-perfectly plastic pile-soil interface, this approach assumes that the pile head settlement is equal to the settlement at the neutral axis depth, where the shaft friction changes from negative to positive. (III) Uncoupled Boundary Element Method**,** this method uses Greenfield settlements and calculates relative displacements from either the pile toe or the pile head and inputs this into an analytical pile program based on Mattes and Poulos (1969) Boundary Element Analyses (Williamson, 2014).

2.6 Conclusion

A variety of methods for the analysis of pile-soil-tunnel interaction problems have been developed and briefly reviewed in this chapter. Researchers have investigated the effects of tunnelling on pile foundations with experiments (in the laboratory or in the field), analytical and numerical methods. In all the centrifuge and laboratory tests carried out, plane strain tunnel was simulated. Recently many works focused on the 3D tunnelling effect on pile foundation through these tests. Previously in numerical methods, 2D model is usually adopted due to the longer running time in 3D analysis, but does not adequately simulate pile-soil interaction. Recently, the three-dimensional analysis is very advantageous owing to its capability to simulate 3D tunnel advancement and pile-soil interaction.

The response of piles to tunnelling-induced movements is generally very sensitive to the relative pile toe-tunnel location, location of pile axis from the tunnel vertical axis (or the clear distance), piles installation method, safety factor, the induced tunnelling volume loss, the ground conditions and the load distribution between base and shaft. Several zones of influence, where large pile settlement may occur, were proposed. Due to group positive effect, several authors proposed to conservatively estimate pile group performance with and without the pile cap considering the tunnel-single pile interaction.

Finally, the combination of previous works on tunnel-pile interaction (TPI) and tunnel-structure interaction (TSI) is necessary to achieve a better representation of the global tunnel-pile-structure interaction (TPSI). In general, tunnelling adjacent to piles (near the pile shaft) induced minimal building distortions as mainly causes lateral bending in piles rather than settlements. Whereas, tunnelling beneath piles (at or below the toes of the piles) induces more settlement, which leads to structural failure. Thus, pile settlements represent the major concern for tunnelling considering the way in which they affect buildings. However, these studies shown that pile failure are not a primary concern in clays and should be better investigated in sands to consider the pile safety factor.

CHAPTER 3

Deep Excavation-Induced Ground Movements

CHAPTER 3

Deep Excavation-Induced Ground Movements

3.1 Introduction

In many cities in densely populated areas around the world, the application of deep excavations for the realisation of underground spaces or for other infrastructure is becoming common practice. Supporting excavations using the retaining structures is a matter of extreme importance to construction safety officials due to the danger posed to life by the ground movements induced by deep excavations. In the field of geotechnical, any excavation induces changes in the stresses in the soil mass. Also, regardless of the construction technique used, deformations occur around the excavation which will propagate into the surrounding massif and can reach the surface. Depending on their nature, their amplitudes, their distribution in space and time, the deformations thus generated are likely to cause disorders in the built environment: buildings, structures, roads, and other underground structures. Several researchers developed to asses ground movement induced by an adjacent excavation. The well-known methods are presented in this chapter.

3.2 Ground movements induced by excavation

The excavation imposes displacements and stress on its surroundings. In general, the excavation construction induces three types of ground movements as shown in Figure 3.1:

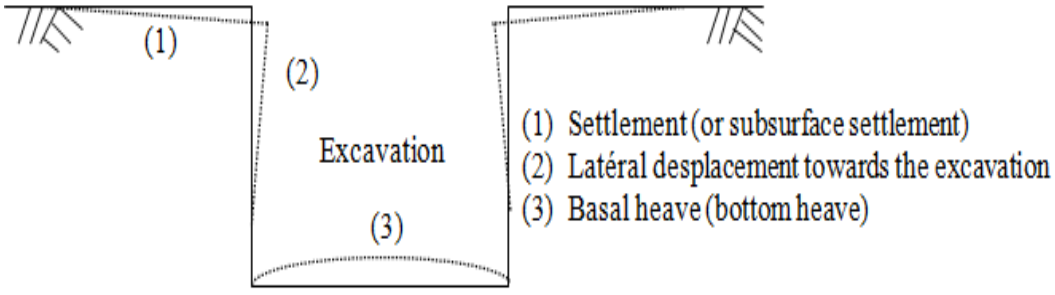

Figure 3.1 Ground movements induced by excavation

3.2.1 Settlement induced by excavation

3.2.1.1 Settlement induced by the construction of diaphragm walls

According to the monitoring results of the rapid transit system in Hong Kong (Cowland and Thorley, 1985), after the completion of the diaphragm walls and before the main excavation, the accumulated deformation can achieve 40-50% of the total deformation after the completion of the main excavation.

Clough and O'Rourke (1990) found that the ratio of the maximum settlement induced by the construction of diaphragm walls to the depth of the trench is 0.15%, according to many in situ monitoring results (see Figure 3.2). We can see that soil settlement in the vicinity of diaphragm wall panels, induced by their construction, is significant and that caution is strictly required to protect adjacent properties (Ou, 2006).

Ou and Yang (2000) studied the monitoring results of the settlement induced by the construction of the diaphragm walls for the excavations in the Taipei Rapid Transit System and found that, under normal construction conditions, the maximum settlement induced by a single panel was about 0.05 H_t% (H_t is the depth of a trench) and the maximum settlement mostly occurred within $0.3H_t$ from the trench panel, as shown in Figure 3.3. The main influence range of settlement was $0.5H_t$ from the trench panel and little settlement occurred beyond $1.0H_t$ from the trench panel. The concrete casting did not cause significant settlement. In sand-clay alternated layers, the maximum settlement induced by a single trench panel is 10-15 mm, in Singapore marine clay, 24 mm (Poh and Wong, 1998).

Ou and Yang (2000) also found that the maximum accumulated settlement after the completion of several test panels was 0.07 H_t% (Figure 3.3) and its location and influence range were basically similar to those of single-panel induced settlement. The maximum amount of accumulated settlement after the completion of the whole diaphragm wall was greater than that induced by a single test panel as well as that by multiple test panels. The maximum amount of total settlement was about $0.13H_t$%, occurring within a distance of $0.3H_t$ from the diaphragm wall. The above maximum amount of total settlement was less than that of Clough and O'Rourke's (1990) envelope ($0.15H_t$%). Settlement became less observable beyond the distance of 1.5-$2H_t$ from the diaphragm wall (Ou, 2006).

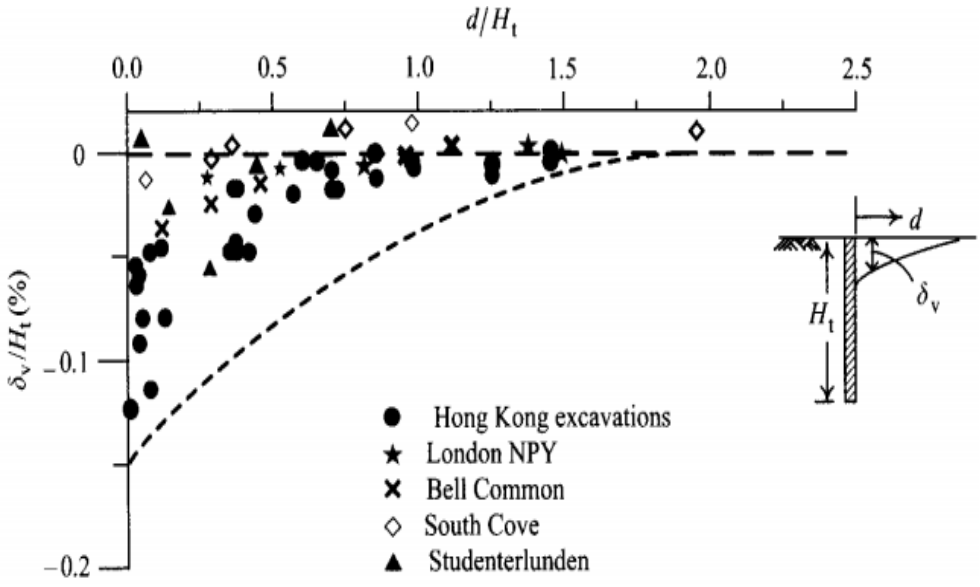

Figure 3.2 Envelope of ground surface settlements induced by trench excavations (Clough and O'Rourke, 1990)

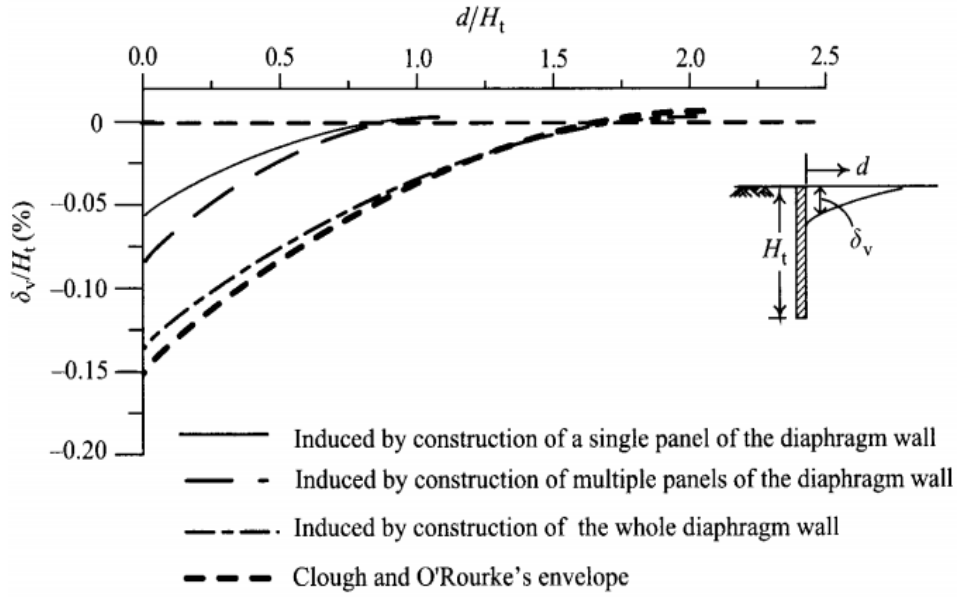

Figure 3.3 Envelopes of ground surface settlement induced by the diaphragm wall construction (Ou and Yang, 2000)

3.2.1.2 Empirical methods to predict ground surface settlements

Several methods exist to determine the ground surface settlement due to excavation. In this section empirical formulas are introduced and the most well-known methods are:

Peck's method

Peck (1969) was the first to propose a method to predict excavation-induced ground surface settlement, based on field observations. He mainly employed the monitoring results of case histories in Chicago and Oslo and established the relation curves between the ground surface settlement (δ_v) and the distance from the wall (d) for different types of soil, as shown in Figure 3.4 (Ou, 2006). The method classifies soil into three types according to the characteristics of soil:

Type I: Sand and soft to stiff clay, average workmanship

Type II: very soft to soft clay

1- Limited depth of clay below the excavation bottom

2- Significant depth of clay below the excavation bottom but $N < N_c$

Type III: very soft to soft clay to a significant depth below the excavation bottom ($N \geq N_c$).

Where N, the stability number of soil, is defined as $\gamma H_e/C_u$, where γ is the unit weight of the soil, H_e is the excavation depth, and C_u is the undrained shear strength of soil, and N_c is the critical stability number against basal heave.

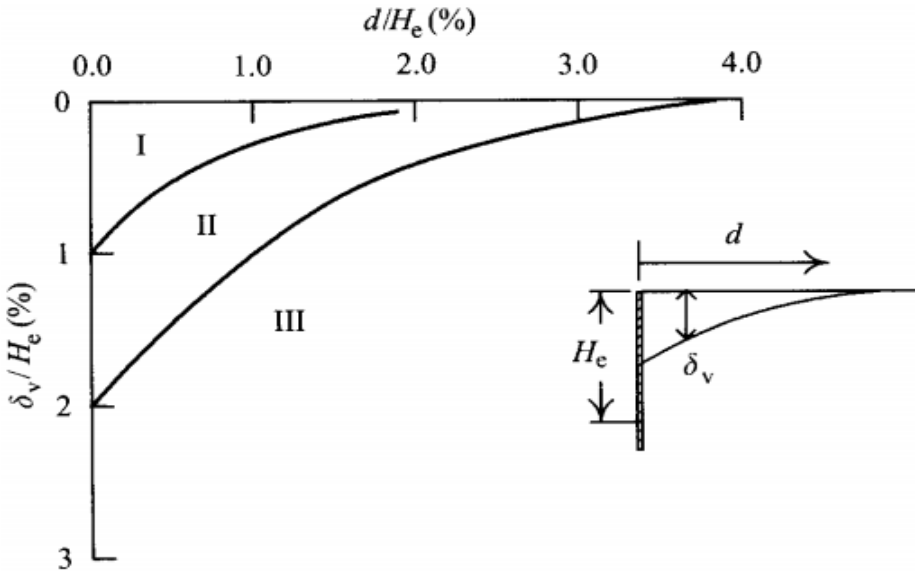

Figure 3.4 Peck's method (1969) for estimating ground surface settlement

In general, larger wall deflection and ground deformations are induced due to excavations in soils with lower strength and stiffness. The relation curves proposed by Peck are not necessarily applicable to all excavations especially in recent years (Since Peck's method took the monitoring results of case histories before 1969). But Peck's method still used by some engineers as it is simple to apply and it's the first to derive an empirical formula to predict the ground surface settlement induced by excavation.

Bowles's method

Bowles (1988) proposed a procedure to estimate excavation-induced ground surface settlements, which can be described as follows (Figure 3.5):

1- Compute the lateral displacement of the wall.

2- Compute the area of the lateral wall deflection (a_d).

3- Estimate the influence range of ground settlement (D) following Capse's method (1966):

$$D = (H_e + H_d)\tan\left(45° - \frac{\varphi}{2}\right) \quad (3.1)$$

Where H_e= the excavation depth; $H_d = B$ if $\varphi = 0°$ and $H_d = 0.5B\tan\left(45° + \frac{\varphi}{2}\right)$ if $\varphi \geq 0°$, where B= the excavation width and φ the parameter if soil strength

4- Suppose the maximum ground surface settlement is located at the intersection of the wall and ground surface. Estimate the maximum ground surface settlement (δ_{vm})

$$\delta_{vm} = \frac{4a_d}{D} \quad (3.2)$$

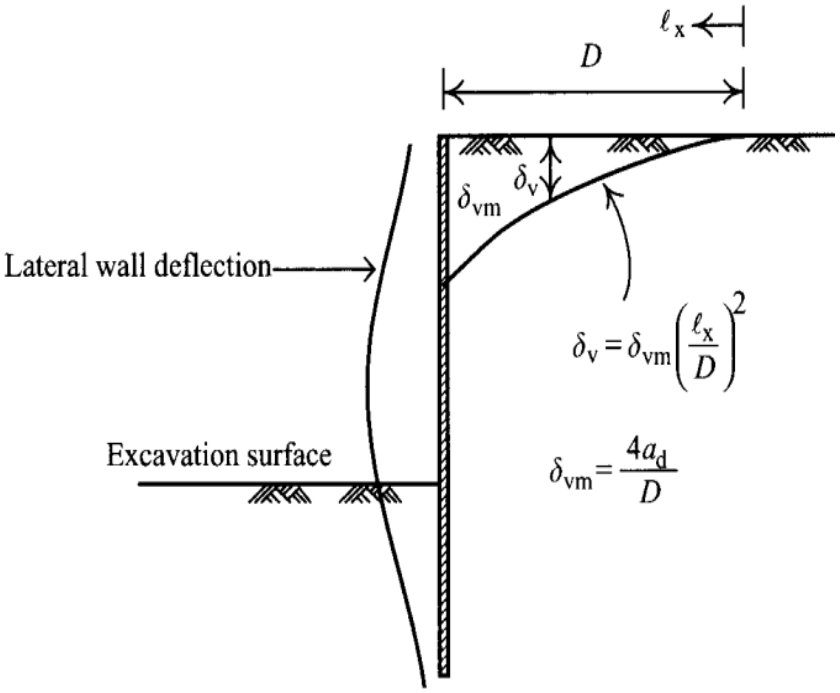

Figure 3.5 Bowles's method (1988) for estimating ground surface settlement

5- Suppose the ground surface settlement exhibits parabolic distribution. The settlement δ_v at l_x can be computed as follows:

$$\delta_v = \delta_{vm}\left(\frac{l_x}{D}\right)^2 \tag{3.3}$$

Where l_x= distance from a point at the distance of D from the wall and δ_v= the settlement at the distance of l_x.

The method suggested by Bowles is clearly only applicable for the spandrel type of ground surface settlement.

Clough and O'Rourke's method

Clough and O'Rourke (1990) proposed various types of envelopes of excavation-induced ground surface settlements for different soils on the basis of case studies. According to their studies, excavation in sand or stiff clay will tend to produce triangular ground surface settlement. For the final excavation depth H_e, the maximum settlement will be found near the retaining wall as shown in Figures 3.6a and 3.6b, whose influence ranges are separately $2H_e$ and $3H_e$. Excavation in soft to medium clay will produce a trapezoidal envelope of ground surface settlement, as shown in Figure 3.6c. The maximum ground surface settlement occurs in the range of $0 < d/H_e < 0.75$ while $0.75 < d/H_e < 2.0$ is the transition zone where settlement decreases from the largest to almost none (Ou, 2006).

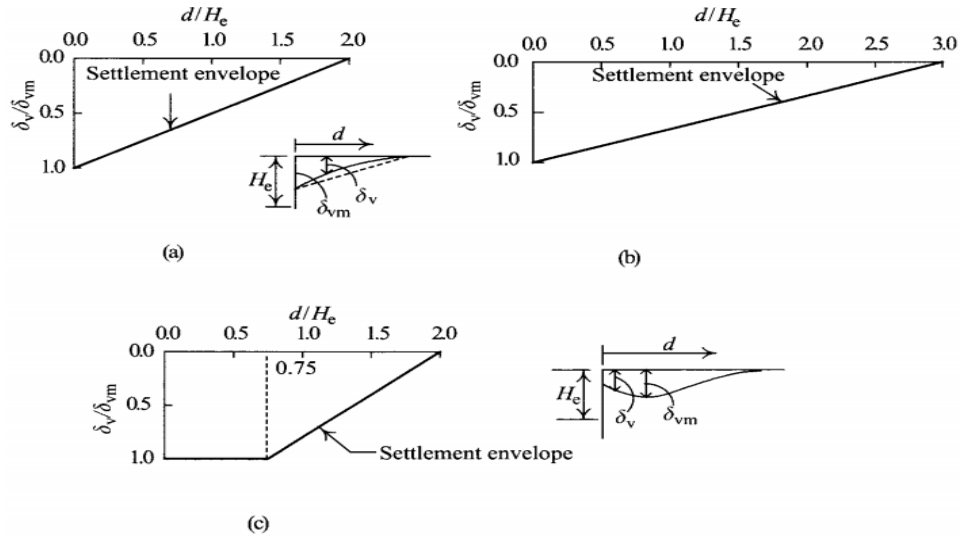

Figure 3.6 Clough and O'Rourke's (1990) method for estimating ground surface settlement (a) sand (b) stiff to very stiff clay, and (c) soft to medium soft clay

Ou and Hsieh's method

Ou and Hsieh (2000), Ou et al. (2005) developed a method to predict the ground surface settlement on the basis of studies of the type of ground surface settlement, the influence zone, the location of the maximum settlement, and the maximum settlement. They proposed settlement curves for the spandrel and the concave types, as shown in Figure 3.7.

Line segment **ab** in Figure 3.7a, with a steeper slope, represents the primary influence zone, which will generate a larger angular distortion as far as the adjacent structures are concerned. Thus, it is necessary to examine the safety of the adjacent structures as long as values of δ_{vm} is large. Line segment **bc** represents the secondary influence zone and has a less steep slope. Under normal conditions, settlement in the **SIZ** has less influence on structures. The maximum settlement is located at the wall when the wall deforms as a cantilever.

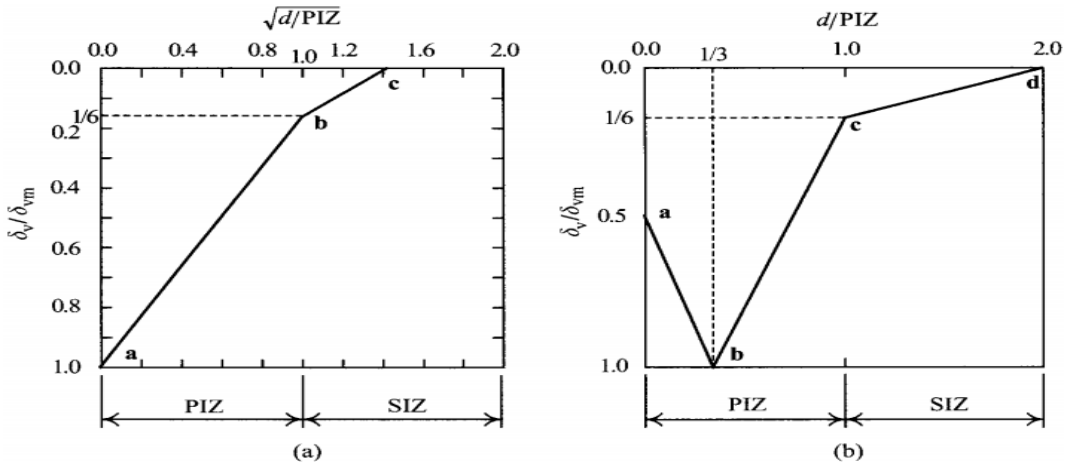

Figure 3.7 Ou and Hsieh's method for estimating ground surface settlement

According to Figure 3.7b, the concave settlement profile for the bulging mode of wall can be described in three line segments. Line segment **abc** represents the primary influence zone and line segment **cd** the secondary influence zone. Their separate influences on structures are the same as described in the spandrel type (Ou, 2006). According to Ou and Hsieh's method, the excavation-induced ground surface settlement in back of the wall can be predicted based on the following procedure:

1- Estimate the maximum lateral displacement of the wall (δ_{hm}): include the simplified method (Figure 3.11), the finite element method, or the beam on elastic foundation method.

2- Determine the type of ground surface settlement: Compute the lateral wall displacement from either the finite element method or the beam on elastic foundation method.

3- Estimate the value of δ_{vm} on the basis of the relations between the maximum settlement (δ_{vm}) and the maximum lateral displacement (δ_{hm}).

4- According to the type of ground surface settlement determined at the second step, compute various settlements occurring in different positions in back of the wall.

3.2.2 Horizontal movements around an excavation

Crofts et al. (1978) proposed to estimate the distribution of horizontal displacements at the soil surface, related to the distance from the edge of the excavation, by means of a diagram similar to that of Peck for the vertical movements (Figure 3.8). However, the curves in this diagram are based on a limited number of in situ data and only provide upper limits of foreseeable movements on a precise site, depending on the soils nature. Indeed, faster declines have been observed as the distance from the edge of the excavation increases (Symons, 1980).

The maximum lateral displacement occurs at a depth which increases with the height of the excavation and is located, with the exception of the first phase of excavation, near the bottom of the excavation. The experimental observations made it possible to specify the variations of the maximum lateral displacement δ_{hm} depending on the maximum excavation depth H_e and wall type:

- For strutted walls, in cohesionless soils, the maximum lateral displacement was about $0.002H_e$ when the support is put in place quickly (Clough and O'Rourke, 1990). In soft clays, the measurements indicate that δ_{hm} can reach $0.01H_e$ to $0.02H_e$. On the other hand, for stiff clays, δ_{hm} was small than $0.002H_e$, and often than $0.001H_e$.

- For diaphragm walls, the maximum lateral displacement observed varies between $0.002H_e$ and $0.005H_e$ (Ou et al. 1993).

- For well-made anchored walls, the maximum lateral displacement is less than $0.002H_e$;

- For sheet pile or Berlin walls, maximum lateral displacement is $\delta_{hm} < 0.01H_e$ (Peck, 1969).

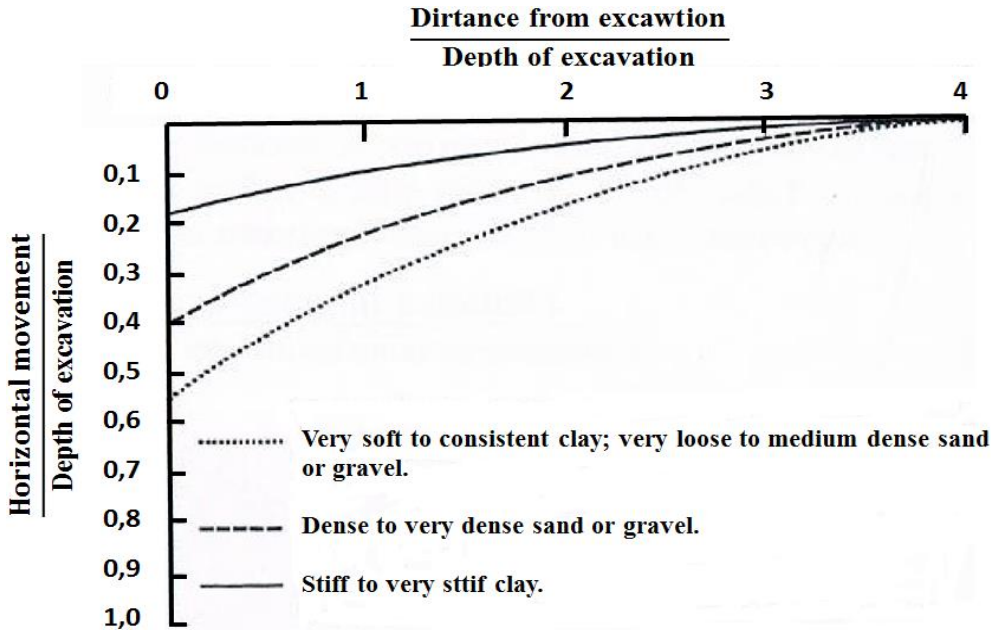

Figure 3.8 Horizontal movements related to distance from excavation (Crofts et al. 1978)

Diaphragm walls generally tend to cause less ground movement than sheet piles or Berlin walls. It should also be noted that, in most cases, the lateral movement increases if the time between excavation and installation of the support increases (Mestat et al. 1999).

3.2.3 Basal heave (bottom movement)

In coherent soils, it is common for the excavation bottom to heave. The magnitude of this movement and the speed at which it occurs depend on the reduction in vertical stresses and the soil nature under the excavation. It can result from three very different phenomena:

• Either elastic unloading of clay over a large thickness;

• Swelling of the clay in the presence of water;

• The phenomenon called “solid renard”. A vertical flow of the soil then occurs, behind the wall towards the bottom of the excavation, which causes the bottom to heave.

3.2.3.1 Factor of safety against basal heave

Clearly the deformation of a retaining wall relates closely to the factor of safety. If the factor of safety is small, weaker the stability of the excavation (strains around the excavation and ground deformations may become large). This possibility of heaves limits the maximum depth that the excavation can reach, regardless of the support system (struts or anchors). If the maximum depth is exceeded, the excavation bottom fails. This fails can be studied as a problem of load-bearing capacity. As in the study of shallow foundations, various plane strain failure mechanisms can be considered as shown in Figure 3.9a. Each mechanism leads to an expression of the maximum excavation depth as given in Table 3.1.

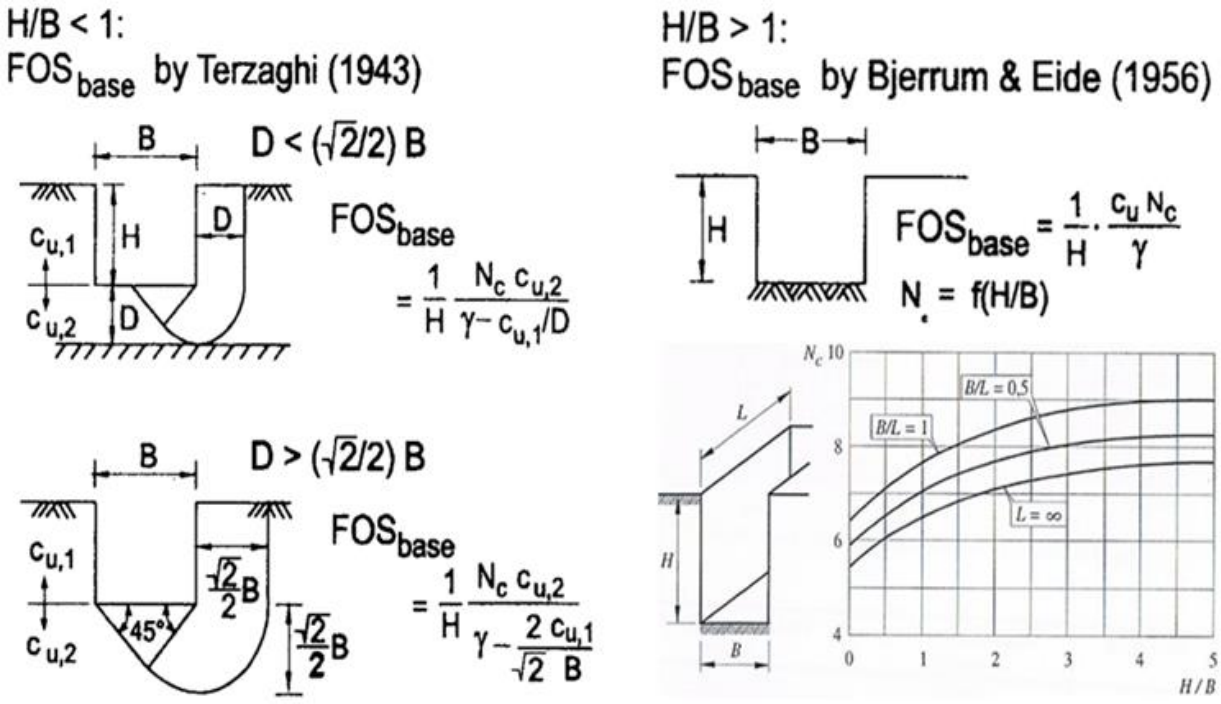

(a) **(b)**

Figure 3.9 Factor of safety against basal heave after (a) Terzaghi (1943), (b) Bjerrum and Eide (1956)

Obviously, these formulas are no longer valid when overloads are applied on the surface, when the soil mass is heterogeneous or when the hypothesis of plane strains is no longer justified. Adaptations have been proposed in the case of three-dimensional excavations (Mestat et al. 1999):

1- The charts of Bjerrum and Eide (1956) shown in Figure 3.9b, which provide values of the stability number $N = \frac{\gamma H}{c_u}$ related to the width B, the length L and the depth H of the excavation. The substratum is supposed to be endless.

2- The formulas of Tschebotarioff (1973), which make it possible to take into account the influence of the indeformable substratum, located at a distance D. The maximum depth of the excavation is then given by the relationships:

- If $L < D$, $H_{max} = \frac{5.14 c_u \left(1+0.44\frac{D}{L}\right)}{\gamma - c_u\left(\frac{1}{D}+\frac{2}{L}\right)}$ (3.4)

- If $L > D$, $H_{max} = \frac{5.14 c_u \left(1+0.44\frac{2D-L}{L}\right)}{\gamma - c_u\left(\frac{1}{D}+\frac{4D-2L}{DL}\right)}$ (3.5)

Table 3.1 Maximum excavation depth without heave risk (Mestat et al. 1999)

Failure mechanisms type	Maximum excavation depth H_{max}
Caquot-Kérisel failure mechanism for deep excavation	$\frac{5.14c_uB}{\gamma B - c_u}$
Terzaghi failure mechanism for narrow excavation	$\frac{5.71c_uB}{\gamma B - c_u\sqrt{2}}$
Terzaghi failure mechanism for large excavation	$\frac{5.71c_uD}{\gamma D - c_u}$
Bjerrum and Eide failure mechanism for H/B>1	See charts (Figure 3.9b)

Mana & Clough (1981) utilized the finite element and the field measurements to relate the maximum wall movements with the factor of safety against basal heave in clays as shown in Figure 3.10. The quasi-constant non-dimensional movement are at high safety factor is an indication of an elastic response. The rapid increase in movements at lower factor of safety is a result of the induced plastic deformations (Ahmed S.M, 2014). The factor of safety against basal failure also affects the shape of the settlement trough associated with deep excavation. Mana & Clough (1981) found by numerical analyses that the width of the settlement trough increases with the increase of the factor of safety.

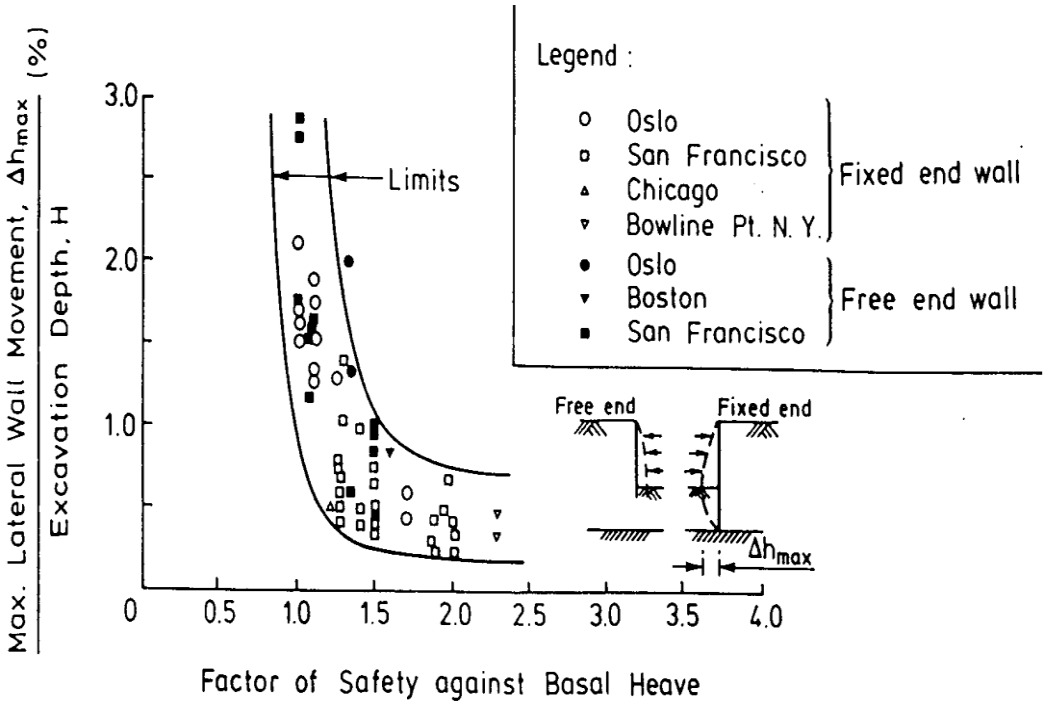

Figure 3.10 Effect of the basal heave stability on the wall deformations induced by deep excavations in clays (Mana & Clough, 1981)

Clough et al. (1989) and Clough & O'Rourke (1990) summarized many excavation case histories and utilized the nonlinear finite elements and field measurements to determine the effect of the wall stiffness on the maximum lateral wall movement in clays that is induced by excavation. They introduced a system stiffness factor for estimating wall stiffness of unit thickness (plane strain) which depends on wall material, section properties and support spacing and the results of their analyses are shown in Figure 3.11. The figure shows that when the factor of safety against basal heave is small, larger deformation of the retaining wall induced, also that the stiffness factors for sheet-pile walls are less than 40 and greater than 300 for diaphragm walls.

Clough at al. (1989) and Clough & O'Rourke (1990) concluded that the wall stiffness is less effective in reducing movements than in cases with high factor of safety against basal instability. However, in case of having low factor of safety against basal heave, the wall stiffness affects the deformation greatly. The aforementioned studies suggest that the maximum lateral wall movement for stiff systems in stable soils is limited to approximately 0.2% of the excavation depth regardless of the system stiffness (Ahmed S.M, 2014).

Zapata-Medina (2007) proposed a revised system stiffness factor which gives more reliable results with the data using the data of 30 case histories that comprise soft, medium and stiff clays. Figure 3.12 shows the favourable correlation between the maximum lateral deformation, the factor of safety against basal heave and revised system stiffness. The factor of safety could reach as low values as 0.65 in the analyses without having a failure of the excavation; instead, large ground deformations were observed (Ahmed S.M, 2014).

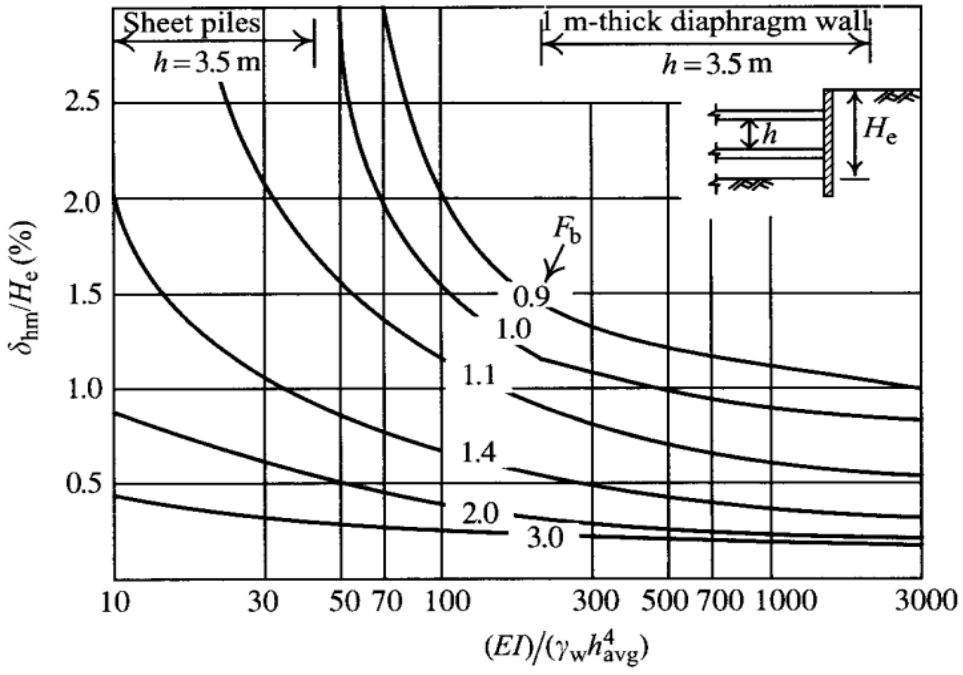

Figure 3.11 Effect of the basal heave stability and the system stiffness on the wall deformations induced by deep excavations in clays (Clough at al. 1989)

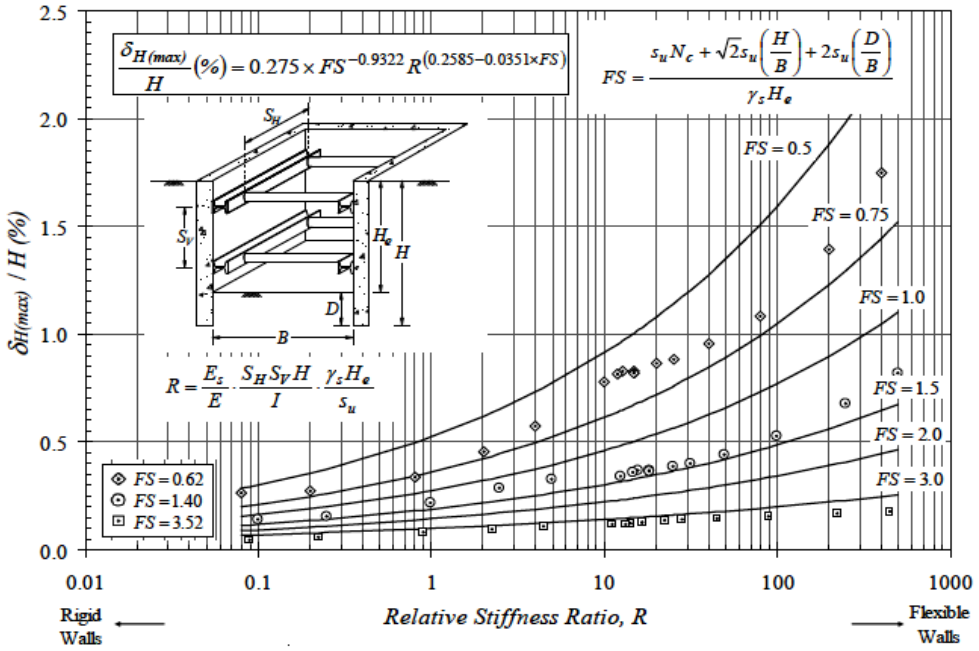

Figure 3.12 Normalized lateral wall movements Vs. relative stiffness ratio (R) for deep excavations in cohesive soils (Zapata-Medina, 2007)

3.3 Conclusion

With the increasing demands for deep excavation in urban areas, it becomes increasingly important to have well-designed support systems for deep excavations that do not only ensure the stability of the excavation itself but also warrant that the excavation will not cause damage to the adjacent buildings and utilities due to potentially excessive ground deformations.

This chapter introduces the types of ground movements induced by excavation such as: the ground surface settlement, the ground lateral movement, and the excavation bottom movement. However, the optimal design for a supporting system for deep excavations includes assessment of the induced ground deformations using empirical/semi-empirical approaches (most of which are empirical formulas or diagrams based on the monitoring results of excavations), analytical methods, and numerical methods.

Numerous empirical methods were envisaged to estimate the ground deformations associated with deep excavations based on the worldwide and local databases of the monitoring observations in deep excavation projects. Generally, empirical/semi-empirical methods focus on the assessment of the maximum settlements behind the wall, maximum lateral deformations of the walls, the widths of the settlement troughs, distributions of settlements and lateral deformations behind the walls. Numerical analysis is suitable method and widely used recently for soil-structure interaction problems that to be undertaken by a geotechnical engineer especially deep excavation problems (the different aspects of the problem can be incorporated into the numerical models).

CHAPTER 4

Excavation-Soil-Pile Interactions

CHAPTER 4

Excavation-Soil-Pile Interactions

4.1 Introduction

In dense urban environments where land is scarce and buildings are very close to one another, excavations projects are widely used for basement construction and development of underground transit facilities. As these excavations are usually carried out close to existing buildings, one of the main design constraints in these projects is to prevent or minimize damage to adjacent buildings and underground utilities. Many buildings and infrastructures are supported by pile foundations to transfer the structural loads to the lower and more competent subsurface strata. However, when the excavations carried out, the ground inevitably moves towards the excavation and causes ground deformations. The main concern is these ground movements resulting from the soil excavation can damage the piles, so cause damage to the building rested on. Thus, the precise prediction of the effects of excavation works on existing piles is a major challenge when designing and practicing in urban geotechnical environments.

Several researches developed to assess the behavior of piles near to deep excavations. In this chapter, an overview of the main studies that address the problem of the effects of deep excavation on piles and piled structures in different types of soils, where, pile responses in both soft soils and stiff soils will be discussed. The review is presented through three main sections; namely (1) Field observations and Analytical methods, (2) Centrifuge and Laboratory Studies, and (3) Numerical Methods.

4.2 Field observations and Analytical methods

Recently, studies address the excavations effect on piles using field data and analytical methods have been reported. Some of these studies will be reviewed briefly in this section.

Finno et al. (1991) gives an interesting example of this class of problem. He reports on the performance of groups of step-tapered piles located adjacent to a 17.7 m deep tieback excavation. The excavation was performed through primarily granular soils (hydraulic fill, alluvial sand) within the footprint of an existing framed structure. The main columns were supported by groups of 21 m long unreinforced or lightly reinforced concrete piles. The temporary tieback sheet-pile wall was located as close as 0.60 m to the pile caps. Field observations, including lateral deformations of the sheet pile wall and lateral and vertical deformations of the main columns, found that several of the pile caps displaced up to 6.4 cm laterally towards the excavation (Figure 4.1). Poulos and Chen (1997) report reasonable comparisons between these measurements and the computed behaviour from a detailed analysis. Design charts were used to estimate the maximum pile deflection and bending moment.

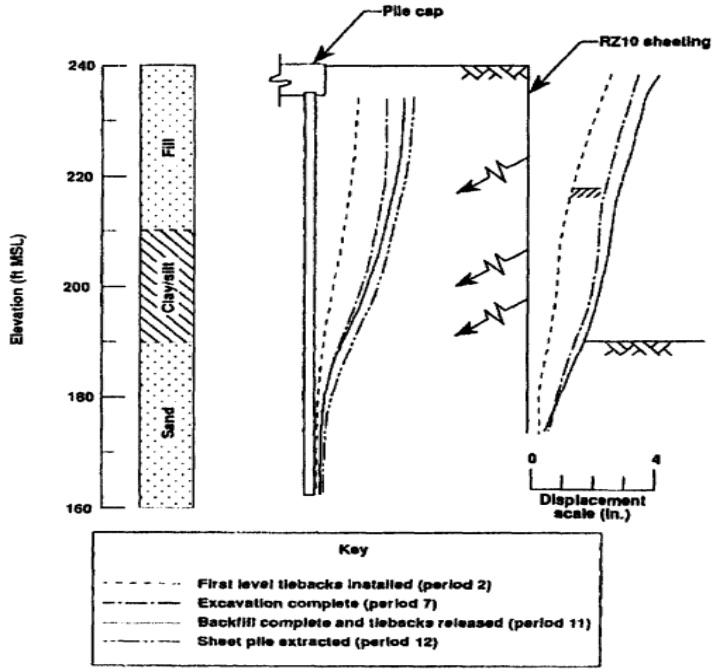

Figure 4.1 Computed sheet-pile and pile movements after Finno et al. (1991)

Poulos and Chen (1996, 1997) described a two-stage analysis to study pile responses due to excavation induced lateral soil movement, focusing on unsupported and braced excavation in clay as shown in Figure 4.2. The TSAM involving (1) determination the green field soil displacements with finite element analysis the computer program AVPULL (2) the soil movement was then used as input to the boundary element program PALLAS to determine the pile responses. A parametric study was conducted in both investigations varying the main parameters like pile location, undrained shear strength, wall stiffness, pile diameter, strut stiffness, strut spacing (the two later are for braces case).

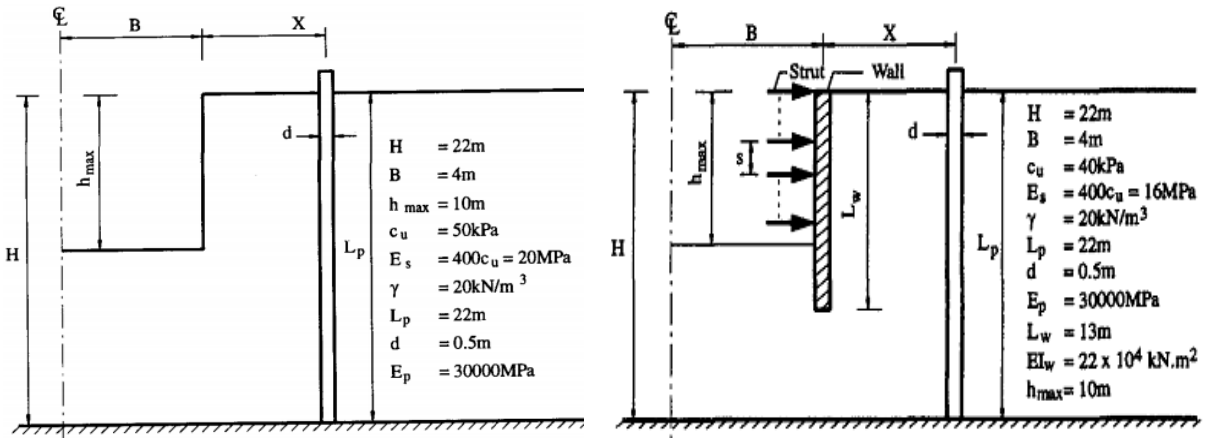

(a) **(b)**

Figure 4.2 Basic problem (a) unsupported system (b) strutting system after Poulos and Chen (1996, 1997)

In general, for both studies, they conclude that pile response increases with increasing stability number $N = \gamma H/c_u$, due to larger lateral soil movements. Pile bending moment increases with increasing pile diameter, and pile deflection decreases when pile diameter increases. It was found that pile responses decreases when distances from the excavation face increases. In braced case, they found that pile response decreases with stiffer excavation support conditions, higher struts stiffness and smaller strut spacing because such support conditions result in smaller soil movements. Based on the parametric, Poulos and Chen (1996, 1997) developed a series of design charts and equations for predicting the maximum deflection and bending moment of a single pile due to excavation-induced lateral soil movements. The predicted maximum pile bending moment and deflection showed fair agreement with existing measured field data.

The boundary element method has a major limitation that it can be only performed on a single pile and a group with non-identical free-head piles, but cannot handle capped pile groups. Poulos and Chen (1996) have examined the effects of the pile head condition on the pile response, and have found that it may have a very substantial effect. The greater the degree of restraint, the greater arc the bending moments induced in the pile.

Goh et al. (2003) describe an actual full-scale instrumented field test. The field test was performed on a free-head drilled shaft with a diameter of 1.0 m and a total embedment length of 46 m. The lateral soil movements at 3 m distance to the diaphragm wall was measured by in-soil inclinometer at stage A and stage B, respectively. This study was carried to examine the behaviour of the existing pile due to nearby excavation activities resulting from the construction of a 16 m deep cut-and-cover tunnel. The pile was located 3 m behind a 0.8 m thick diaphragm wall. The excavation is supported by struts spaced at 3 m vertically and 9 m horizontally (see Figure 4.3).

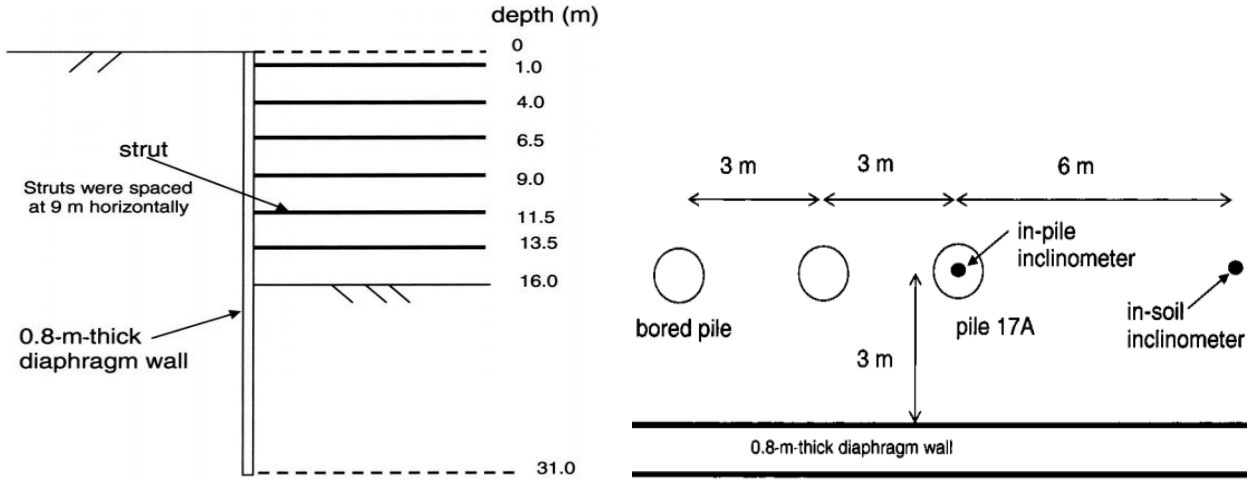

Figure 4.3 (a) Cross section of excavation (b) positions of piles and inclinometers (Goh et al. 2003)

Excavation to the formation level that was 16 m below the ground surface resulted in a maximum lateral pile movement of 28 mm. A simplified numerical procedure based on the finite-element method (BCPILE) was used to analyse the pile response. Generally, the theoretical predictions were in reasonable agreement with the measured results.

Zhang et al. (2011b) developed a similar two-stage approach, in which the deflection of the retaining wall is determined by a beam on elastic spring method and the soil movement behind the wall by the source-sink method defined by Sagaseta (1987). Zhang then uses hyperbolic description of the friction behaviour between pile and soil, with unloading hysteresis to describe the soil-pile interaction. This requires the pile to be divided in segments and a solution with boundary conditions and linearization of the equations, while taking into account the existence of a working load on the pile. Zhang confirmed his work by comparing his results with solutions from BEM from Chen et al. (1999) and centrifuge test data from Loganathan et al. (2000) with satisfying results.

Korff (2012) established an analytical method and tested for the behaviour of piled buildings near excavations. Korff (2012) explores the building displacements related to deep excavations for a case study from the Netherlands: the construction of the North South Metro Line in Amsterdam. Figure 4.4 shows a cross section of Ceintuurbaan station, soil profile & extensometer locations. This method includes the reduction of pile capacity due to lower stress levels, settlement due to soil deformations below the base of the pile and development of negative (or positive) skin friction due to relative movements of the soil and the pile shaft.

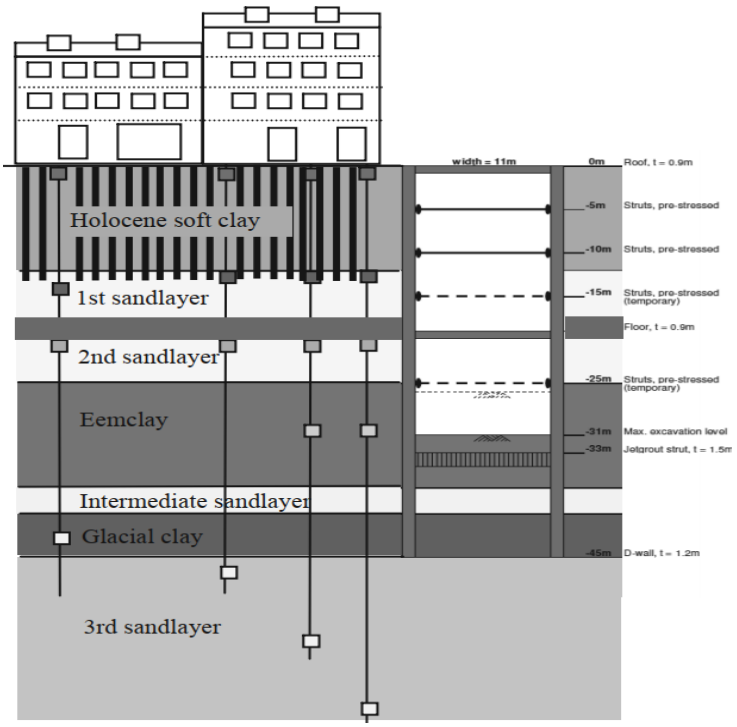

Figure 4.4 Cross section of Ceintuurbaan station, soil profile & extensometer locations (Korff, 2012)

Liang et al. (2013) investigate the response of an axially loaded pile group (with free heads or a pinned pile cap) subjected to lateral soil movement. They solved the equations of axially loaded piles subjected to lateral soil movement based on the flexural differential equations of elastic piles and the Winkler's spring model of pile-soil interaction. In the derivation, the flexural differential equations were established using a two-stage method and solved by the finite difference method. The behaviour of the pile group was evaluated by adding the deflections and bending moments of single piles and considering the shielding effect of the front piles on the rear piles. The shielding effect between piles was considered using Mindlin's solution. A parametric study was conducted to investigate the influence of pile spacing, piles number, location and magnitude of the axial load.

Korff et al. (2016) established an analytical model relating axial pile deformation to the vertical soil movement due to deep excavation and also proposes ways to determine the pile response to lateral displacements. In this model, they modelled the non-linear load transfer mechanisms depending on relative soil pile displacements as well as pile axial deformations/strains were. They found that the settlement of piles with a large component of shaft friction is determined principally by the actual load on the pile relative to the pile ultimate capacity. The lateral pile response is controlled mainly by the relative stiffness of the pile to the soil.

4.3 Centrifuge and Laboratory Studies

Physical model tests both (1g) model and centrifuge model can be adopted to simulate and investigate pile responses due to deep excavation-induced soil movement. Some published works carried out using these techniques are reviewed in this section.

At the National University of Singapore (NUS), centrifuge model tests have been conducted by Shen (1999) and Lim (2001) to study the behaviour of a single pile and pile groups due to nearby an excavation-induced soil movement in sand. It was found that the induced bending moment on the piles increased with excavation depth. It's interesting that the induced bending moment did not increase consequently with the large lateral soil movement due to wall collapse. It was assumed that the sand just flowed around the pile without applying any additional load on the piles after the wall had failed. Lim (2001) also pointed out that if clay was used instead of sand, the pile bending moment and deflection reduced over time in the case of a collapsed wall.

Leung et al. (2000) used the centrifuge model test to investigate the behaviour of single pile subject to deformation induced by unstrutted deep excavations in dry Toyoura dense sand as shown in Figure 4.5a. The centrifuge model tests were conducted at 50g on the National University of Singapore Geotechnical Centrifuge. An appropriate thickness of sand in front of the wall was removed, a latex bag containing zinc chloride ZnCl2 solution having the same density as the sand is placed in the excavated area, and then the excavation was simulated in-flight by draining away the ZnCl2 solution from latex membrane.

LVDTs (linear variable displacement transformers) are used to measure lateral displacement (deflection), and rotation angle, also LVDTs used to measure the ground surface settlements. The test takes into consideration the depth of excavation, head conditions, length of pile, distance of pile from wall and the soil properties. Two cases of wall stability are investigated, stable wall and unstable wall.

The test results were analysed using a numerical model developed by Chow and Yong (1996). They found that, the theoretical predictions were generally in good agreement with the measured values for the case of a pile situated within relatively stable ground (either behind a stable wall or outside the soil failure zone of a failed wall). For the case of a pile located within the soil failure, the analytical approaches do not give accurate results of the pile deformation and moments.

Leung et al. (2003) performed a series of centrifuge tests on free-head and capped-head pile groups involving two, four, and six piles nearby unstrutted deep excavation in dry sand as shown in Figure 4.6a. They found that the interaction effect between the individual piles is insignificant in case of two piles arranged in a row parallel to the retaining wall for both configuration free- or capped-head. When two piles are arranged in a line perpendicular to the retaining wall, the existence of a front pile diminishes the significant effect of the excavation on the rear pile. For free-head 4- or 6-pile groups, the induced bending moment decreases by increasing the piles number. Either front or rear centre pile, they always experience lower bending moments than those of peripheral piles as the latter are more adversely affected by soil movement. In capped-head 4- or 6-pile groups, the existence of a pile cap reduces the pile-group deflection. The rear piles are less affected by soil movement as they are located farther away from the wall which would drag the front piles back.

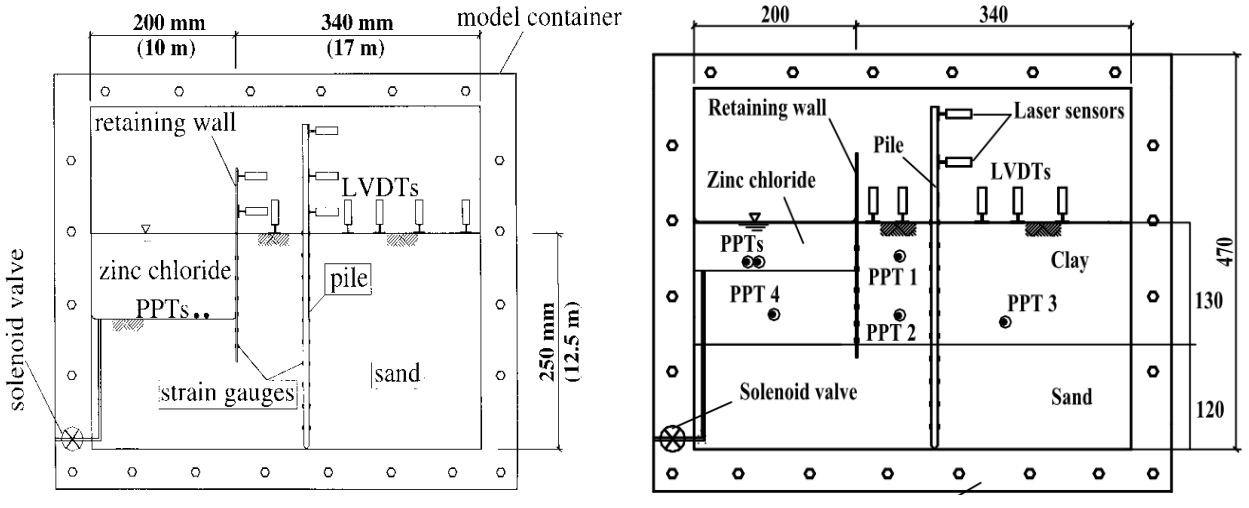

(a) **(b)**

Figure 4.5 Centrifuge setup for single pile case (a) Leung et al. (2000), (b) Ong (2004) and Ong et al. (2006a)

Ong et al. (2003) used the centrifuge model tests to study the time-dependent behaviour of a single pile subjected to lateral soil movements in an unstrutted excavation in kaolin clay overlying dense sand. The results reveal that the time-dependent pile behaviour is totally different in cases of a stable and collapsed wall. The time-dependent pile behaviour may be attributed to the existence of fissures on the clay layer, progressive wall and soil deformations, and pore water pressure redistribution that leads to soil reconsolidation. In case of collapsed wall (excessive soil movements), the occurrence of tension cracks prevent the transmission of full soil pressures to the pile. Thus, bending moments are reduced over time.

Ong (2004) indicated using centrifuge tests in clay (see Figure 4.5b) that the development of bending moments and deflection in piles adjacent to deep excavations is time dependent. The results show that the limit soil pressure/soil strength ratio for piles subject to soil movement is significantly less than that of loading piles, especially when the magnitudes of soil movement are large. Ong (2004) found that the induced maximum bending moment for pile groups was always lower than that of the corresponding single pile. The induced bending moment of the front pile, which experiences greater soil movement, is moderated through the pile cap.

Leung et al. (2006) discuss the effect of excavation on the single pile behaviour in clayey soil by using centrifuge model tests. The pile deflection and bending moment were observed during the excavation until wall failure. They found out that the induced bending moment increases with progressing excavation and it was reduced again when the excavation completed (reduced even before ending the excavation for the walls that experienced failure).

Ong et al. (2006a) carried out a series of centrifuge model test to investigate the behaviour of single pile subjected to excavation induced soil moment behind a stable retaining wall and the excavation up to the wall collapse. They carried out the test by varying the distance between the pile and the excavation. Centrifuge model setup is the same as that used in Ong (2004) study (see Figure 4.5b). A numerical model was used to back-analyse centrifuge test data which gives reasonably good prediction.

Ong et al. (2009) carried out a series of centrifuge model test to investigate the behaviour of pile group using various sizes and configuration behind the retaining wall in very soft clay overlying dense sand as shown in Figure 4.6b. The test results reveal that the induced bending moment on a single pile in a free-head pile group is always smaller than that on a corresponding single pile located at the same distance behind the wall due to the shadowing and reinforcing effects of other piles within the group. The degree of shadowing experienced by a pile depends on its relative position in the pile group. Though subjected to different magnitudes of soil movement, the individual piles in capped-head pile group are forced to interact in unison. The induced bending moment on the front piles is moderated by the rear piles through the pile cap, despite being subjected to a larger soil movement. A finite element program developed at the National University of Singapore is employed to back-analyse the centrifuge test data.

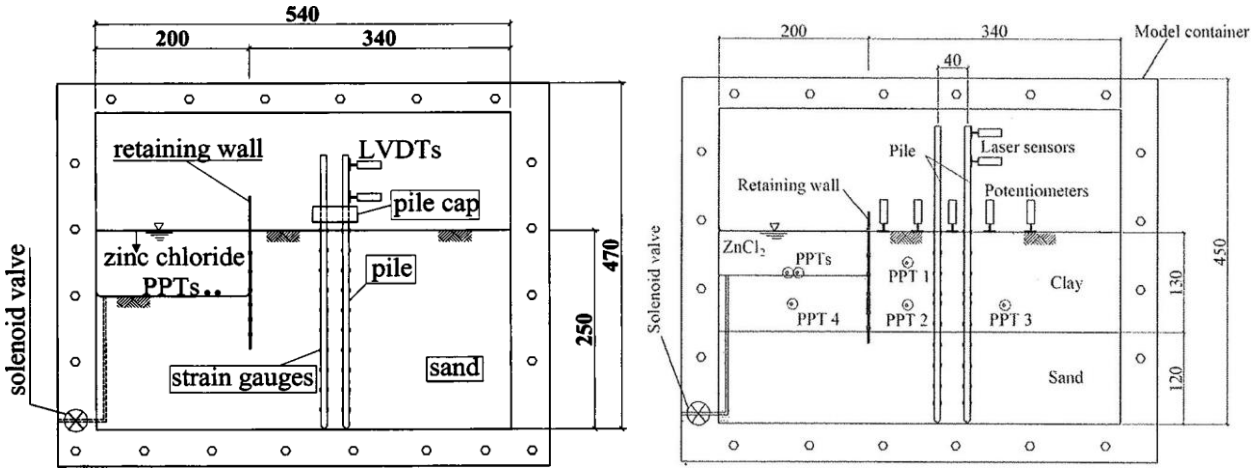

(a) **(b)**

Figure 4.6 Centrifuge model setup for pile group case (a) Leung et al. (2003) (b) Ong et al. (2009)

Ng et al. (2017) investigated the effects of multipropped excavation in-flight on vertically loaded floating piles in dry Toyoura sand through three centrifuge tests, which help designers and engineers to address the adverse effects on the safety and serviceability of adjacent pile foundations due to the construction of such geotechnical problems. Piles were laterally restrained in terms of rotation and deflection right at or above ground surface in the three different tests. To better understand the load transfer mechanism and pile–soil interaction, three-dimensional numerical analyses using the finite element program ABAQUS with a hypoplastic soil constitutive model were carried out to back analyse the centrifuge tests. Pile settlement, axial force, and bending moment were measured during the in-flight excavation. In each test, in-flight excavation was carried out step by step with installation of props at target levels. Figure 4.7 shows the schematic plan view and elevation view of the centrifuge models.

The results show that the pile-raft settled a similar amount as the free-head pile and the elevated pile group. Although different pile head conditions in the three tests, piles settlement was quite similar. While it was found that the lateral restraints imposed on the pile head have a substantial influence on induced pile bending moment in particular in the upper part of the pile (the effect in the lower part is limited). Induced bending moment due to excavation can exceed the pile bending capacity especially for piles in pile-raft foundations.

Madhumathi and Ilamparuthi (2018) investigated the response of single pile embedded in sand (see Figure 4.8) by adopting suitable scaling law, against supported excavation induced soil movement by conducting model tests at unit gravity (1g). The response of pile was studied by varying the relative stiffness of pile and soil, distance between pile and retaining wall, and pile length. The model tests are back-analysed numerically using the finite element program PLAXIS.

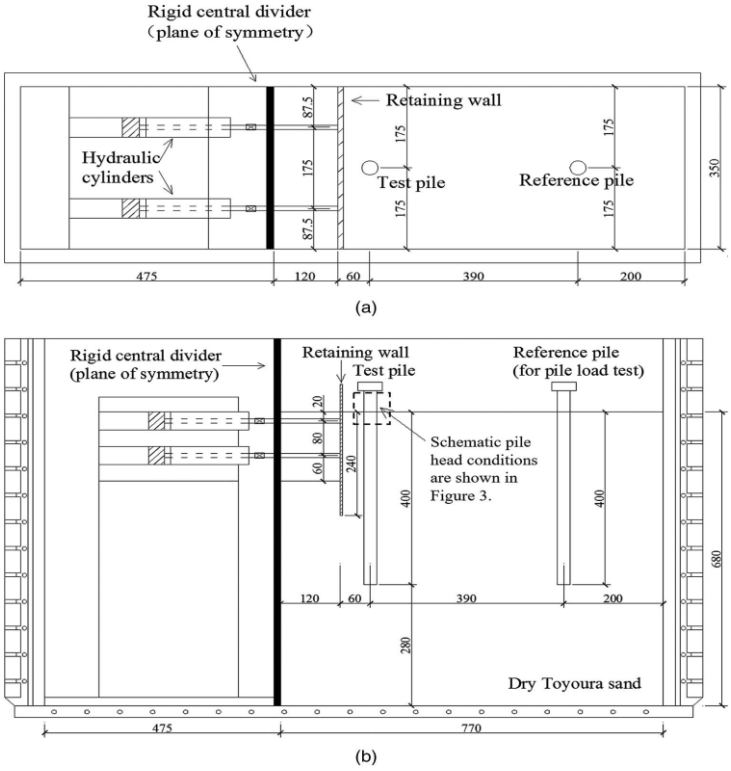

Figure 4.7 Centrifuge model setup (a) plan view (b) elevation view (Ng et al. 2017)

The test results show that the pile head deflection and the induced bending moment decrease significantly with increasing distance between the pile and the wall irrespective of pile length. The results show that the shorter pile (stiff pile) deflects more when compared to a long pile (flexible pile). The numerical analysis results are reasonably good with those obtained in the test. Design charts are included to predict pile head deflection, and the maximum bending moment.

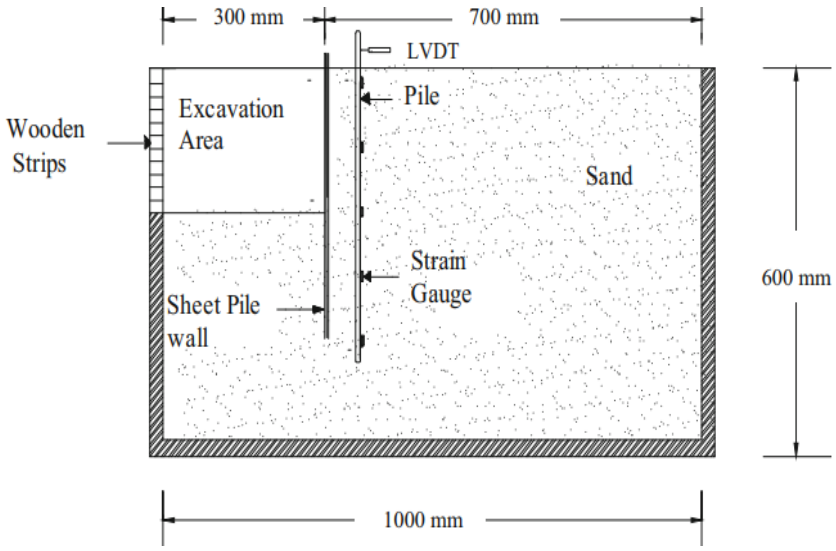

Figure 4.8 Side view of the centrifuge model setup (Madhumathi and Ilamparuthi, 2018)

4.4 Numerical Methods

Li et al. (2014a) and Li et al. (2014b) performed three finite difference numerical studies to investigate single pile response due to unstrutted and braceded excavation-induced lateral soil movement, respectively. In both cases, the study carried out using finite difference code FLAC3D. They focus their study on pile deflection, bending moment and lateral soil pressure. The studies investigate the effect of some key parameters on pile behaviour including excavation depth, distance from the excavation, wall stiffness, pile stiffness, pile-head condition, pile length and axial load. The Modified Cam Clay (MCC) constitutive model was employed to model the non-linear stress-strain soil behaviour. They found that the pile response such as pile deflection, bending moment and lateral soil pressure is different from that caused by unstructted excavation but the laws of the effect of some parameter on pile behaviour are similar.

Liyanapathirana and Nishanthan (2016) used the numerical method to study the effect of excavation on adjacent single pile. They verified their numerical simulation using the centrifuge test results reported by Ong et al. (2006a). They performed a parametric study to investigate the effects of the depth of excavation, soil properties, wall support system, pile head fixity conditions and pile location away from the excavation on pile behaviour. The study carried out using finite element program ABAQUS with the Modified Cam Clay (MCC) model for the Malaysian kaolin clay. Figure 4.9 shows the problem geometry and the finite element mesh used for the analysis.

The test results show that pile lateral deformation and bending moment increases significantly with excavation depth. Increasing the axial load does not have a significant influence on the pile behaviour. While pile head fixity condition, stiffness and spacing of the wall support system have a significant influence on the pile performance adjacent to the excavation. For a particular excavation depth, the maximum lateral deformation and bending moment of the pile decrease exponentially with the distance from the excavation. With increasing over-consolidation ratio (influence of stress history), the maximum pile response decreases. Based on the parametric study, they provided design charts for the case of single pile behaviour near excavation by taking into account the depth of excavation, undrained shear strength, width of the pile, spring stiffness, spacing of vertical supports, and unsupported depth of the excavation (depth where the first level of props is installed).

The capability of the proposed design charts are demonstrated using a 3D finite element analysis, a case study from the literature and a previously published simplified analysis procedure (Finno et al. 1991; Poulos and Chen 1997). These charts are useful in predicting maximum pile lateral deflection and bending moment during an adjacent excavation but valid only for piles founded in clayey soils, within 40 m from the wall.

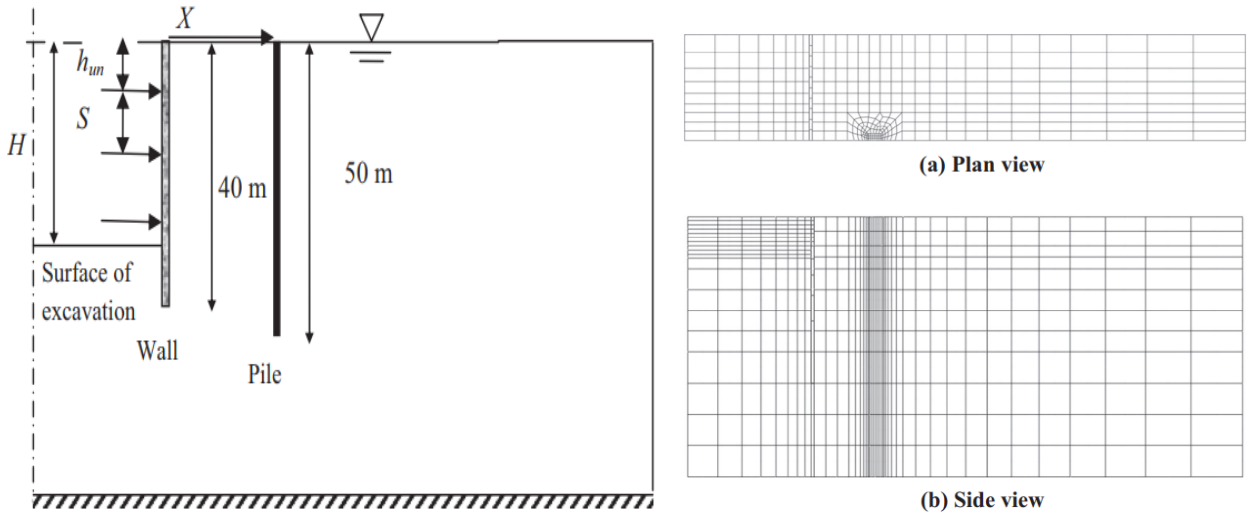

Figure 4.9 Liyanapathirana and Nishanthan (2016) basic problem (a) Excavation geometry (side view) (b) the finite element mesh used for the analysis

Nishanthan et al. (2017) investigate pile group response due to adjacent deep unbraced and braced excavations induced lateral soil movement. The braced excavation is considered in particular in soft clay soils, where the struts are used to support the wall during the excavation. They are performed the numerical simulations based on the finite element method to investigate the shielding effect within free-head and capped-head piles group using three different pile group configurations. The numerical model is validated by simulating a series of centrifuge tests reported by Ong et al. (2009). A parametric study is carried out to investigate the shielding effect of piles in a group, varying pile group configuration and head conditions. Nishanthan et al. (2017) investigate also the single pile responses as shown in Figure 4.10.

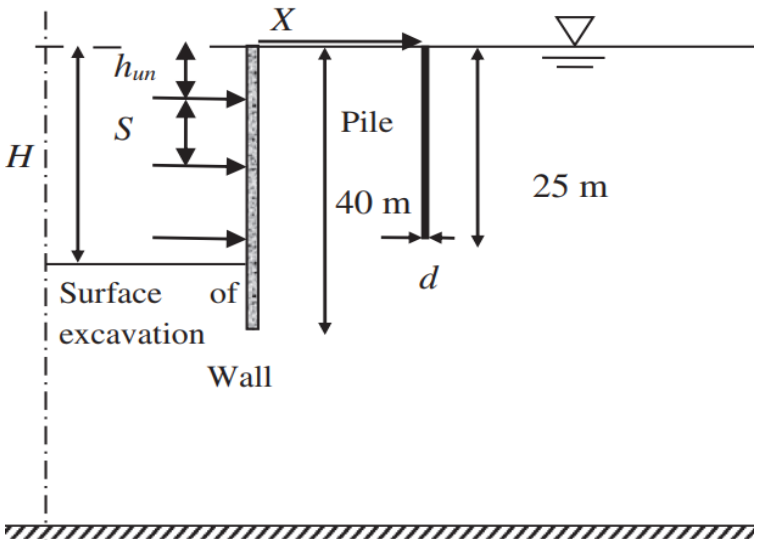

Figure 4.10 Side view of excavation (Nishanthan et al. 2017)

Shakeel and Ng (2018) used the finite element program PLAXIS to perform 3D coupled consolidation analysis to investigate the response of a 2×2 floating pile group adjacent to deep excavation in soft Kaolin clay. Their study considers the settlement, tilting and load transfer mechanism of the pile group. The finite element model is validated using the centrifuge test results reported by Ong et al. (2009). Some key parameters are systematically studied such as: the excavation depth, pile length (see Figure 4.11), pile group location from excavation, supporting system stiffness, soil state, soil permeability, and working load.

The analysis results revealed that the magnitude of settlement and tilting depends strongly on the relative pile toe position with reference to the excavation level. Pile group settlement and tilting increase with increase in the excavation depth. It is also observed that the pile responses decrease with the increase in the stiffness of the supporting system. Higher effects of the applied working load on pile group settlement but smaller effects on pile group tilting. Due to excavation, the excess negative pore water pressures generated in the soil leads to a progressive long term settlement pile group. Two distinct load transfer mechanisms are identified: downward load transfer from shaft to toe of pile till L_p/H_e= 0.45 and then upward load transfer from toe to shaft of pile. A significant bending moment is induced when pile toe is located below the final excavation depth than when it is located at the same level.

Shakeel et al. (2018) used a validated finite element model to investigate the influence of excavation depth to pile length ratio (H_e/L_p) on settlement and tilting of pile group. Also, relative density of sand (D_r) on an existing adjacent pile group are investigated. The analysis results show that the pile group settlement increases with the advancement of excavation and decreases with an increase of D_r (denser sand has higher soil stiffness). Pile group tilting does not follow any trend with the excavation depth for all the D_r (pile group tilts continuously increases towards the excavation with the increase of H_e/L_p).

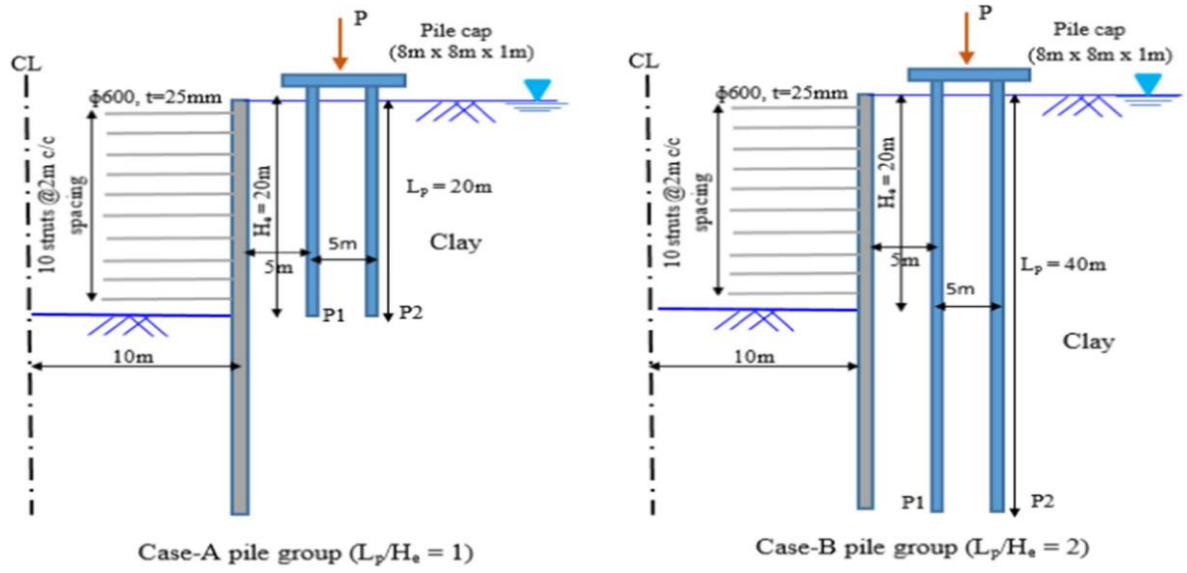

Figure 4.11 Typical geometry problem selected in Shakeel and Ng (2018) analysis

Soomro et al. (2018b) investigate the settlement, tilting, load transfer and load redistribution of an elevated (2×2) pile group due to adjacent excavation using a three dimensional coupled consolidation finite element analysis with the hypoplastic model for the saturated silty clay. The results indicate that due to excavation induced stress release (degradation of clay stiffness around the piles in the group) reduced the shaft resistance, thus, a non-linear pile group settlement was induced. Therefore, the pile had to settle substantially to further mobilise end-bearing. Owing to non-uniform stress release, pile group tilted towards the excavation by of 0.14%. Due to excavation-induced stress release and dragload, head load of rear piles was reduced and transferred to front piles. This load transfer can increase the axial force in front piles by 94%. Differential settlement was induced between the two pile rows, thus, tilting of the pile group. This attributed to the non-uniform change in vertical effective stress.

Shi et al. (2019) conducted 3D numerical analysis to investigate the behaviour of a floating pile due to adjacent excavation by using hypoplastic sand model. This model had the capability to capture small-strain soil stiffness and stress-path dependent soil behaviour. The numerical model was verified based on the results of a centrifuge test reported by Ng et al. (2017). Using the FE software ABAQUS, parametric studies were conducted to study the effect of excavation depth, pile location, working load, sand density and support system stiffness. Figure 4.12 shows a schematic diagram of the problem. The results reveal that when the pile located farther away from the retaining wall, negligible pile head settlements are observed. Reducing FOS before excavation from 3.0 to 1.5 double pile settlements. By increasing the relative sand density 30-90%, the pile settlement decreases by up to 66%. Less influence of support system stiffness for shallow excavation ($H_e/L_p < 0.4$) on pile head settlement. Downward and upward load transfer mechanisms are observed at different excavation stages, depending on the ratio (H_e/L_p).

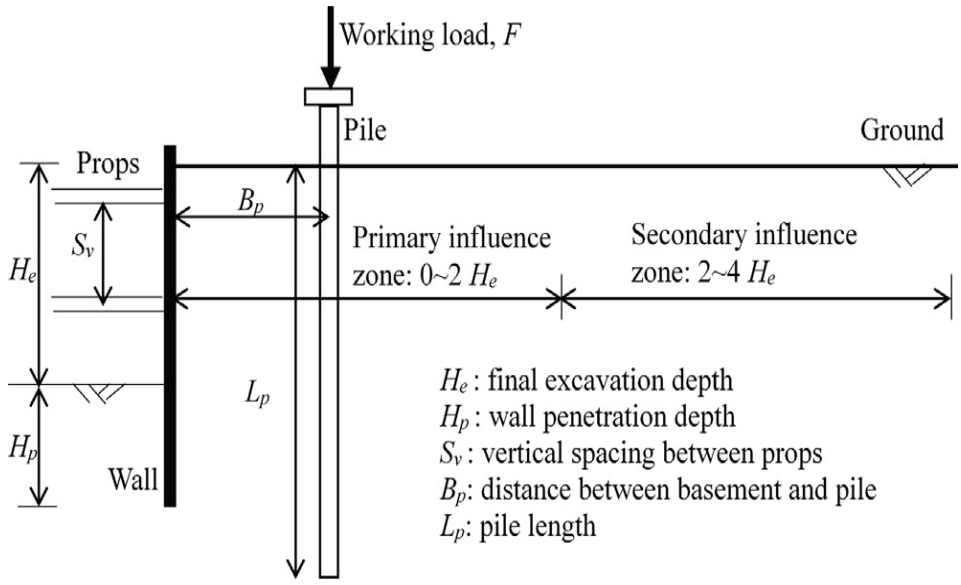

Figure 4.12 Schematic diagram of Shi et al. (2019) study

Soomro et al. (2019a) performed a three-dimensional numerical parametric study using an advanced hypoplastic model which takes into account of small-strain stiffness to investigate a loaded single floating pile responses to adjacent excavations in soft ground (Kaolin clay). The numerical model parameters are calibrated and validated using centrifuge test results reported in literature (Ong et al. 2006a). The effects of excavation depths relative to pile (H_e/L_p) were investigated via three cases. The excavation is simulated near the pile shaft (i.e., H_e/L_p= 0.67), next to (H_e/L_p= 1.00) and below the pile toe (H_e/L_p= 1.33) as shown in Figure 4.13. The pile head conditions and working load were also studied. Their studies focus on pile settlement, axial load, deflection and the induced bending moment distribution. Also the effective stress changes and excessive pore pressure developed during excavation are reported and discussed.

It is found that the excavation depth as well as the embedded depth of the wall significantly affects the pile responses. For a large embedded depth of the wall, the induced pile settlement was smaller than that in cases when the embedded depth of the wall is small. With different wall depth in each case, pile responses at the same stage of the excavation were different in the three cases.

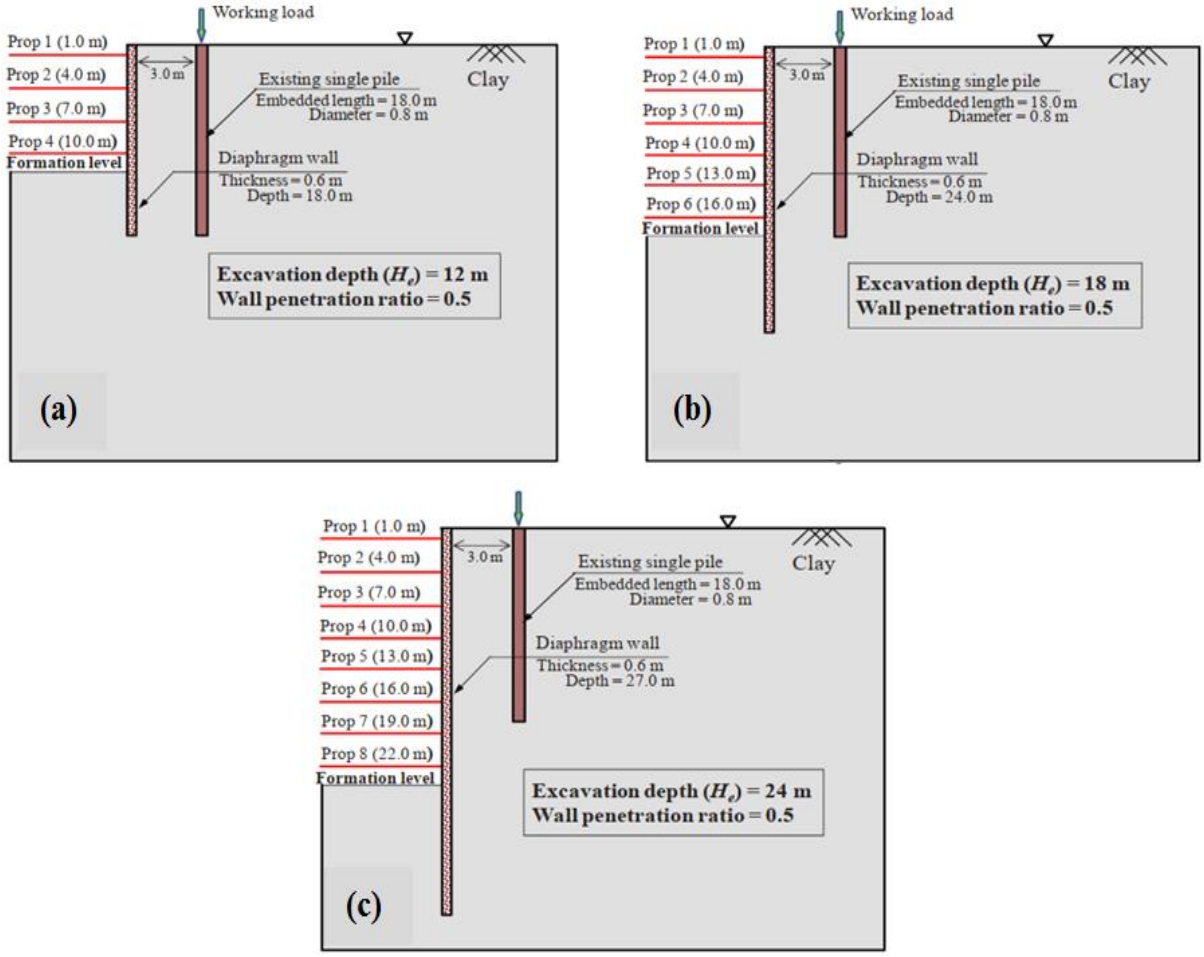

Figure 4.13 Elevation views of H_e/L_p cases (a) 0.67 (b) 1 and (c) 1.33 (Soomro et al. 2019a)

The results show that the excavation in case of H_e/L_p= 1.33 caused the largest pile settlement. While, the largest pile deflection was induced in case of H_e/L_p= 0.67. It is found that on completion of the excavation in each case the insignificant bending moment and changes in axial load distribution are induced in the pile. The maximum induced bending moment in all the three cases is much less than the pile bending moment capacity (i.e., 800 kNm). Significant effects of pile head conditions on bending moment distribution was observed (in particular with fixed head condition) and less impact on pile settlements. The different working loads (with FOS = 3.0 and 1.5) influence induced pile settlement but have relatively minor effect on induced bending moment.

Soomro et al. (2019b) performed 3D coupled consolidation analyses to study the responses of a floating and end bearing pile due to nearby excavation at different excavation depths in soft Kaolin clay (see Figure 4.14). To obtain a satisfactory numerical model, the hypoplastic constitutive model which takes account of small-strain stiffness is used for the clay. The effects of excavation depths relative to pile (H_e/L_p) were investigated by simulating the excavation near the pile shaft (case S) and next to toe (case T). Lateral deflection, bending moment, lateral forces and axial load distribution along the pile and stress changes during excavation are reported and discussed. The results show that after completion the excavation, end-bearing piles (case T) experienced smaller induced deflection but higher induced axial force, bending moment and lateral load compared to floating pile (case S). They found that in all the cases, the induced bending moment is significantly affected by the pile toe positions. The maximum induced bending moment in both types of piles after the ending of excavation is much less and not even reach the pile bending moment capacity (i.e. 800 kNm).

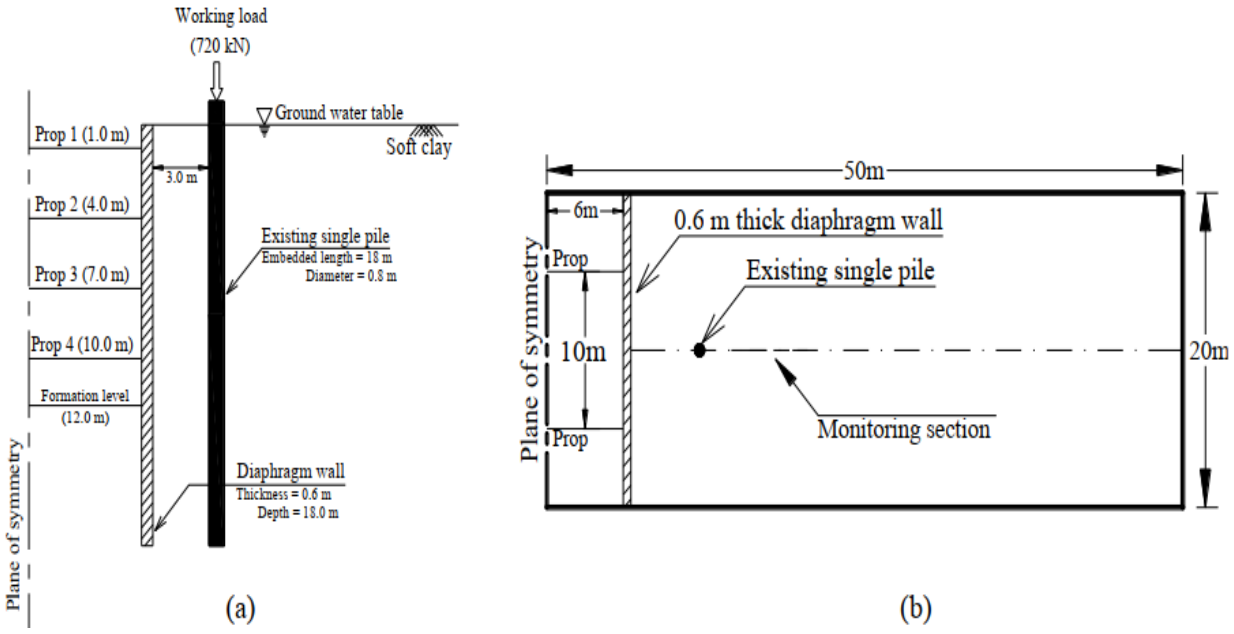

Figure 4.14 Typical geometry in Soomro et al. (2019b) analysis (a) elevation & (b) plan view

As the pile toe is resting on the hard stratum, the excavation has negligible effect on the end-bearing pile toe movement. Additionally, after excavation, the end-bearing piles were subjected to significant drag load owing to negative skin friction. In contrast, no significant changes in load distribution along floating piles were observed. However, the progressive changes in excess pore water pressure and long-term behaviour of the both types of piles are studied and show significant effect on pile behaviour.

Soomro et al. (2020a) investigate the deformation mechanism of a 20-storey building sitting on a (4×4) piled raft in sand due to multipropped deep excavation (25 m deep basement excavation as shown in Figure 4.15). A three-dimensional numerical parametric study was conducted using an advanced hypoplastic model. The results show that excavation adjacent to a building resting on the piled raft induced significant settlement, differential settlement, lateral deflection, and inter storey drift in the building. Bilinear increment in induced settlement was observed with increasing of excavation depth due to degradation of soil stiffness. The total settlements of the building exceed the maximum allowable foundation settlement (50 mm). Negligible differential settlement was induced in first excavation step and then increased with excavation depths. This led the building to move laterally towards the excavation which caused the building permanent inter storey drifts. Also, significant bending moment, shear forces, and changes in axial load distribution along pile length were induced.

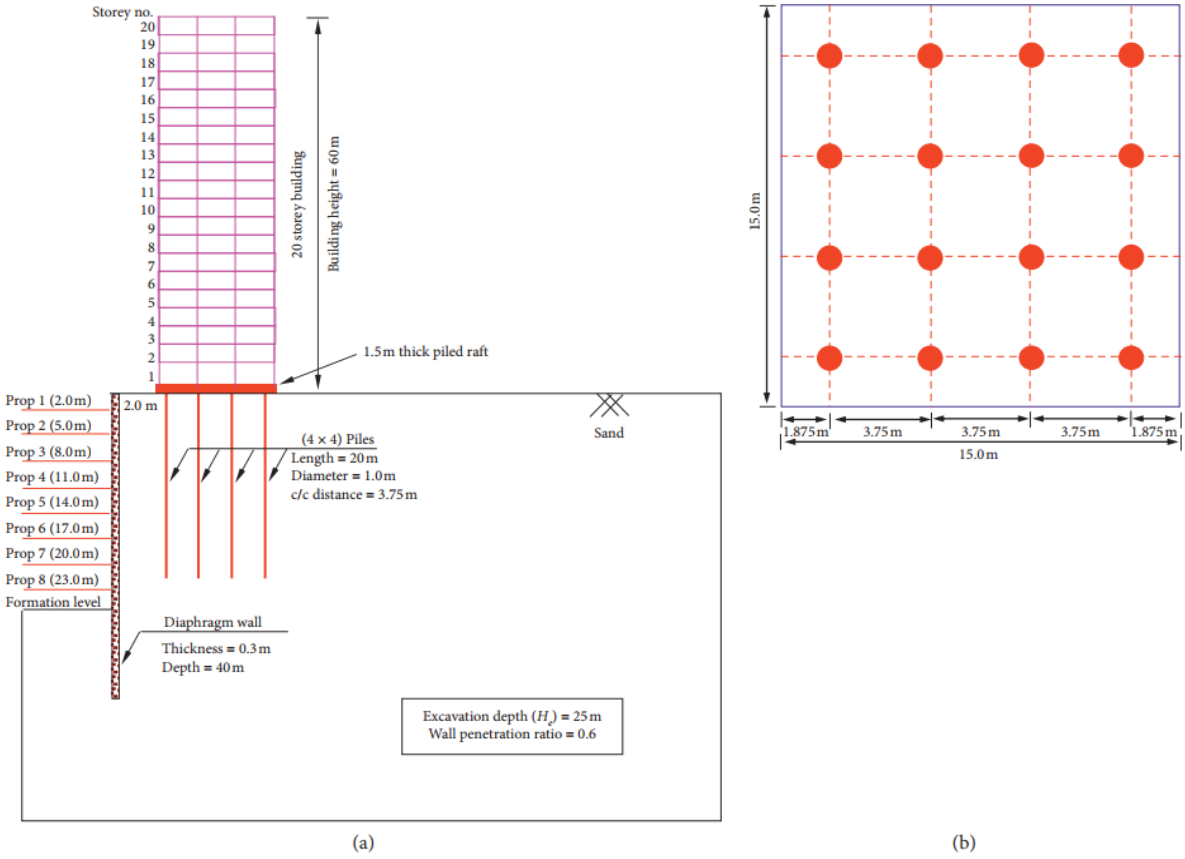

Figure 4.15 Soomro et al. (2020a) analysis (a) geometry (b) piles arrangement in the raft

Zhang et al. (2021) used the finite element analyses to investigate the behaviour of pile due to adjacent excavation. The Hardening Soil model with small-strain stiffness (HSs) implemented in the FE code PLAXIS was employed to model the non-linear stress-strain soil behaviour. A parametric study were carried out by varying the depth of excavation, pile diameter, pile length, pile location, pile-head fixity, unsupported depth of excavation and axial load applied on the pile head. The numerical model is based on the full-scale instrumented case history reported by Goh et al. (2003). The water table was about 4 m below the ground surface. The typical 2D numerical model is shown in Figure 4.16. The results show that the excavation depth, pile length, pile diameter and pile location have the most substantial influences on pile responses (lateral deformations and bending moments). Less impact of the axial load was observed. Pile-head fixity obviously affects the bending moments along the pile, as well as pile lateral deflection. Based on parametric study results, and for a single passive pile, a set of design charts are proposed to estimate the pile responses.

Ng et al. (2021) performed a series of 3D centrifuge model tests and numerical simulations to investigate the influence of raft contact on the response of an existing 2×2 piled rafts in comparison to that of an elevated pile group when subjected to a nearby multipropped deep excavation in dry Toyoura sand. Four centrifuge tests are performed, including a pile group load test. Numerical back analyses are performed using the FE program PLAXIS 3D with a hypoplastic sand constitutive model to study the settlement, tilting, the load transfer mechanism, and the raft-soil-pile interaction mechanism. Load distribution among piles and the stress paths are discussed to clarify the load distribution and load transfer mechanisms.

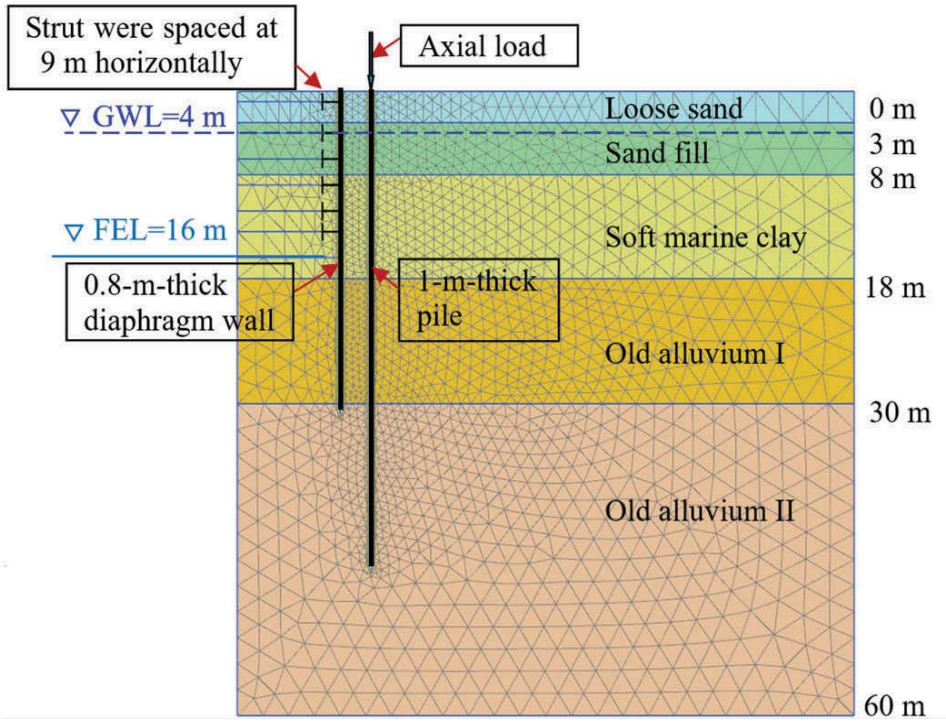

Figure 4.16 Finite element mesh used in Zhang et al. (2021) study

Due to stress release and soil movement due to 8 m deep excavation, an increasing of pile head load by 21% and 3% for the nearest pile to the excavation for the piled raft and pile group foundations, respectively. The analysis of pile settlement, subsurface soil settlement and raft contact pressure shows that a gap formed beneath the raft and ground surface in the piled raft, thus, a load transfer from the raft to the piles. Larger settlement was observed in the piled raft foundation than in the pile group (about 20%), thus, shaft and end bearing resistances further mobilized to maintain the vertical equilibrium. Besides, 30% additional pile bending moment was induced due to excavation.

4.5 Conclusion

Deep excavation one of the main sources that caused ground movements which therefore can have a significant effect on adjacent buildings supported by piles foundations. A variety of methods for the analysis of pile-soil-excavation interaction problems in different types of soils have been developed and briefly reviewed in this chapter, which are categorised into: field and analytical methods, experimental studies, and numerical methods.

The review show that owing to such phenomena in excavation works, soil movement (deformation) can pose a serious threat to the retaining structure and nearby existing structures supported on pile foundations. Although an excavation will cause both vertical and lateral soil movements, the second component is considered to be more critical, as piles are usually designed to sustain significant vertical loads (many previous studies mainly focus on the piles lateral responses).

Generally, there is a lack of field data to verify the piles responses. Several analytical methods have been developed and compared to some physical tests and field studies, and shows reasonably good agreement. Several experimental studies have also been conducted to explore the pile-soil-excavation interaction phenomena. Recently, the numerical analysis is very advantageous owing to its capability to simulate 3D excavation procedures, pile-soil interaction, and to perform parametric studies to investigate the effect of different parameters on pile performance. The above methods have been conducted to explore the effect of various parameters on pile behaviour such as: excavation depth, pile length, distance of pile from excavation, pile stiffness, wall stiffness, pile head conditions, struts space and stiffness (braceded excavation), working load, and varying soil properties. The same parameters used for pile group case using various configurations. The main effects of ground movements due to deep excavation are the development of additional movements (deflection and settlement), axial forces and bending moments in the piles, and thus the key design aspects are related to movements and to the structural integrity of the pile.

Second Part
Numerical Modelling

CHAPTER 5

3D Numerical Analysis of the Effects of Tunnelling-Induced Ground Movements on Nearby Piles

CHAPTER 5

3D Numerical Analysis of the Effects of Tunnelling-Induced Ground Movements on Nearby Piles

5.1 Introduction

Traffic jams in large cities often require the proliferation of underground structures such as tunnels. In most cases, due to space constraints, tunneling may be required to be carried out not far from nearby edifices. The stress release caused by the digging of a particularly shallow tunnel can lead to excessive vertical and lateral ground movements. As a result, it is very likely that the behavior of the closest pile foundations will be influenced. It is therefore necessary to better understand the multifaceted phenomenon of pile-soil-tunnel interactions and its impact on pile performance, which in turn affects the safety and functionality of neighboring buildings.

Due to the overlap of many factors, the precise assessment of the impact of tunneling works on existing nearby piles remains a topical area of research.

Several researchers investigated the pile performance due to tunneling by analytical methods (Chen et al. 1999; Loganathan et al. 2001; Huang et al. 2009; Zhang et al. 2011; Huang and Mu, 2012; Basile, 2014; Marshall and Haji, 2015; Franza et al. 2017; Zhang et al. 2018). Current analytical studies have mainly employed the plane strain analysis and do not take into account the multiple interactions between the different elements constituting the problem. The reactions of exposed piles to ground movements induced by tunnelling were also assessed using the basic method recognized as the two stage analysis method (TSAM). First: Greenfield soil movements induced by tunneling are estimated using empirical methods and also analytical closed-form solutions (Peck, 1969; Clough & Schmidt, 1981; Mair et al. 1993; Loganathan and Polous, 1998). In the second stage, these soil movements are imposed on the pile using simplified boundary element analysis to compute the pile responses. It is worth mentioning that this approach assumes that the soil mass is homogeneous and has a linear elastic behaviour; this is what makes it unsuitable to non-linear problems and non-homogeneous soils.

Various studies have investigated the tunnel-soil-pile interactions through field monitoring (Kaalberg et al. 2005; Selemetas et al. 2006; Coutts and Wang, 2017). Centrifuge modelling technique and model tests were also carried out to study the responses of single piles or piles group subjected to tunnelling. (Loganathan et al. 2000; Jacobsz et al. 2004a; Ong et al. 2006b; Lee and Chiang, 2007; Ng et al. 2013; Hong et al. 2015b; Soomro et al. 2017, 2018a; Leung et al. 2019). These experimental methods divulge some fundamental features of the problem. Nevertheless, for the pre-project phase, these approaches can be costly and time-consuming. The 3D numerical calculation by finite element or by finite difference has therefore become indispensable, since the complex geometry and the multiple interactions between the

different components of the problem can be explicitly considered (Mroueh and Shahrour, 2002; Kitiyodom et al. 2005; Cheng et al. 2007; Yang et al. 2011; Lee, 2012a, 2013; Zidan and Ramadan, 2015; Soomro et al. 2015; Lee et al. 2016; Al-Omari et al. 2019; Soomro et al. 2020b). Most of the studies carried out have focused on tunneling-induced pile responses in homogeneous soils. However, the study of the problem in a multi-layer soil remains very limited.

The analyses of the induced soil movements and the response of the piles due to tunneling have been studied by various researchers using numerical methods by decoupled loadings in plane deformation. However, experimental studies have highlighted the limitations of the 2D approach, due to the restricted assumptions on which the formulations are based, and have confirmed that the problem is clearly three-dimensional. Thus, a full three-dimensional coupled numerical analysis of the problem, which takes into account the real tunnel-soil-pile interactions, has become an important contribution to a thorough understanding of the observed phenomena.

In this chapter, a full 3D numerical analysis is performed to study the effect of ground movements caused by tunneling on the adjacent piled foundations in a non-homogeneous geological context. The different constituents of the problem (tunnel, pile, soil) and the different stages of tunnel construction were modeled using the PLAXIS 3D software (Brinkgreve et al. 2016). The numerical analyses mainly focus on both vertical and horizontal single pile responses. The validation of the numerical model was performed by comparison with the results of a centrifuge test conducted at an acceleration field of 100g according to Ong (2009). The relevance of the three-dimensional model is also judged by comparison with the plane strain model using PLAXIS 2D code (Brinkgreve et al. 2017).

From a 3D numerical reference model, a series of parametric analyzes were performed to gain a deeper understanding of the tunneling-induced pile responses. The tests focus mainly on the effect of tunnel advancement steps (front location of the tunnel in relation to the pile location), volume loss, pile position, pile extent, pile diameter, clay over consolidation ratio (OCR), tunnel depth, and tunnel diameter on single piles behaviour. To give supplementary comprehensions concerning groups of piles, a 2×2 pile group with two different pile head conditions (free and capped) was considered.

5.2 Validation of 3D finite element model against centrifuge test results

5.2.1 Description of the centrifuge test

The centrifuge test, used for the validity of the finite element modelling approach performed in this study, was carried out using the Geotechnical Centrifuge facility at the National University of Singapore by Ong (2009). The centrifuge test was conducted at an acceleration field of 100g to investigate tunneling-induced soil deformations in clay overlying dense sand and their effects on adjacent free-headed single pile.

The model was prepared and tested in a plane strain strong box (plane strain model of long tunnel section). The container used is made of stainless steel alloy and has internal dimensions of 525 mm×200 mm×490 mm (length×width×height). Figure 5.1a shows the side view of the centrifuge test. The centrifuge model was carried out to simulate the inward tunnel deformation (soil move towards the tunnel lining using an innovative model tunnelling technique). The tunnel is made of a circular rigid outer plate and a hollow metallic circular tube of 60 mm diameter, simulating a 6 m tunnel diameter at 100g. The gap parameter GAP as proposed by Lee et al. (1992) was used to model the over-cut of the tunnel. To achieve the volume loss of 3% in 100g, a GAP parameter of 100 mm in prototype scale is needed. The tunnel is 200 mm long, and 150 mm depth. The whole mechanism works as such when there is a force pushing the aluminium sliding rod, the small rods will fall onto the three thinner parts of sliding rod of smaller cross-sectional area. This causes an 'immediate' closure of the GAP and simulating the inward tunnel deformation.

Regarding the adjacent piles, two different types of pile pattern are used in the test, and each pile is placed on either side of the tunnel. The piles were fabricated using square aluminum tube 9.53 mm in width and 1.59 mm thick. Ten pairs of strain gauges were attached along the piles shaft to measure bending moments and axial forces of piles. Thin layer of epoxy coating was used to protect strain gauges from damage. The final external width of pile is 12.6 mm which simulates a prototype width of 1.26 m at 100g.

The soil used in the test is kaolin clay and Toyoura sand. Sand was first rained into the model's container. Clay was prepared in slurry form by mixing water to dry clay powder to 1.5 time's liquid limit of the clay. The clay slurry was then consolidated under a small pressure of 20 kPa in the laboratory at 1g (earth gravitational field). The Malaysian kaolin clay has a compression index C_c of 0.56, swelling index C_s of 0.12, initial void ratio e_{init} of 2.25, liquid limit (LL) of 80%, plastic limit (PL) of 40%, and plasticity index (PI) of 40 %. The coefficient of permeability of kaolin clay normally consolidated at a consolidation pressure of 100 kPa has been determined to be approximately 2×10^{-8} m/s. The clay has an effective internal friction angle φ' of 23°, a coefficient of earth pressure at rest of about 0.6, and a specific gravity of 2.65 (Ong, 2009). The undrained shear strength C_u of the clay is on average 0.25 of the effective overburden pressure. Mechanical properties of Toyoura sand are well documented by Teh and Wong (1995). The sand has a relative density RD = 90%, an average particle size of 0.2 mm, and a unit weight of 15.78 kN/m^3. The critical state friction angle and the effective cohesion are 32°, 0 kPa, respectively. The sand also presents an average particle size of 0.16 mm, uniformity coefficient of 1.3, maximum and minimum void ratio of 0.977 and 0.605; respectively. The sand underlying the clay serves as a drainage channel and interlocking for the pile.

Potentiometers were employed to measure the ground and pile head settlement during the test. Pore pressure transducers (PPTs) were inserted into the sample to measure the pore water pressure at various locations. Non-Contact Laser Transducers were used to measure the lateral pile head deflections during and after tunnel excavation.

5.2.2 Numerical finite element modelling

The numerical modeling was carried out using the PLAXIS 3D software (Brinkgreve et al. 2016), which is a flexible device for analysing nonlinear 3D soil–structures interaction problems. The 3D mesh of the numerical model used to simulate the centrifuge test is shown in Figure 5.1b. Due to symmetry, only one-half of the centrifuge setup was modeled. The finite element model has an overall dimension similar to the centrifuge container size at 100g, i.e. length of 26.5 m, width of 20 m, and height of 27 m. The pile and tunnel lining (the hollow metallic circular tube) are modelled using "Embedded pile" and "plate" structural elements, respectively.

The pile model has a bending stiffness EI_p of 3.97×10^6 kNm^2 and an axial rigidity EA_P of 3.64×10^7 kN. The total pile length is 22 m (embedded 3 m in the dense sand). The single pile is located at 6 m from the vertical axis of the tunnel. Both pile and tunnel lining were modelled using an isotropic linear elastic model with Young's modulus *E*= 23.5 and 200 GPa, respectively. Concerning the boundary conditions, no horizontal displacement is authorized on the nodes of the vertical boundaries of the numerical model. However, the nodes of the bottom boundary are fully fixed in both vertical and horizontal directions. The right vertical boundary corresponds to the symmetry axis of the problem. In hydraulic terms, these boundaries are assumed to be impervious.

The behaviour of the interface between the shaft of the pile and the soil is governed by a linear elastic constitutive law with restricted strength. The mobilization of the resistances of the shaft and the base of the pile is governed by the relative displacement between the soil and the pile as well as by the soil shear modulus. The development of negative shear stress along the shaft of the pile is permitted, which is practical for modelling negative lateral friction.

The Hardening Soil Model with small-strain rigidity (HSsmall), implemented in PLAXIS 3D, was used in this study to model the non-linear stress-strain soil behaviour. The HSsmall model is an innovative model suitable for both rigid and soft soils subject to loading - unloading phenomenon. The HSsmall model has the benefit of using the same parameters of the Hardening Soil Model by only two additional material parameters needed to governor the strain and stress history dependent stiffness. These parameters are the initial shear modulus (G_0^{ref}) and the shear strain ($\gamma_{0.7}$) at which the shear modulus has decayed to 70% of its initial value.

The HSsmall model involves four various stiffness moduli namely E_{oed}^{ref}, E_{50}^{ref}, E_{ur}^{ref}, and G_0^{ref}, each of them estimates the reference rigidity in a specific stress path for a given reference pressure (P^{ref}). For a detailed description of the HSsmall model, see Benz et al. (2007) and Brinkgreve et al. (2016).

Based on the relative density (*RD*), the following formulas developed by Brinkgreve et al. (2010) were used in this numerical study to deduce the stiffness parameters of the HSsmall model for Toyoura sand:

$$E_{50}^{ref} = E_{oed}^{ref} = 60000.RD/100 \quad [kN/m^2] \tag{5.1}$$

$$E_{ur}^{ref} = 3\,E_{oed}^{ref} \tag{5.2}$$

$$G_o^{ref} = 60000 + 68000.RD/100 \quad [kN/m^2] \tag{5.3}$$

Regarding soft soils, such as Kaolin clay, the stiffness parameters can be calculated using the relationships in the PLAXIS material model manual, as follows:

$$C_c = \frac{2.3(1+e_{init})P_{ref}}{E_{oed}^{ref}} \tag{5.4}$$

$$C_s = \frac{2.3(1+e_{init})(1+v)(1-2v)P_{ref}}{(1-v)E_{ur}^{ref}K_0} \tag{5.5}$$

$$E_{50}^{ref} = 1\text{-}2\ E_{oed}^{ref} \tag{5.6}$$

$$G_0^{ref} = \frac{5\ E_{ur}^{ref}}{(1+v)} \tag{5.7}$$

Hence, using the relationships mentioned above and the different soil properties reported by Ong (2009), the required parameters of the HSsmall model for both layers (soft clay and dense sand) are deduced and summarized in Table 5.1.

Experimentally, the Poisson's ratio ν_{ur}, the unloading modulus E_{ur} and the first loading modulus E_{50} (secant modulus) are determined from triaxial compression tests with primary loading and unloading-reloading. However the oedometric modulus E_{oed} is determined using the oedometer test. The realization of ''loading-unloading-reloading'' cycles provides useful information and accessing to a state that can be reasonably close to the in situ behavior.

Table 5.1 Soil parameters used in the analyses

Soil	γ_{unsat} ($\frac{kN}{m^3}$)	γ_{sat} ($\frac{kN}{m^3}$)	E_{50}^{ref} (MPa)	E_{oed}^{ref} (MPa)	E_{ur}^{ref} (MPa)	m	ν_{ur}	P^{ref} ($\frac{kN}{m^2}$)	C_{ref} ($\frac{kN}{m^2}$)	φ (°)	K_0^{nc}	$\gamma_{0.7}$	G_0^{ref} (MPa)
Kaolin Clay	16	18	26	13	90.5	1	0.2	100	3	23	0.6	2×10^{-4}	37
Toyoura Sand	18.5	20.5	54	54	162	0.4	0.2	100	0.01	39	0.37	1.1×10^{-4}	121.2

Notes: γ: Unit weight, E_{50}^{ref}: Reference secant stiffness modulus, E_{oed}^{ref}: Reference tangent stiffness modulus, E_{ur}^{ref}: Reference unloading-reloading stiffness modulus, m: Power for stress dependent stiffness, C_{ref}: Effective cohesion, φ: Friction angle, ν_{ur}: Poisson's ratio for unloading-reloading, P^{ref}: Reference stress for stiffness, K_0^{nc}: Coefficient of earth pressure for normal consolidation, G_0^{ref}: Reference shear modulus, $\gamma_{0.7}$: Shear strain.

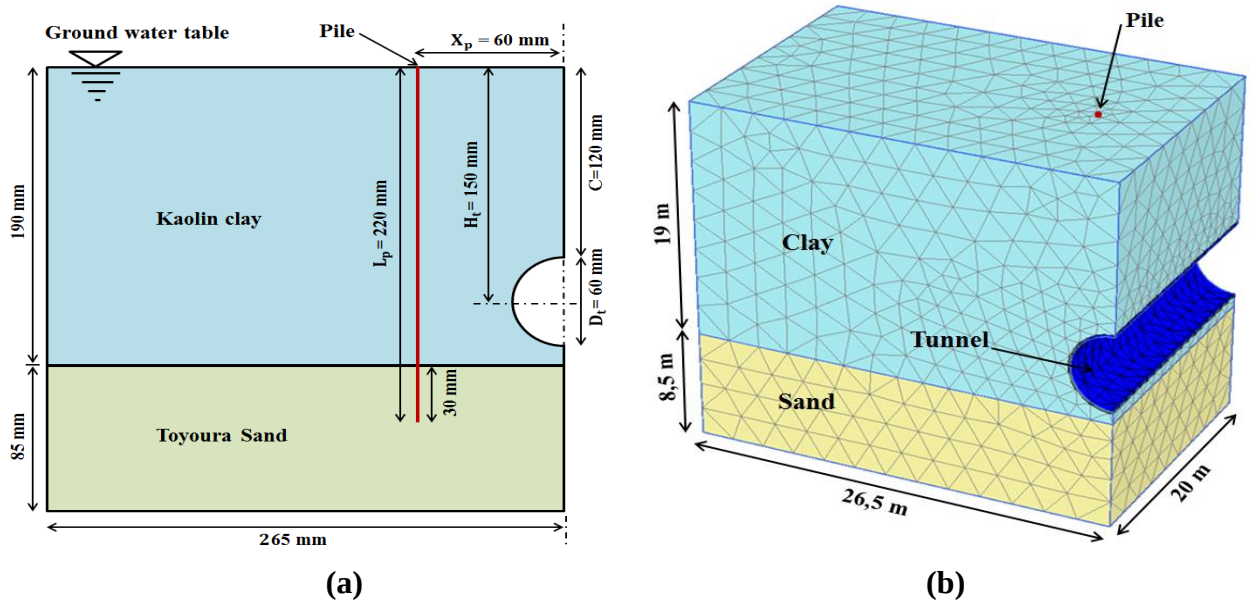

Figure 5.1 Details of the centrifuge test (a) Side view (b) Finite element mesh

The numerical modeling procedure is the same as for the centrifuge test, as follows:

1. Generate the initial stresses using the K_0 procedure at 1g

2. Activate the pile model (wished-in-place)

3. Increase the amount of gravity to 100g using $\sum M_{Weight}$ wich is the total multiplier for the material weight

4. Simulate tunnel excavation: to simulate the plain strain condition, the entire length of the tunnel model has been excavated all at once by deactivating soil elements inside. Successively, activate the tunnel lining (Plate), and then apply the volume loss (3% according to the test) using the contraction function.

5.2.3 Comparison of numerical and measured results

To judge the relevance of the numerical model, the pile responses in terms of bending moment and lateral displacement, were compared to the measurements as shown in Figure 5.2. From Figure 5.2a, the pile deflected towards the tunnel with a cantilever-type deformation for the centrifuge test, while the numerical model shows a deflection shape close to a straight line. However, the deflection trend at the top of the pile appears to be similar for both results, with almost the same maximum deflection (about 3mm) at the pile head. Figure 5.2b shows that the computed bending moment significantly overestimates the measurements in the upper part of the pile. However in the lower part ($0.45L_p$ and $0.8L_p$), a good agreement was found between the measurements and the calculations, where both indicate the same maximum bending moment (about 150 kN) which occurred at the same depth (i.e. near the horizontal axis of the tunnel).

Because pile head was not constrained, zero bending moments were obtained at pile head. Some of the unimportant difference seen in the pile responses between measurements and numerical calculations may have been due to the use of a thin layer of epoxy coating, to protect the strain gauges used in the test, making the lateral surface of the pile much smoother than that of the concrete pile. Generally, the numerical results slightly overestimate the pile responses and are thus on the conservative side. However, the obtained results reveal that there is an ability to perform a numerical parametric study (effect of some key parameters) to investigate single pile and pile group behaviour near tunnel excavation using the HSs model.

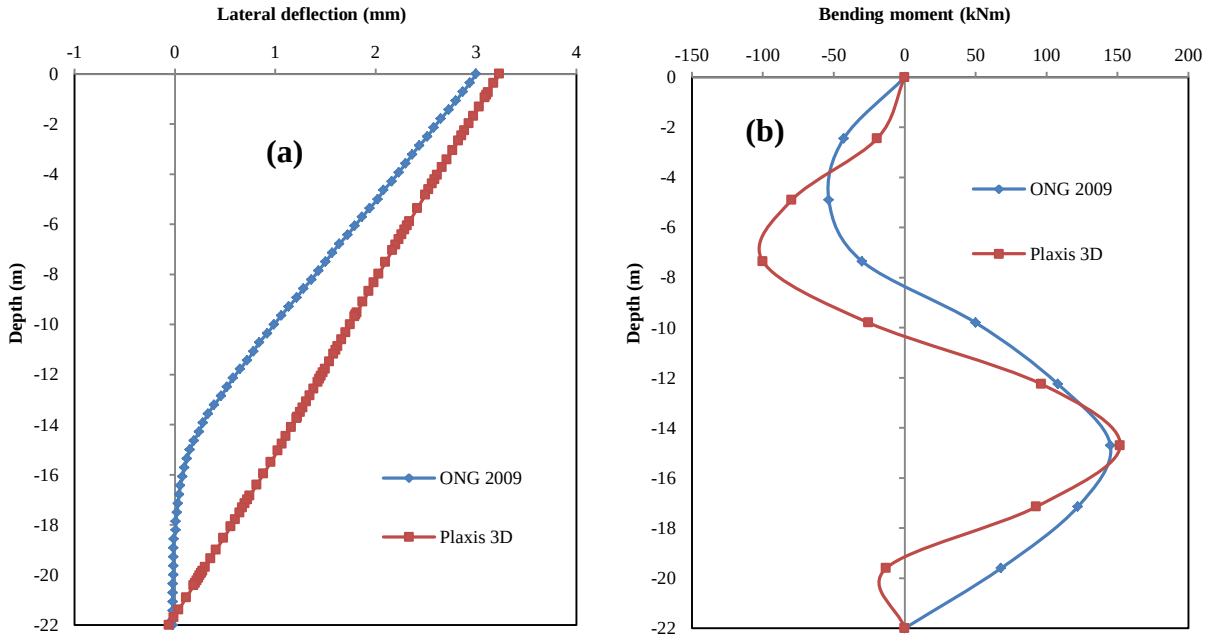

Figure 5.2 Comparison of the computed and measured results (a) pile lateral deflection (b) induced bending moment

5.3 Numerical reference model used for the parametric analyses

5.3.1 General presentation of the model

Unlike of the centrifuge test, the main object of this numerical analysis is to study the pile behaviour before, during, and after the passage of the tunnel face. In this paper, the construction of the tunnel was performed using the shield tunnel boring machine (TBM). The shields provide protection against collapse of the tunnel walls and the excavation front before the installation of the tunnel lining.

Using the PLAXIS 3D finite element numerical code, a full 3Dnumerical analysis was carried out to investigate the effects of tunnel construction on nearby pile foundation. The subsoil of the model consists of two layers. The upper layer is saturated soft clay and extends to a depth of 18 m. Underneath there is a very dense layer of sand, which extends to a large depth.

To model the nonlinear stress-strain soil behaviour, the Hardening Soil model with small-strain stiffness mode (HSsmall) was used. The input parameters of the HSsmall model for both layers are the same as those of the centrifuge test (see Table 5.1). Due to the symmetry of the problem, only half of the model is analysed.

Figure 5.3 shows the model geometry used for the analysis (side and longitudinal views). The ground domain extends for a distance equal to 3.5 times the tunnel diameter (3.5 D_t) in the lateral and vertical directions (Yang et al. 2011; Zidan and Ramadan, 2015). In the longitudinal direction (Figure 5.3b), the soil domain extends eight times the diameter of the tunnel (8 D_t). Consequently, the reference 3D numerical model sizes are 64 m×28 m×28 m (length × width × height). These dimensions are appropriate to permit for any possible failure mechanism to develop and to avoid any influence of the model boundaries. Soil was simulated using a 10-node tetrahedral element.

Figure 5.4 shows the three dimensional finite element mesh used in the numerical analyses. The mesh consisted of 15745 soil elements and 21919 nodes. The diameter (D_t), and depth (H_t) of the tunnel are 8 m and 16 m ($2D_t$), respectively. To ensure a sufficiently high safety factor, the excavation was supported by t_l= 0.25 m thick concrete lining. The pile was assumed to be 24 m in length ($L_p = 3D_t$) and 1 m in diameter (d_p= $0.125D_t$). The horizontal distance between tunnel vertical axis and the free headed single pile was X_p= 8 m ($1D_t$).

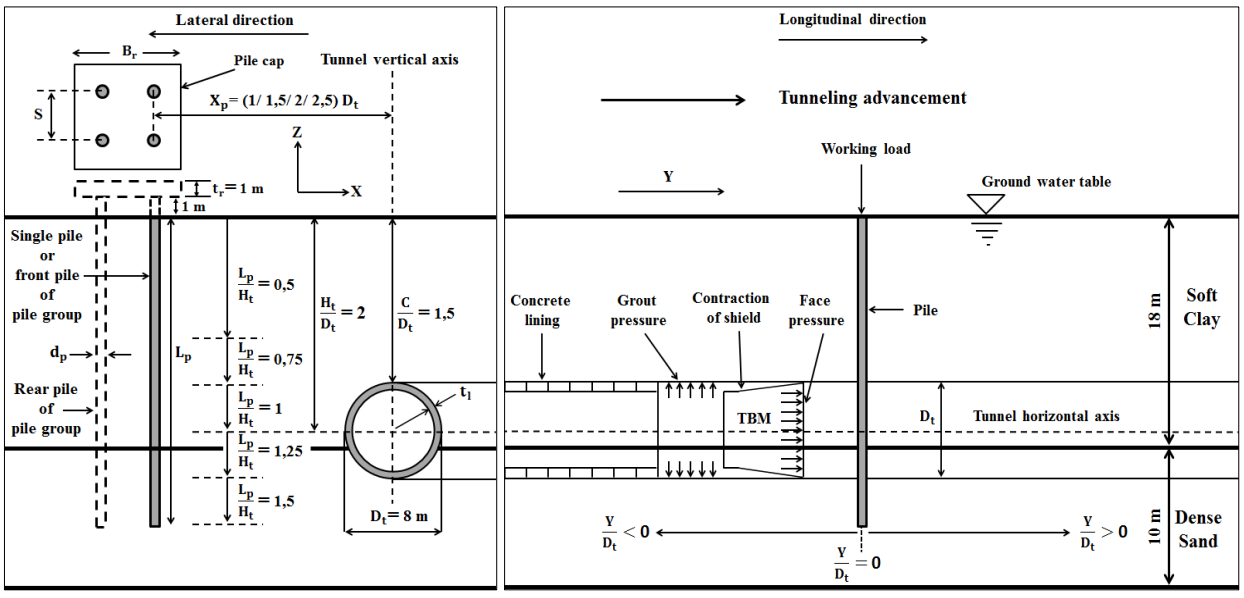

Figure 5.3 Typical geometry of the model used in this study (a) side view (b) longitudinal view

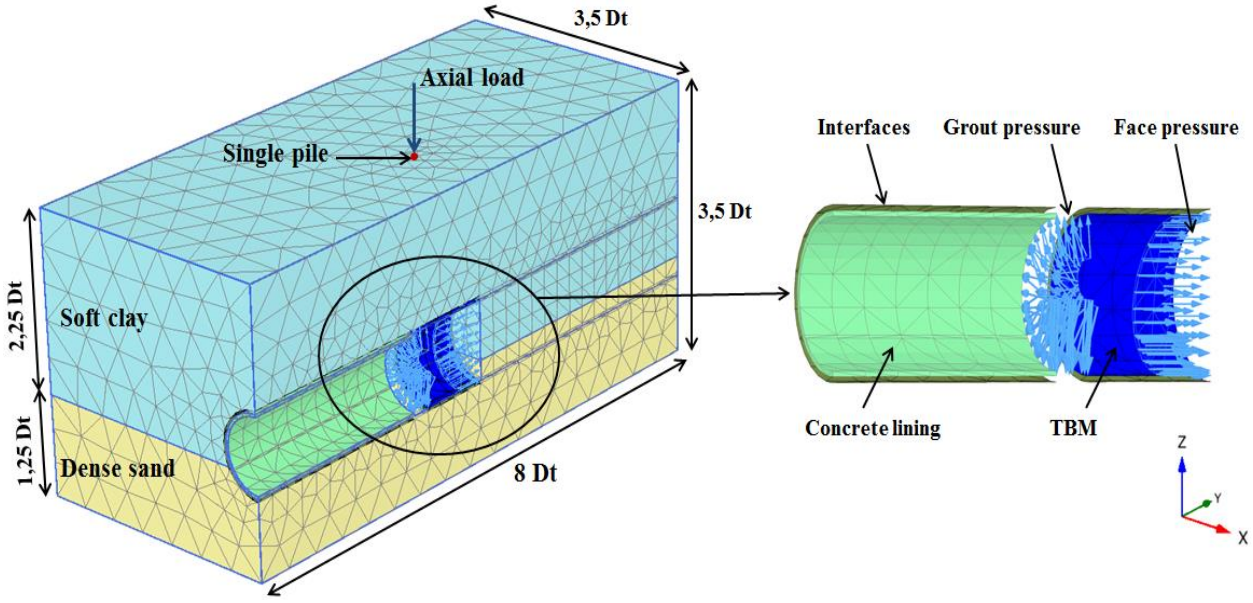

Figure 5.4 Three dimension finite element mesh

The pile was modelled using the embedded pile structural element. It consists of beam elements with special interface elements providing the interaction pile-soil. Material properties of the embedded pile used in this analysis are summarised in Table 5.2. The water table is at the ground surface and the pore pressure distribution is assumed to be hydrostatic. The tunnel boring machine shield (TBM) is 8 m long, and it was modelled using a 6-node triangular plate element. The concrete tunnel lining are modelled using 10-node volume elements with a specific weight γ = 24 kN/m^2, Young's modulus E_l = 30 GPa, and Poisson's ratio ν = 0.2.

To take into account the soil-structure interaction, positive interface elements of 12 nodes have been added to the plate element (around the TBM). The behaviour of the pile, tunnel lining, and the TBM is assumed to be elastic, linear and isotropic.

Table 5.2 Material properties of the embedded pile (L_p= 24 m)

Description/ Parameter/ Unit	Value
Unit weight, γ (kN/m^3)	24
Young modulus, E (GPa)	30
Diameter, d_p (m)	1
Skin resistance at top layer, T (kN/m) for Z_p=0→ 18 m	0→135.5
Skin resistance at bottom layer, T (kN/m) for Z_p=18→ 28 m	135.5→145
Base resistance (kN)	16560

5.3.2 Construction sequences

In practice, tunnel construction can be realized with different Tunnel Boring Machine (TBM) techniques: Open Face TBM, Slurry Pressure Balance (SPB), Earth Pressure Balance (EPB), and compressed-air TBM. In the current study the Slurry Pressure Balance technique (SPB) is used.

The whole construction activities included excavation, installation of the TBM, installation of tunnel lining, grouting the gap between the soil and the newly installed lining, and application of the support pressure to prevent active failure at the tunnel face. In each phase of tunnel advancement, the same construction sequences are repeated. The sequence of the installation of the pile itself is not taken into account; therefore the pile is assumed as "wished in place".

5.3.3 Numerical modelling procedures

The numerical modelling procedures consisted of three mainly steps: initial geostatic equilibrium, application of the working load at the pile head, and tunnel excavation. Due to the fact that TBM advances at a quite low speed and the permeability of sand layer is high, drained analysis was performed to examine the pile behaviour in long-term. Location of the tunnel face at any step is normalised by tunnel diameter (Y/D_t). Tunnel excavation was simulated from Y/D_t= -4 to +4 (-32 m to +32 m) in the longitudinal direction (Y), as shown in Figure 5.3. The pile axis was located at $Y/D_t = 0$.

In order to model the advancement of the TBM, computations are carried out in 32 successive steps after the application of pile loading. Therefore, at each step, the tunnelling rate of 2 m/day was assumed. The first four excavation steps represent the installation of the TBM shield. Next, grout pressure is applied 2m behind the shield. Followed by the laying of the precast concrete lining (each slice is 2 m in length and 0.25 m in thickness).

In order to simulate the volume losses due to the overcut zone and the conicity of TBM, contraction factor is used. Thus, contraction is applied to the TBM to simulate the reduction of the tunnel cross section. The TBM is slightly conical, and the tail diameter is assumed to be 8 cm less than the front one. This effect has been modelled using a total contraction of 1% in volume. The TBM causes a gap between the external diameter of the shield and the erected concrete lining at the tail end of the TBM which is filled with grout during the TBM advancement. The grouting process is important to lead the settlement of the soil surface to be within acceptable limits and provides stability for the surrounding soil. Thereafter it is assumed that the grout has settled and dewatered enough that no additional deformations are produced.

In the numerical simulation, the grouting pressure is modelled by a non-uniformly distributed load acting on the soil elements that directly follow the shield to avoid the collapse of surrounding soil. This distribution is kept constant with the advancement of the TBM. The grout

pressure has been set to 194.5 kN/m^2 at the top (tunnel crown), increasing to 328.5 kN/m^2at the bottom (increases linearly with depth by a rate of 16.5 $kN/m^2/m$). To prevent collapse of the soil in front of the TBM, the face support pressure is applied at the excavation face. The frontal tunnel pressure in this study is assumed to be 178.5 kN/m^2 at the top, increasing to 260.5 kN/m^2 at the bottom (tunnel invert). The pressure at the tunnel face is a bentonite-based pressure. Table 3 summarise the numerical modelling procedure.

Table 5.3 Numerical modelling procedures

Steps	Description
1	Generating the initial effective stresses using the K_0 procedure $K_0 = 1 - \sin\varphi'$.
2	Activate the single pile (modelled as 'wished in place').
3	Apply the working load at the single pile head (1.5 MN determined from pile load test), and allow excess pore pressure induced due to applied working load to dissipate.
4	Excavate the first 2 m by deactivating the soil element in 1 day for an excavated volume of 100 m^3, activateplate elements represent the TBM shield, interface elements, and application of contraction. After that applying a support pressure at the tunnel face.
5, 6	Repeat Phase 4 by excavating 2 m in each phase until excavates 6 m of the soil. Due to the TBM slight cone shape and the reduction of the diameter over the first 6 m length of the TBM, a linear contraction with a reference value C_{ref}= 1%, and increment $C_{inc,axial}$= -0.167 was activated in each phase.
7	In this phase the TBM advances from Y= 6 m to Y= 8 m ($1D_t$), with the same steps as the previous one, only apply to the last 2 m of the TBM a uniform contraction of 1% (the tail which has a constant diameter).
8	In this phase another tunnel advancement from Y= 8 m (1 Dt) to Y= 10 m, followed by application of the grout pressure to the back of the TBM.
9	In this phase another advances of the TBM (Y= 10 m to Y= 12 m), followed by the activation of the volume element representing the concrete lining.
10	Continue the construction process by the same rate of excavation 2m/day, until the last phase of excavation (i.e., Y = $+4D_t$) is completed in 32 days.

5.3.4 Two-dimensional numerical analysis

To judge the relevance of the 3D model, a two-dimensional numerical analysis using the PLAXIS 2D code with an assumption of plane strains (Brinkgreve et al. 2017), was also carried out. The characteristics for both layers (the soft clay and the dense sand) used in the 2D analysis

are the same as those of the 3D analysis. Both the model pile and tunnel lining are simulated using "Plate" structural element with thickness of 1 m and 0.35 m, respectively. The tunnel excavation was simulated by deactivating the two soil clusters inside the tunnel and the water pressure was eliminated by making the excavated area dry, then the lining was put in place (modelled using elastic plate elements). Using the contraction function, the volumetric contraction was then applied at the tunnel centre in the following calculation step to simulate the tunnelling-induced volume loss. The grout pressure, face pressure, and tunnel boring machine (TBM) advancement it cannot be modeled in 2D analysis. Figure 5.5 shows the 2D mesh of the numerical model.

Ong (2008) performed a comparative study of finite element analysis using PLAXIS 2D versus centrifuge modeling to investigate pile behavior subjected to lateral ground movement and the effect of smearing the properties of a 3D pile in a 2D finite element environment.

In 2D plane-strain finite element analysis, it is not possible to model the 3D nature of a pile because of the difficulty in selecting adequate parameters to represent 3D effect. As such, the actual properties of a 3D pile are "smeared" in the plane strain direction to obtain the "equivalent" pile properties per meter width. Indeed, the 3D nature of a pile is now represented by an equivalent wall. This can be done by considering the contact areas of a cylinder and a rectangular wall as shown schematically in Figure 5.6 for a single pile and a pile group.

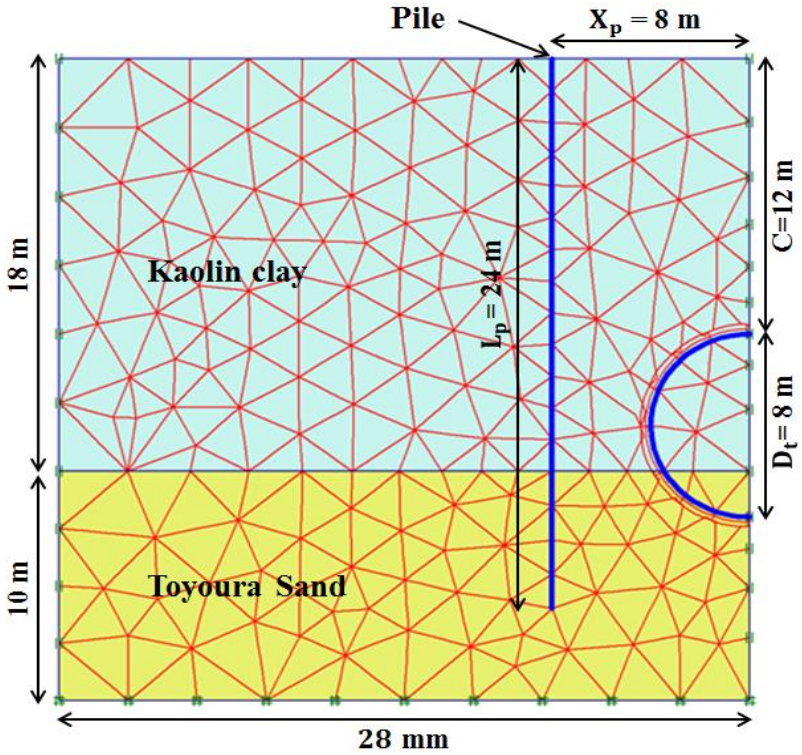

Figure 5.5 2D Finite element mesh

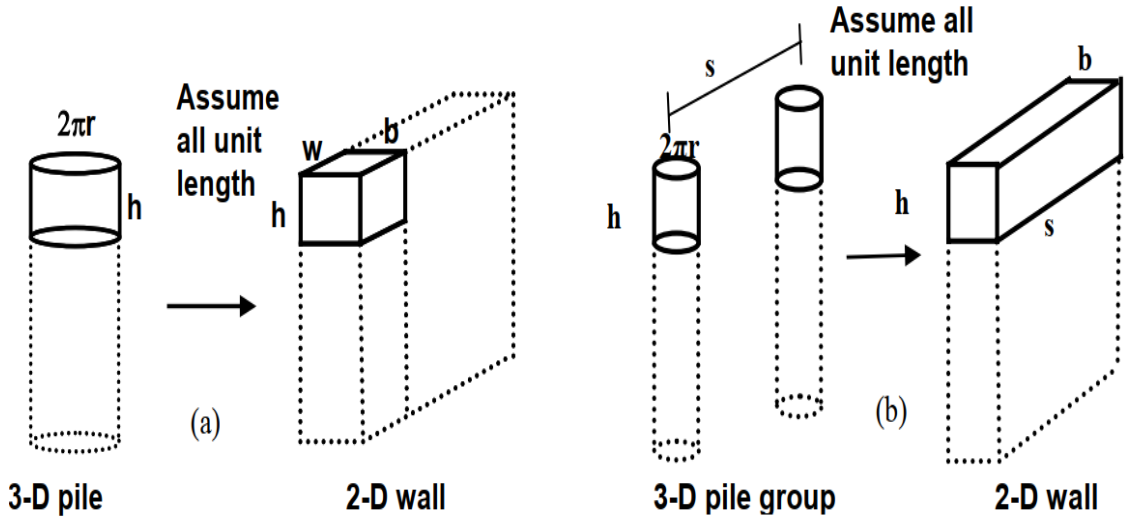

Figure 5.6 Method of smearing 3D pile to an equivalent 2D wall (a) single pile (b) pile-group, from Ong (2008)

Table 5.4 Method of converting response of equivalent wall to that of a pile for the case of a single pile

Pile response	**Quantity per linear m of wall as output by PLAXIS**	**Conversion to quantity per pile**
Bending moment (BM)	BM in kNm/m	BM×3d to obtain kNm
Axial or shear forces (F)	F in kN/m	F×3d to obtain kN

Table 5.5 Method of converting response of equivalent wall to that of a pile for the case of a group of piles

Pile response	**Quantity per linear m of wall as output by PLAXIS**	**Conversion to quantity per pile**
Bending moment (BM)	BM in kNm/m	BM×[(n-1)×s]/n to obtain kNm
Axial or shear forces (F)	F in kN/m	F×[(n-1)×s]/n to obtain kN

- **Single pile**

In the case of a single pile, by assuming all unit length for parameters r, h, w and b (i.e. all with value 1), the unit contact areas of the cylinder ($2\times\pi\times r\times h$) and the rectangular wall ($2\times h\times w$) are 2π and 2, respectively. This shows that the contact area of a 3D cylinder is actually larger by π (=3.142) than that of a 2D rectangular wall, thus the development of Equations (5.8) and (5.9). This value is important in the case of a single pile as it represents the extent of influence imposed by the single pile. In general, the formulations used to obtain a 2D equivalent wall for the case of a single pile can be written as:

Axial rigidity: $(E_pA_p) / (3d)$ (5.8)

Bending rigidity: $(E_pI_p) / (3d)$ (5.9)

Where E_p, A_p, I_p and d are the Young's modulus, sectional area, second moment of area and diameter of the pile, respectively.

- **Group of piles**

For the case of a pile group, the 3D single pile properties are multiplied by the number of similar piles in the plane-strain direction and smeared (divided) by the pile group centre-to-centre spacing, s, in the plane-strain direction as shown in Figure 5.6b. In general, the formulations used to obtain a 2D equivalent wall for a group of piles in the plane strain direction can be written as:

Axial rigidity: $n(E_pA_p) / [(n-1)(s)]$ (5.10)

Bending rigidity: $n(E_pI_p) / [(n-1)(s)]$ (5.11)

Where n is the number of piles in the plane strain direction and s is the centre-to-centre pile spacing between 2 piles in the plane strain direction.

By converting 3D piles to equivalent 2D wall, the magnitudes of bending moment and forces (axial or shear) will be output as kNm/m and kN/m, respectively. In order to obtain the "actual" pile bending moment and forces, multiplication of smeared dimensions is necessary. Tables 5.4 and 5.5 show the methods of converting response of equivalent wall to that of a pile for a single pile and group of piles, respectively. Nevertheless, the resulted deflections and rotations remain similar.

5.3.5 Determination of the axial load-carrying capacity of single pile and pile group

Excavating a tunnel close to a pile (single or in a group) not only causes soil deformations and stress release, but can also reduce the bearing capacity of the pile. Therefore, prior to tunnelling, it is necessary to determine the bearing capacity of the pile so that the working load to be applied on the pile could be deduced.

To achieve this objective a pile load test was thus carried out with absence of tunnel. Figure 5.7a shows the relationship between axial load and pile settlement for pile length of 24 m (L_p/H_t= 1.5). The settlement is normalized by the pile diameter (d_p). The ultimate load capacity of pile was determined using the displacement-based failure criterion proposed by Ng et al. (2001) for single pile with large diameter (greater than 0.6 m). The failure criterion is given by the following expression:

$$\delta_{ph,max} \cong 0.045\, d_p + \frac{1}{2}\frac{P_h L_p}{A_p E_p} \tag{5.12}$$

Where $\delta_{ph,max}$ is the maximum pile head settlement that defines the ultimate load capacity of the pile, d_p is the pile diameter, P_h is the pile head load, L_p is the pile length, E_p is the Young's modulus of the pile shaft, and A_p is the cross-sectional area of the pile.

For the reference model (L_p= 24 m), the load applied to the pile head was gradually increased to 5 MN with an increment of 250 kN. Based on the load settlement curve, the ultimate capacity of the pile was 4.5 MN. A working load of 1.5 MN was adopted with a factor of safety (FOS) of 3. A pile settlement of 0.29% d_p (2.9 mm) due to the applied working load was observed.

From the failure criterion, it is clear that the working load depend on the pile geometry, and soil conditions. Other loading tests were performed for different pile lengths and pile diameters as shown in Figure 5.8 (which will be used later).

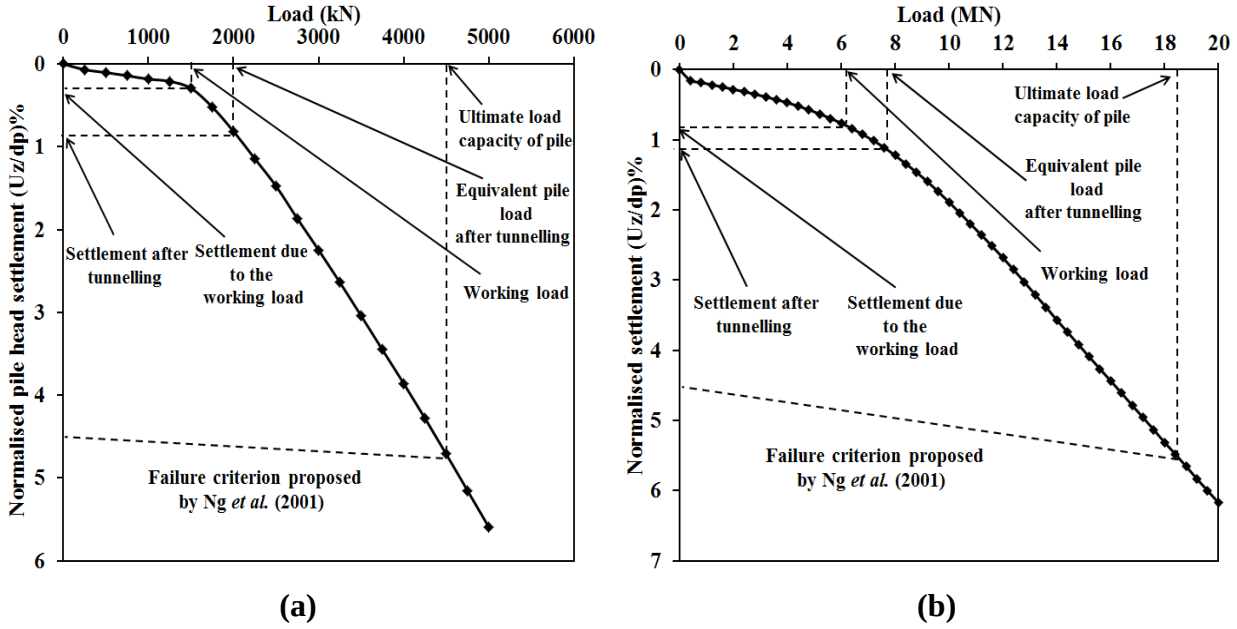

Figure 5.7 Load settlement relationship obtained from load test for (a) single pile (b) pile group

In order to highlight the pile length effect, pile responses are investigated using five different pile lengths (i.e. L_p/H_t = 0.5/ 0.75/ 1/ 1.25/ and 1.5). Using the failure criterion indicates that the working load is determined to be 92, 165, 360, 1180, 1500 kN, respectively. Pile diameters variation testing revealed that the working load is determined to be 1000, 1200, 1500, and 1800 kN, for pile diameters of d_p= 0.6/ 0.8/ 1/ and 1.2 m, respectively. For the case of L_p/H_t = 1.25 and 1.5, the pile head was loaded gradually to higher values as it is embedded in the sand layer (end bearing pile). Since the numerical model inincludes two layers, the analysis was carried out using two different piles, namely floating and end bearing pile.

As there is no failure criterion available for pile group, the failure criterion proposed by Ng et al. (2001) for single pile is adopted in many researches and in the current study to determine the ultimate pile group capacity as shown in Figure 5.7b. An axial load is applied on the pile cap and gradually increased to 20 MN corresponding to 24 m long pile group. Based on the adopted failure criterion, the ultimate load-carrying capacity of pile group is 18.3 MN. With a factor of safety of 3, the working load is determined to be 6.1 MN. For the case of free-head pile group, the working load determined from load test of single pile was applied to each pile head individually.

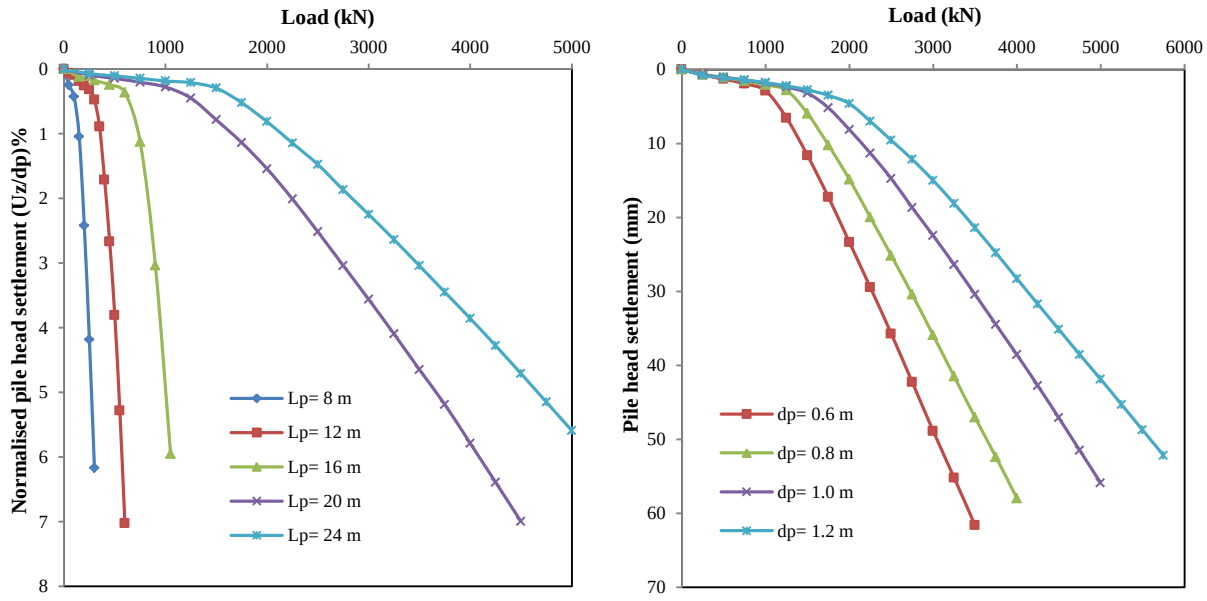

(a) **(b)**

Figure 5.8 Load settlement relationships (load tests) for different (a) pile lengths (b) pile diameters

5.3.6 Results and discussions

5.3.6.1 Soil movements in Greenfield conditions

The ground movements caused by tunnel construction need to be evaluated for safety issue implications on adjacent structures. Greenfield conditions (or free-field soil movements) are considered to be those occurring solely through tunnelling without interaction with nearby structures or foundations (i.e. without the presence of piles).

In this section, ground movements obtained from the numerical analysis (both 3D and 2D simulation) are compared with some existing empirical methods and also with some analytical closed-form solutions proposed in the literature. The tunnelling process is associated with surface settlement, subsurface settlement, and lateral deformations. The shapes of surface settlement trough during tunnel excavation are well described by a Gaussian distribution function (Peck, 1969). Ground surface settlement, S, is defined as:

$$S = S_{max} \exp\left(-\frac{X^2}{2i_x^2}\right) \tag{5.13}$$

with

$$S_{max} = \frac{V_s}{i_x\sqrt{2\pi}} = \frac{0.313\, V_l D_t^2}{i_x} \tag{5.14}$$

O'Reilly and New (1982) proposed $i_x = 0.5z_0$ for cohesive soils (clay, silt). Also Clough & Schmidt (1981) proposed an empirical relationship to estimate the settlement trough width as:

$$i_x = R\left(\frac{z_0}{D_t}\right)^{0.8} \tag{5.15}$$

Loganathan & Poulos (1998) proposed a closed-form analytical solution to predict surface settlements trough as:

$$S_{z=0} = 4\varepsilon_0(1-\nu)\, R^2 \frac{H}{H^2+x^2} \exp\left(-\frac{1.38x^2}{(H+R)^2}\right) \tag{5.16}$$

where: $S = S_{z=0}$ = vertical settlement trough at distance X/ S_{max} = maximum settlement above the tunnel axis/ X = lateral distance from the tunnel centerline/ i_x = trough width parameter (distance from the tunnel centreline to the point of inflection)/ $z_0 = H$ = tunnel depth/ V_s = the volume of settlement trough/ $V_l = \varepsilon_0 = \frac{V_s}{V_t}$ = ground loss ratio (volume loss)/ V_t = volume to be excavated/ R= tunnel radius/ D_t = tunnel diameter/ ν = soil poisson ratio.

For a volume loss of 1% and at the monitoring section (Y/D_t= 0), the surface settlement trough at the final step of tunnel excavation are shown in Figure 5.9a. The distance from the tunnel axis and the soil settlement are normalized by the tunnel diameter (D_t). The results

obtained from numerical analysis are compared to those obtained by the Gaussian distribution function (Peck, 1969) using the trough width parameter proposed by O'Reilly and New (1982) and Clough & Schmidt (1981), where i_x is 8 m and 6.97 m, respectively. The trough width i_x in our case is about 8.5 m.

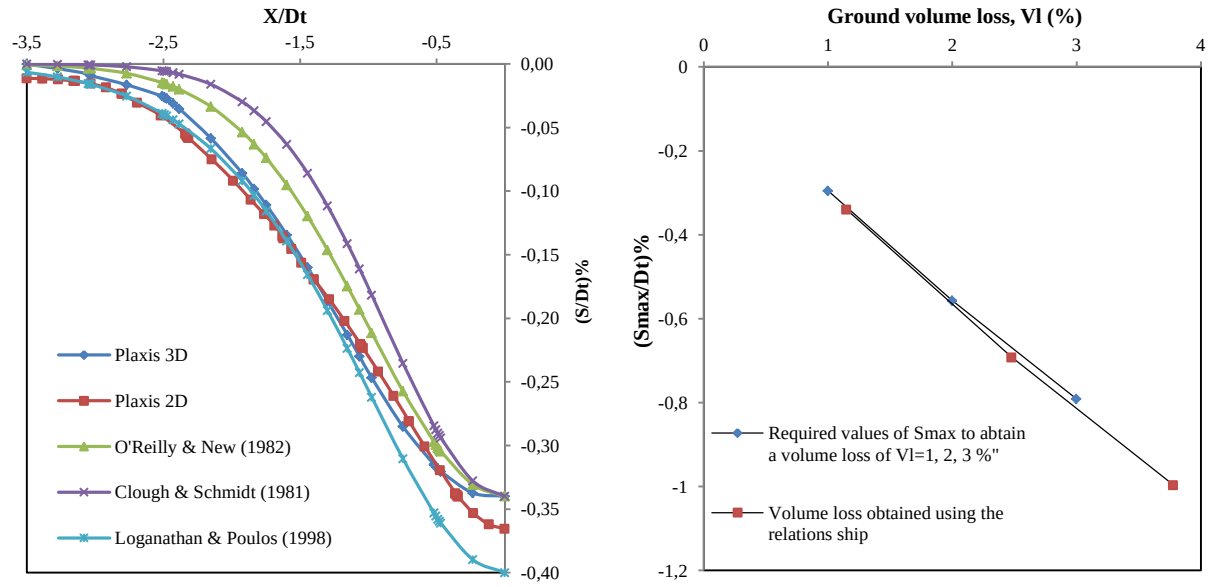

(a) **(b)**

Figure 5.9 Soil settlement (a) surface settlement trough in transverse direction at (Y/D_t= 0) for the last step (Y/D_t = +4), (b) relationship between maximum ground settlement and volume loss

The results showed that the maximum ground settlement S_{max} above the tunnel centreline is equal to 27.2 mm (about 0.34%D_t) for the numerical results and those obtained using the Gaussian distribution function. While S_{max} is relatively large for the solution proposed by Loganathan & Poulos (1998). However, this comparison reveals that the empirical and analytical results agree well with those of the numerical analysis in terms of the shape and the amplitude of the settlement trough. The numerical results showed that the maximum vertical displacement at the tunnel crown $S_{c,max}$ is eqoual to 32 mm (0.4D_t) which represent 1.2 times of S_{max}.

The settlement trough is also characterized by its total volume V_s. This volume is expressed as a function of the maximum settlement S_{max} and the parameter i_x as follows:

$$V_s = i_x \sqrt{2\pi}\, S_{max}. \qquad (5.17)$$

Compared to the theoretical excavated volume (V_t =50.24 m^2/m), the volume of the settlement trough is equal to 0.58 m^2 (1.15% V_t). For a trough width of 8.5 m, and S_{max} of 27.2 mm, the volume loss V_l =1.15% is very close to the inserted value in PLAXIS (1%).

In this study, three different values of volume loss considered V_l =1/ 2/ and 3%, which gives three different values of S_{max} = 27.2, 55.4, and 79.76 mm, respectively. Therefore, trough width of i_x = 8.5/ 9/ and 9.5m. Using V_s function, the obtained volume loss is V_l = 1.15, 2.38, and 3.78%, respectively, as shown in Figure 5.9b. This figure illustrates also the required values of S_{max} that should be abtained to reach a volume loss of V_l= 1, 2, 3 %. Also it's evident that an approximate linear relationship exists between maximum settlement and volume loss. The results show that for $V_l \geq$1%, the contraction function used in PLAXIS gives slightly conservative results, this explain the adopted reference model with an inserted volume loss of V_l =1%.

To estimate the subsurface settlement S_z at any depth z, Loganathan & Poulos (1998) and Mair et al. (1993), presented a closed-form solution and an empirical method given by Eqs 5.18 and 5.19, respectively.

$$S_z = \varepsilon_0 R^2 \left(-\frac{(z-H)}{x^2+(z-H)^2} + \frac{(3-4\nu)(z+H)}{x^2+(z+H)^2} - \frac{2z\left[x^2-(z+H)^2\right]}{[x^2+(z+H)^2]^2}\right) \exp\left[-\left(\frac{1.38x^2}{(H+R)^2} + \frac{0.69z^2}{H^2}\right)\right] \quad (5.18)$$

$$S_z = \left(\frac{1.25*V_l}{0.175+(0.325*(1-z/z_0))} * \frac{R^2}{z_0}\right) \exp\left(-\frac{x^2}{2*\left(\frac{0.175+(0.325*(1-z/z_0))}{(1-z/z_0)}\right)^2 *(z_0-z)^2}\right) \quad (5.19)$$

Figure 5.10a shows the subsurface settlement profiles at the tunnel centreline obtained from the numerical analysis compared to those estimated from Mair et al. (1993) and Loganathan & Poulos (1998). The results showed that at the ground surface and at the tunnel crown, the subsurface settlement S_z is equal to the maximum ground settlement S_{max}, and to the maximum vertical displacement at the tunnel crown $S_{c,max}$, respectively.

For the horizontal movements, Loganathan & Poulos (1998) presented a closed-form solution to predict the lateral ground movements S_x, as follows:

$$S_x = -\varepsilon_0 R^2 x \left(\frac{1}{x^2+(H-z)^2} + \frac{3-4\nu}{x^2+(H+z)^2} - \frac{4z(z-H)}{(x^2+(H+z)^2)^2}\right) \exp\left[-\left(\frac{1.38x^2}{(H+R)^2} + \frac{0.69z^2}{H^2}\right)\right] \quad (5.20)$$

Besides, O'Reilly and New (1982) approximated the surface horizontal displacements by:

$$S_x = -\frac{x*S}{z_0} \quad (5.21)$$

Figure 5.10b compare the surface horizontal displacements in Greenfield conditions (PLAXIS 3D) with those obtained using equations 5.20 and 5.21. The Figure shows good agreement between the results especially in the proximity of the tunnel centreline ($1> X/D_t >0$). The results reveal that the maximum values are induced at a distance of $X/D_t = 1.15$ (about 9 m from tunnel centreline).

The results of the 2D calculation are plotted in the same figures for comparison with those of the 3D calculation. A good agreement is noticed in terms of surface settlement and subsurface settlement. While in terms of horizontal displacements, the 2D numerical results are over-estimated.

Figure 5.11a shows the deformed mesh when the tunnel face is located at $Y/D_t = 0$. In this Figure, the settlement trough above the tunnel is clearly visible and the maximum settlement is occured at the tunnel centreline. The results from the calculations are quite realistic and agree well to the field measurements and the typical Greenfield ground movements associated with tunnelling (Attewell et al. 1986). Figure 5.11b shows the shadings of the total displacements of the soil and Figure 5.11c shows the settlement trough at the ground surface at the same location. These figures confirm the obtained results of the deformed mesh and show in more details where the largest displacements occur (i.e. just above the tunnel crown), which are somewhat larger than that at the soil surface.

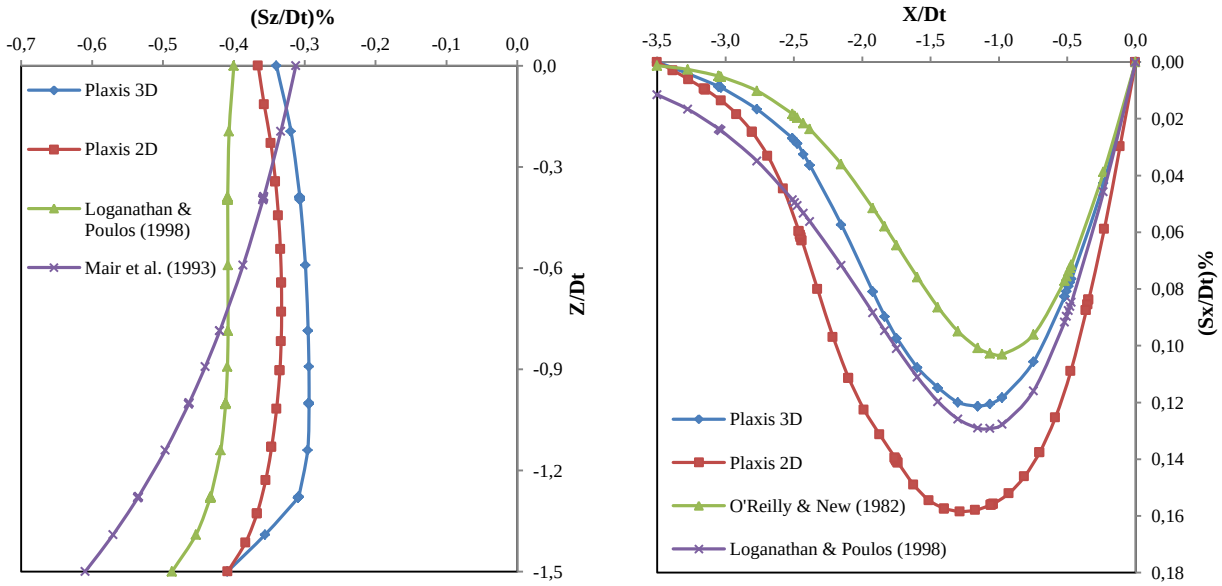

(a) **(b)**

Figure 5.10 Comparison of soil movements (a) subsurface settlement (b) lateral movement ($Y/D_t = +4$)

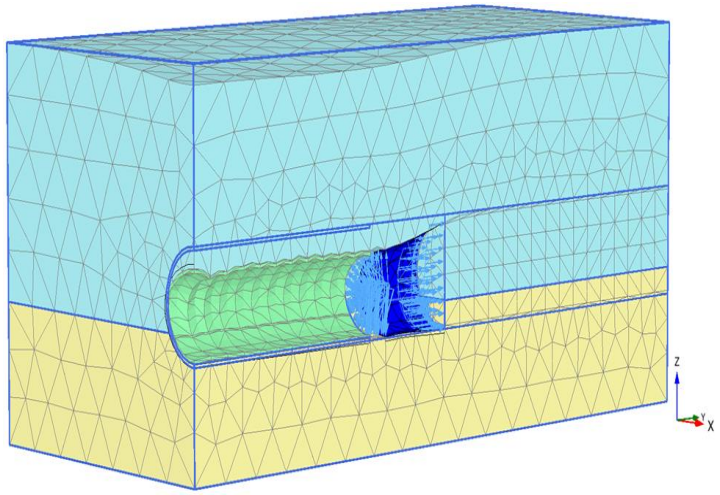

(a)

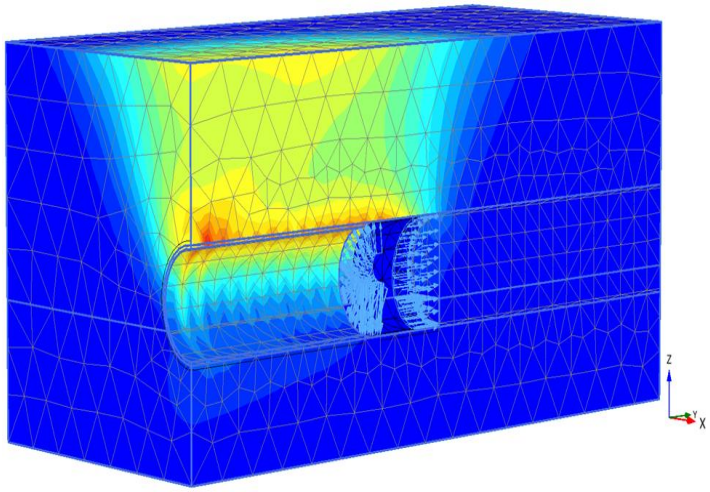

(b)

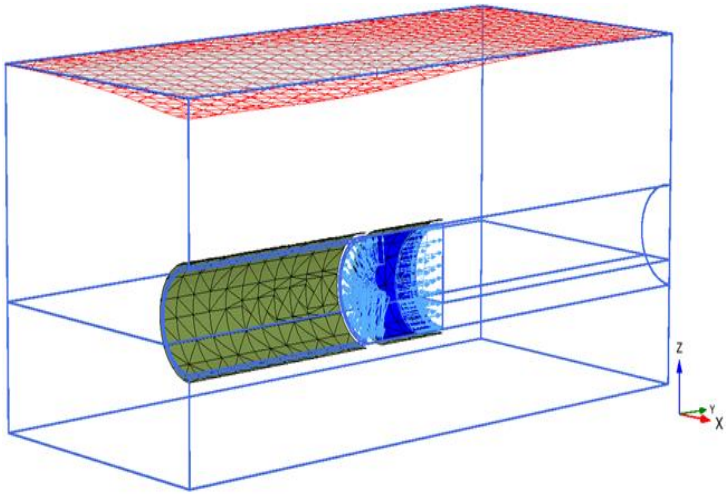

(c)

Figure 5.11 PLAXIS 3D output results (Greenfield condition) at tunnel face location of ($Y/D_t = 0$) (a) deformed mesh (b) shadings of the total displacements of the soil (c) settlement trough at ground surface level

5.3.6.2 Pile responses

The digging of a shallow tunnel induces more or less significant disruptions in the internal balance of the surrounding soil volume, which causes deformations and displacements of the soil in both horizontal and vertical directions. In urban areas, this phenomenon can affect the stability of adjacent structures, which makes estimating the effects of these movements on existing pile foundations a major challenge for designers.

5.3.6.2.1 Pile lateral responses

Figures 5.12a and 5.12b show the distributions of the lateral deflection induced along the pile in the transverse and longitudinal directions due to the tunnelling operations. The results reveal that during tunnel excavation, the lateral pile deflection in the longitudinal direction depends on the current location of the tunnel face; a movement of the pile towards the excavation face is noted with the advancement of this one, which means a tilting backwards when the front approaches, then forwards after it has passed.

Unlike in the longitudinal direction, in the transverse direction, the pile deflection is always oriented towards the tunnel axis (a cantilever type deflection) regardless of the location of the working face. Figure 5.12a shows that the lateral deflection U_x increases with tunnel advancement. Also, the maximum deflection occurred at the pile head and decreased with depth until the pile toe.When the tunnel face reaches and then passes the pile location ($Y/D_t \geq 0$), the lower part deflects away from the tunnel with slight shift of the pile toe even with 6 m of pile embedment in the underlying dense sand layer (about $0.25\mathrm{L_p}$). This figure also reveals that the lateral displacement of the pile U_x reaches its maximum value of about 7.14 mm ($0.714\%d_p$) when the tunnel face is at a distance of ($Y/D_t \geq 2$) and stops increasing when the tunnel face exceeds this distance.

Figure 5.12b shows that the pile deflection in the longitudinal direction U_y is induced mainly before the passage of the tunnel face ($Y/D_t < 0$). The maximum value occurs at pile head when the tunnel face reaches the pile position ($Y/D_t = 0$) and it is about 4.5 mm ($0.45\%d_p$), which is 1.6 times less than the maximum value occurred in the transverse direction. After the passage of the tunnel face, a decrease of pile deflection is observed. This may be because of lining installation (especially when the lining installs at the level of pile location) which helps soil stabilisation behind tunnel face. Thus, a combined upward heave-longitudinal soil movement is induced ($Y/D_t \geq 1$) which pushes the pile forward. When the tunnel face pass from ($Y/D_t = 0$) to ($Y/D_t = +4$), pile deflection becomes less about 4.5 times.

Figures 5.12c and 5.12d show the distributions of the tunnelling-induced bending moment along the pile in the transverse and longitudinal directions, respectively. For both directions, the maximum values of the induced bending moment occur near the horizontal axis of the tunnel (Z_p=$0.67L_p$). A slight bending moment induced in the lower part due to 6 m of pile embedding in the underlying dense sand layer. Since the pile head was unconstrained, zero

bending moments were obtained from the numerical results at the pile head. Figures 5.12c shows that the bending moment in the transverse direction (M_{yy}) increases significantly due to the increasing in lateral deflection with tunnel advancement, and it remains negative almost all along the pile(Z_p=0.87L_p).

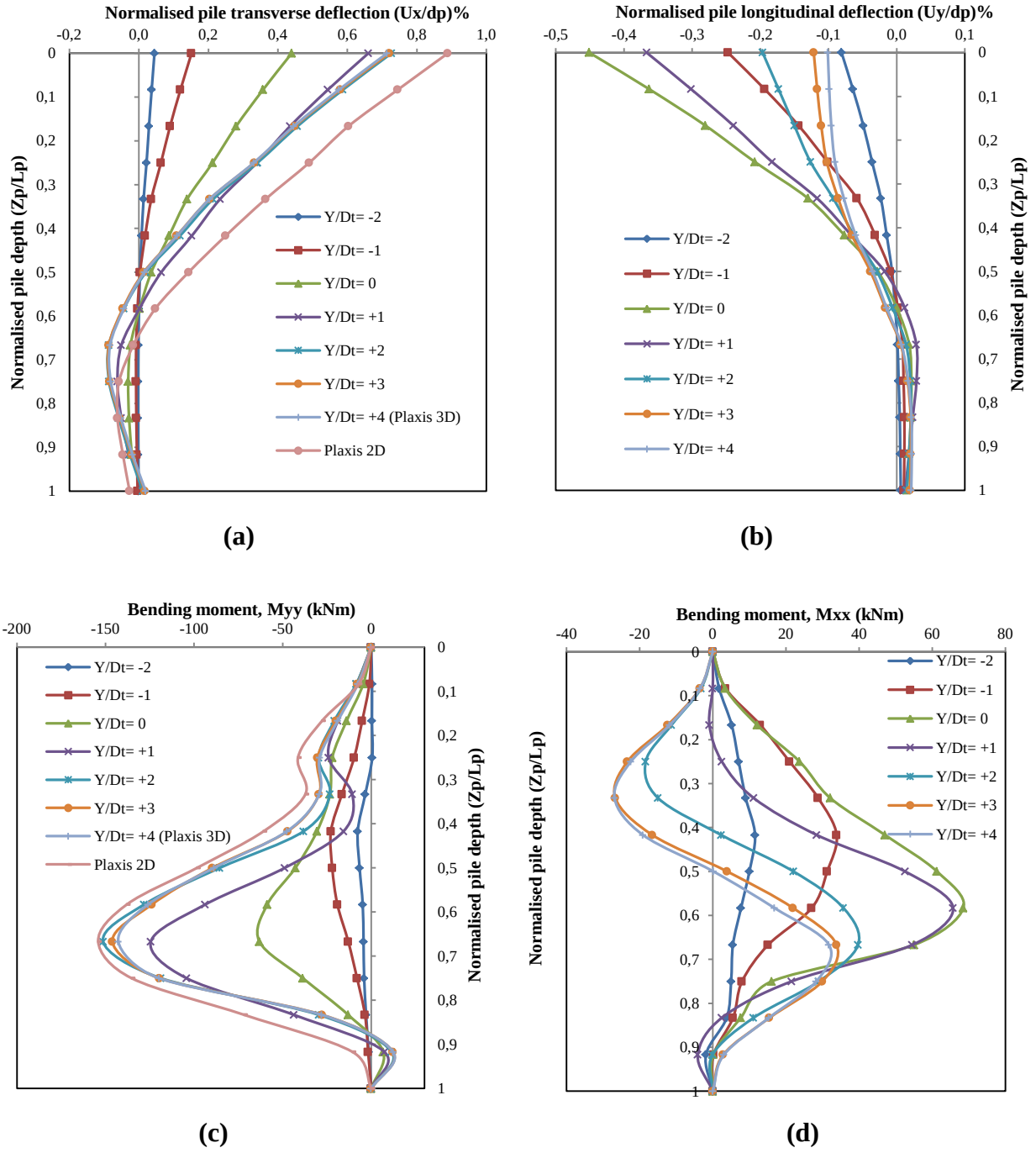

Figure 5.12 Pile lateral responses in transverse and longitudinal directions

Figure 5.12d shows that the bending moment in the longitudinal direction (M_{xx}) is mainly induced before the passage of the tunnel face due to the increase in lateral deflection from Y/D_t =-2 to Y/D_t =0. The bending moment along the whole pile is positive. When the tunnel face location becomes greater than $Y/D_t \geq 0$, a negative bending moment has developed at the top of the pile (Z_p=0.5L_p). Comparing Figure 5.12c and 5.12d, the magnitude of maximum bending moments is higher in the transverse direction about twice than that in the longitudinal direction.

In order to properly compare the results of the 2D model with those of the 3D model, the results of the 2D calculations are reported on the same figures. The deflection and bending moment profiles of the pile in the transverse direction show good agreement with the 3D calculations, both for the form of the curves and for the order of magnitude. Nevertheless the maximum lateral displacement of the 2D analysis is overestimated by 25%. This difference may be due partly to the fact that tunneling is inherently a three-dimensional problem (Houhou et al. 2016; Migliazza et al. 2009), and partly to the numerical modeling method of the pile itself.

In fact in the 2D model, it is very difficult to perform the 3D effect of a pile due to the difficulty in specifying the suitable pile parameters. In the 2D model, the pile is simulated by a plate element, whereas in 3D analysis it is simulated by an embedded pile element. So, the real properties of a pile are smeared in the direction of the plane strain model to obtain the equivalent properties of the pile per meter of width (performed by an equivalent 2D wall).

5.3.6.2.2 Pile vertical responses

Figure 5.13a shows the distributions of normalized pile settlement along the pile depending on the advancement of the working face. It should be noted that U_z is the total pile settlement combined with the effect of service pile loading and tunnelling process. It can be seen that the developed settlement increases with the progress of the tunneling and a maximum value of 8.4 mm (0.84%d_p) is observed at the pile head.

Figure 5.13b illustrates the skin resistance evolution along the normalised pile depth (Z_p/L_p). It can be seen that when the pile is in front of the working face (Y/D_t <0), a positive skin resistance develops along the entire length of the pile to bear the applied load and increases linearly in depth until the pile toe reaching a maximum skin resistance of 145 kN/m. Consequently, the normalised axial load decreased from the pile head to the toe, as shown in Figures 5.13c, where P is the axial pile force at a certain depth and P_w is the working load applied on the pile head before tunnelling (1500 kN). However, when the tunnel face exceeds the vertical axis of the pile ($Y/D_t \geq 0$), negative skin friction is developed along the upper part of the pile (above the tunnel horizontal axis), as a result the axial load increased from the pile head and achieves a maximum value of (P/P_w=1.25) at a depth of (Z_p/L_p=0.45). The negative skin friction leads to a drag load in the pile and therefore to an increase in pile settlement, as shown in Figure 5.13a.

Figure 5.13c also reveals that no significant change in the axial load at the pile head, while at the pile toe the axial force increases with the advancement of the tunnel face (more loads transferred to the tip of the pile), which affects the performance of the pile in service.

From Figure 5.13, it can be seen that when the face of the tunnel becomes sufficiently forward of the vertical axis of the pile ($Y/D_t \geq 1$), pile settlement, axial load and skin friction stagnate (does not change in shape or magnitude viewpoint).

By comparing 3D and 2D results, in terms of vertical displacement U_z and induced axial force, it is found that the 2D numerical results are overestimated.

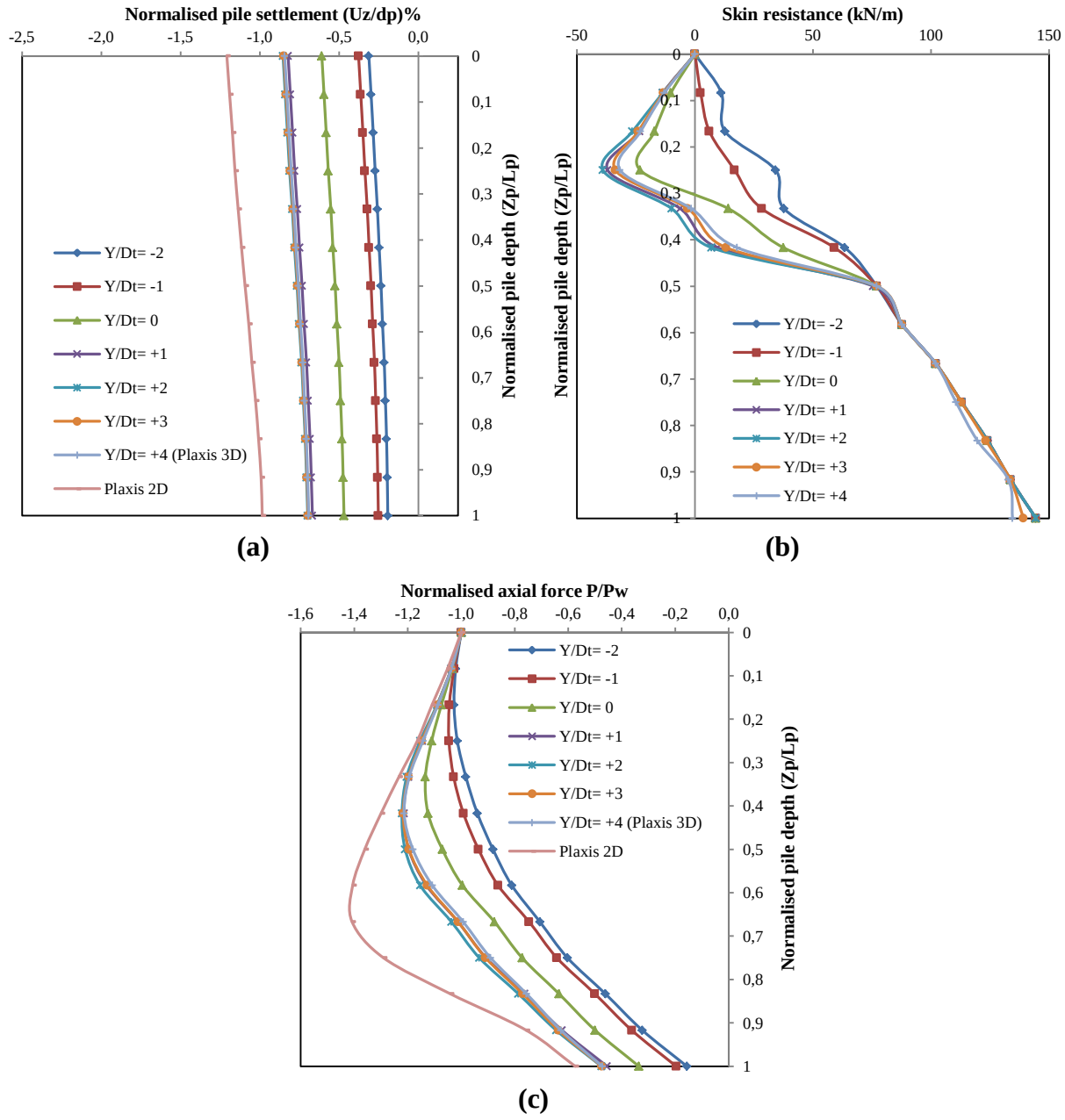

Figure 5.13 Pile vertical responses (a) pile settlement (b) skin resistance (c) axial load

From Figure 5.14 which shows the contours of the total displacement of the soil around the pile and tunnel, it can be noted that the soil as well as the pile undergo the same movement laterally towards the tunnel. This phenomenon of movement is due to the loosening of the soil during the digging of the tunnel (Stresses relief around the excavated zone). It should also be noted that most of the movements occur in the upper part of the pile (above the tunnel crown level) reflecting a cantilever type displacement profile (see Fig. 5.12a).

By comparing the behavior of the soil in the 3D model with that of the plane strain model, it can be seen that the soil volume mobilized in the 2D model is relatively greater. The extent of the ground movement both at the surface and in depth is larger in the 2D model.

At depth, the soil movements in the 2D model slightly exceed the pile toe (Fig. 5.14b), while in 3D model it does not even reach the toe of the pile (Fig. 5.14a).Thus, as already observed in Figure 5.12a, the movements obtained by the plane strain analysis are relatively overestimated. Therefore, it was shown that plane strain simulations could give conservative results.

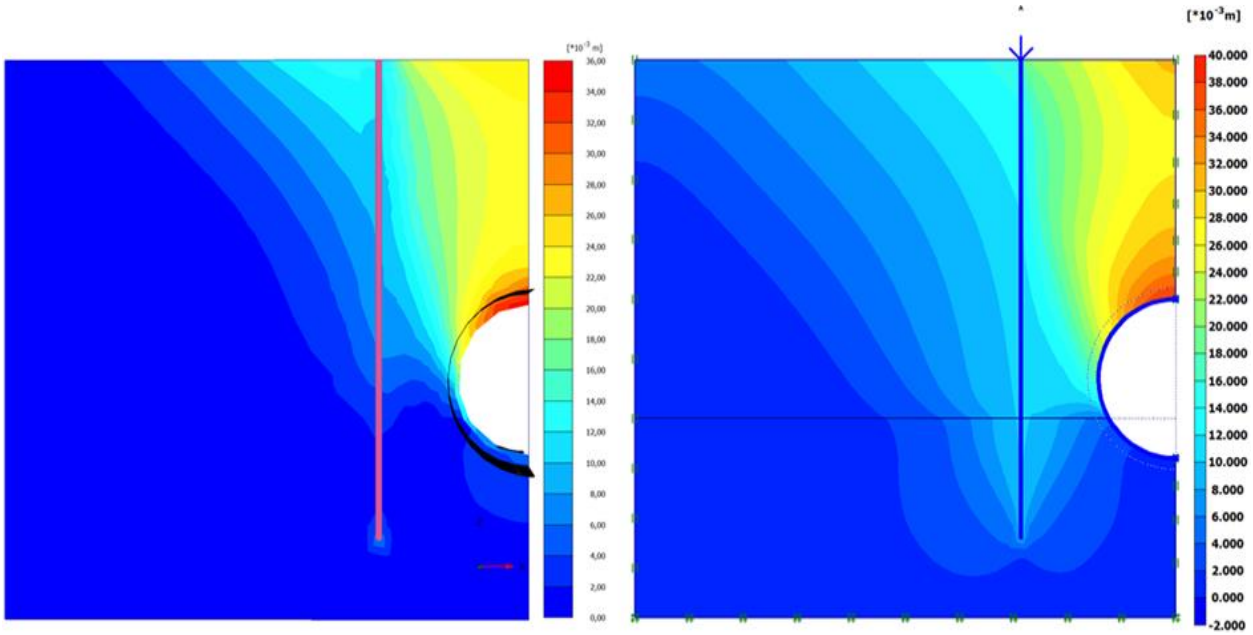

(a) **(b)**

Figure 5.14 Total displacement contours of the soil at (Y/D_t =0) (a) 3D simulation (b) 2D simulation

5.4 Parametric study

Given full soil-structure interactions, a 3D parametric study was carried out by varying certain key parameters to study their influence on single pile performance. The numerical model already studied in section 3 is used as a reference model for this parametric investigation. Table 5.6 summarizes the key parameters used in this parametric analysis. In addition, the pile group effect has also been investigated. For this purpose a configuration of 2×2 pile group with two cases of pile head conditions was considered.

Table 5.6 Parameters used in the parametric analysis

Parameters	Notations	Units	Variations
Normalised pile location	X_p/D_t	/	1 (ref)/ 1.5/ 2/ 2.5
Volume loss	V_l	[%]	1(ref), 2, 3
Normalised pile length	L_p/H_t	/	0.5/ 0.75/ 1/ 1.25/ 1.5 (ref)
Diameter of the tunnel	D_t	[m]	6/ 8 (ref)/ 10
Normalised tunnel depth	H_t/D_t	[m]	1.5 / 2(ref)/ 2.5
Pile diameter	d_p	[m]	0.6/ 0.8/ 1 (ref)/ 1.2
Over consolidation ratio	OCR	/	1 (ref)/ 1.25/ 1.5

5.4.1 Effect of volume loss

The effect of volume loss on ultimate pile responses for different positions of the tunnel face is shown in Figure 5.15. In this analysis, three different values of volume loss were considered V_l =1, 2 and 3%. It can be seen that all peak pile responses increase exponentially with increasing volume loss. As long as the face of the tunnel is relatively far from the pile location ($Y/D_t \leq$ -2), it can be said that the pile responses are considered negligible regardless of the volume loss.

From Figures 5.15a, 5.15b, 5.15c, and 5.15d, which represent the evolution of the maximum of the normalised pile head settlement (U_z/d_p), normalised pile lateral deflection (U_x/d_p), pile bending moment in lateral direction (M_{yy}), and normalised pile axial force during the advancement of the tunnel face, respectively, it can be seen that the maximum pile responses increase significantly with increasing volume loss when the tunnel face passes from Y/D_t = -2 to +2. These figures also reveal that there is no additional effect of the volume loss on the behavior of the pile when the tunnel face progress further away from the position of the pile ($Y/D_t \geq$2).

When the volume loss increases from 1% to 3%, the pile head settlement, pile lateral deflection, pile bending moment, and pile axial force increase by a maximum of 83%, 140%, 53%, and 12%, respectively.

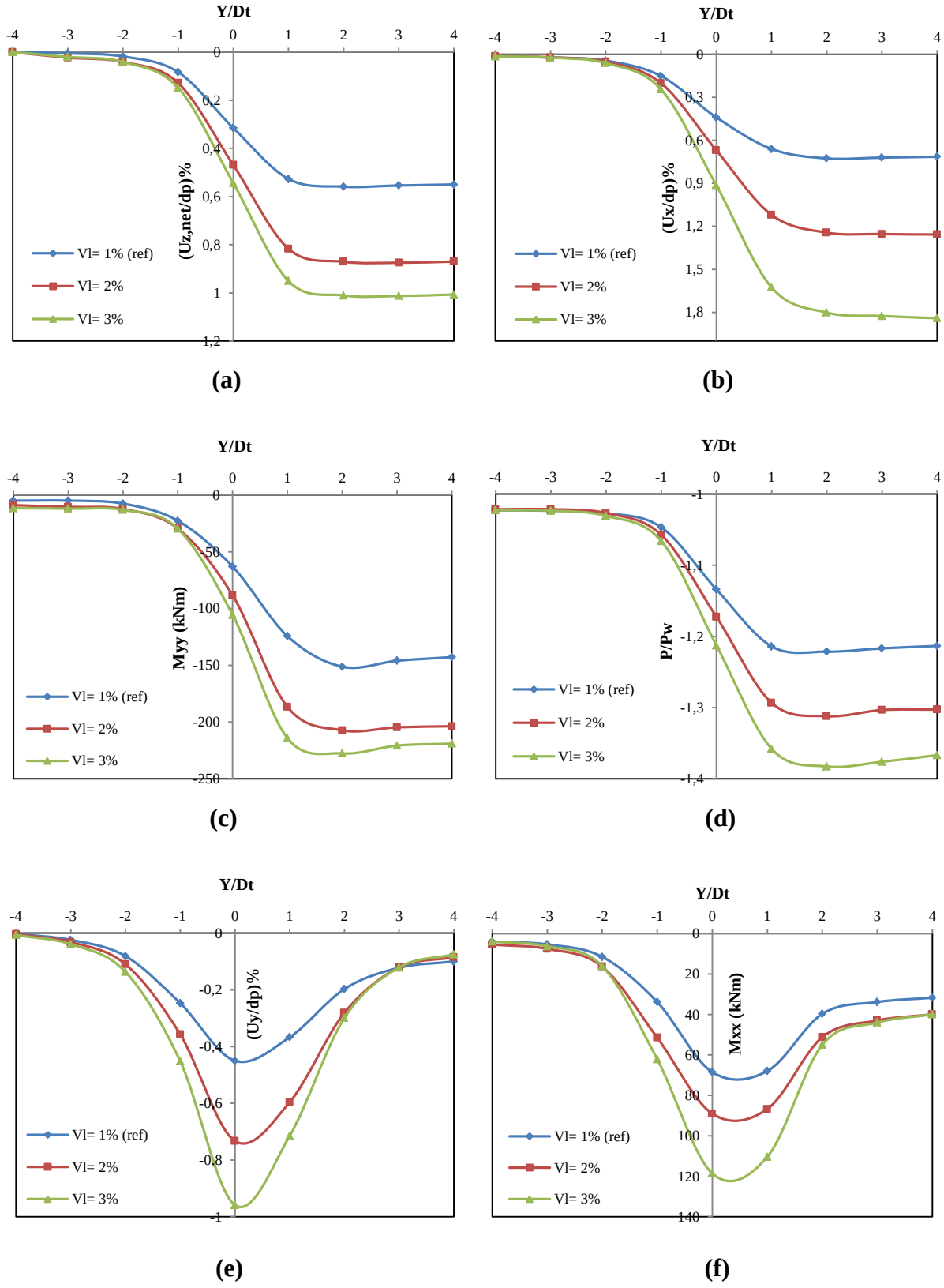

Figure 5.15 Effect of volume loss on ultimate pile responses during tunnel advancement

With regard to the behavior of the pile in the longitudinal direction, it can be seen that the pile behaves differently than in the transverse direction as shown in figures 5.15e and 5.15f. The maximum bending moment (M_{yy}) and deflection (U_y) are induced mainly when the tunnel face reaches the pile location ($Y/D_t = 0$), then tend to decrease until the face of the tunnel is away from the pile by three times the diameter of the tunnel ($+3D_t$). However, beyond this distance, the behavior remains unchanged.

Excavating a tunnel close to a pile not only causes ground deformations, but also can reduce the pile bearing capacity. Some researchers have used centrifuge tests or numerical analyzes to study the tunnel impact on the pile bearing capacity (Ng et al. 2001, 2013; Soomro et al. 2020b).

Pile bearing capacity is often inferred using settlement criteria, and pile settlements induced by tunnel excavation were correlated with the apparent loss of pile capacity (ALPC). Owing to the initial applied working load (1.5 MN), the pile has settled 2.94 mm in the case of 1% volume loss, and an additional pile head settlement of 5.5 mm ($0.55\%d_p$) was induced due to tunnelling. Therefore, a total pile settlement of 8.44 mm is deduced (combined effect of applied load and tunnelling). So, based on these results and using the load-settlement relationship obtained by Ng et al. (2013) from load test for single pile with and without tunnelling, an equivalent pile load after tunnelling of 2 MN is deduced (see Figure 5.7a). Thus, an additional load of 0.5 MN is induced due to tunnelling. Based on the failure criterion proposed by Ng et al. (2013), the ultimate load capacity of the pile was 4.5 MN. Therefore, it can be considered that an ALPC of 11% occurred due to tunnelling. In the case of volume loss of 2% and 3%, the total pile settlement is 11.64 and 13 mm, and the deduced equivalent applied loads are 2.25 and 2.4 MN, respectively. As a result, the apparent loss of pile capacity (ALPC) is17% and 20%, respectively.

Based on the results of the apparent loss of pile capacity (ALPC), it is suggested that the serviceability limit state of the pile should be taken into account for the design of the piles due to tunnelling.

5.4.2 Effect of pile location

In order to study the effect of pile location on pile responses at the last phase of the tunnel excavation ($Y= +4D_t$), the numerical reference model has been tested for four different normalised values of the pile location with respect to the vertical axis of the tunnel ($X_p/D_t = 1$; 1.5; 2; 2.5). The maximum distance X_p has been set to $2.5D_t$ so that it corresponds at the maximum vertical limit of the tunneling influence zone defined by Mroueh and Shahrour (2002) and Al-Omari et al. (2019).

Figure 5.16 shows the distributions of bending moment (M_{yy}), lateral deflection U_x, pile settlement U_z, and axial force of a single pile with length L_p= 24 m located at different distances X_p from the tunnel axis. Generally the numerical results indicate that the pile location has a significant effect on pile behaviour. It can be seen that pile responses decrease significatlly with

increasing pile location. As for the shape of the curves, they are quite similar with that of the reference case. Figure 5.16 indicates that in all cases the maximum values of the normalised lateral deflection U_x and normalized pile settlement U_z occured at the pile head. On the other hand, the results show that there is slight shift upwards of the maximum induced bending moment (M_{yy}) and normalised axial load (P/P_w) with decreasing of pile location. From the Figure 5.16, it can also be noted that when X_p increases from 8 m to 20 m, the maximum response of the pile decreases by about 80% for the lateral deflection, 57% for the pile settlement, 72% for the bending moment, and 15% for the axial load.

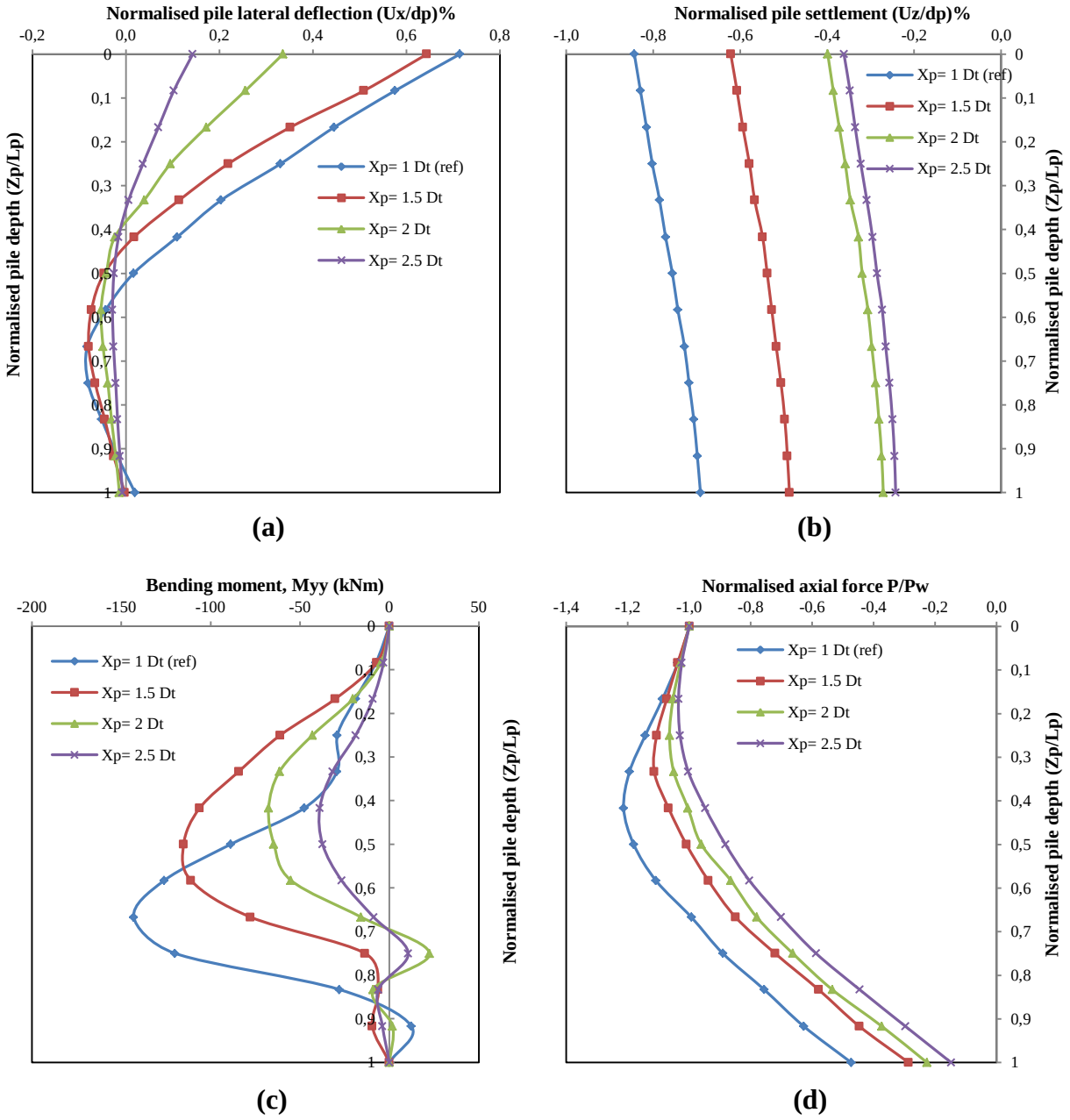

Figure 5.16 Effect of pile location (X_p) on (a) pile lateral deflection (b) pile settlement (c) bending moment (d) axial load (Y/D_t = +4)

For each pile location value, to better understand the single pile behaviour, the pile response was also analyzed for several values of the pile length. Figure 5.17 shows the distribution, for different pile lengths, of the maximum induced lateral bending moment, normalised lateral deflection, normalized pile settlement, and the axial force of a single pile located at different distances X_p from the tunnel vertical axis.

The curves shown in Figure 5.17 indicate that when the pile is farther from the tunnel axis and for any pile length, the pile responses decrease exponentially. In terms of axial load and bending moment of the pile, this tendency is more obvious when the pile length is relatively important ($L_p/H_t>1$). However, in terms of horizontal and vertical pile displacements, this trend is more marked when the pile length is relatively short ($L_p/H_t<1$).

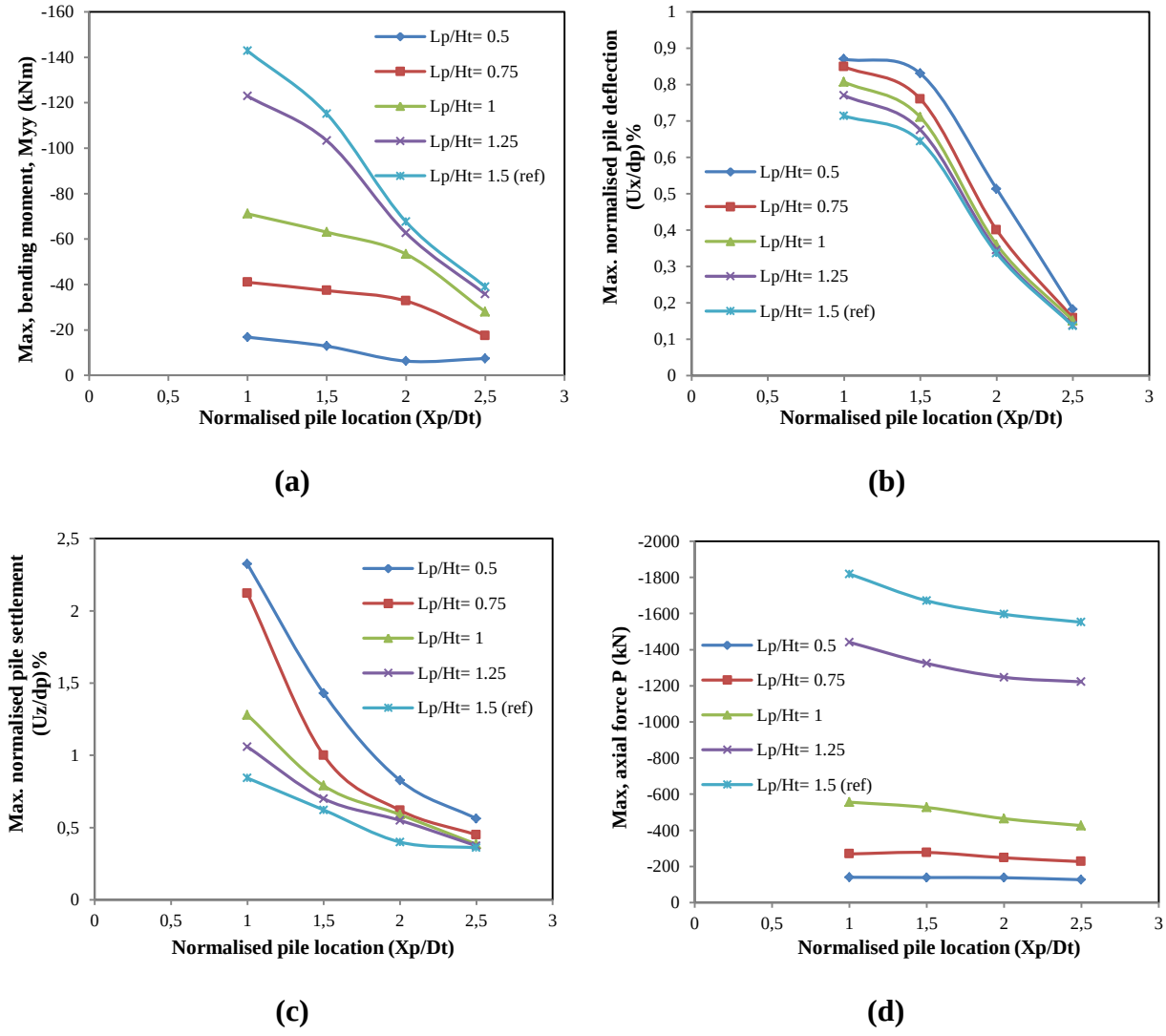

Figure 5.17 Effect of pile location on (a) pile bending moment (b) pile lateral deformation (c) pile settlement (d) pile axial load, for different pile lengths

When the pile is situated at 20 m (i.e. $2.5D_t$) from the tunnel vertical axis, the effect of pile length on pile responses becomes negligible, except for the response of the pile in terms of axial load where the effect of pile length remains significant. This is due to the fact that the pile axial force is not only due to the tunnelling but also due to the workload applied at the head of the pile which is independent of the pile location. In the case of pile length equal to 24 m (L_p/H_t=1.5), when X_P increases from $1D_t$ to $2.5D_t$, the maximum response of the pile decreases by about 73,81, 57, and15% for the bending moment, lateral deflection, pile settlement, and axial force, respectively.

5.4.3 Effect of pile length

For the last excavation stage where the working face is located ahead at a distance Y = $4D_t$, in order to highlight the effect of pile length on pile responses due to tunnelling, the numerical model was tested for five different normalised values of pile length ($L_p/H_t = 0.5$; 0.75; 1.0; 1.25; 1.5).

According to Figure 5.18a which shows the evolution of the normalized lateral deflection of the pile according to its length, it can be seen that in all cases the pile moves towards the tunnel. This is due to the stress relief induced by tunnelling and the ground movement towards the tunnel. Figure 5.18a shows that the maximum deflection decreases with increasing pile length and always occurs at the pile head. When the normalised pile length increases from 0.5 to 1.5, the pile lateral deflection decreases by a maximum of 18%. The figure also shows that when the normalized pile length is relatively large ($L_p/H_t \geq 1$), the lower part of the pile deflects away from the tunnel and a significant negative displacement is observed at the level of the tunnel horizontal axis. The more the pile is embedded in the underlying dense sand layer, the more this negative displacement decreases until it becomes negligible (extreme case of $L_p/H_t = 1.5$).

Figure 5.18b shows the distributions of the induced bending moment along the pile in the lateral direction for the different cases considered. In contrast to the lateral displacement of the pile, the bending moment constantly increases with the increase in the pile length. Increasing the normalized pile length from 0.5 to 1.5 causes an increase in the maximum bending moment of about 7 times. It is also observed that when the end of the pile remains in the overlying soft clay layer (L_p/H_t <1.25), the bending moment along the whole pile remains negative (response of a floating pile) and the maximum of this bending moment is observed almost at mid-depth of each pile. When the tip of the pile is situated below the tunnel horizontal axis (L_p/H_t >1) and within the dense sand, the maximum bending moments are induced almost at the level of the horizontal axis of the tunnel (Z_p=0.67L_p). From Figure 5.18b, it should also be noted that in all cases no bending moment is induced at the pile head, because there was no rigid restriction at this level (the head of the pile was free to move and rotate).

Figure 5.18c shows the axial load distribution for different pile lengths. Using single pile load test, the corresponding working load for each pile length: $L_p/H_t = 0.5; 0.75; 1.0; 1.25; 1.5$ was 92, 165, 360, 1180, and 1500 kN, respectively. It should be noted that the axial load increases dramatically with increasing pile length, and in any case the pile remains compressed. When the normalised pile length increases three times (from 0.5 to 1.5), the peak axial force increases about 13 times.

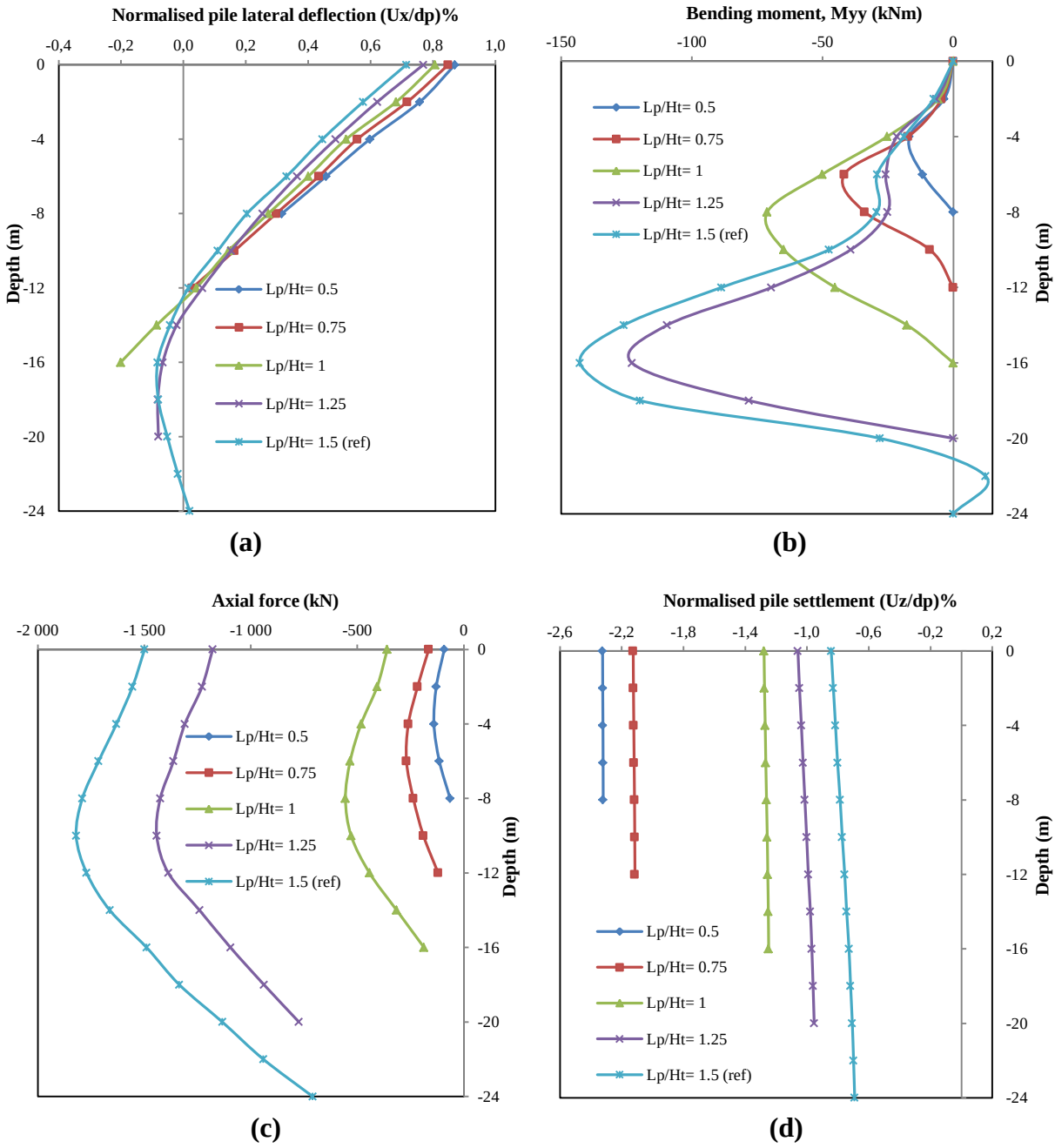

Figure 5.18 Effect of pile length on (a) lateral deflection (b) pile bending moment (c) axial load (d) pile settlement

In cases where $L_p/H_t \leq 1$ (floating piles), the majority of the working load is mobilised by the positive skin resistance developed along the shaft of the pile. Due to the negative skin friction developed along the top of the end bearing piles (L_p/H_t=1.25 and 1.5), the axial load increases from the top up to the depth of $0.5L_p$ where it reaches its maximum value, then it decreases up to the pile tip because of the positive skin resistance mobilized in the lower part of the piles.

The impact of pile length on pile settlement was also investigated, as shown in Figure 5.18d. This figure shows that the normalised pile settlement decreases with increasing pile length. By increasing the length of the pile from 8 m to 24 m, the pile head settlement decreases by approximately 63%. The pile experiences greater settlement if the pile toe is located above the horizontal axis of the tunnel. This is because the pile tip is subjected to the greatest stress release, which results in a large reduction in the pile tip strength.

5.4.4 Effect of tunnel diameter

In order to investigate the effect of tunnel diameter (D_t) on pile responses when the tunnel face is in front of the pile position by a distance Y= 4Dt, the numerical reference model was tested for three values of D_t; namely D_t= 6 m, 8 m and 10 m.

In general, the results obtained indicate that the tunnel diameter has a significant influence on the pile behaviour as shown in Figure 5.19. Due to the increase in the theoretical excavated volume (V_t), the excavation induced more stress release and soil movement towards the tunnel opening, which will affect the pile responses.

As shown in Figure 5.19, pile responses increase with increasing tunnel diameter. When D_t increases from 6 m to 10 m, the magnitude of the maximum pile response increases by about 120%, 63%, 10%, and 75% for the lateral deflection, induced bending moment, axial load, and the pile settlement, respectively. However, the diameter of the tunnel has no impact on the shape of the pile response curves.

From Figures 5.19b and 5.19c, it is observed that the position of peak bending moment and axial load shifts slightly downward with increasing tunnel diameter.

Figure 5.20, which represents the shadings of the total displacements of the soil around the tunnel and the pile when the working face reaches the position ($Y/D_t = +4$), clearly shows the increase in the amplitude of the soil displacements around the pile and the tunnel with the increase in the diameter of the tunnel.

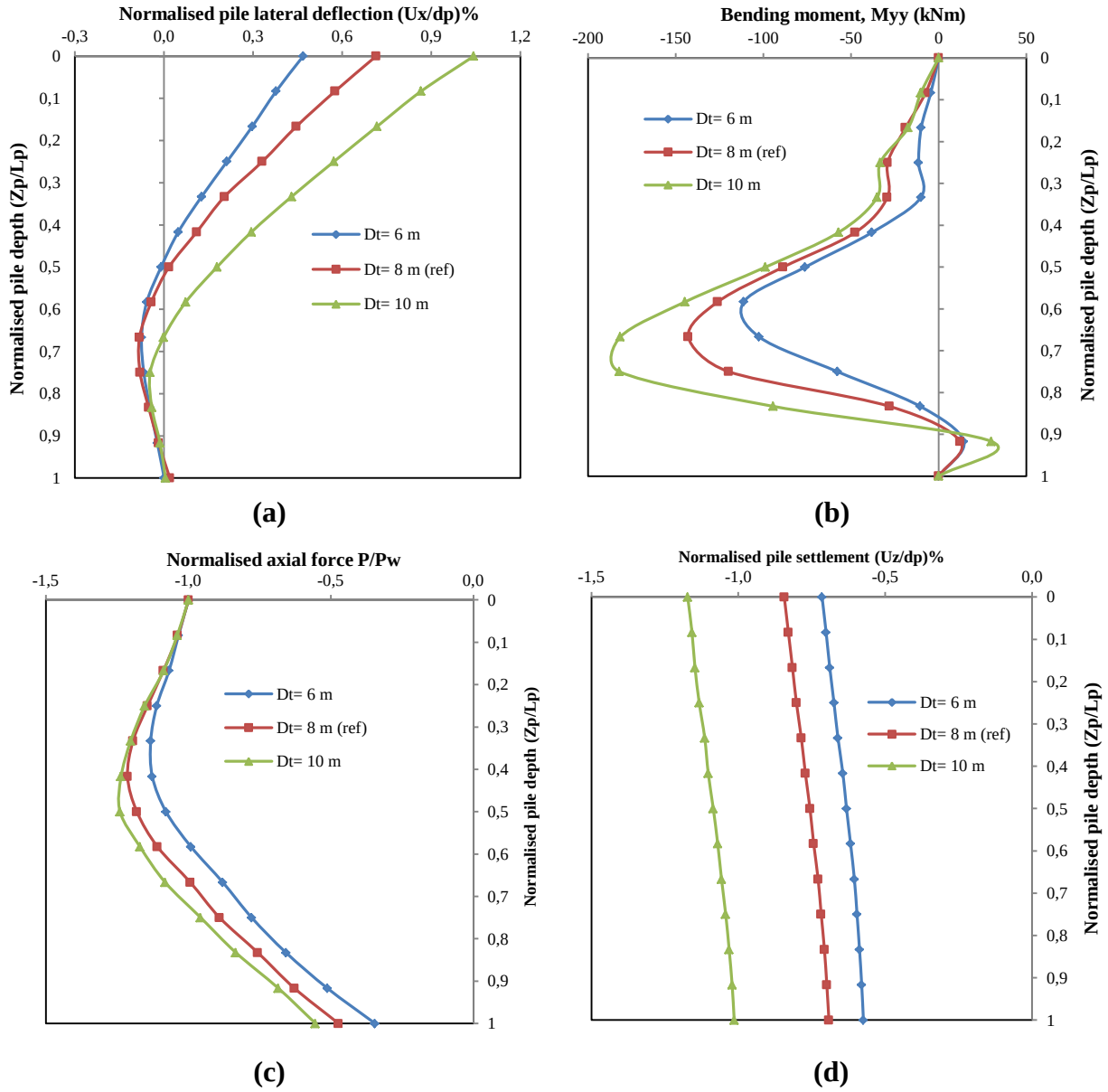

Figure 5.19 Effect of tunnel diameter on (a) lateral deformation (b) pile bending moment (c) axial load (d) pile settlement

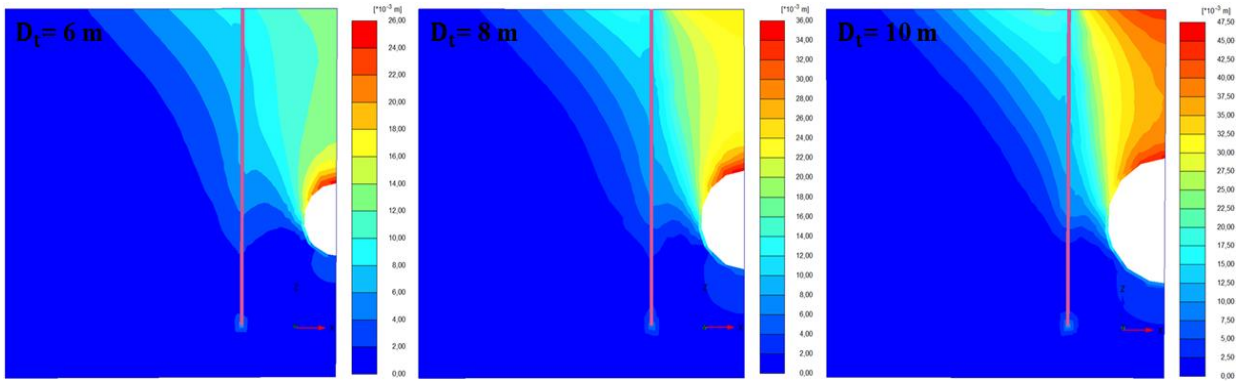

Figure 5.20 Total displacement shadings at (Y/D_t = +4) for three cases of tunnel diameter

5.4.5 Effect of tunnel depth

For the last stage of tunneling activities (Y/D_t = +4), in order to study the tunnel depth effect (H_t) on pile responses, the analyses are carried out for tunnels placed at three different normalised depths i.e., H_t = 1.5D_t (shallow tunnel), 2D_t (intermediate tunnel), 2.5D_t (deep tunnel) as shown in Figure 5.21. For the cases of shallow and intermediate tunnel, the excavation is carried out in the soft clay layer. Whereas in the case of the deep tunnel, the tunneling taken place in the dense sand layer.

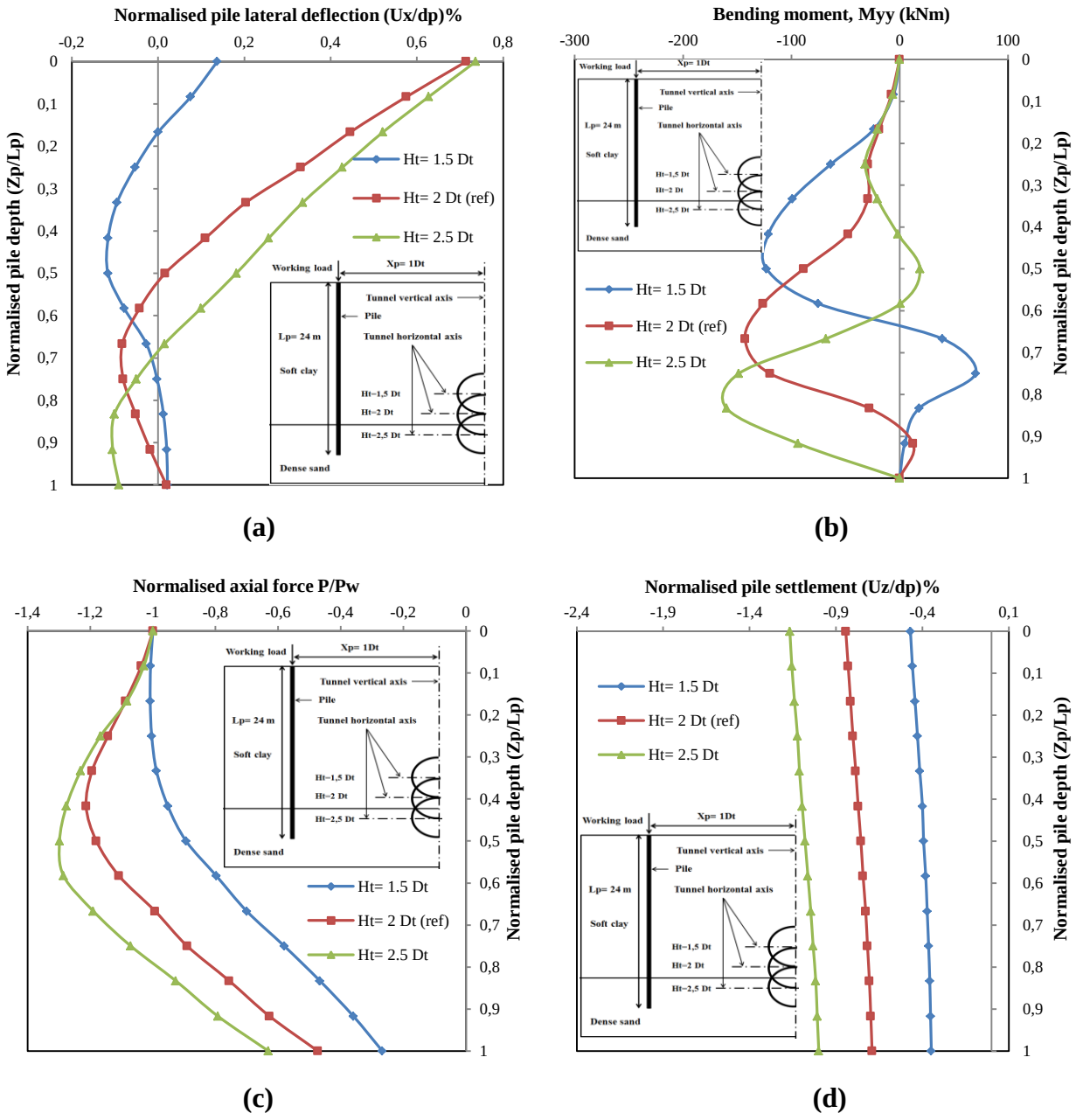

Figure 5.21 Effect of tunnel depth on (a) lateral deflection (b) pile bending moment (c) axial load (d) pile settlement

Variation in tunnel placement depth significantly influences the behaviour of the single pile, as shown in Figure 5.21. It was found that an increase in tunnel axis depth from $1.5D_t$ to $2.5D_t$ results in an increase in the maximum magnitude of lateral deflection, bending moment, axial load, and pile settlement of approximately 420%, 32%, 30%, and 146%, respectively.

From Figures 5.21a and 5.21d, it can be observed that the maximum normalised lateral deflection (U_x/d_p) and the normalised settlement of the pile (U_z/d_p) , whatever the value of the tunnel depth, are induced at the pile head. However, as shown in Figures 5.21b and 5.21c, the location of the induced maximum bending moment (M_{yy}) and normalised axial load (P/P_w) is shifted significantly downwards with increasing tunnel axis depth. Nevertheless, the maximum bending moment always occurs at the tunnel depth.

From Figure 5.21, it can also be seen that for the shallow tunnel (H_t/D_t = 1.5), unlike the other cases, the pile shaft around the tunnel depth deflects away from the tunnel, a significant positive bending moment develops in the lower part of the pile, and the maximum axial force is induced at the pile head then decreases to the pile toe.

In the case of the deep tunnel (H_t/D_t = 2.5) the pile behaves almost in the same way as that in the reference case (intermediate tunnel, H_t = $2D_t$). Most of the bending moment is negative along the pile; the deflection is generally towards the tunnel with a form of cantilever, except at the bottom where the pile moves slightly away from the tunnel).

Figure 5.22 presents the shadings of soil total displacements at the final step of excavation for the three considered depths of the tunnel. This figure confirms the above results and shows that increasing in tunnel depth affects the soil movement and increases its amplitude especially at ground surface. The width and the shape of the shadings of the total ground displacements indicate that the soil deformations correspond well with observations obtained from pile lateral deflections and pile settlements. As the tunnel axis got closer to the pile toe the effect of excavation on the pile response increases (the pile toe is subjected to the greatest release of stress).

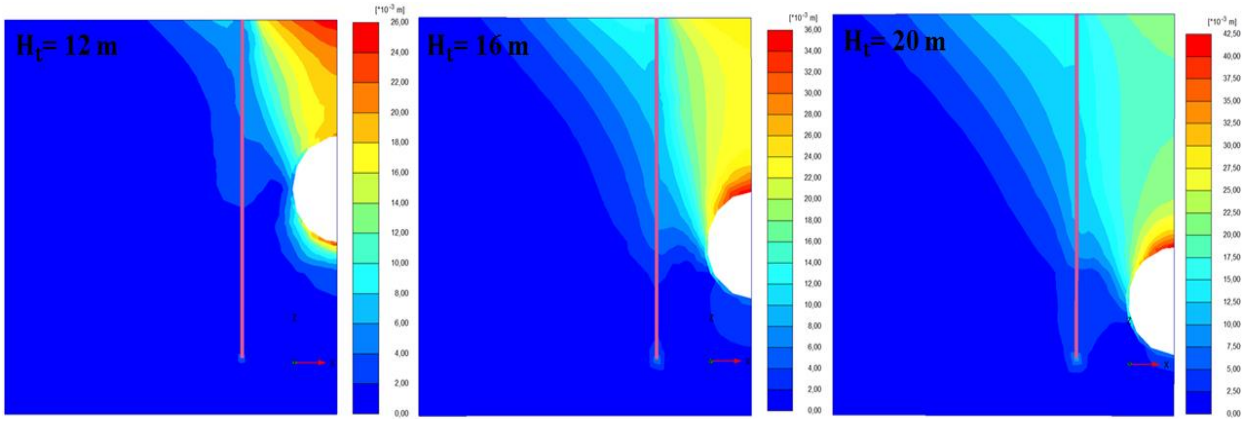

Figure 5.22 Shadings of the total displacements around the tunnel and pile at (Y/D_t = +4) for three different tunnel depth

5.4.6 Effect of pile diameter

Using different pile diameters, the influence of pile stiffness on pile performance for the last step of excavation (Y/D_t= +4) is investigated. For the results given in Figure 5.23, the pile is located at 8 m away from the tunnel centreline, and for three different values of volume loss V_l =1/ 2/ and 3%. Using pile load test, the working load for each pile (i.e. d_p= 0.6/ 0.8/ 1/ and 1.2 m) is determined to be 1000, 1210, 1500, and 1800 kN, respectively (see Figure 5.8b).

From Figure 5.23a, it can be seen that the induced bending moment increases almost constantly with increasing of pile rigidity. It can also be noted that the distribution of the maximum bending moment is quite similar in shape for the different cases considered for the volume loss. However the pile lateral deflection decreases with increasing of pile diameter as shown in Figure 5.23b

The numerical results reveal that the pile diameter significantly affects the induced bending moment for all cases of volume loss. In the case of V_l = 3%, when the pile diameter increases from 0.6 to 1.2 m, the maximum bending moment increases by about 750%. Noting that the effect of the volume loss is all the more important as the diameter of the pile is large. In the case of d_p = 0.6m, the increase in the loss of volume from 1% to 3% causes an increase in the bending moment of 45%. Whereas for d_p = 1.2 m, this same increase in volume loss causes an increase in the bending moment of 55%.

From Figure 5.23b, it can be noted that the effect of increasing the diameter of the pile is only palpable in the case of significant volume loss (V_l = 3%). In other words, for low values of volume loss ($V_l \leq 2\%$), the stiffness of the pile has no significant influence on the deflection of the pile. For V_l = 3%, when pile diameter is varied from 0.6 to 1.2 m, the maximum pile lateral deflection decreases by about 25%.

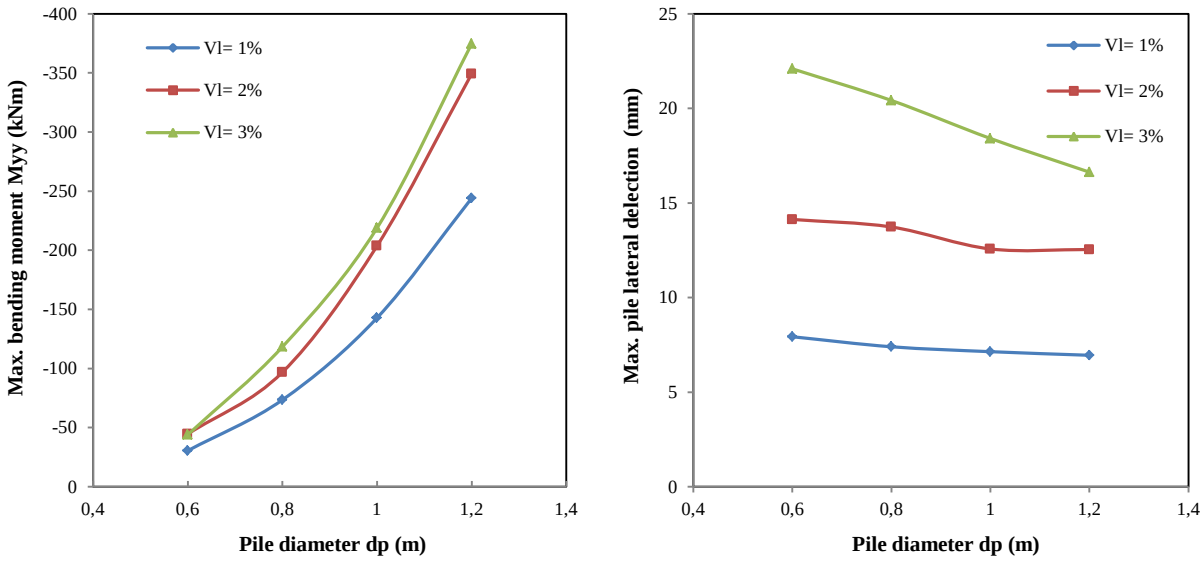

Figure 5.23 Effect of pile diameter on (a) pile bending moment (b) pile lateral deflection

5.4.7 Effect of over consolidation ratio (OCR)

The effect of stress history of the soil on the pile behaviour is investigated by analyzing the over consolidation ratio (OCR) effect. Since the HSs model was used to model the constitutive behaviour of soil, the over consolidation ratio (OCR) was considered using three different values (OCR= 1, 1.25 and 1.5). It should be noted that a uniform over consolidation ratio value were considered only through the depth of clay layer, while the over consolidation ratio of the dense sand layer is fixed to (OCR= 1).

Figure 5.24a and 5.24b shows the effect of OCR on the maximum induced pile bending moment and lateral deformation, respectively. The effect of OCR was tested for three different values of volume loss V_l= 1, 2, and 3%. As expected, the stress soil history significantly affects the pile response. It can be seen that for overconsolidated soils with high OCR values (OCR>1), both the induced bending moments and pile lateral deflection decreases. When the OCR increases from 1 to 1.5, for $V_l = 3\%$, the maximum bending moment and the lateral deflection of the pile decrease by about 60% and 58%, respectively.

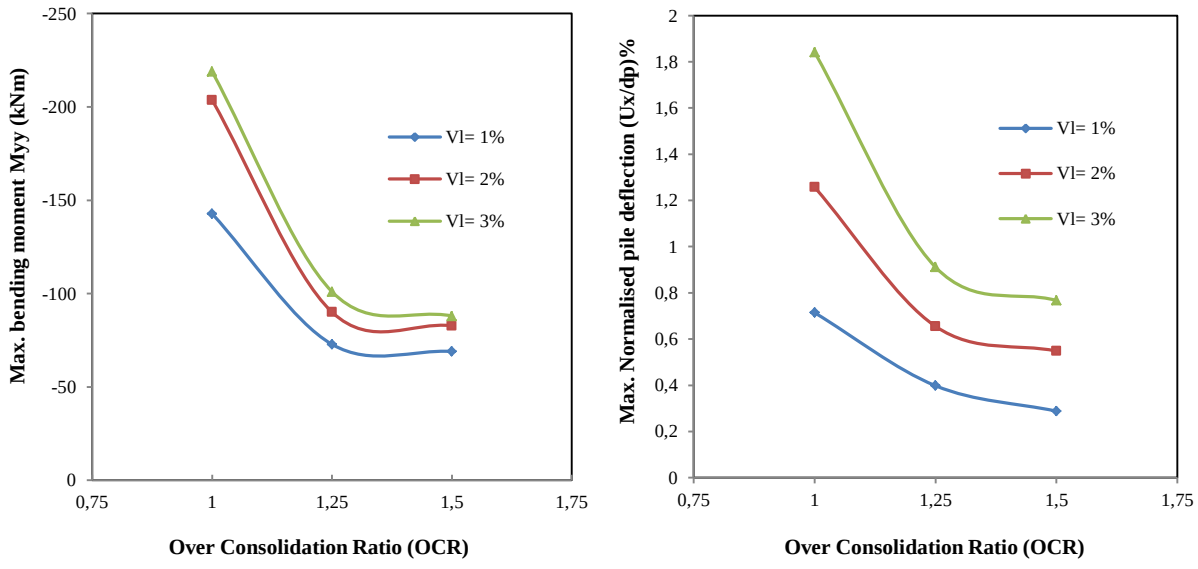

(a) **(b)**

Figure 5.24 Effect of overconsolidation ratio (OCR) on pile (a) bending moment (b) lateral deflection

5.4.8 Effect of pile group

In urban environments, piles are often used in groups (piled raft or group of piles). In this perspective, a parametric analysis is performed to study the responses of the piles in groups during the final phase of the excavation activities (Y/D_t = +4). For this aim, a configuration of 2×2 pile group was considered. To study the effect of head support conditions of the piles, two pile head condition types were considered, namely free and capped. The geometry of the 3D numerical model used for this parametric analysis has been shown in Figure 3. Both pile group

configurations (free and capped) involve two pairs of piles, front and rear, located at horizontal distances of $X_p = 1D_t$ and $X_p = 1.5D_t$, respectively, from the tunnel centreline (spacing between piles is 4 m ($4d_p$)).

The raft used for capped the four identical piles is square (7 m × 7 m) with a thickness of 1 m and it is elevated enough so that it does not touch the ground surface. The raft model has a bending stiffness EI_p of 17.5×10^6 kNm^2 and an axial rigidity EA_P of 2.10×10^7 kN. The raft as the piles is modelled with elastic properties.

Computed pile responses of the two configurations (free and capped) are presented in Figures 25 and 26. The responses obtained from tests of a single pile located at an equal horizontal distance with the front and rear piles are shown in the same figures for comparison purposes. In general, the pile responses are lower in the pile group than in the single pile case, indicating a positive group effect. It should also be noted that the responses of the front piles are constantly greater than those of the rear piles. This is because the front piles undergo the uppermost impact due to tunnelling. It's like the front piles play the role of a shelter on the back piles.

The results in terms of normalised pile lateral deflection are shown in Figure 25. It can be seen that, whether for front or rear piles (free and capped), the lateral pile deflection is quite similar in shape to single pile cases. It is also observed that in all cases, the maximum deflection occurred at the pile head and the lower half of the pile deflects slightly away from the tunnel. As shown in Figure 25, the maximum deflection of the front or rear piles, in the free or capped case, is lower than that of a single pile located at the same distance from the tunnel centerline. This could be due to the positive effect of the pile group.

The results obtained from Figure 25a indicate that the maximum deflection of the front piles is less than that of the single pile by almost 25% and 33%, respectively in the capped and free head case. From Figure 25b, it can be noted that the peak deflection of the rear piles is lower than that of the single pile by approximately 26% and 31%, in the case of capped and free head, respectively. It should also be noted that the rear piles (free or capped) undergo a maximum displacement lower by 11% than that of the front piles. This may be due to the shading effect of the row of front piles on that of the rear piles.

From Figure 26 It can be noticed that the induced bending moment curves of the group piles, whether for front or rear piles, are quite comparable in shape to those of the single piles, in particular in the case of free head. The pile head being free, the generated bending moment is zero at the pile head. Due to the restraint of the pile cap, an important bending moment is induced at the top of the front and rear piles. It should also be noted that a positive bending moment is developed in the lower part of the rear piles (free and capped head), which is not the case for the front piles.

From Figure 26a, the results obtained show that the maximum bending moment of the front piles is smaller than that of the single pile by almost 15% and 24%, respectively in the free

and capped head case. Regarding the rear piles (Figure 26b), the maximum pile bending moment is lower than that of the single pile by approximately 28% in the case of free head. However in the case of capped head, the maximum bending moment (induced at the head) remains greater than that of the single pile by about 35%. The numerical results show that the maximum bending moment of the front piles is larger than that of the rear piles by about 47% in the case of free head. However in the capped head case, the maximum bending moment of the front piles is smaller than that of the rear piles by about 30%.

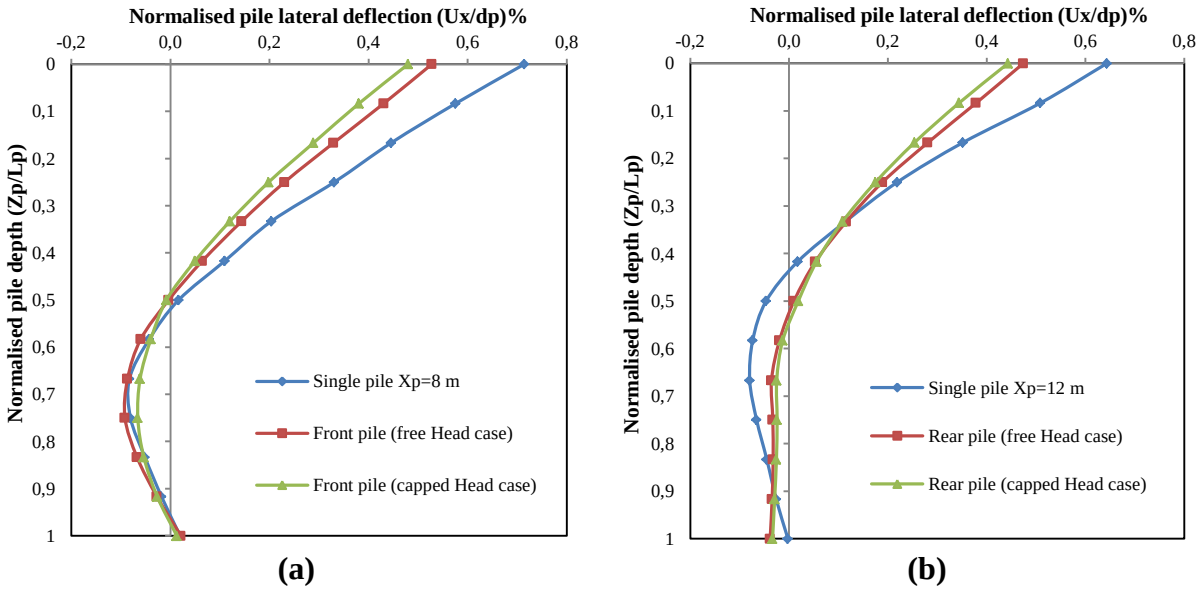

Figure 5.25 Comparison of pile lateral deflection (U_x) (a) Front pile (b) Rear pile

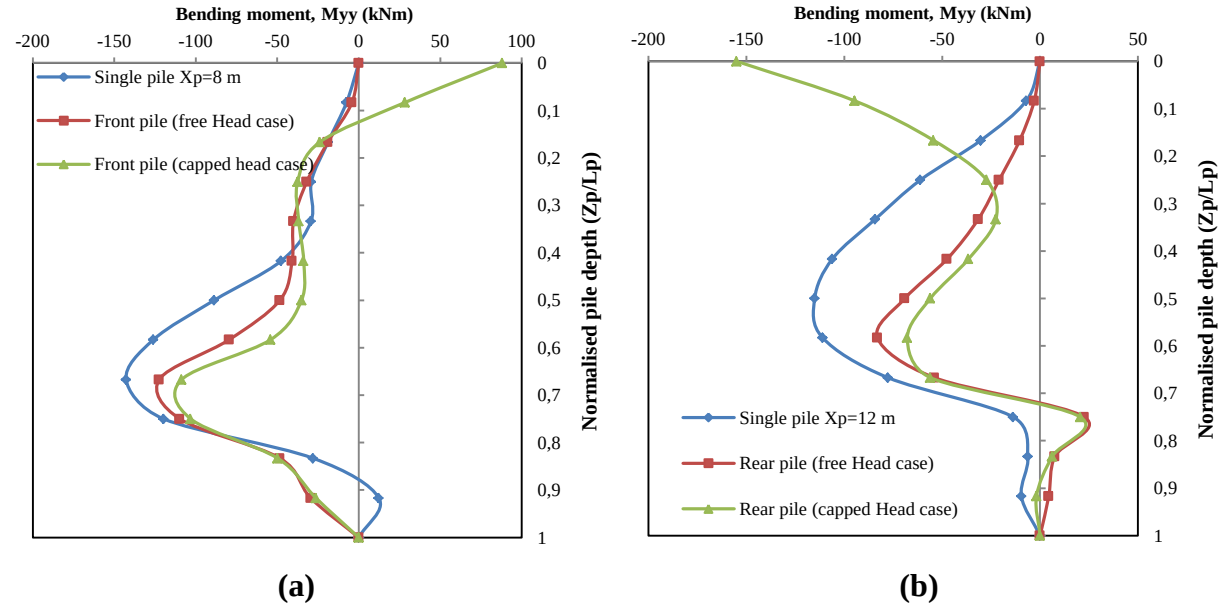

Figure 5.26 Comparison of induced bending moment (M_{yy}) (a) Front pile (b) Rear pile

In order to study the influence of the presence of the pile group on the surface ground movement, Figure 5.27 shows the transverse troughs of the surface settlement at the section (Y/D_t= 0) for single pile, pile group and Greenfield cases. It can be seen that the presence of the piles affects the settlement troughs distributions (reduced the soil settlement notably for pile group case). It is also notable that when there is a pile in the ground, the settlement trough does not follow exactly the well-known Gaussian settlement trough. The settlement troughs for the single pile and pile groups become similar to the Greenfield settlement trough only when X/D_t is almost 2.25. This figure reveal that the estimation of pile settlement due to tunnelling using the Greenfield condition may result in overestimation of pile settlement, in particular for the piles in groups (positive group effect). To express the settlement trough, settlement distribution patterns other than the Gaussian curve may be needed when there are pre-existing piles in the ground (Lee, 2013).

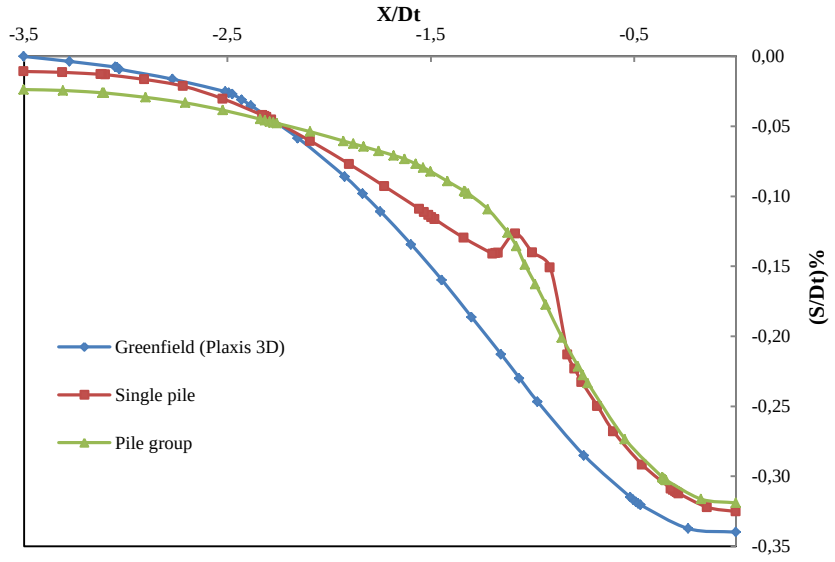

Figure 5.27 Surface settlement troughs for single pile, pile group and Greenfield cases at the last step of tunnel excavation (Y/D_t =+4)

5.5 Conclusion

In this chapter, a full 3D numerical analysis is carried out to study the response of vertical single piles due to tunneling induced soil movements in soft clay overlying dense sand. Among the various tunnel boring machines (TBM), the Slurry Pressure Balance (SPB) technique is used in this study to simulate the construction of the tunnel. The numerical model has been validated on the basis of the results of a centrifuge test published in the literature. The pertinence of the three-dimensional model was also assessed by comparison with a 2D plane strain numerical model. An extensive parametric study was conducted to investigate the effect of some key parameters such as tunnel advancement, volume loss, pile location, pile length, tunnel diameter, tunnel depth, and clay over consolidation ratio (OCR). The group effect on pile responses was also studied using two pile group configurations.

The results obtained from the 3D numerical modelling show that due to tunnelling-induced soil movements, the pile response in terms of transverse bending moment, axial force, shaft resistance, transverse deflection and pile settlement increases considerably with the advancement of the tunnel. Pile responses seem stabilized once the tunnel face is in front of the pile by a distance of twice the tunnel diameter. In the longitudinal direction, the maximum pile responses (bending moment and deflection) occur when the working face is at the same level as the pile location. Nevertheless the magnitude of the pile responses remains very low compared to those in the transverse direction (a reduction coefficient up to 2.3 was observed).

Except bending moment, where the 2D analysis shows good agreement with the 3D simulation, the pile responses using 2D numerical analysis are overestimated. Thus, 2D plane strain modelling could give conservative results.

As the volume loss increases from 1% to 3%, pile head settlement, lateral deflection, bending moment, and axial force increase by 83%, 140%, 53%, and 12% maximum, respectively. The effect of volume loss on pile responses only becomes noticeable when the tunnel face is located from a back distance of 2 times the tunnel diameter. Noting that the effect of the volume loss is all the more important as the diameter of the pile is large. Excavating a tunnel close to a pile not only causes ground deformations, but also can reduce the pile bearing capacity. By increasing the volume loss from 1% to 3% the apparent loss of pile capacity (ALPC) increases from 11% to 20%.

The variation in pile length revealed that the pile performance depends on the position of the pile toe with respect to the tunnel depth. The pile experiences greater settlement if the pile toe is located above the tunnel horizontal axis. This is because the pile tip is subjected to the greatest stress release, which results in a large reduction in the pile tip strength and shaft resistance. By increasing the pile length from $0.5H_t$ to $1.5H_t$, the maximum pile head settlement and lateral deflection decrease by about 63% and 18%, respectively. In contrast to the pile displacements, the induced bending moment and axial load constantly increases with the increase in the pile length. When the pile length increases from $0.5H_t$ to $1.5H_t$, the maximum bending moment and axial load increase by about 7 and 13 times, respectively.

For any pile length, pile responses decrease exponentially with lateral distance from the tunnel axis. When the pile is located at a distance of $2.5D_t$, the pile responses become insignificant. The increase in theoretical excavated volume (V_t) induces more stress release and soil movement towards the tunnel, which will affect the pile responses. The 3D results showed that increasing the tunnel diameter from 6 m to 10 m results in a 120%, 75% and 63% increase in maximum lateral deflection, pile settlement and bending moment, respectively.

Variation in tunnel placement depth significantly influences the behaviour of single piles. It was found that an increase in tunnel axis depth from $1.5D_t$ to $2.5D_t$ (with $L_p = 3D_t$) results in an increase in the maximum magnitude of lateral deflection, pile settlement, bending moment, and axial load of about 420%, 146%, 32%, and 30%, respectively.

As expected, the stress soil history significantly affects the pile response. When the OCR increases from 1 to 1.5, for $V_l = 3\%$, the maximum bending moment and lateral deflection of the pile decrease by about 59%.

In general, the results obtained showed that the pile responses are lower in the pile group than in the single pile case, indicating a positive group effect. The response of a pile within a pile group depends, among other parameters, on its location in the group (front or rear pile), and pile head conditions (free or capped head).

CHAPTER 6

3D Numerical Analysis of Pile Response Due to Deep Excavation-Induced Ground Movements

CHAPTER 6

3D Numerical Analysis of Pile Response Due to Deep Excavation-Induced Ground Movements

6.1 Introduction

The development of urban areas leads to an increased demand for underground constructions which often require deep excavations supported by strutted or anchored diaphragm walls and therefore, the diaphragm wall is often found to be located at a close distance from adjacent existing buildings. As the excavation progresses in depth, the soil inevitably moves towards the excavation and causes both horizontal and vertical deformations. Consequently, the nearby pile foundation will be potentially affected (Poulos and Chen, 1997; Schanz and Vermeer, 1998; Leung et al. 2006; Ng et al. 2017). Hence, it is essential to have a thorough understanding of the harmful effects of excavation on adjacent piles, especially concrete piles, as they are generally not designed to withstand large lateral loads.

The estimation of additional deformations and internal forces in existing piles induced by a nearby deep excavation has been and continues to be the topic of much numerical and experimental research. One can refer to the research work of Poulos and Chen (1996, 1997), Leung et al. (2000), Liyanapathirana and Nishanthan (2016), Ng et al. (2017), Nishanthan et al. (2017), Soomro et al. (2018b, 2019a) or Shakeel and Ng (2018).

In first approach, the analysis is generally based on model tests (Chen et al., 1997) and centrifuge modeling technique in sand (Leung et al. 2003; Zheng et al. 2012; Ng et al. 2017; Shi et al. 2019) and in clay (Leung et al. 2006; Ong et al. 2009). These investigations reveal some basic characteristics of this problem. However, for the preliminary design, the experimental methods can be time consuming and expensive.

The responses of piles subjected to excavation-induced soil movements were also evaluated using simplified method known as two-stage analysis method "TSAM" (Poulos and Chen, 1996, 1997). However, this approach estimates the soil mass as a homogeneous linear elastic material under plane strain conditions, which makes it problematic to extend to nonlinear problems and multilayered soils. The three-dimensional numerical computation using finite difference or finite element method has therefore become indispensable (Shi et al. 2019; Soomro et al. 2018, 2019a, 2019b).

Results obtained from previous studies show that the response of piles subjected to ground movements induced by deep excavations is related to a complex phenomenon of soil-structure-pile interactions. As a result, the comparison of the numerical modelling of such structures with instrumented sites or laboratory tests is often marked by disagreements. Thereby,

advance studies are required to develop more insight on the mechanical behavior of the pile foundation system subjected to soil movements induced by the excavation.

In this chapter, a full three-dimensional numerical analysis is carried out to investigate single pile and pile group responses due to deep excavation-induced soil movement in bilayer soil. The explicit finite element numerical code PLAXIS 3D (Brinkgreve et al. 2016) is used to model the various phases of excavation in the presence of piles. The numerical model was validated based on the results of a centrifuge test reported by Ong et al. (2006a). The relevance of the 3D model is also judged by comparison with the 2D plane strain model. To better understand the single pile behaviour near deep braced excavations, a parametric study was carried out using 3D numerical model. The parametric study focuses on the effects of excavation depth, pile location, sand density, support system, pile stiffness, head conditions, and pile length. The effect of pile group on pile performance was also investigated using different pile group configurations. In order to provide further insights about the response of pile group system, the interactions between the different individual piles through the pile cap are investigated by varying some parameters as the number of piles and the piles location from the wall. For a preliminary design, this numerical study can serve as a practical basis for similar projects.

6.2 Validation of 3D finite element model using a centrifuge test data

6.2.1 Description of the centrifuge test

The centrifuge test, used for the validity of the numerical modeling procedure carried out in this study, was conducted at 50g in the Geotechnical Centrifuge of the National University of Singapore by Ong et al. (2006a) to assess excavations-induced ground deformations in clay and their effects on adjacent pile foundation. The container used in the test is made of aluminum alloy and has internal dimensions of 540mm×200mm×470mm (length×width×height). Figure 6.1a shows the geometry of the centrifuge test (side view). The retaining wall is made of aluminum alloy plate. The model pile was fabricated from a hollow square aluminum tube covered with thin layer of epoxy coating was used to protect strain gauges from damage with an external width of 12.6 mm. The pile is embedded at the base of the box (rested at the bottom of the box which simulates rigid stratum). The soil used in the test is kaolin clay overlying a layer of Toyoura sand.

The Malaysian kaolin clay has a liquid limit (LL) of 80%, plastic limit (PL) of 40%, plasticity index (PI) of 40 %, compression index C_c of 0.64, swelling index C_s of 0.14, and initial void ratio e_{init} of 2.3 (Ong et al. 2006a). Compression and swelling indexes are determined using the oedometer tests. The coefficient of permeability of normally consolidated kaolin clay at a consolidation pressure of 100 kPa was determined to be about 1.36×10^{-8} m/s.

The effective internal friction angle φ' is 23°. The clay has a coefficient of earth pressure at rest of about 0.6, and a specific gravity of 2.65. The undrained shear strength C_u of the clay is 0.20 to 0.30 of the effective overburden pressure. The variation of undrained shear strength of

the clay with depth obtained using a T-bar penetrometer test (Ong et al. 2006a). However, the failure characteristics of clay in drained behaviour (c' and φ') are obtained from (CU + U) triaxial tests.

The sand used is Toyoura sand (a type of quartz sand), whose mechanical properties are well documented by Tatsuoka et al. (1986). The unit weight and relative density *RD* of the sand were measured to be 15.78 kN/m^3 and 90%, respectively. For a confining stress ranging from 50-100 kPa, the friction and dilation angles of the sand at the given density, from triaxial compression test data of Tatsuoka et al. (1986), are determined to be about 43° and 12°, respectively. The effective cohesion is 0 kPa, and the Young's modulus is 6z MPa, where z is the depth below the ground surface in meters. The coefficient of earth pressure at rest K_0 of sand is about 0.32. Measurements of the coefficient K_0 are carried out from K_0 oedometer tests with measurement of lateral stresses. In addition, this sand has an average particle size of 0.16 mm, uniformity coefficient of 1.3, maximum void ratio e_{max} of 0.977, minimum void ratio e_{min} of 0.605, and specific gravity of soil particles of 2.64. The main soil parameters used are summarized in Table 6.1.

An appropriate thickness of clay in front of the retaining wall was removed, and a latex bag containing $ZnCl_2$ solution, having the same density as the clay, is placed in the excavated area, then the excavation was simulated in-flight by draining away the $ZnCl_2$ solution from latex membrane. Linear variable displacement transformers (LVDTs) are used to measure pile lateral deflection, rotation, and ground surface settlement. For more details about the soil parameters and the measures obtained, the reader should refer to the research work of Ong et al. (2006a).

6.2.2 Three-dimensional finite element modelling

The numerical simulation was performed with the finite element code PLAXIS 3D (Brinkgreve et al. 2016), which is a flexible tool for the analysis of 3D nonlinear soil-structure interaction problems. Figure 6.1b shows the 3D mesh of the numerical model used to simulate the centrifuge test. Due to symmetry, only one-half was modeled. Model dimensions are determined so that they are equivalent to those of the centrifuge model at 50g (i.e. length of 27 m, width of 10 m, and height of 12.5 m). It is assumed that no horizontal and vertical displacement at the bottom boundary by providing pin supports to the base of the mesh. However, the vertical sides of the mesh were restrained from moving laterally but free to settle by using roller supports. The retaining wall consists of a sheet pile (approximately equivalent to that of a FSP-IIA sheet pile wall) with an equivalent thickness at 50g of 15.87 cm and depth of 8 m. The equivalents embedment depth (L_p) and external width (d_p) of the pile at 50g are 12.5 m and 0.63 m, respectively.

The pile is modelled using the embedded pile feature available in PLAXIS 3D with a bending rigidity EI_p of 2.2×10^5 kNm^2, and the retaining wall is simulated using the plate element with a bending stiffness EI_w of 24×10^3 kNm^2/m. Both pile and retaining wall were

modelled using an isotropic linear elastic model. The behavior of the interface between the pile shaft and the surrounding soil in the axial direction is governed by a linear-elastic constitutive law with limited strength. Similar behavior is also adopted to simulate the response at the tip of the pile. The mobilization of the shaft and base resistances is governed by the relative displacement between the pile and the soil and also by the shear modulus of the soil. The development of a negative shear stress along the pile shaft is allowed, which is useful for modelling negative skin friction.

To model the small-strain nonlinear behaviour of the soil, the Hardening soil model with small-strain stiffness (HSs), implemented in PLAXIS, was used in this analysis.

Thus, using the relationships mentioned in chapter 5 (see Eqs. 5.1 to 5.7) and the various soil properties reported by Ong et al. (2006a), the different parameters of the HSs model for both layers (soft clay and dense sand) are deduced and summarized in Table 6.1.

The numerical modelling procedure is the same as that of the centrifuge test:

1. Generation of the initial effective stresses using the K_0 procedure at 1g;
2. Activate pile and retaining wall (modelled as "wished-in-place");
3. Apply hydrostatic pressures to simulate the $ZnCl_2$ solution pressure on the wall;
4. Increase the amount of gravity to 50g using $\sum M_{Weight}$ (total multiplier for the material weight);
5. Simulate the excavation by decreasing the pressure.

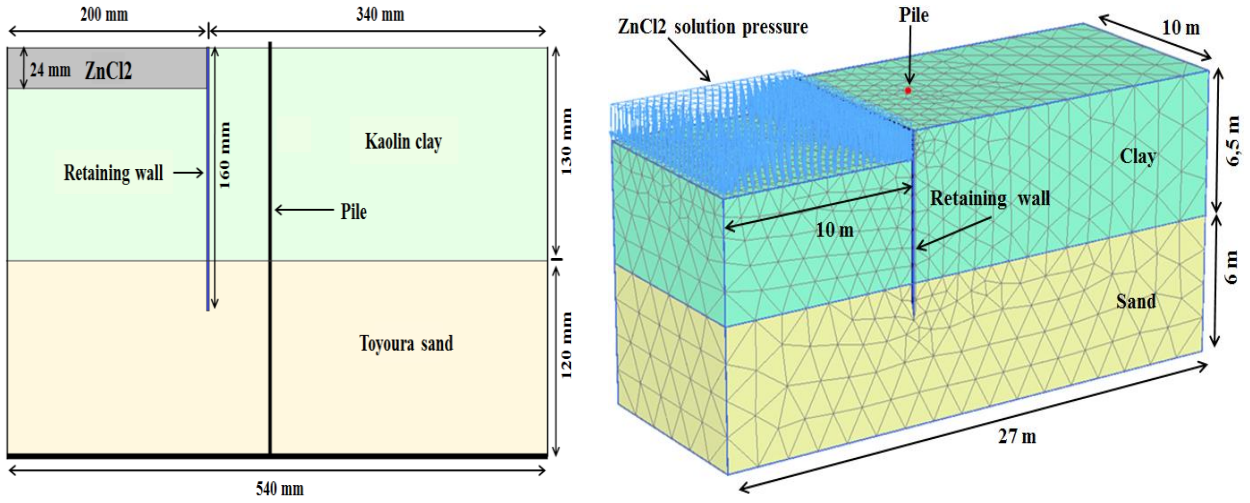

Figure 6.1 Details of the centrifuge test (a) Side view (b) 3D Finite element mesh

Table 6.1 Soil parameters used for the validation of 3D finite element model

Soil	γ_{unsat} ($\frac{kN}{m^3}$)	γ_{sat} ($\frac{kN}{m^3}$)	E_{50}^{ref} (MPa)	E_{oed}^{ref} (MPa)	E_{ur}^{ref} (MPa)	m	v_{ur}	P^{ref} ($\frac{kN}{m^2}$)	C_{ref} ($\frac{kN}{m^2}$)	$\varphi°$	K_0^{nc}	$\gamma_{0.7}$	G_0^{ref} (MPa)
Clay	16	18	24	12	87.5	1	0.2	100	3	23	0.6	2×10^{-4}	33
Sand	18.5	20.5	54	54	162	0.4	0.2	100	0.01	39.2	0.37	1.1×10^{-4}	121.2

Notes: γ= unit weight, $E_{50}^{ref}/E_{oed}^{ref}/E_{ur}^{ref}$= reference secant/tangent/unloading-reloading stiffness, m= power for stress dependent stiffness, C_{ref}= effective cohesion, $\varphi°$= effective friction angle, v_{ur}= Poisson's ratio for unloading-reloading, P^{ref}= reference stress for stiffness, K_0^{nc}= coefficient of earth pressure for normal consolidation, G_0^{ref}= reference shear modulus at very small strains, $\gamma_{0.7}$ = shear strain.

6.2.3 Comparison of computed and measured results

Figure 6.2 shows comparison between the measured and computed pile responses at the end of excavation in terms of bending moment and lateral deflection. Figure 6.2a shows that the measured maximum induced bending moment is 86 kNm at the end of the test (single pile located at 3 m from the wall) and occurred at a depth of 0.6 L_p (this depth also represents the wall toe level). For the computed results, the maximum bending moment reaches 92 kNm at a depth of $0.52L_p$, which coincides with the base of the clay layer. From Figure 6.2b, it can be seen that due to excavation procedures, the pile deflected towards the excavation with cantilever type deformation, since the wall is unsupported during excavation. Consequently, both for the computed results and the centrifuge test observations, the maximum horizontal displacement occurred at the pile head (free-head) then decreases with depth until reaching a negligible value at the pile toe, since the latter was embedded in rigid stratum, which means restrained movements in all directions. For the centrifuge test, the pile deflection profile can be obtained by integrating the bending moment twice, using the measured pile head deflection and rotation as the input boundary condition. The magnitude of the maximum measured and computed pile deflection is 12.5 mm ($2.1\%d_p$) and 12 mm ($2\%d_p$), respectively.

By comparing the results of the present numerical model to the centrifuge test measurements, a good agreement is observed both in terms of pile lateral deflection and bending moment (both for the curves shapes and magnitudes). Nevertheless, the position of the maximum bending moment is slightly shifted upwards in the numerical model.

The obtained results reveal that there is an ability to perform a numerical parametric study (effect of some key parameters) to investigate pile and pile group behaviour near deep excavation using the HSs soil model.

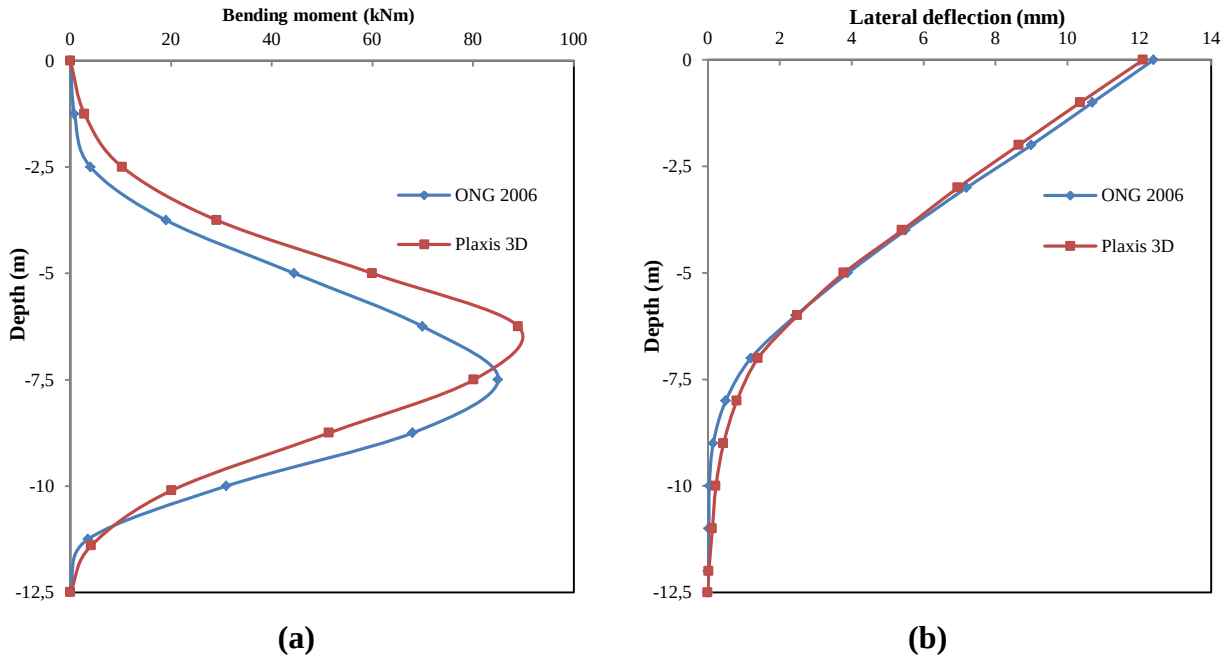

Figure 6.2 Comparison of the computed and measured results (a) pile bending moment (b) pile lateral deflection

6.3 Reference 3D numerical model used for the parametric study

Using the finite element numerical code PLAXIS 3D, a full three-dimensional numerical analysis was conducted to investigate the pile response due to nearby deep multi-strutted excavation. The method of strutted diaphragm walls is one of the most commonly used methods of deep excavation support. In practice, the construction of a deep excavation nearby to existing pile foundations is a process that can consist of several phases. First the wall is installed to the desired depth. Then some excavation is carried out to create space to install an anchor or a strut to support the retaining wall. Then the soil is gradually removed to the final depth of the excavation. Special measures are usually taken to keep the groundwater out of the excavation (dewatering). The analysis neglects installation effects of the wall on existing piles and concentrates only on the pile behavior due to excavation induced ground deformations.

6.3.1 General description of the model

In this reference model, the upper 28 meters of the ground consist of a layer of saturated soft clay (the same as that reported in section 6.2.1). Underneath this clay layer there is a dense stiffer layer of sand, which extends to a large depth (32 m of the sand layer are considered in the model). It was adopted the same sand used in the centrifuge test but with different relative density. The Hardening soil model with small-strain stiffness mode was adopted to model the nonlinear stress-strain soil behaviour. The input parameters of the HSs model for the clay layer are the same as those used for the validation test (see Table 6.1). However, the sand layer parameters are those which correspond to a relative density *RD* of 60% as shown in Table 6.2.

The sand has an internal friction angle of 35.5°, dilation angle of 10°, permeability of 1.38×10^{-6} m/s, and an effective cohesion of zero. The lateral earth pressure coefficient at rest, K_0, for the sand is 0.42, and the Poisson's ratio is assumed to be 0.2. The initial shear modulus G_0^{ref} defined for the reference pressure of 100 kPa is 100.8 MPa. The tangent reference modulus of rigidity E_{oed}^{ref} and the unloading-reloading modulus stiffness E_{ur}^{ref} are 54 MPa and 162 MPa, respectively.

Due to symmetry of the problem, only one half of the model is analysed (the right side). The 3D numerical model dimensions are 100m×20m×60m (width×length×height). These dimensions are sufficient to allow any possible collapse mechanism to develop and to avoid any effect of the model boundaries. Figure 6.3 shows the geometry of the model used for the analysis (side and plan views). The volume to be excavated has dimensions of (10×20×20) m^3 which is equivalent to half width (B), length, and maximum depth of excavation (H_e), respectively. To ensure a sufficiently high safety factor against the stability of the structure, the excavation was supported by 1 m thick, 40 m long diaphragm wall (which represents two times the final excavation depth), and ten levels of steel props with axial rigidity of EA=81×10^3 kNm. The first level of props is installed at depth h_{uns} (unsupported excavation depth) of 1 m (Figure 6.3a). The average vertical props spacing h_{avg} is 2 m, while the horizontal spacing is 4 m.

The embedded length (L_p) and diameter (d_p) of the pile are 40 m and 1 m, respectively. The pile is located at a horizontal distance X_p of 4 m (i.e. $4d_p$) from the diaphragm wall. The pile was modelled using "Embedded pile" structural element which consists of beam element (3-node line elements) with special interface elements providing interactions soil-pile. The embedded pile element used in this numerical analysis has six degrees of freedom per node: three translations (U_x, U_y and U_z) and three rotations ($\emptyset_x$, $\emptyset_y$ and $\emptyset_z$). In this reference model it was adopted the case of free-head (both translations and rotations are free). Material properties of embedded pile are summarised in Table 6.3.

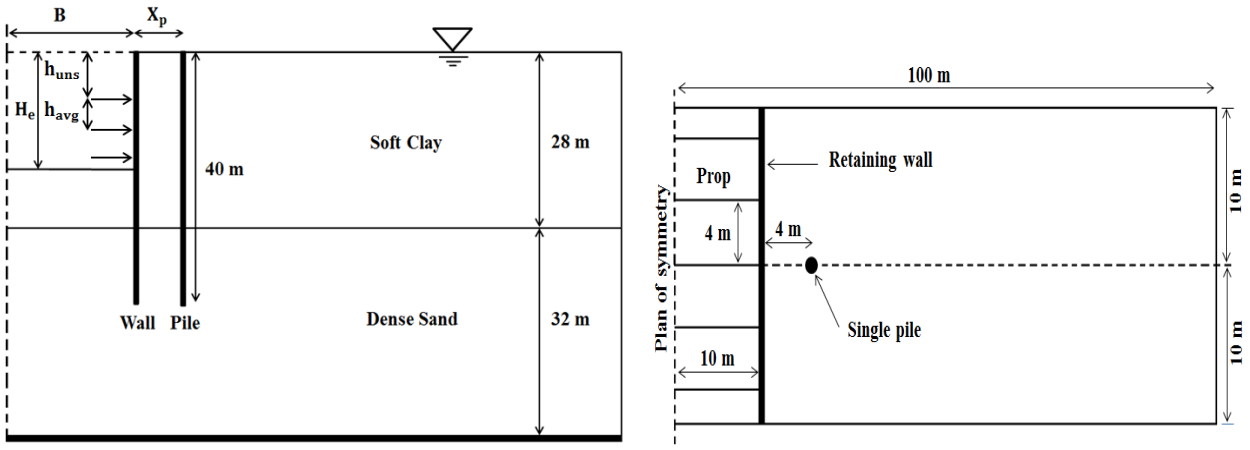

(a) **(b)**

Figure 6.3 Typical geometry of the reference model (a) side view (b) plan view

Soil was simulated using a 10-node tetrahedral element. The soil mesh surrounding the single pile was refined (fineness factor is 0.3536) and becomes coarser further away from the pile. Finally, the mesh consisted of 12841 soil elements and 20266 nodes (Figure 6.4). Retaining wall was modelled using a 6-node triangular plate element. The props and diaphragm wall are modelled using anchors and plate elements, respectively. The behaviour of wall, pile and props is assumed to be elastic, linear and isotropic. For a proper modelling of soil-wall interaction, interface elements of 12-nodes were inserted between the soil and the wall. Interfaces are joint elements consist of pairs of nodes, compatible with the 6-noded triangular side of a soil element or plate element. The interfaces allow for the specification of a reduced wall friction compared to the friction in the soil. Initially, the water table is at the soil surface and the pore pressure is hydrostatic.

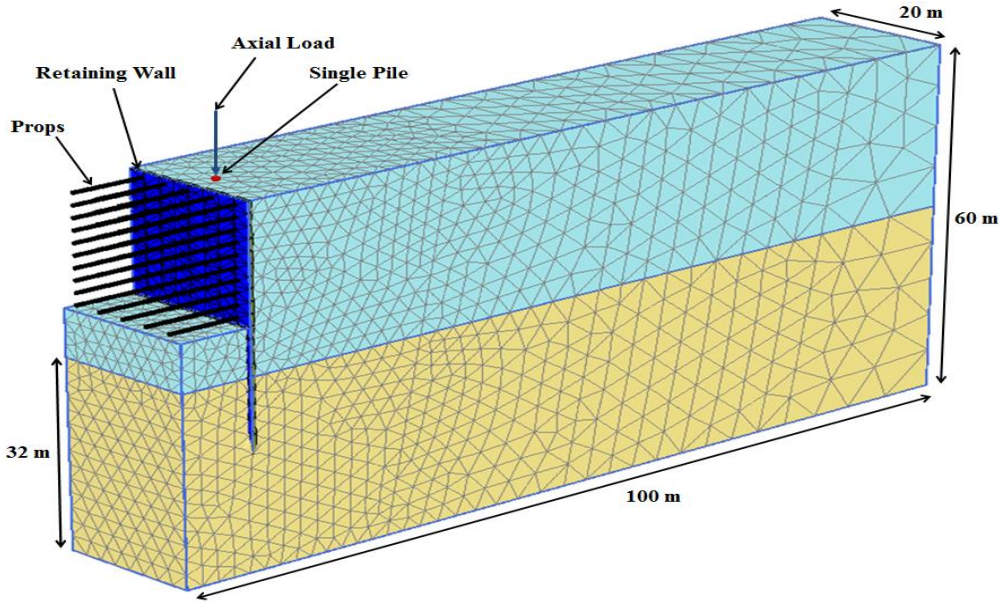

Figure 6.4 3D finite element mesh

Table 6.2 Soil parameters used for the reference 3D numerical model

Soil	γ_{unsat} $(\frac{kN}{m^3})$	γ_{sat} $(\frac{kN}{m^3})$	E_{50}^{ref} (MPa)	E_{oed}^{ref} (MPa)	E_{ur}^{ref} (MPa)	m	ν_{ur}	P^{ref} $(\frac{kN}{m^2})$	C_{ref} $(\frac{kN}{m^2})$	φ°	K_0^{nc}	$\gamma_{0.7}$	G_0^{ref} (MPa)
Clay	16	18	24	12	87.5	1	0.2	100	3	23	0.6	2×10^{-4}	33
Sand	17	20	36	36	108	0.5	0.2	100	0.01	35.5	0.42	1.4×10^{-4}	100.8

Table 6.3 Material properties of the embedded pile (L_p= 40 m)

Description/ Parameter/ Unit	Value
Unit weight, γ (kN/m^3)	24
Young modulus, E (GPa)	30
Diameter, d_p (m)	1
Skin resistance at top layer, T (kN/m) for Z_p=0→ 28 m	0→175
Skin resistance at bottom layer, T (kN/m) for Z_p=28→ 40 m	175→245
Base resistance (kN)	17000

6.3.2 Construction sequences

The whole construction activities included staged dewatering, excavation and strutting. At each stage, dewatering is first performed to lower the ground water table down to 1m below the bottom of the subsequent stage of excavation, and then the soil is removed and followed by the installation of all the struts at 1 m above the bottom of the excavation. Step by step, the subsequent staged dewatering, excavation and strutting phases can follow each other until the final bottom of excavation is reached. Table 6.4 summarise the numerical modelling procedure.

6.3.3 Numerical modelling procedures

In general, excavation was simulated by deactivating the soil element and making the excavated area dry. The water table inside the excavation was progressively lowered with the excavation of the soil during each phase, which is likely to correspond to the situation where a pumping inside the excavation. Below the excavation level water condition was simulated by using interpolate option. The displacements are reset to zero before starting of the excavation to ensure that all deformations referred to hereafter are only a result of the excavation procedures.

Using the PLAXIS code, the systematic steps of methodology of the numerical simulation of the problem are defined as follows:

1. General setting: The type of finite elements must be specified, the minimum dimensions of the draw area must also be given here;

2. Creating a geometry model: A geometry model should include a representative division of the subsoil into distinct soil layers, structural objects, construction stages and loadings;

3. Boundary conditions: Standard boundary conditions were adopted;

4. Material data sets: The soil model and appropriate material parameters must be assigned to the geometry. For structures (like walls, plates, piles, struts, etc.) the system is similar;

5. Mesh generation: PLAXIS allows for a fully automatic mesh generation;

6. Initial conditions: Before starting the calculations, however, the initial conditions must be generated. The initial conditions comprise the initial groundwater conditions, the initial geometry configuration and the initial effective stress state;

7. Performing calculations: The construction process of an excavation can be simulated with the ***Staged construction*** calculation option. The different stages of calculation are detailed in Table 6.4;

8. Viewing output results: Once the calculation has been completed, the results can be evaluated in the output program.

Table 6.4 Numerical modelling procedure

Steps	Description
1	Establish the initial phase using the K_0 procedure: $K_0 = 1 - \sin\varphi'$.
2	Activate the single pile (modelled as "wished in place")
3	Apply the working load on the single pile, and allow excess pore pressure induced due to applied working load to dissipate. With a factor of safety of 4.0, the working load is determined to be 5500 kN.
4	Install wished-in-place diaphragm wall by activate plate and the interface elements.
5	Excavate the first 2 m by deactivating the soil element in 8 days for an excavated volume of 400 m^3 (equivalent to that reported in centrifuge test by 50 m^3/day), then the first level of props is installed at 1 m below the ground surface (h_{uns}=1 m).
6	Excavate to 4 m below the ground surface with the same rate of excavation, followed by the second rows of props at 1 m above the excavation level.
7	Repeat phase 6 by excavating 2 m in each phase followed by props installation with h_{avg}= 2 m until the last phase of excavation (i.e., H_e= 20 m) is completed in 80 days.

6.3.4 Two-dimensional numerical analysis

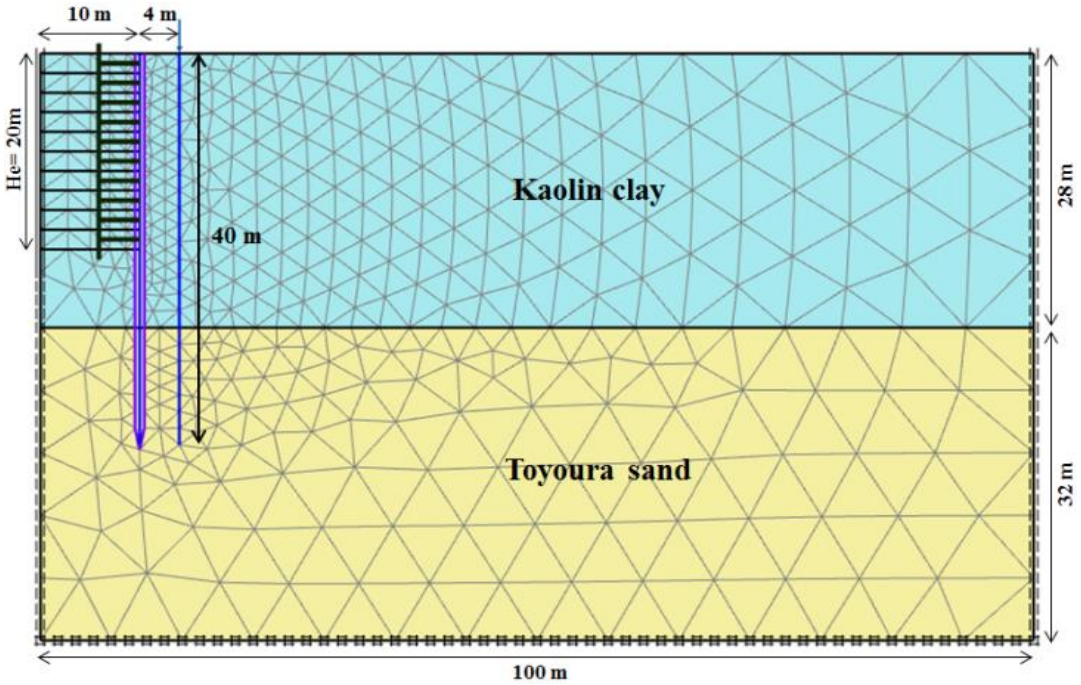

Figure 6.5 2D Finite element mesh

A two-dimensional numerical analysis, using the Plaxis 2D code with an hypothesis of plane strains (Brinkgreve et al. 2017), was also performed in parallel to the three-dimensional analysis so that the results of the two analyzes could be compared to assess the significance of the 3D behaviour. Both the retaining wall and the pile are simulated using "Plate" structural element with thickness of 1 m. The props are modelled using anchors structural elements with spacing out of plane L_s of 4 m (simulates the horizontal space between props). Plates in the 2D finite element model are composed of beam elements (line elements) with three degrees of freedom per node: two translational (U_x, and U_y) and one rotational. The dimensions, characteristics of the soil, and all the structural elements used in the 2D analysis are the same as those of the 3D analysis. Figure 6.5 shows the 2D mesh of the numerical model.

6.3.5 Results and discussions

The pile responses in terms of bending moment, lateral deflection, skin resistance, axial load, and settlement, for this reference model are shown in Figures 6.6 and 6.7. In general, it can be seen that the pile responses increase with the depth of excavation; this is due to the stress relief, soil movement due to excavation, and the dewatering.

From Figure 6.6a, it can be noted that in each stage and until the final excavation depth (Z_p/L_p= 0.5), the maximum induced bending moment occurred near the corresponding excavated depth. At the final depth of excavation, the pile bends towards the excavation as indicated by the negative bending moment magnitude (approximately $0.75L_p$ of the pile is in compression). While a positive bending moment is developed in the lower part due to 12 m of pile embedding in the dense sand layer (about $0.25L_p$ of the pile is in tension). The positive value of bending moment indicates that the side of the pile which is far away from the excavation is in tension. Because pile head was not constrained (free), zero bending moments were obtained at pile head.

During the early steps of excavation, a cantilever type deformation was observed for pile lateral deflection as shown in Figure 6.6b. For H_e= 2÷10 m, the maximum deflection occurred at the pile head and then decreased till the pile toe. As the excavation progresses in depth (H_e>10 m), due to the kinematics of the deflection in depth of the wall and the influence of props rigidity, the pile shows a deep inward displacement profile with a maximum displacement observed in depth after being at the head of the pile.

At the end of the excavation, the maximum normalised lateral displacement of the pile reaches $32\%d_p$ and occurs at a depth of $0.45L_p$, which almost corresponds to the final depth of the excavation. When the excavation depth H_e increases from 2 to 20 m, the maximum pile deflection increases from 2 to 31.8 cm which represent an increase of about 15 times. It is also observed that the displacement at the pile head is about half of the maximum displacement.

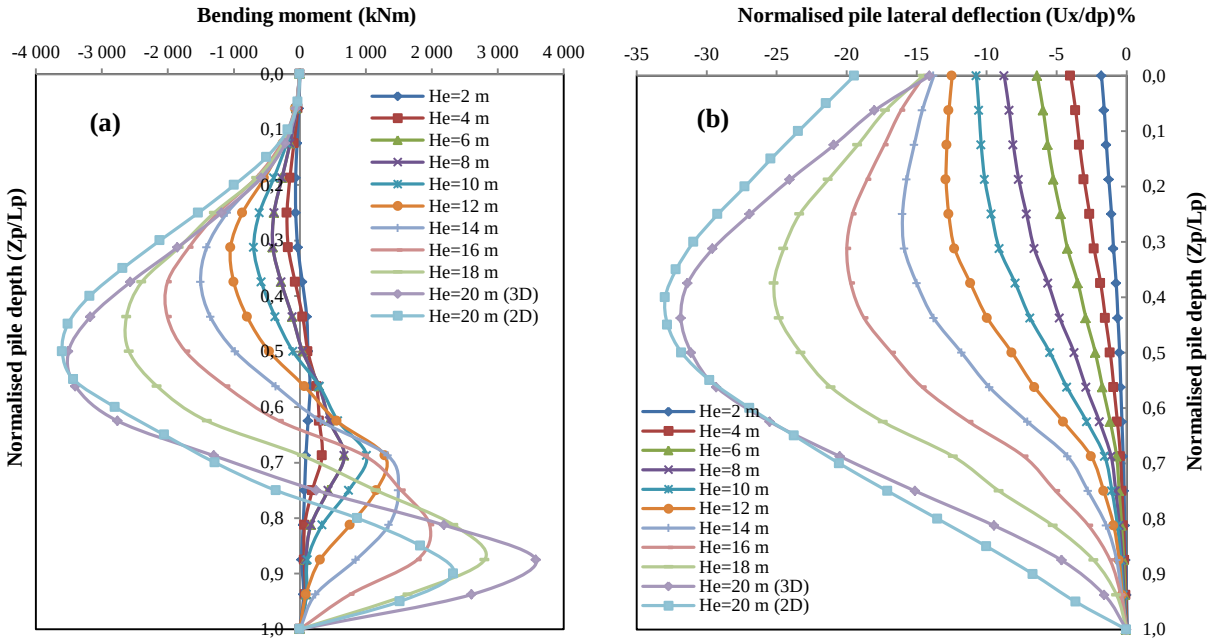

Figure 6.6 Effect of excavation on (a) pile bending moment (b) pile lateral deformation

Figure 6.7a shows the skin resistance distribution along the normalised pile length (Z_p/L_p) for different excavation phases. It can be seen that in the early stages of excavation (up to H_e= 6 m), a positive skin resistance developed almost along the pile length to support the applied load, and increases linearly with depth until reaching a maximum of 245 kN/m at the pile toe. As a result, the pile axial load decreased from the head to the pile toe as shown in Figure 6.7b. However, at the final stage of excavation, a negative skin friction is developed along the pile to a depth of $0.75L_p$ and consequently the pile axial load increased from the top to Z_p= $0.75L_p$, then decreases up to the toe of the pile due to the mobilization of positive skin friction.

The negative skin friction results in drag in the pile, and consequently in an increase in pile settlement as shown in Figure 6.7c. By analysing the results of Figures 6.6b and 6.7c, it can be noted that the maximum pile lateral deflection is about three times the maximum pile settlement (U_x/U_z= 3).

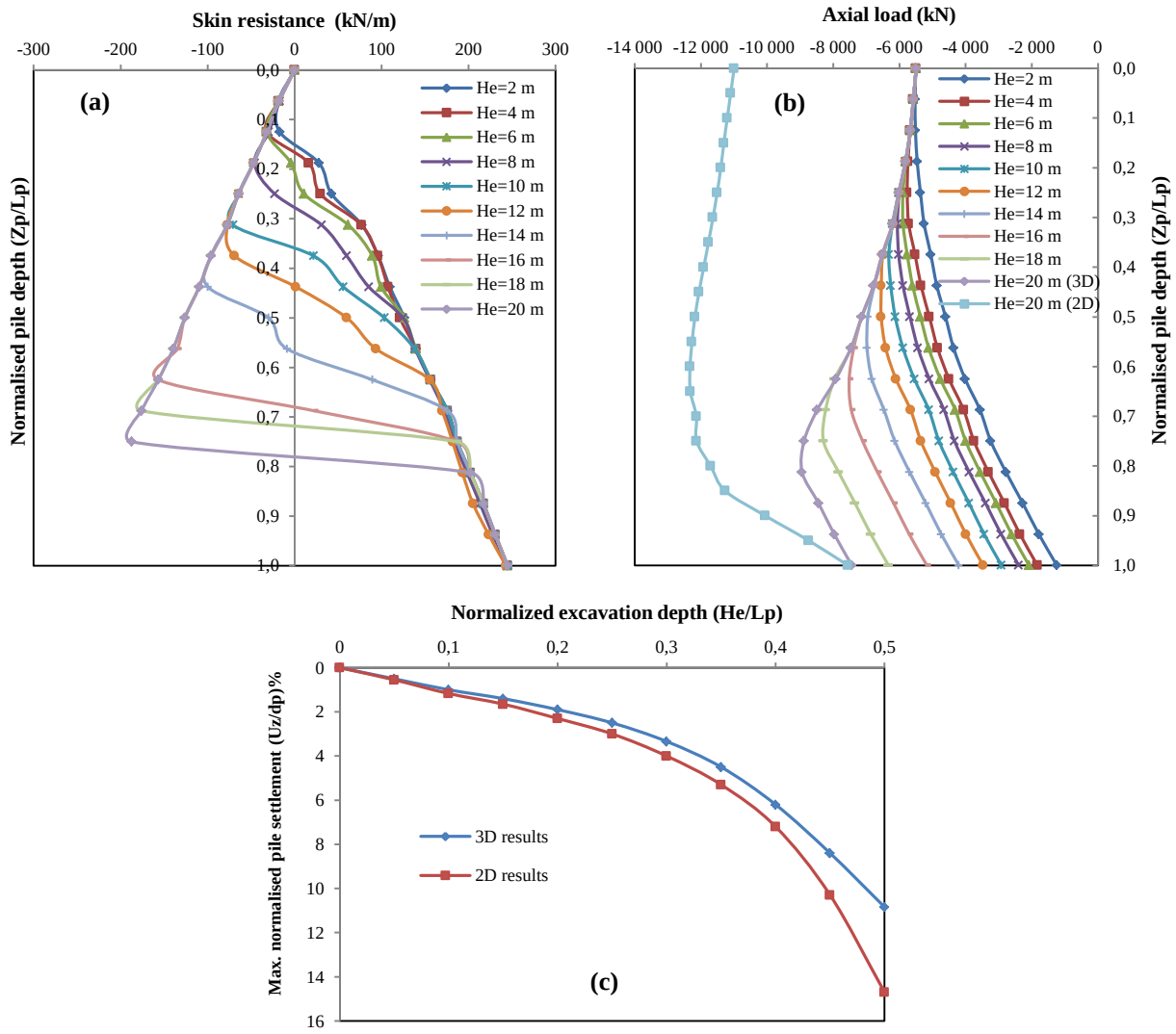

Figure 6.7 Effect of excavation on (a) pile skin resistance (b) axial load distribution (c) pile settlement

To better compare the results of the 2D model with those of the 3D model, the 2D calculation results are plotted in the same figures. The bending moment profiles and normalised pile lateral deflection at the final phase of excavation show reasonably good agreement compared to the 3D calculation, both for the shape of the curves and for the order of magnitude, nevertheless the maximum pile bending moment and lateral deflection of the 2D analysis are overestimated by 3% and 4%, respectively. Regarding the axial load and pile settlement, it can be noted that the 2D results are significantly overestimated. At the final phase of excavation, the maximum axial load and normalised pile settlement of the 2D analysis overestimates the 3D results by about 38% and 36%, respectively. These differences may be due on the one hand to the fact that the multi-propped deep excavations are in nature three-dimensional problems (Wang et al. 2010; Hong et al. 2015a; Houhou et al. 2019, 2021), and on the other hand to the simulation of the pile itself. Indeed in the plane strain model, it is not possible to represent the

3D effect of a pile because of the difficulty in selecting adequate pile parameters. In fact the pile is modelled by a plate element in 2D while in 3D analyses it is modelled by an embedded pile element. Thus, the actual properties of a 3D pile are "smeared" in the plane strain direction to obtain the equivalent pile properties per meter of width (represented by an equivalent 2D wall). For more details on formulations used to obtain the 2D equivalent wall and to converting his responses to that of a 3D pile, one can refer to section 5.3.4 of chapter 5.

From Figure 6.8 and Figure 6.9, it can be seen that there is a significant upward heave ahead the wall, however behind the wall and pile, the ground surface mainly moves in the lateral direction towards the excavation. This significant uplift ahead the wall is due to soil movements beneath the bottom of the excavation. Stresses relief beneath the excavated zone (reduction of the apparent weight of the soil) due to excavation induces a heave over the excavated bottom. As a result, soil around the lower part of the pile and wall flows in the horizontal direction towards the excavation.

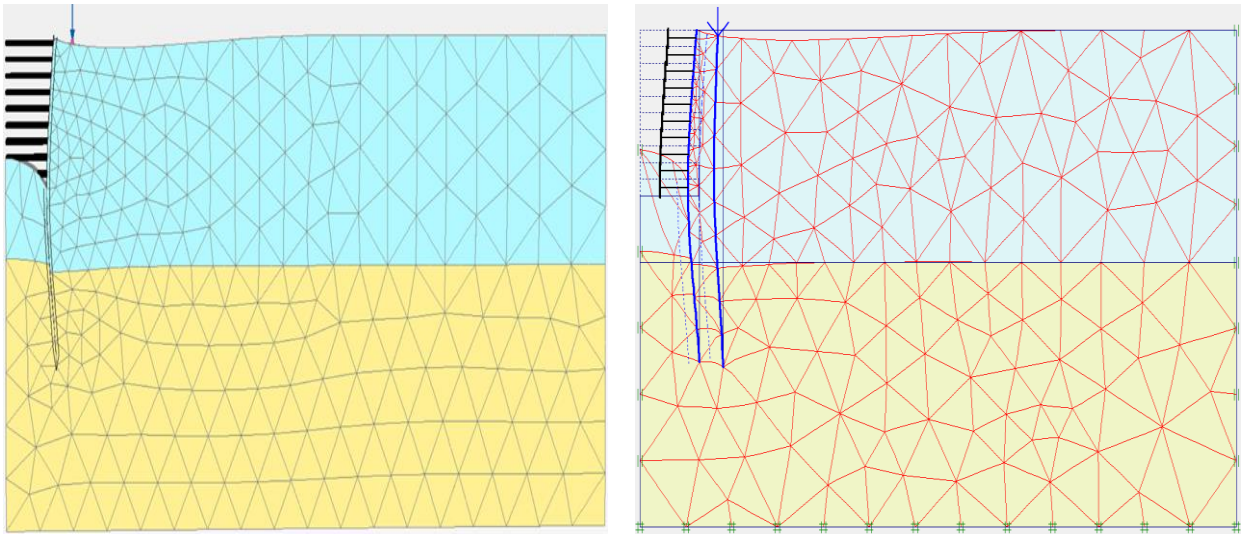

(a) **(b)**

Figure 6.8 Deformed mesh at final excavation depth. (a) 3D simulation, (b) 2D simulation

According to Figure 6.10 which represents the horizontal displacement contours of the soil, it can be seen that the pile as well as the wall undergoes the same movement as the ground towards the excavation. It should also be noted that the movements are concentrated more in the middle zone of the pile and the wall reflecting a displacement profile of deep inward type (see Figure 6.6b). Despite the final embedded length of the wall and pile is rather important in relation to the excavation bottom, a global rotation movement is observed in the lower part of the wall and pile.

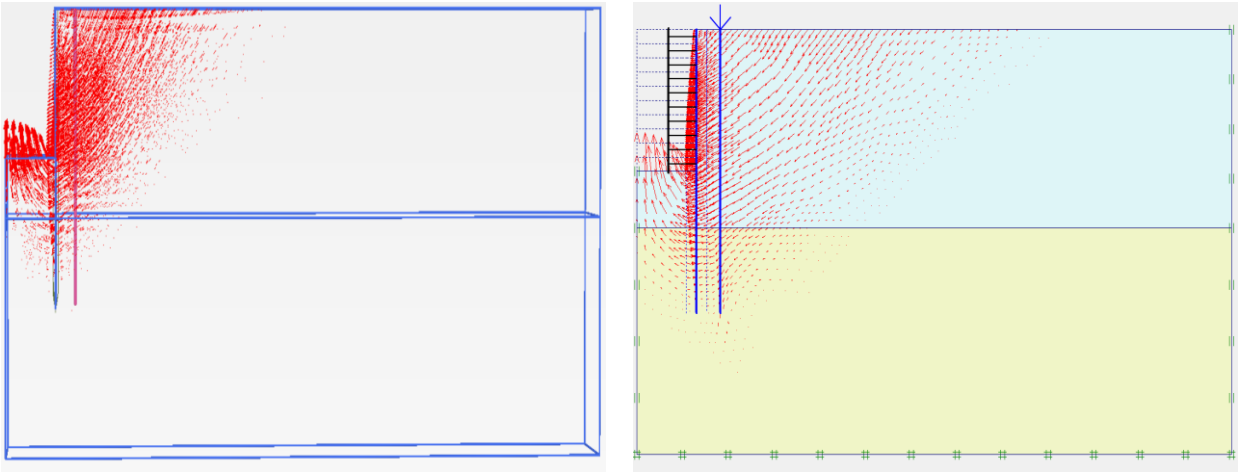

(a) **(b)**

Figure 6.9 Total displacements vector around the wall and pile at final excavation depth (H_e= 20m). (a) 3D simulation, (b) 2D simulation

By comparing the behavior in 2D and 3D, it can be noted that the volume of the ground mobilized in the two-dimensional case is more important. The extent of the movement on the surface as well as in depth is greater in the 2D case. In depth the ground movement in 2D slightly exceeds the tip of the pile (Figure 6.9b), while in 3D does not even reach the pile tip. So, as it has already been observed in Figure 6.6, movements predicted by the 2D analysis are relatively overestimated. Thus, it has been shown that the plane strain simulations might give conservative results.

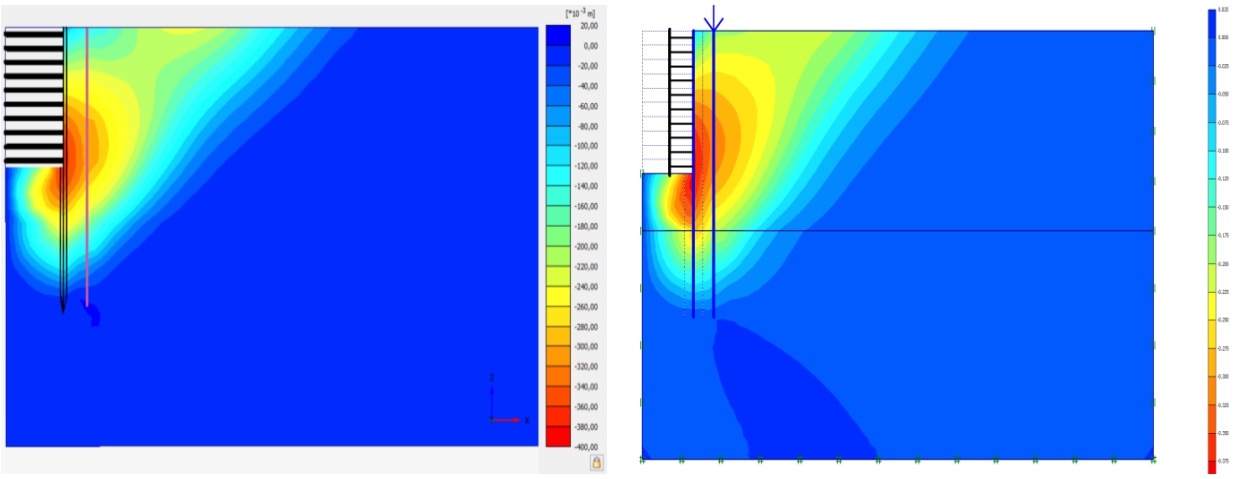

(a) **(b)**

Figure 6.10 Horizontal displacements U_x contours around the wall and pile at final excavation depth (H_e= 20m). (a) 3D simulation, (b) 2D simulation

6.4 Parametric study

Considering the full interactions, a three-dimensional parametric study was conducted to investigate the effects of some key parameters on mechanical behavior of single pile subjected to ground deformations induced by an adjacent deep braced excavation embedded in a bilayer soil. The numerical model studied in section 6.3 was used as the basic model for this parametric analysis. The main parameters used in this parametric study are summarized in Table 6.5. In addition, pile group effect was also studied. So several pile configurations were considered, including two, four, and six pile groups, for each pile configuration two cases of head conditions were examined as shown in Figure 6.20.

Table 6.5 Main parameters used in the parametric study

Parameters	**Values**
Pile location X_p [m]	4 (ref), 8, 12, 20, 30, 40, 60
Sand density D_r [%]	30, 60 (ref), 90
Wall stiffness $EI_w \times 10^6$ [kNm^2/m]	0.33/ 0.83/ 1.67/ 2.5/ 3.33 (ref)/ 16.7/ 33.3
Pile diameter d_p [m]	0.4, 0.6, 0.8, 1 (ref), 1.2
Pile length L_p [m]	10, 20, 30, 40 (ref)
Head condition	Free, pinned, fixed
Props Stiffness EA [MN]	40, 80 (ref), 120, 160, 200, 350, 500, 1000

6.4.1 Effect of pile location

Figure 6.11 shows, for different excavation depths, the distributions of maximum induced bending moment and normalised lateral deflection of a single pile located at various distances X_p from the retaining wall. In all cases, pile toe is located at two times of the final excavation depth (H_e= 20 m). These curves reveal that when the pile located farther away from the retaining wall and for any excavation depth, the induced bending moment and pile deflection decreased exponentially. This trend is more pronounced when the excavation depth is important. When the pile is located at 60 m (i.e. three times of the final excavation depth $3H_e$), the excavation does not have a significant effect on the pile behaviour and the pile response become negligible whatever the excavation depth.

At the final excavation depth, when X_p increases from $0.2H_e$ to $2H_e$ (i.e. increases 10 times), the maximum pile bending moment and lateral deflection decrease by about 87% and 80%, respectively. Figure 6.11 also shows that for any specific pile location, maximum bending moment and lateral deflection varies linearly with excavation depth. The rapid decrease of the pile bending moment with respect to the decrease of the pile lateral displacement, moving away from the excavation, indicates that the pile is subject to flowing rather than bending as it moves away from the excavation.

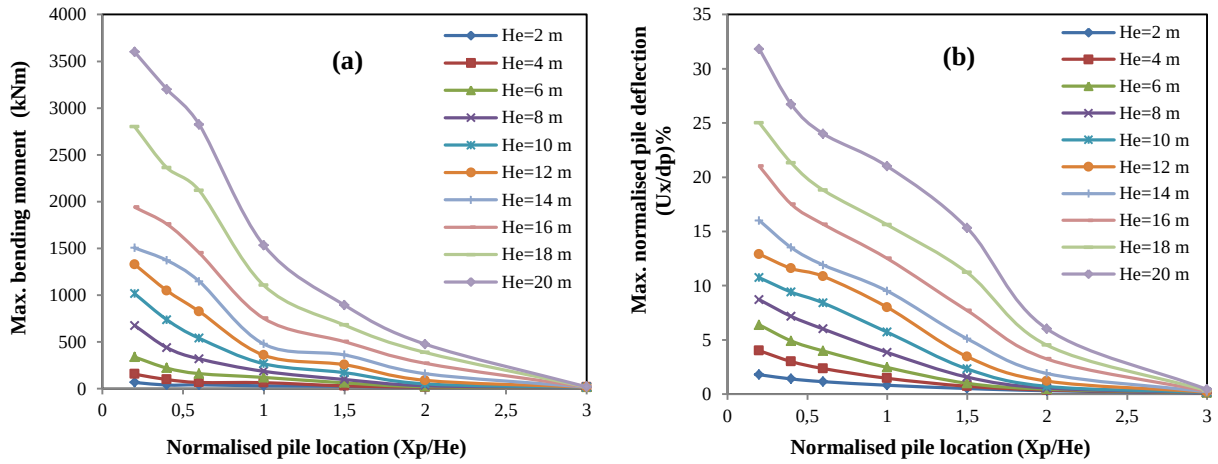

Figure 6.11 Effect of pile location on (a) pile bending moment and (b) pile lateral deflection

6.4.2 Effect of sand density

Because the pile is embedded 12 m in the underlying sand layer (about $0.3L_p$), pile responses are investigated for three cases of relative sand densities D_r= 30, 60 and 90%. Figures 6.12a and 6.12b show the bending moment and lateral deflection distribution at the final stage of excavation, respectively. While Figure 6.12c shows the maximum pile settlement for different excavation depths. Generally the numerical results indicate that the sand density has a significant effect on pile behaviour. It can be seen that pile responses decrease with increasing sand density. As for the shape of the curves, it is the same in all cases. For all cases of sand densities, the maximum value of pile responses is observed near to the final excavation depth ($0.5L_p$). From Figure 6.12a, it is also noted that with decreasing sand density, bending moment tends to shift to the negative side of the curve. It is interesting that when the pile moves toward the excavation, there is no change in pile head deflection in spite of the decreasing of sand density (Figure 6.12b). This may be due to the use of struts and the relatively high stiffness of the diaphragm wall. As the relative density of sand increases from 30% to 90%, the maximum pile responses decrease by approximately 27%, 30%, and 47% for bending moment, lateral deflection, and pile settlement, respectively. These results indicate that sand density have a major effect on pile tip resistance, where increasing sand density helps more to mobilise the working load.

It can be seen from the Figure 6.12c that bilinear increase in settlements was observed with increasing normalised excavation depth (H_e/L_p) in each case. The pile settlement increased linearly with excavation depth, nevertheless, the rate of induced settlement increased with further excavation steps in each case. The maximum pile settlement U_z is about 15% d_p, 10.8% d_p, and 8% d_p for D_r= 30, 60 and 90%, respectively.

Through the results of these tests, it should also be noted that the ratio between the maximum horizontal displacement U_x and the maximum settlement U_z is not constant but increases with increasing the density of the sand. U_x/U_z = 2.5, 3, and 3.5 for D_r = 30, 60 and 90%, respectively.

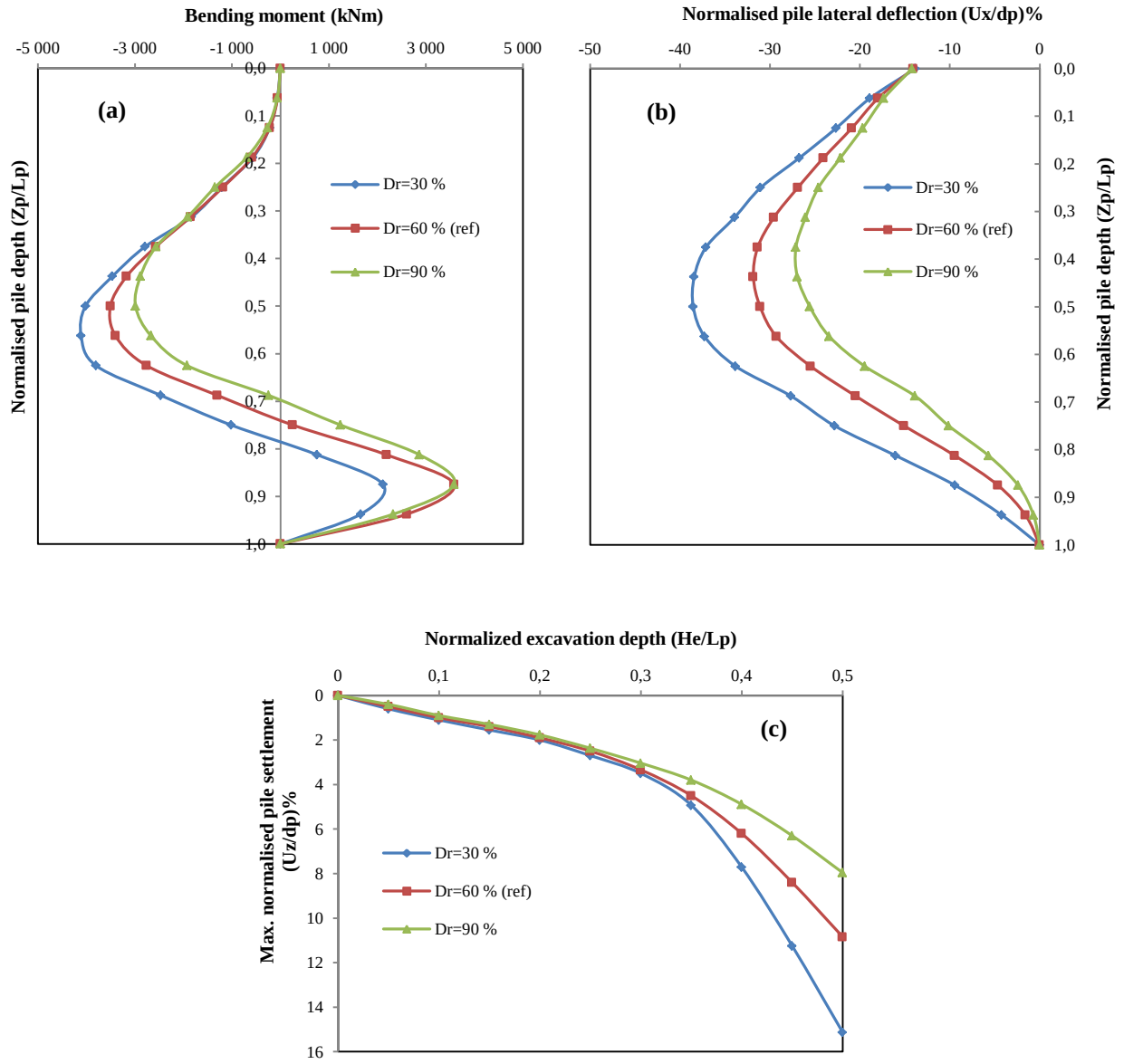

Figure 6.12 Effect of sand density on (a) pile bending moment, (b) pile lateral deflection, and (c) pile settlement

6.4.3 Effect of excavation support system

The rigidity of the retaining wall, the number and stiffness of the struts are essential parameters for controlling the movements induced by the excavation. The total rigidity of the support system which includes among others the rigidity of the wall and struts spacing has been much considered. There is many ways to study the influence of excavation support system. In this study only the effect of system stiffness factor, the unsupported excavation depth h_{uns}, props axial stiffness EA, and the excavation width are investigated.

6.4.3.1 Effect of system stiffness factor and unsupported excavation depth

In the literature there are several proposals to define the rigidity of the support system. In addition to the flexural stiffness of the wall (EI_w), often used by its logarithm, Clough and O'Rourke (1990) introduce the approach of the stiffness of the wall-support system through the average vertical spacing of struts (h_{avg}): $S = (EI_w)/(\gamma_w h_{avg}^4)$. They developed the approach for strutted excavation to compute the normalised lateral wall displacement (δ_{hm}/H_e) for soft to medium clays. For h_{avg}= 2 m, the influence of system stiffness factor (S) on pile behaviour was studied by varying wall bending stiffness EI_w (see Table 6.5). Figure 6.13 shows the influence of the system stiffness factor (S) on the pile behavior, at the intermediate and final excavation phases, for different values of unsupported excavation depth h_{uns}.

According to Figure 6.13, there is a significant effect of support system factor on pile behavior in particular in the final phase of excavation. Bending moment and normalized lateral deflection of the pile decrease exponentially with increasing support system factor. At the final phase of excavation with h_{uns}= 5 m, it is found that increasing the support system factor up to 10^5 decreases the pile bending moment and lateral deformation by approximately 71% and 57%, respectively. It should be noted that in the case of h_{uns}= 1 m, the pile response decreases by 78% and 42% for the bending moment and the deflection, respectively. Thus, increasing the factor (S) up to 10^5 is more beneficial when h_{uns} becomes lower.

It is clear that when the support system factor increases beyond 10^5, there is no further significant reduction in maximum bending moment and lateral movements of the pile.

The trend shown in Figure 6.13 highlights the negative impact of the unsupported excavation depth on pile performance and the need for enforcing a strict restriction on this depth to limit pile movements to acceptable levels, especially in the case of low system stiffness factor.

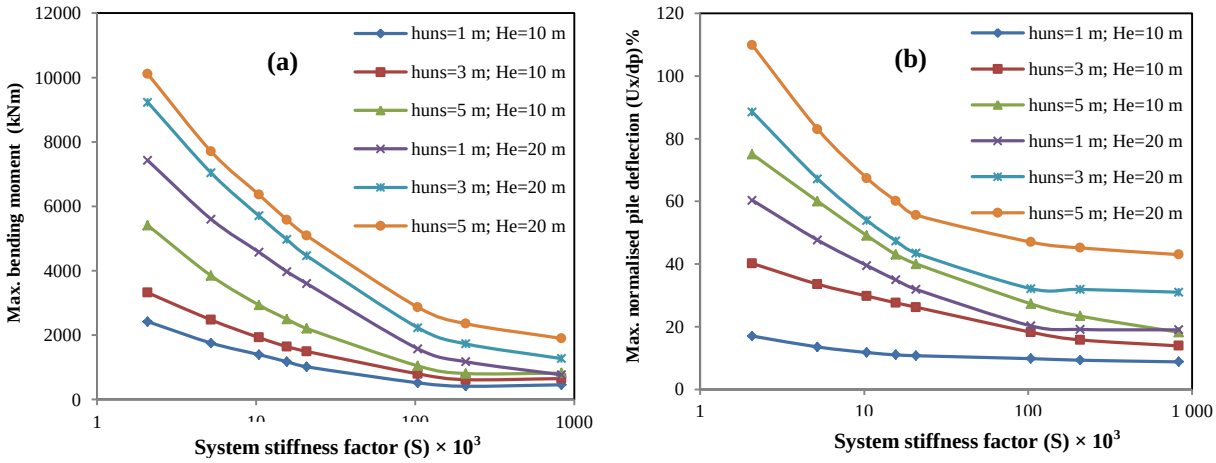

Figure 6.13 Effect of system stiffness factor on (a) pile bending moment and (b) pile lateral deflection

6.4.3.2 Effect of props axial stiffness and excavation width

To better understand the effect of the support system on the pile performance, the axial stiffness of the props (EA) was also studied. Figure 6.14 shows the variation of the maximum bending moment and normalised lateral deflection with *EA*, for a range of excavation width (B/H_e), at the final stage of excavation (H_e= 20 m). The props are spaced 2 m vertically and 4 m horizontally for a pile located 4 m ($4d_p$) away from the retaining wall. It can be noted that the pile response decreases exponentially with increasing *EA*, especially in terms of lateral deformations. This tendency being more pronounced for a higher value of B/H_e.

It should be noted that there is a significant reduction in pile responses in the range 40 to 500 MN. While by increasing *EA* beyond 500 MN, no palpable influence is recorded on the behavior of the pile. For B/H_e= 1, an increase in *EA* from 40 to 500 MN causes a decrease in the maximum pile bending moment and lateral deflection of more than 40% and 70%, respectively. On the other hand, the curves reveal that whatever the value of the props stiffness, the maximum bending moment and the lateral deformations of the pile increase by increasing B/H_e. In the case of low axial rigidity (EA = 40 MN), it may be noted that when B/H_e ranges from 0.25 to 1, the maximum pile bending moment and lateral deflection increase by almost 100% and 230%, respectively. Almost the same tendency was observed in the case of significant rigidities.

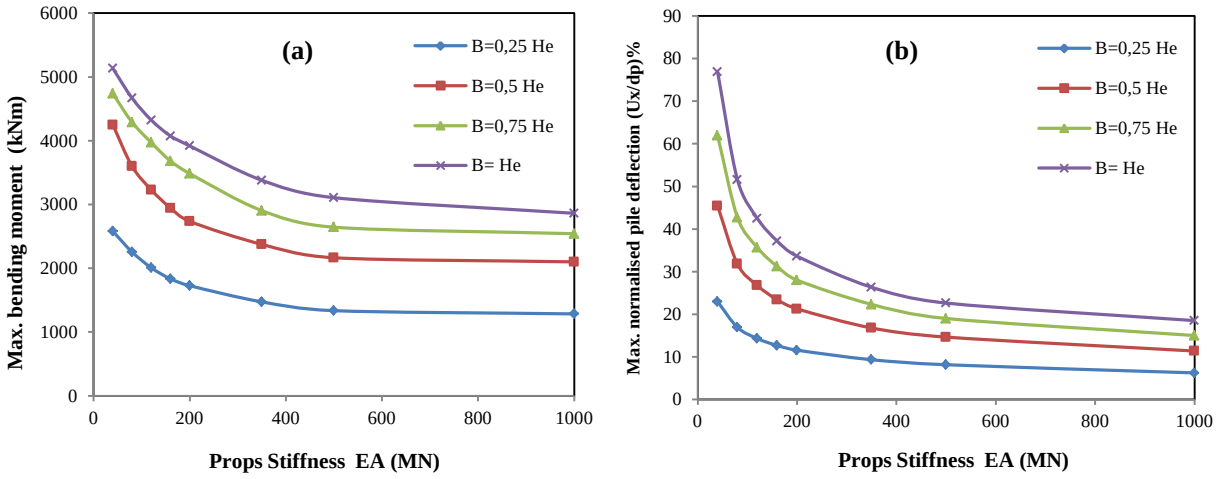

Figure 6.14 Effects of Props axial stiffness and normalised excavation width on (a) bending moment and (b) pile lateral deflection (H_e= 20 m)

6.4.3.3 Effect of props horizontal and vertical spaces

Figure 6.15 and Figure 6.16 shows the pile maximum induced bending moment and pile lateral deflection with various props horizontal and vertical spaces for the six last stages of the excavation. In Figure 6.15, the vertical space was fixed to h_{avg}= 2 m and the horizontal space were changed. While in Figure 6.16, the horizontal space is fixed to 4 m and the vertical space was changed. It should be noted that in both cases, the first level of props is installed at depth

h_{uns}= 1 m. For vertical space case, the number of props levels depends on the studied case (varying of vertical space), therefore depends on the geometry of each case.

It can be seen that the evolution of the max bending moment is quite similar to that of the lateral deflection. From these figures, it appears that whatever the excavation depth, the response of the pile increases significantly with the increase in the horizontal and vertical space of the struts. When the excavation depth is relatively low (H_e=10, 12 m), the effect of the horizontal and vertical spacing of the props is less important on the behaviour of the pile. However, when the excavation progresses in depth (H_e=14÷ 20 m), the effect becomes more obvious. Moreover, for a depth of excavation 0.5L_p, when the horizontal space of the props decreases from 10m to 2m, the pile response decreases to about half. Almost the same remark is valid for the props vertical space effect.

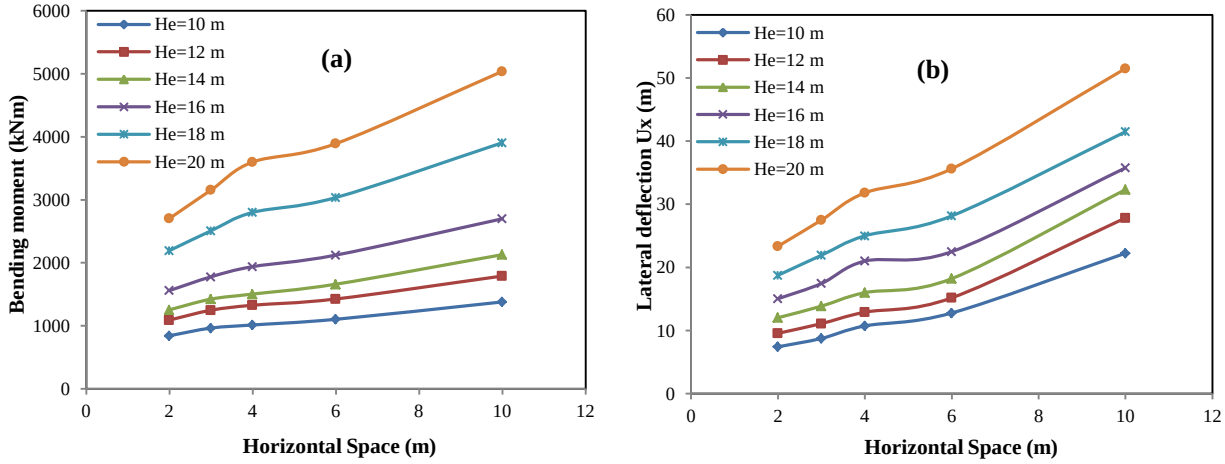

Figure 6.15 Props horizontal space effect on (a) bending moment (b) lateral deflection

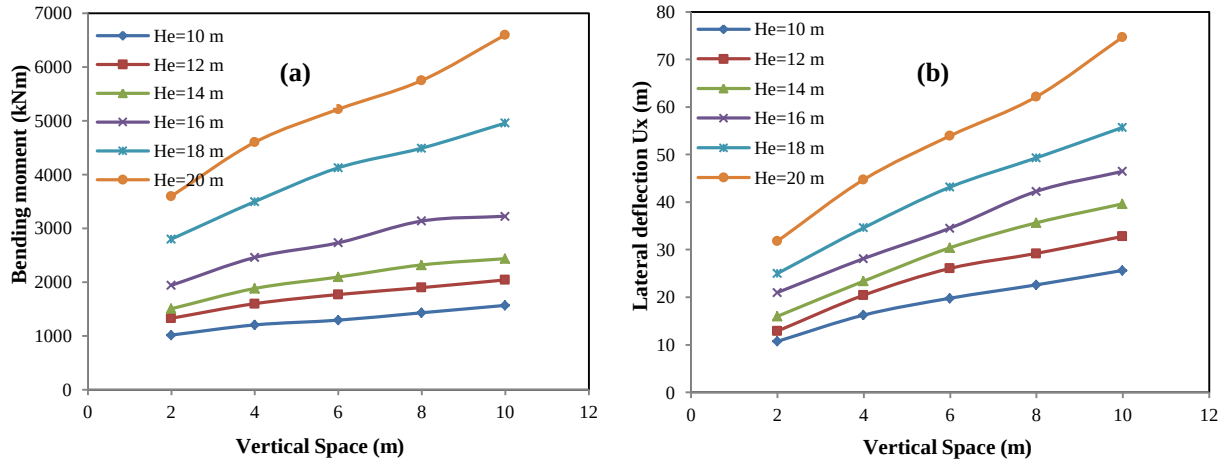

Figure 6.16 Props vertical space effect on (a) bending moment (b) lateral deflection

6.4.4 Effect of pile stiffness

Using different pile diameters (see Table 6.5), the influence of pile stiffness on pile behaviour for the maximum excavation depth H_e= 20 m are investigated (Young's modulus is fixed at 30 GPa). For the results given in Figure 6.17, the pile is located at $4d_p$ away from the wall, which is supported by props spaced 2 m vertically and 4 m horizontally, having axial rigidity of EA= 81×10^3 kNm. The results show that the distribution of bending moment and lateral deflection are quite similar in shape. It can be seen that the induced bending moment increases with increasing of pile stiffness as shown in Figure 6.17a. While Figure 6.17b reveal that the maximum pile lateral deflection decreases with increasing of pile stiffness.

When the pile diameter varies from 0.4 to 0.8 m, the maximum bending moment occurred in the lower part of the pile at Z_p= $0.875L_p$. While for d_p= 1 and 1.2 m, the maximum negative bending moment is higher in magnitude than the positive one (observed in the upper part of pile near to Z_p= $0.5L_p$). It's noted also that for d_p= 0.4÷0.8 m, the pile rigidity does not have a significant influence on the pile deflection. It is noted that with increasing the pile stiffness, the pile head deflect towards the wall from $11d_p$% to $17d_p$% for d_p = 0.4 to 1.2 m, respectively. These results show good agreement with studies conducted by (Poulos et al. 1997) to investigate pile stiffness effect on pile behaviour using the two stage analysis method (TSAM). Where due to its larger stiffness (solid pile), pile deflection decrease slightly with increasing pile diameter but generally follows the soil movement unless the pile is very stiff (d >1 m).

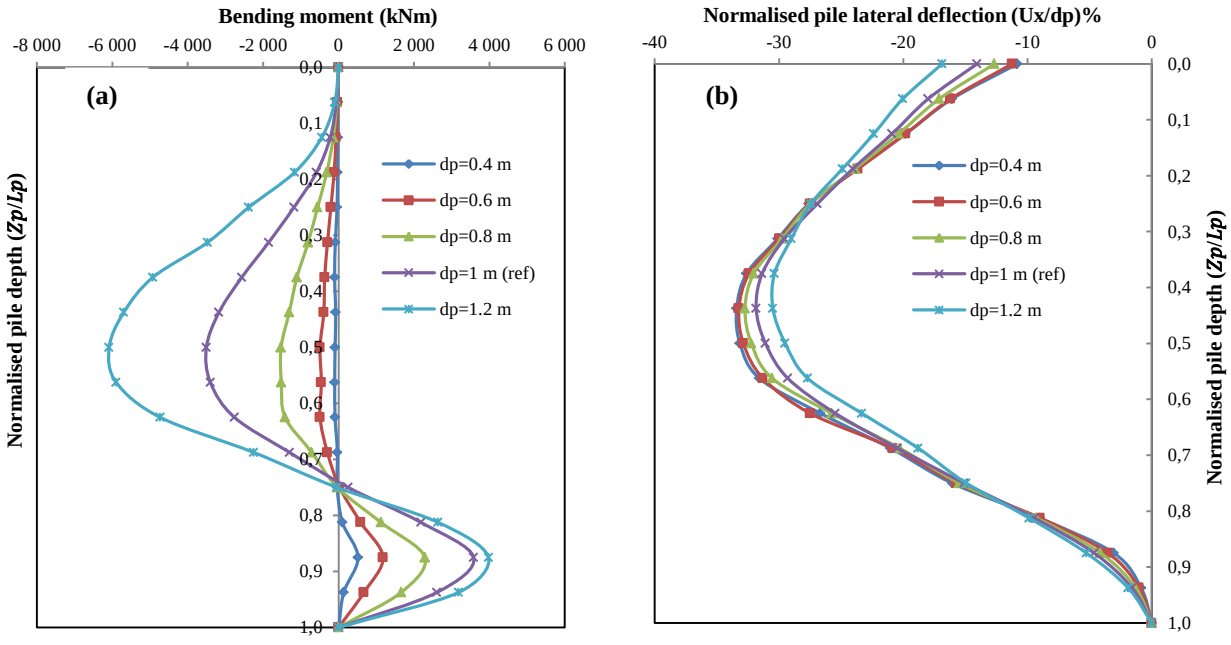

Figure 6.17 Effect of pile stiffness on (a) pile bending moment (b) pile lateral deflection (H_e= 20 m)

6.4.5 Effect of pile length

For the final excavation depth (H_e= 20 m), in order to highlight the pile length effect, pile responses are investigated using four different pile lengths (i.e. L_p/H_e= 0.5; 1; 1.5; 2), consequently using different working load (i.e. 415 kN; 958 kN; 2140 kN; 5500 kN, respectively). From Figures 6.18a and 6.18b, it can be seen that when the base of the pile is still in the soft clay layer (L_p/H_e= 0.5 and 1), the bending moment along the entire pile is negative, and the pile deflection is almost linear (the toe of the pile moves more than its head). So this is the response of a floating pile due to excavation-induced soil movements. When the pile toe is located below the final excavation level and within the dense sand layer (end bearing pile), maximum bending moment and lateral deflection always occurred at the final excavation level, and then reduced till the pile toe. Up to a pile length equal to $1.5H_e$, the bending moment remains negative along the pile (which implies that the tensile fiber is located on the face of pile opposite to excavation), whereas in the case L_p/H_e= 2, positive bending moment is developed in the lower part of the pile.

From Figure 6.18a it can be seen that no bending moment was induced at/near pile head in all the 4 cases, since there was no rigid constraint at the pile head (pile head was free to move and rotate). Figure 6.18b shows, in all cases studied, that the pile head remains almost unchangeable and represents almost half of the maximum deflection, it can also be noted that as excavation was carried out, the pile deflected towards excavation in all the four cases. This is because of excavation-induced effective stress relief and soil movement towards excavation.

From Figure 6.18c, it can be seen that the axial load increases with the increase of pile length, and in all cases the pile is subjected to a compressive force. In the cases of floating pile (L_p/H_e= 0.5 and 1), most of the working load is mobilised by the positive skin resistance developed along the pile, and the maximum axial load occurs at the pile head and then continues to decrease until the pile toe. For end bearing piles (L_p/H_e= 1.5 and 2), due to negative skin friction developed along the upper part, the axial load increases from the pile head to reach a maximum value at the depth $0.75L_p$, then it decreases until pile toe due to the positive skin resistance developed in the lower part of the pile. As the pile length increases from 10 to 40 m, the maximum axial load increases by about 22 times. According to the 3D results obtained in this study (Figure 6.19), when the axial load applied at the pile head increased from 2140 kN (L_p/H_e= 1.5) to 5500 kN (L_p/H_e= 2), the increase in induced pile lateral deflection and bending moment are negligible.

Figure 6.18d shows the normalised pile vertical settlement (U_z/d_p) profile along the pile length after the final excavation depth in all four cases (i.e. L_p/H_e= 0.5; 1; 1.5; 2). It can be seen that the pile head settlement increases with decrease of pile length. The single pile experienced maximum settlements (due to the excavation work and the existence of working-load) of 108 mm, 187 mm, 263 mm and 277 mm (i.e., 10.8%, 18.7%, 26.3% and 27.7% of pile diameter) in case of L_p/H_e= 2, L_p/H_e= 1.5, L_p/H_e= 1 and L_p/H_e= 0.5, respectively. Which means that the

pile experiences higher settlement if the pile toe is located closer to the final excavation level (pile toe is subjected to the largest stress release, leading to a large reduction in pile toe resistance). On the other hand, the pile settlement profile is uniform along its depth. This is because of higher stiffness of concrete as comparative to soil.

These results reveal that the pile performance depends, among other parameters, on the relative position of the pile toe with respect to the excavation level.

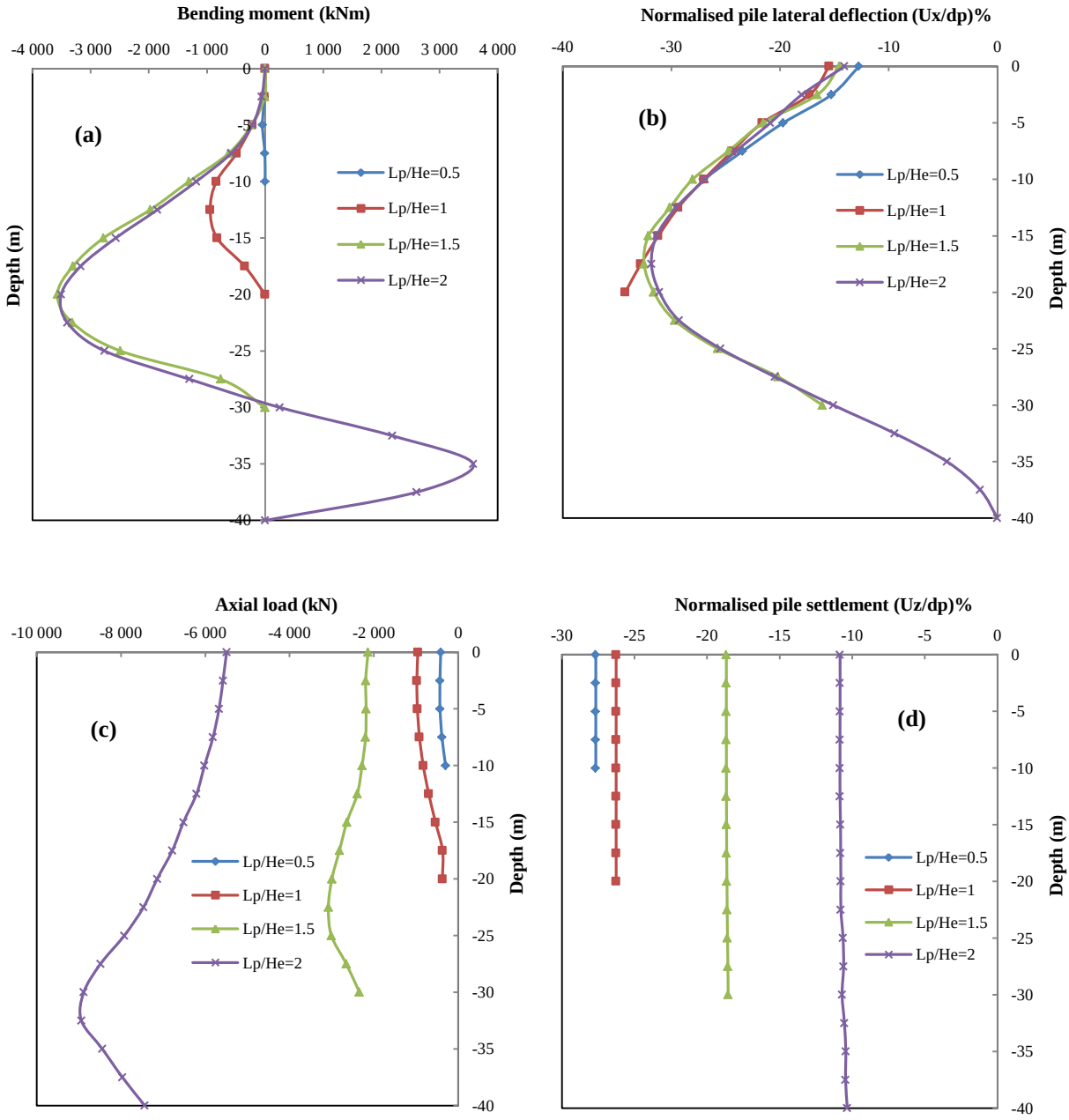

Figure 6.18 Effect of pile length on (a) pile bending moment (b) lateral deformation (c) axial load (d) pile settlement (H_e= 20 m)

6.4.6 Effect of head conditions

Several researches show that the pile head conditions have major effects on pile performance, either by using centrifuge tests (Leung et al. 2000; Leung et al. 2003) or using numerical methods (Liyanapathirana and Nishanthan, 2016; Soomro et al. 2019a), particularly on the induced bending moments and pile lateral deflection. Poulos et al. (1996) study the free translation and fixed rotation as another type of head condition. The embedded pile element used in this numerical analysis has six degrees of freedom per node: three translations (U_x, U_y and U_z) and three rotations ($\emptyset_x, \emptyset_y,$ and $\emptyset_z$). The *create point prescribed displacement option* implemented in PLAXIS 3D is used to study the effect of the support conditions of the pile head, where three cases were investigated: free head, pinned head, and fixed head.

Simulation of the three cases as follows: free case is simulated by a free head pile (both translation and rotation are free). The case of pinned head is simulated by fixing only the translation U_x and U_y, which is likely to correspond to the situation where the pile head-pile cap connection is pinned, or where single piles supporting superstructure columns are often connected by tie beams to enhance the overall foundation stability. In fixed case, all translation (U_x, U_y and U_z) and rotation ($\emptyset_x, \emptyset_y$ and $\emptyset_z$) are fixed, which is likely to correspond to the situation where a massive pile cap is restrained by ground beams, or when the pile is part of a pile raft foundation for a large structure.

Figure 6.19 shows the pile responses at the last stage of an adjacent excavation. It shows that the pile head conditions play an important role and affect the pile responses, especially in the upper part of the pile, while there is no great change noticed in the lower part. For both the induced bending moment and pile lateral deflection, the maximum values were occurred near the final excavation depth $H_e = 0.5L_p$ except the fixed case. From Figure 6.19, in general, it appears that the shape of the curves is quite similar for all cases considered, whether for the bending moment or the deflection of the pile.

As the pile head is free, it can be seen that the induced bending moment is zero at pile head. In terms of lateral displacements, the deflection at the pile head is approximately 50% of the maximum deflection that occurred in the middle of the pile length.

In pinned case, it can be seen that the bending moment at pile head is zero because the pile head was still free to rotate. However, a large negative bending moment developed at the upper part of the pile. The pile head deflection has been effectively eliminated in this case.

In fixed case, a significant positive bending moment develops at the upper part of the pile (maximum value about 5300 kNm at pile head), which can increase the risk of possible structural damage to the pile. However, the pile head deflection is totally eliminated, and the deflection in the upper half section of the pile is relatively less than the previous cases, so that the maximum deflection decreased about 11%.

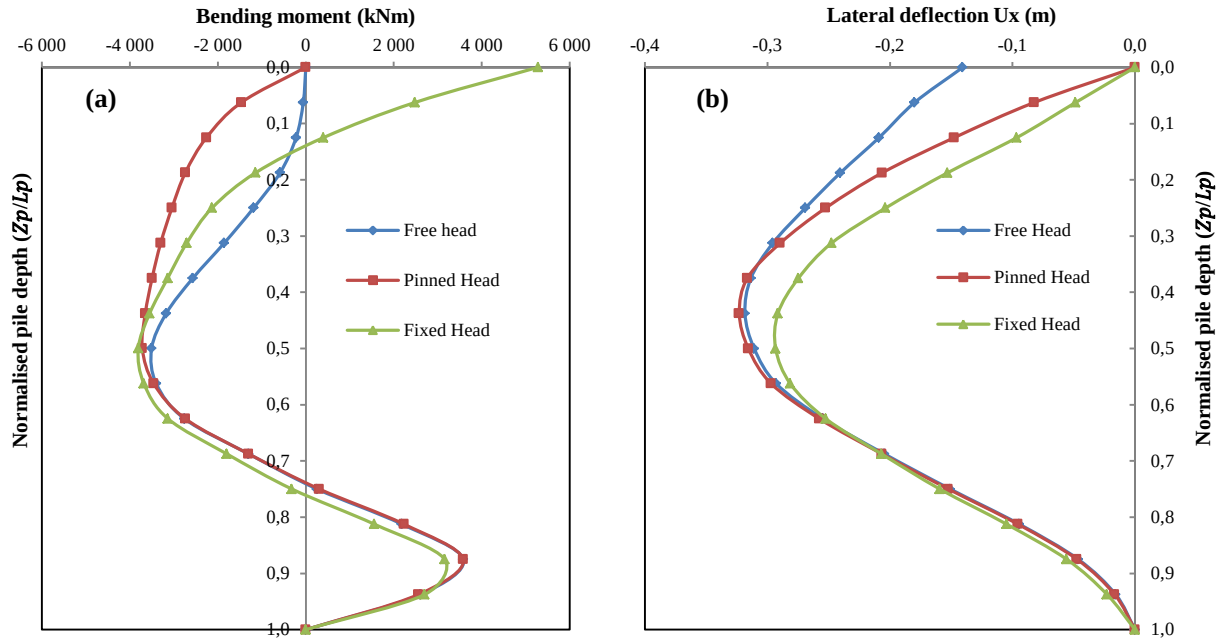

Figure 6.19 Effect of head conditions on (a) bending moment and (b) pile deflection

6.4.7 Effect of pile group

In practice, piles are frequently used in groups especially in urban areas. Both numerical and experimental studies have been carried out to investigate the influence of ground movement on pile group response during nearby excavations. One can refer to the research work used the centrifuge tests (Leung et al. 2003; Ong et al. 2009), or using numerical methods to study these types of geotechnical problems (Nishanthan et al. 2017; Shakeel and Ng, 2018; Soomro et al. 2018b). In this context a parametric study is carried out to investigate the behaviour of piles in groups at the final stage of excavation (H_e= 20 m). For this purpose, several configurations of pile group were considered including two, three, four and six single piles. Each configuration has been tested for two different pile head condition cases, namely free and capped. Schematic configurations for all pile group tests are presented in Figure 6.20. The dimensions, characteristics of the soil and all the structural elements (wall, props, and piles) used in the analysis are the same as those of the single pile case. The horizontal distance between the retaining wall and the front piles row is X_p= 4 m. For the horizontal direction X and Y, the center-to-center spacing between piles was $4d_p$ except test 6 (S_p= $2d_p$). In capped-head case, the pile cap was assumed to be at 1.0 m above ground surface to avoid interactions between the pile cap and the soil surface. But this does not prevent the different interactions that can occur between the different individual piles through the pile cap. The pile cap is made from reinforced concrete with thickness of 1.0 m which is modeled as a linear elastic material using a 6-node triangular plate element with a Young's modulus of 30 GPa and Poisson's ratio of 0.2. The pile cap bending rigidity depends on the configuration of the piles facing the excavation.

Test No.	1, 2, and 3	4	5	6, and 7	8	9, and 10	11	12	13	14	15	16
Pile Group Configuration												
Pile Head Condition	Free	Free	Capped	Free	Capped	Free	Free	Capped	Free	Capped	Free	Capped
Geometric Parameters	For all tests, the front piles are located at distance from the wall X_p=4 m and centre-to-centre S_p=4d_p, Except : - Test 02 and Test 03: Xp= 8 and 12 m, respectively. - Test 07: X_p=8 m and centre-to-centre S_p=4d_p - Test 10: X_p=6 m and centre-to-centre S_p=2d_p ; • Pile; d_p:Pile diameter; Retaining wall; Pile cap											

Figure 6.20 Pile group configurations used in the analysis

6.4.7.1 Two and three-pile groups

Figure 6.21a shows the induced bending moment distribution of 2-pile group parallel to the wall configuration, where tests 4 and 5 investigate the free-head and capped-head cases, respectively. Due to symmetry, only one pile responses were presented. The test result of a single pile case located at the same position labelled test 1 is plotted in the same figure for comparison. It can be seen that the distribution of bending moment are quite similar in shape. In each case, the maximum induced bending moment occurred near the final excavated depth H_e= 20 m. Pile response in the upper part is very close to that of the single pile. A positive value of bending moment in the lower part is developed. A negligible bending moment developed in pile head for test 5 (due to the presence of pile cap). However, the results indicate that the induced bending moment of the single pile was larger than that of the pile group. The same remark for the maximum lateral deflection as shown in Table 6.6. It's noted also that the pile deflects by the same magnitude for tests 4 and 5.

Figure 6.21b shows the distribution of the induced bending moment of a group of 2 piles arranged perpendicular to the wall for two configurations, the free-head and capped-head cases which represent test 6 and test 8 respectively. The front and rear piles are located at 4 and 8 m away from the retaining wall, respectively. Whether in test 6 or 8, the distributions of bending moment are quite similar in shape for the front and rear piles. It can be seen that the front piles experiences the highest effect from the excavation. It is clear that the existence of the front pile which is located inside the wedge of weakened soil reduces the harmful effects of the deep excavation on the rear pile.

Because the pile head is restrained for the capped-head 2-pile group case (test 8), a positive bending moment has developed in the upper part of the pile (Z_p= 0.25L_p) for the front and rear piles. In both tests, the piles deflected by approximately the same maximum value as shown in Table 6.6.

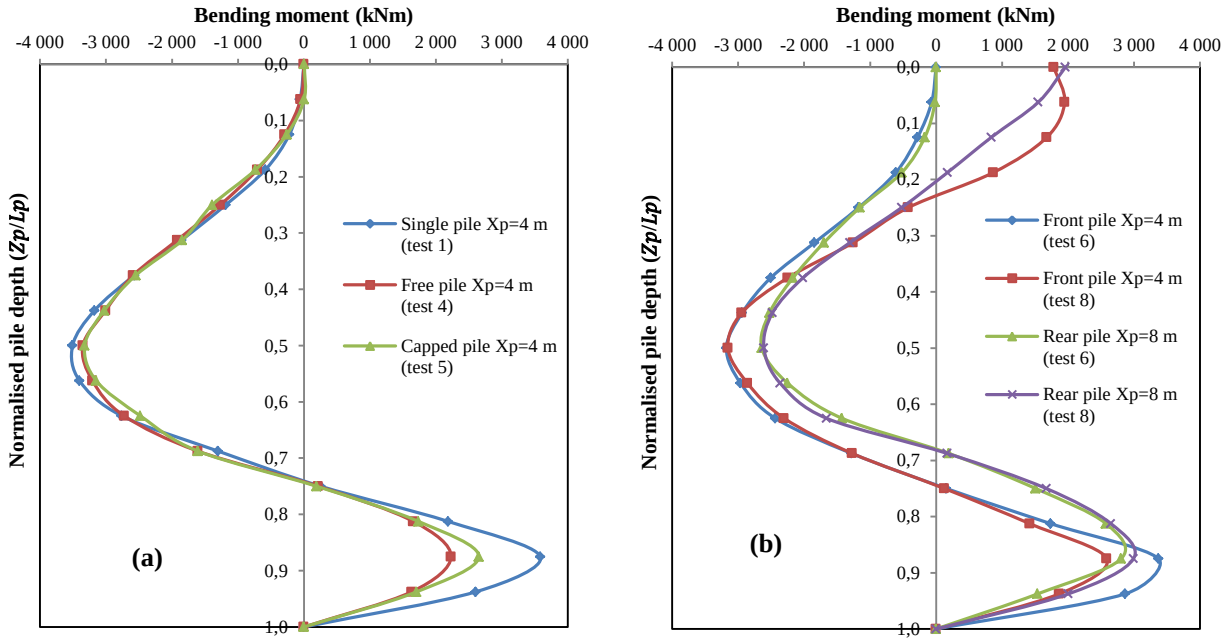

Figure 6.21 Pile response for (a) 2-pile parallel to the wall (b) 2-pile perpendicular to the wall (H_e=20 m)

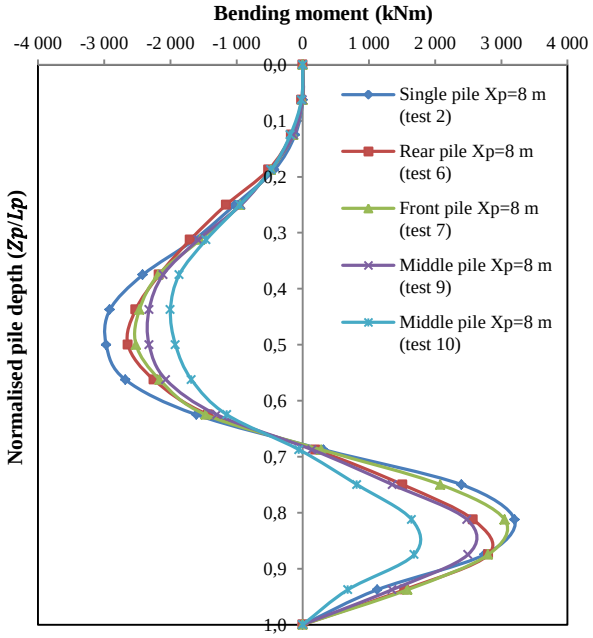

Figure 6.22 Bending moment of pile situated at X_p=8 m from the wall

A third case presented to study the behaviour of a pile situated at the same distance from the wall in 2, and 3-pile group configuration (Figure 6.22). Only free-head pile group case is presented. The intended pile is that located 8 m from the wall. In test 6 and test 7 it represents front pile and rear pile, respectively. While it represents the middle pile with $4d_p$ and $2d_p$ centre-to-centre spacing between piles for test 9 and 10, respectively. For comparison, the test result of a single pile case located at the same position labelled test 2 is plotted in the same figure. It can be seen that the distribution of bending moment profiles are quite similar in shape for the five tests. Because of group effect, the magnitude of induced bending moment of the pile has reduced (test 6, 7, 9, and 10), in particular for the middle pile case when compared to that of single pile at the same location (test 2). The pile in test 7 is playing the role of the front one unlike in test 6 where the existence of the front pile diminishes the detrimental effects of excavation on the rear pile.

Test 9 and 10 was conducted also to study the effect of centre-to-centre spacing between piles. It appears that when centre-to-centre spacing decreases from $4d_p$ to $2d_p$ the pile response decreases. Figure 6.22 also reveals, after comparing the groups of 2 and 3 piles, that as the number of piles increases, the response of the piles decreases. For these tests (pile located at $8d_p$ from the wall), the corresponding pile deflection is slightly reduced as shown in Tables 6.6. It can be seen that the front pile experiences the highest deflection followed by the middle and rear pile, respectively.

6.4.7.2 Four-pile groups

Tests 11 and 12 were conducted involving a free-head and capped-head four-pile group, respectively. These tests include a pair of front piles and another pair of rear piles located at 4 and 8 m from the wall, respectively. Due to symmetrical arrangement of piles relative to the excavation face, only two piles behaviour is presented (one at 4 m and another at 8 m from the wall). The results of these 2 tests in terms of pile bending moment are shown in Figure 6.23. The results of two tests labelled test 1 and test 2 (single pile located at X_p= 4 m and 8 m, respectively) are plotted in the same figure for comparison with those of the front and rear piles.

It can be seen that either for test 11 or test 12 (front or rear piles), the distributions of induced bending moment are quite similar in shape with that of single pile cases. In each case, the maximum bending moment occurred near the final excavated depth (H_e= 20 m). A positive value of bending moment in the lower part is developed owing to 12 m (about $0.3L_p$) of pile embedment into the underlying dense sand layer. As the pile head is free (test 1, 2, and 11), the induced bending moment is zero at pile head. Due to pile cap restraint (test 12), significant positive bending moment is developed in the upper part (Z_p= $0.2L_p$) for both front and rear piles. In both configurations (free and capped head), the pile response is always higher when the pile is in the forward position than when it is in the rear position, in other words, front piles experience the highest effect of excavation. Therefore, the existence of front piles row reduces the harmful effects of excavation on the rear piles.

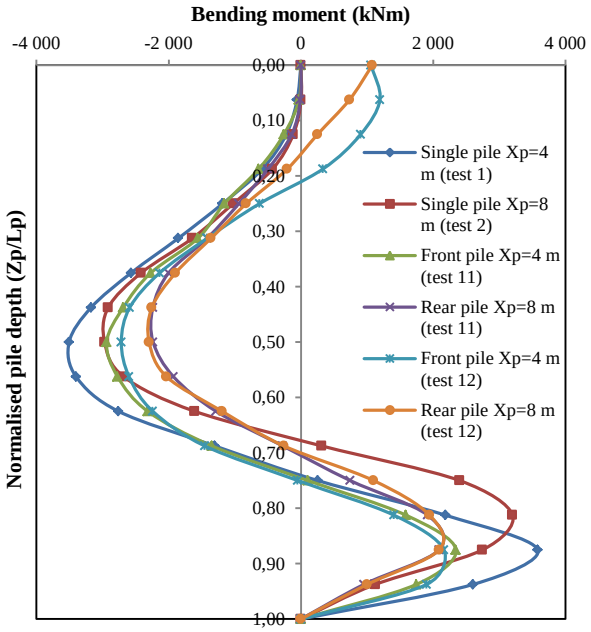

Figure 6.23 Pile bending moment of free and capped-head 4-pile group (Test 11 and Test 12)

The 3D numerical results show that the maximum bending moment of the front pile is greater than that of rear pile by about 29% and 19% in the free and capped case, respectively. The curves reveal also that the induced maximum pile bending moments in 4-pile group are smaller than those of the single pile case (test 1 and 2) due to group positive effect. By comparing the results of tests 11 and 12, the magnitude of the induced bending moment for the capped-head pile group (front or rear pile) is slightly smaller than that of the free-head case due to group interaction effect, and because of the presence of the pile cap which diminishes the effect of the working load (where this pile cap are used to first transmit the working load to the connected piles and then transmit it to the underlying bedrock), unlike when apply directly an axial load on every single pile in free-head pile group case. From Figure 6.23, it can also be noted that the maximum front pile bending moment in the free case is larger than that in capped case by only 8%, however the maximum bending moment of the rear pile in the free or capped case is almost the same.

As to the piles lateral deflection, the results are consistent with those found for the induced bending moment. As shown in Table 6.6, the maximum pile lateral deflection of the front or the rear piles in the 4-pile groups (tests 11 and 12) is smaller than that of a single pile situated at the same distance behind the diaphragm wall (tests 1 and 2). This may be due to the positive effect of the group and to the "shadowing" effect of the front pile over the rear pile.

The results show that the maximum lateral deflection of front pile (test 11 or 12) is smaller than that of single pile located at the same distance from the wall (test 1) by about 10%, however the deflection of rear pile is lesser (test 11 or 12) than that of single pile situated at X_p= 8 m (test 2) by about only 7.5%. However it is noted that the value of the maximum lateral

deflection of the front piles in the free-head case (test 11) is almost the same as that of the front piles in the capped-head case (test 12). This also applies to the rear piles.

In Table 6.6, it can also be noted that the maximum pile lateral deflection of the front pile is greater than that of rear pile by about 18% and 16% in the free and capped case (test 11 and 12), respectively.

Table 6.6 Maximum pile lateral deflection for different pile group configurations (H_e =20 m)

Tests No.	Maximum pile lateral deflection in (cm)		
	Front Piles	**Middle Piles**	**Rear Piles**
1	31.8	/	/
2	26.7	/	/
3	24	/	/
4	31	/	/
5	31	/	/
6	30	/	26
7	25.3	/	21.56
8	29.9	/	25.6
9	29.8	25	21.3
10	26.4	24.7	23.7
11	29	/	24.6
12	28.5	/	24.5
13	28	25	20.9
14	27.25	22.7	20.5
15 (centre piles)	27.8	/	24
16 (centre piles)	27.3	/	23.45

For comparison and using the PLAXIS 2D code (Brinkgreve et al. 2017), a two-dimensional analysis was also performed in parallel with that case of three-dimensional analysis (four-pile group configuration (2×2)). The 3D single pile properties are multiplied by the number of similar piles in the plane strain direction and smeared (divided) by the pile group centre-to-centre spacing (s) in the plane-strain direction as shown in Figure 5.6b (see chapter 5), while the deflection results remain similar.

Figure 6.24a and 6.24b shows comparison between 2D and 3D computed bending moment for test 11 and 12, respectively. In general, the curves have similar shapes and the results show that there is a good agreement between the two models, except for the rear piles which are less predicted by the 2D model compared to those of the 3D analysis. The same cannot be said for the maximum lateral deflection, which is very close to that of the 3D calculation: 29 and 26 cm for test 11, while 28.5 and 27.8 cm for test 12, for front and rear piles, respectively.

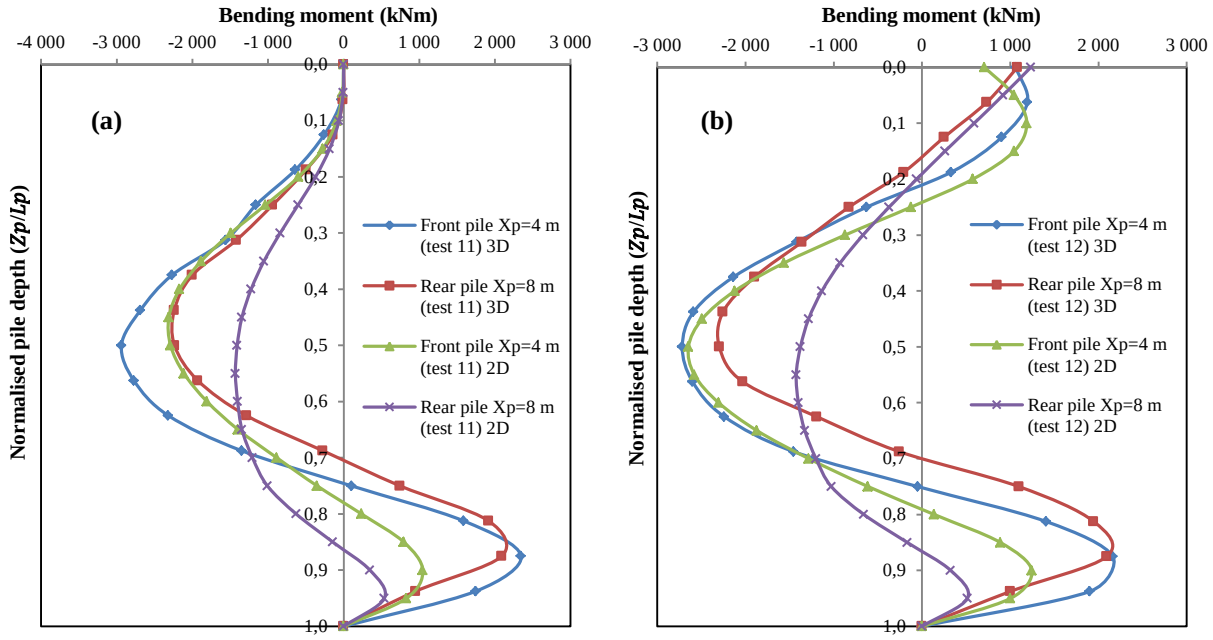

Figure 6.24 Comparison of bending moment in 2D and 3D FE for 4-pile group (a) free-head (b) capped-head (H_e=20 m)

6.4.7.3 Six-pile groups

Four tests were performed to study piles responses for the six-pile group configuration. Two tests of (2 piles×3 rows) configuration were conducted for free and capped-head cases labeled test 13 and test 14, respectively (see Figure 6.20). These tests involved three pair of piles: front, middle, and rear piles, located at 4, 8, and 12 m behind the wall, respectively. In addition, two other tests labeled test 15 and 16 were carried out; it is the (3 piles×2 rows) configuration.

Figure 6.25a shows the distribution of bending moment for the 2×3 configuration (tests 13 and 14). Since the response of the piles located at the same distance from the wall is identical due to the symmetry of the model in the longitudinal direction, only three piles behavior is presented (those located at 4, 8, and 12 m from the wall). It can be seen that when the piles was located further away from the wall, the induced bending moment decreased exponentially. As can be observed, the first pair of piles experiences the highest bending moment, followed by the middle piles, with the rear pair experiencing the lowest bending moment. From Figure 6.25a, the maximum bending moment of the front piles (test 13) is higher than that of middle, and rear piles by about 25% and 83%, respectively. Between Z_p= 0.3L_p and Z_p= 0.8L_p, for both tests 13 and 14, the front, middle and rear piles behave almost the same.

By comparing the piles located at the same distance from the wall, it is found that the bending moment of the capped-head pile group is slightly smaller than that of the free-head case.

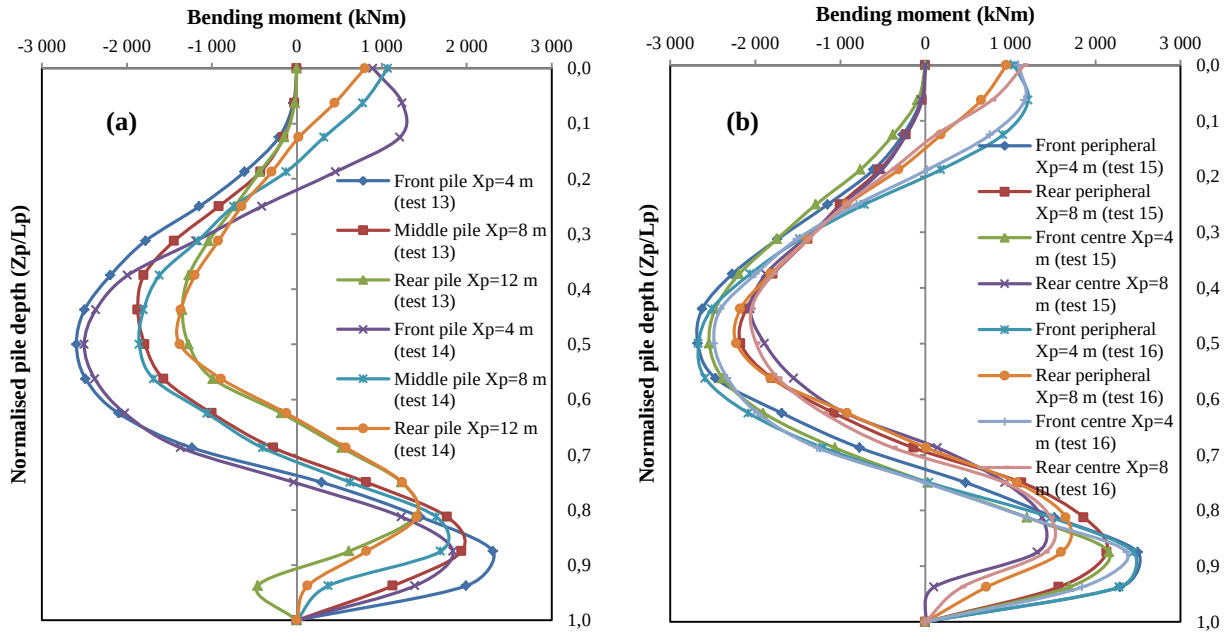

Figure 6.25 Bending moment for 6-pile groups (a) 2×3 configurations "test 13 and 14" (b) 3×2 configurations "test 15 and 16"

Due to the influence of the group and the interaction through the pile cap, a substantial positive bending moment developed at the pile head for test 14. According to the results obtained in the previous section, it should be noted that the pile bending moment of a group of 6 piles is in order lesser than that of a group of 4 piles and single pile. In addition to the shadowing effect, it is thought that the diminution in ground movements is due to increased piles reinforcing the soil behind.

Consistent with the observed pile bending moment in Figure 6.25a, the maximum lateral deflection of the front piles is the largest, followed by the middle piles, and then finally by the rear piles (see Table 6.6). However, there is no significant difference between the maximum deflection of the piles of the free and capped-head cases.

In tests 15 and 16, four types of piles named as follows: front peripheral, rear peripheral, front centre and rear centre pile are used to illustrate the behaviour of piles in 3×2 configurations (2 rows of 3 piles) as shown in Figure 6.25b. The curves of this figure reveal that the induced bending moment profiles are similar in shape. Whatever type of pile, peripheral or centre, the responses of the front piles are more important than those of the rear piles, which agrees well with the previous findings (tests 11, 12, 13 and 14). From Figure 6.25b, the maximum bending moment of front piles (peripheral or centre) is greater than that of rear piles (peripheral or centre) by about 20% in the case of free-head (test 15). In the case of capped-head (test 16), due to pile cap restraint, a significant positive bending moment is developed at piles head. It should also be noted that peripheral piles experience the highest effect of ground movements due to excavation. It is obvious that peripheral piles protect and reduce the impact of soil movement imposed on

central piles, in particular rear piles. Figure 6.25b also shows that the maximum bending moment of peripheral piles (front or rear) is higher than that of the centre piles (front or rear) by almost 10% in the case of capped-head. Analysis of the results shows that the responses of the piles in the 2×3 pile group are smaller compared to those of the 3×2 configurations. Indeed, in the 2×3 configuration, the last two pairs of piles (middle and rear piles) represent two thirds of the group which is located relatively far from the wall, unlike the 3×2 configuration (2 rows of 3 piles) where the first row, which represents half of the group, is in the primary influence zone (very close to the wall).

Concerning the piles lateral deformations, the results obtained are consistent with those obtained for the induced bending moment. As shown in Table 6.6, the deflection of front centre pile is slightly higher than that of rear pile.

6.5 Conclusion

In this chapter, single pile behaviour due to deep braced excavation-induced soil movements embedded in bilayer soil (soft clay overlying dense sand) was investigated using a full three-dimensional numerical analysis, which was verified using some centrifuge test results found in the literature. The relevance of the 3D model is also judged by comparison with a 2D model. A thorough parametric study is carried out to investigate the effects of excavation depth, pile location with respect to the excavation wall, sand density, stiffness of the support system, pile stiffness, head conditions, and pile length. The effect of pile group on pile performance was also investigated using different pile group configurations.

The 3D results obtained indicate that due to soil movements, the dewatering, and soil stress relief upon excavation, the pile response in terms of bending moment, lateral deflection, axial load, skin resistance, and pile settlement increases significantly with excavation depth. Bending moment and pile lateral deflection using 2D analysis show good agreement compared to those of the 3D calculation. However the 2D plane strain model might give conservative results. Regardless of the excavation depth, the maximum lateral displacement and the bending moment of the pile decrease exponentially with the distance from the excavation. They become negligible when the pile is located at a distance of $3H_e$ from the wall. At the final excavation depth, when the sand relative density increases from 30% to 90%, the maximum pile responses decrease by approximately 27%, 30%, and 47% for bending moment, lateral deflection, and pile settlement, respectively. With increasing the support system factor, both pile lateral deformation and maximum bending moment decrease exponentially. However, when the support system factor exceeds 10^5, support system has no noticeable influence on pile behaviour. It should be noted that the increase of the system stiffness (Without exceeding 10^5) becomes more beneficial when the unsupported excavation depth h_{uns} is low. The maximum pile bending moment and lateral displacement decreases exponentially with increasing props axial stiffness *EA* (particularly the

lateral deformations). This tendency is more pronounced as the normalised excavation width (B/H_e) increases. When *EA* exceeds 500 MN, no perceptible influence on the pile behaviour is recorded. Whatever the value of *EA*, the maximums of the bending moment and the lateral deformation of the pile increase by increasing B/H_e.

Pile head condition has a massive impact on the pile performance with increasing degree of pile head fixity, especially near pile cap in terms of induced bending moment, and pile lateral deflection. In other words, the development of bending moment is very high in upper part of the pile and the deflection is totally eliminated (pinned and fixed cases). Pile length variation testing revealed that pile performances depend on the pile toe position relative to the excavation level. As the pile length increases from 10 to 40 m, the maximum axial load increases by about 22 times. In the case of floating pile (when the pile toe is still in the soft clay layer, L_p/H_e= 0.5 and 1), the pile experiences higher settlement because the pile toe is subjected to the largest stress release, resulting in a significant reduction in the pile toe resistance. When the pile toe is below the final excavation level (the case of end bearing pile), a positive bending moment and skin resistance develop in the lower part of the pile.

The bending moment and lateral deflection of pile within a pile group depends, among other parameters, on its location with respect to the other piles of the pile group (front, middle, or rear pile), its distance from the retaining wall, pile head condition (free-head or capped-head), the number of piles in the group, and centre-to-centre spacing.

General Conclusion

The research work presented in this thesis focuses on the numerical analysis of the effect of ground movements induced by the construction of underground structures on adjacent pile foundations. The objective of this research work is to investigate single pile and pile group responses due to tunnelling or deep excavation induced soil movements in soft clay overlying dense sand using the explicit finite element code PLAXIS 2D & 3D. The response of vertical piles to excavation-induced movements is evaluated in terms of: bending moment distribution, lateral pile deflection, axial force induced in the pile (compression, tension), pile settlement, skin resistance distribution, and pile bearing capacity.

Unlike previous studies which investigated the problem in homogeneous geological context (sand or clay), in this thesis, the pile response was thoroughly studied in bilayer soil. To take into account the small-strain nonlinear behaviour of the soil, the Hardening soil model with small-strain stiffness (HSs) was used in the present numerical analyses.

This thesis consists of two main parts:

The first part is devoted to a bibliographic study containing four chapters, the first two chapters presents a literature review on methods developed by researchers to predict tunnelling induced ground movements in sands and clays, and the various studies that address the problem of the effects of tunnelling on piles and piled structures (pile-soil-tunnel interaction problems). The second two chapters presents a literature review on the various popular methods available to predict ground movements due to deep excavation, and the various existing methods to investigate piles responses due to ground movement induced by adjacent deep excavation (wall-soil-pile interaction problems).

The second part, which includes two chapters, is the subject of the various contributions made in this research. It involves numerical modeling to observe the additional responses of the adjacent piles due to the effect of the movements of the surrounding ground induced by the digging of the underground works, namely tunnels or deep excavations. The numerical modeling of these underground structures includes four main aspects: construction phasing, three-dimensional effects, hydromechanical coupling and soil-pile-structure interactions.

The validation of the numerical models was based on the results of centrifuge tests found in the literature. The relevance of the 3D models was also judged by comparison with the 2D plane strain models using the PLAXIS 2D code. The various numerical calculations carried out show that the movements of the ground around the underground structures and consequently the responses of the piles in the vicinity depend on a multitude of parameters: the geometry and in particular the size and depth of the structural elements, the behavior of the soil mass, the stiffness of the various elements constituting the problem, the geometric configuration of pile groups, and construction phasing.

First, a full 3D numerical analysis is carried out to study the effect of ground movements caused by tunneling on the behavior of adjacent piles in soft clay overlying dense sand. The Slurry Pressure Balance (SPB) technique is used in this study to simulate the construction of the tunnel. The numerical analyses mainly focus on both vertical and horizontal single pile responses. From a 3D numerical reference model, an extensive parametric study was conducted to investigate the effect of some key parameters such as tunnel advancement, volume loss, pile location, pile length, pile diameter, tunnel diameter, over consolidation ratio of the clay, and tunnel depth. To give supplementary comprehensions concerning groups of piles, a 2×2 pile group with two different pile head conditions (free and capped) was considered. Based on the numerical analyses results obtained and within the range of the parameters tested and soil conditions, the following conclusions can be drawn:

- The results obtained from the 3D numerical modelling show that due to tunnelling-induced soil movements, the pile response in terms of transverse bending moment, axial force, shaft resistance, transverse deflection and pile settlement increases considerably with the advancement of the tunnel**.** Pile responses seem stabilized once the tunnel face is in front of the pile by a distance of twice the tunnel diameter. However in the longitudinal direction, the maximum pile responses (bending moment and deflection) occur when the working face is at the same level as the pile location. Nevertheless the magnitude of the pile responses remains very low compared to those in the transverse direction (a reduction coefficient up to 2.3 was observed).
- Except bending moment, where the 2D analysis shows good agreement with the 3D simulation, the pile responses using 2D numerical analysis are overestimated. Thus, 2D plane strain modelling could give conservative results.
- As the volume loss increases from 1% to 3%, pile head settlement, lateral deflection, bending moment, and axial force increase by 83%, 140%, 53%, and 12% maximum, respectively. The effect of volume loss on pile responses only becomes noticeable when the tunnel face is located from a back distance of 2 times the tunnel diameter. Noting that the effect of the volume loss is all the more important as the diameter of the pile is large.
- Excavating a tunnel close to a pile not only causes ground deformations, but also can reduce the pile bearing capacity. By increasing the volume loss from 1% to 3% the apparent loss of pile capacity (ALPC) increases from 11% to 20%.
- The variation in pile length revealed that the pile performance depends on the position of the pile toe with respect to the tunnel depth. The pile experiences greater settlement if the pile toe is located above the tunnel horizontal axis. This is because the pile tip is subjected to the greatest stress release, which results in a large reduction in the pile tip strength and shaft resistance**.** By increasing the pile length from $0.5H_t$ to $1.5H_t$, the maximum pile head settlement and lateral deflection decrease by about 63% and 18%, respectively. In contrast to the pile displacements, the induced bending moment and axial load constantly increases with the increase in the pile length. When the pile length

increases from $0.5H_t$ to $1.5H_t$, the maximum bending moment and axial load increase by about 7 and 13 times, respectively.

- For any pile length, pile responses decrease exponentially with lateral distance from the tunnel axis. When the pile is located at a distance beyond $2.5D_t$, the pile responses become insignificant.
- The increase in theoretical excavated volume (V_t) induces more stress release and soil movement towards the tunnel, which will affect the pile responses. The 3D results showed that increasing the tunnel diameter from 6 m to 10 m results in a 120%, 75% and 63% increase in maximum lateral deflection, pile settlement and bending moment, respectively.
- Variation in tunnel depth significantly influences the behaviour of single piles. It was found that an increase in tunnel axis depth from $1.5D_t$ to $2.5D_t$ (with $L_p = 3D_t$) results in an increase in the maximum magnitude of lateral deflection, pile settlement, bending moment, and axial force of about 420%, 146%, 32%, and 30%, respectively.
- As expected, the stress soil history significantly affects the pile response. When the OCR of the clay increases from 1 to 1.5, for $V_l = 3\%$, the maximum bending moment and lateral deflection of the pile decrease by about 59%.
- Increasing of pile rigidity increases the bending moment and decreases lateral deflection.
- In general, the results obtained showed that the pile responses are lower in the pile group than in the single pile case, indicating a positive group effect. The response of a pile within a pile group depends, among other parameters, on its location in the group (front or rear pile), and pile head conditions (free or capped head).

Secondly, a full three-dimensional numerical analysis is performed to investigate single pile and pile group responses due to deep excavation-induced soil movement in bilayer soil. To better understand the single pile behaviour, a thorough parametric study was carried out using 3D numerical model. It focuses on the effects of excavation depth, pile location, sand density, support system rigidity, pile stiffness, head conditions, and pile length. In order to provide further insights about the response of pile group system, several configurations of pile group were considered including two, three, four and six single piles. Each configuration has been tested for two different pile head condition cases, namely free and capped. Based on numerical results and analysis presented herein, the following conclusions can be drawn:

- The 3D results obtained indicate that due to soil movements, the dewatering, and soil stress relief upon excavation, the pile response in terms of bending moment, lateral deflection, axial load, skin resistance, and pile settlement increases significantly with excavation depth.
- Bending moment and lateral deflection using 2D analysis show good agreement compared to those of the 3D calculation. However the 2D plane strain model might give conservative results.

- Regardless of the excavation depth, the maximum lateral displacement and the bending moment of the pile decrease exponentially with the distance from the excavation. They become negligible when the pile is located at a distance of $3H_e$ from the wall.
- At the final excavation depth, when the sand relative density increases from 30% to 90%, the maximum pile responses decrease by approximately 27%, 30%, and 47% for bending moment, lateral deflection, and pile settlement, respectively.
- With increasing the support system factor, both pile lateral deformation and maximum bending moment decrease exponentially. However, when the support system factor exceeds 10^5, support system has no noticeable influence on pile behaviour. It should be noted that the increase of the system stiffness (Without exceeding 10^5) becomes more beneficial when the unsupported excavation depth h_{uns} is low.
- The maximum pile bending moment and lateral displacement decreases exponentially with increasing props axial stiffness *EA* (particularly the lateral deformations). This tendency is more pronounced as the normalised excavation width (B/H_e) increases. When *EA* exceeds 500 MN, no perceptible influence on the pile behaviour is recorded. Whatever the value of *EA*, the maximum bending moment and pile lateral deformation increase by increasing B/H_e.
- Variation of pile diameter indicates that the bending moment in the pile increases with increasing of pile stiffness. However the pile lateral deflection decreases with increasing of pile stiffness.
- Pile length variation testing revealed that pile performances depend on the pile toe position relative to the excavation level. As the pile length increases from 10 to 40 m, the maximum axial load increases by about 22 times. In the case of floating pile (L_p/H_e= 0.5 and 1), the pile experiences higher settlement because the pile toe is subjected to the largest stress release, resulting in a significant reduction in the pile toe resistance. When the pile toe is below the final excavation level (the case of end bearing pile), a positive bending moment and a skin resistance develop in the lower part of the pile.
- Pile head condition has a significant impact on the pile performance with increasing degree of pile head fixity, especially near pile cap in terms of induced bending moment, and pile lateral deflection. In other words, the development of bending moment is very high in upper part of the pile and the deflection is totally eliminated (pinned and fixed cases).
- The bending moment and lateral deflection of pile within a pile group depends, among other parameters, on its location with respect to the other piles of the pile group (front, middle, or rear pile), its distance from the retaining wall, pile head condition (free-head or capped-head), the number of piles in the group, and centre-to-centre spacing.

For a preliminary design, the numerical analyzes studied in this thesis can serve as a practical basis for similar projects.

References

Ahmed, S. M. (2014). State-of-the-art report: deformations associated with deep excavation and their effects on nearby structures. Ain Shams University, Cairo, Egypt, p. 164.

Al-Omari, R. R., Al-Soud, M. S., & Al-Zuhairi, O. I. (2019). Effect of tunnel progress on the settlement of existing piled foundation. Studia Geotechnica Et Mechanica, 41(2): p. 102-113.

Amari, T., & Houhou, M. N. (2021). 3D numerical analysis of pile response due to soil movements induced by an adjacent deep excavation. World Journal of Engineering, ISSN 1708-5284, DOI 10-1108/WJE-03-2021-0132.

Ata, A. A. (1996). Ground settlements induced by slurry shield tunneling in stratified soils. Proc. North Amercian Tunneling'96, ed. L Ozdemir, Vol. 1, pp. 43-50.

Atkinson, J., & Potts, D. M. (1977). Stability of a shallow circular tunnel in cohesionless soil. Geotechnique, 27(2): 203-215.

Attewell, P. B., Yeates, J., and Selby, A. R. (1986). Soil movements induced by tunnelling and their effects on pipelines and structures. Blackie and Son Ltd, London, UK.

Attewell, P.B. (1977). Ground movements caused by tunnelling in soil. In Proceedings of the International Conference on Large Ground Movements and Structures, Cardiff. Pentech Press, London, pp. 812-948.

Attewell, P.B., and Woodman, J. P. (1982). Predicting the dynamics of ground settlement and its derivatives caused by tunnelling in soil. Ground Engineering, 15(8): p. 13-36.

Basile, F. (2014). Effects of tunnelling on pile foundations. Soils and Foundations, 54(3):p. 280–295.

Benz, T. (2007). Small-strain stiffness of soils and its numerical consequences. PhD Thesis, Institute of Geotechnical Engineering, University of Stuttgart, Stuttgart, p. 209.

Bjerrum, L., Eide, O. (1956). Stability of strutted excavations in clay. Geotechnique, 6, p. 32– 47.

Boonsiri, I., and Takemura, J. (2015). Observation of ground movement with existing pile groups due to tunneling in sand using centrifuge modelling. Geotechnical and Geological Engineering, 33(3):621–640.

Bowles, J.E. (1988). Foundation analysis and design, 4th edtion. McGraw-Hill Book Company, New York, p. 1004.

Brinkgreve, R.B., Engin, E., and Engin, H.K. (2010). Validation of empirical formulas to derive model parameters for sands. Numerical methods in geotechnical engineering, 7thEuropean Conference, Vol.1, pp. 137-142.

Brinkgreve, R.B., Engin, E., and Swolfs, W.M. (2017). Plaxis 2D Version 9.0, Material Models Manual, PLAXISBV, Delft, p. 218.

Brinkgreve, R.B., Kumarswamy, S., and Swolfs, W.M. (2016). Plaxis 2016, PLAXISBV, Delft.

Caspe, M. S. (1966). Surface settlement adjacent to braced open cuts. Journal of Soil Mechanics and Foundations division, ASCE 92(SM4): pp 51-59.

Celestino, T. B., Gomes, R. A. M. P., and Bortolucci, A. A. (2000). Errors in ground distortions due to settlement trough adjustment. Tunnelling and Underground Space Technology, 15(1):97–100.

Chen, L.T., Poulos, H.G., and Hull, T.S. (1997). Model tests on pile groups subjected to lateral soil movement. Soils and Foundations, Vol. 37 No. 1, pp. 1-12.

Chen, L.T., Poulos, H.G., and Loganathan, N. (1999). Pile responses caused by tunneling. Journal of Geotechnical and geoenvironmental engineering, 125(3): p. 207-215.

Cheng, C. Y. (2003). Finite element study of tunnel-soil-pile interaction. Masters of Engineering thesis submitted for examination, National University of Singapore, p. 160.

Cheng, C. Y., Dasari, G. R., Chow, Y. K., and Leung, C. F. (2007). Finite element analysis of tunnel-soil-pile interaction using displacement controlled model. Tunnelling and Underground Space Technology, 22(4):450–466.

Cheng, C. Y., Dasari, G. R., Leung, C. F., Chow, Y. K., & Rosser, H. B. (2004). 3D numerical study of tunnel-soil-pile interaction. Tunnelling and Underground Space Technology, 19(4), 381-382.

Chow, Y. K., and Yong, K. Y. (1996). Analysis of piles subject to lateral soil movements. Journal of The Institution of Engineers Singapore, Vol. 36, No. 2, pp. 43-49.

Clough, G. W., and O'Rourke, J. M. (1990). Construction induced movements of insitu walls. Proc. Conf. Design and performance of earth retraining structures, In: ASCE: Geotech. Spec Cornell University, New York, 25: pp. 439–470.

Clough, G.W., and Schmidt, B. (1981). Design and performance of excavations and tunnels in soft clays. Soft clay engineering, Amsterdam, pp. 567–634.

Clough, G.W., Smith, E.M., Sweeny, B.R. (1989). Movement control of excavation support system by iterative design. Proc. ASCE Foundation Engineering: Current Principles and Practices. Vol. 2. ASCE, New York, p. 869-884.

Cording, E. J. (1991). Control of ground movements around tunnels in soil. In Proceeding of the 9th Pan-American Conference on Soil Mechanics and Foundation Engineering, volume 4, pages 2195–2244.

Coutts, D. R., and Wang, J. (2017). Monitoring of reinforced concrete piles under horizontal and vertical loads due to tunnelling. Tunnels and Underground Structures, pp. 541-546.

Cowland, J.W., & Thorley, C.B.B. (1985). Ground and building settlement associated with adjacent slurry trench excavation. Ground Movements and Structures – Proc., Third Int. Conf., University of Wales Institute of Science and Technology, London, England, pp. 723-738.

Crofts J. E., Menzies B. K.,Tarzi A. I. (1978). Reply to discussions on Lateral displacement of shallow buried pipelines due to adjacent deep trench excavations. Géotechnique, Vol. 28, n° 2, p. 217-220.

Devriendt, M., and Williamson, M. (2011). Validation of methods for assessing tunnelling induced settlements on piles. Ground Engineering, 44(3):pages 25–30.

Dyer, M., Hutchinson, M., and Evans, N. (1996). Sudden valley sewer: a case history. In International symposium on geotechnical aspects of underground construction in soft ground, London, pages 671–676.

Farrell, R. (2010). Tunnelling in sands and the response of buildings. PhD Thesis, Cambridge University.

Feng, S. H. (2003). Centrifuge modeling of tunnel-pile interaction. Masters of Engineering thesis, National University of Singapore, p. 159.

Finno, R. J., Lawrence, S. A., Allawh, N. F., and Harahap, I. S. (1991). Analysis of Performance of Pile Groups Adjacent to Deep Excavation. Journal of Geotechnical Engineering, 117 (6), pp. 934–955.

Franza, A. (2017). Tunnelling and its effects on piles and piled structures. PhD thesis, University of Nottingham, p. 251.

Franza, A., & Marshall, A. M. (2018). Centrifuge modeling study of the response of piled structures to tunneling. Journal of Geotechnical and Geoenvironmental Engineering, 144(2), 04017109.

Franza, A., Marshall, A. M., Haji, T., Abdelatif, A. O., Carbonari, S., and Morici, M. (2017). A simplified elastic analysis of tunnel-piled structure interaction. Tunnelling and Underground Space Technology, 61:104–121.

Goh, A. T. C., Wong, K. S., Teh, C. I., and Wen, D. (2003). Pile Response Adjacent to Braced Excavation. Journal of Geotechnical and Geoenvironmental Engineering, 129 (4), pp. 383–386.

Grant, R. J. (1998). Movements around a tunnel in two-layer ground. PhD thesis, City University, London.

Grant, R. J., and Taylor, R. N. (1996). Centrifuge modeling of ground movements due to tunneling in layered ground. Proc. Int. Symposium on Geotechnical Ascepts of Underground Construction in Soft Ground, London, Balkema, pp. 507-512.

Grant, R. J., and Taylor, R. N. (2000). Tunnelling-induced ground movements in clay. Proceedings of the ICE - Geotechnical Engineering, 143(1):43–55.

Hergarden, H. J. A. M., Van der Poel, J. T., and Van der Schrier, J. S. (1996). Ground movements due to tunnelling: Influence on pile foundations. Proceedings of the 2nd International Symposium on Geotechnical aspects of underground construction in soft ground, Balkema, London, 519–524.

Hong, S. W., and Bae, G. J. (1995). Ground movements associated with subway tunneling in Korea. Proc of the 94th International Symposium on Underground Construction in Soft Ground, New Delhi, India, 229-232.

Hong, Y., Ng, C.W.W., Liu, G.B., and Liu, T. (2015a). Three-dimensional deformation behaviour of a multi-propped excavation at a “greenfield” site at Shanghai soft clay. Tunnelling and Underground Space Technology, Vol. 45, pp. 249-259.

Hong, Y., Soomro, M.A., and Ng, C.W.W. (2015b). Settlement and load transfer mechanism of pile group due to side-by-side twin tunnelling. Computers and Geotechnics, 64: p. 105-119.

Houhou, M. N., Belounar, A., Amari, T., and Brouthen, A. (2021). 3D numerical back-analysis of an instrumented underpass road. World Journal of Engineering, Vol. 18 No. 1, pp. 94-105.

Houhou, M. N., Emeriault, F. and Belounar, A. (2019). Three-dimensional numerical back-analysis of a monitored deep excavation retained by strutted diaphragm walls. Tunnelling and Underground Space Technology, Vol. 83, pp. 153-164.

Houhou, M. N., Emeriault, F., & Vanoudheusden, É. (2016). Three-dimensional back-analysis of an instrumented shallow tunnel excavated by a conventional method. Geotechnical and Geological Engineering, 34(4), 1101-1117.

Houhou, M. N., Emeriault, F., Kastner, R., & Benmebarek, S. (2010). Rétro-analyse tridimensionnelle d'une excavation profonde multisupportée instrumentée. European journal of environmental and civil engineering, 14(1), 55-86.

Huang, M., and Mu, L. (2012). Vertical response of pile raft foundations subjected to tunneling-induced ground movements in layered soil. International journal for numerical and analytical methods in geomechanics, 36(8): p. 977-1001.

Huang, M., Zhang, C., and Li, Z. (2009). A simplified analysis method for the influence of tunneling on grouped piles. Tunnelling and Underground Space Technology, 24(4):410–422.

Jacobsz, S. W. (2002). The effects of tunnelling on piled foundations. PhD Thesis, Cambridge University.

Jacobsz, S. W., Standing, J. R., Mair, R. J., Hagiwara, T., and Sugiyama, T. (2004a). Centrifuge modelling of tunnelling near driven piles. Soils and Foundations, 44(1):49–56.

Jacobsz, S.W., Standing, J.R., and Mair, R.J. (2002). Centrifuge modeling of tunnelling near driven piles. In Proceedings of the 4th International Symposium on Geotechncial Aspects of Underground Construction in Soft Ground, Toulouse, pages 89-94.

Jacobsz, S.W., Standing, J.R., and Mair, R.J. (2004b). Tunnelling effects on pile groups in sand. Advances in Geotechnical Engineering: The Skempton Conference, London, vol. 2, p. 1056-1067.

Jongpradist, P., Kaewsri, T., Sawatparnich, A., Suwansawat, S., Youwai, S., Kongkitkul, W., and Sunitsakul, J. (2013). Development of tunneling influence zones for adjacent pile foundations by numerical analyses. Tunnelling and Underground Space Technology, 34:96–109.

Kaalberg, F. J., Teunissen, E. A. H., Van Tol, A. F., and Bosch, J. W. (2005). Dutch research on the impact of shield tunnelling on pile foundations. In Proceedings of the 5th International Symposium on Geotechnical Aspects of Underground Construction in Soft Ground, Amsterdam, the Netherlands, pages 123-131.

Kitiyodom, P., Matsumoto, T., and Kawaguchi, K. (2005). A simplified analysis method for piled raft foundations subjected to ground movements induced by tunnelling. International journal for numerical and analytical methods in geomechanics, 29(15): p. 1485-1507.

Korff, M. (2012). Response of piled buildings to the construction of deep excavations. PhD Thesis, University of Cambridge.

Korff, M., Mair, R. J., & Van Tol, F. A. (2016). Pile-soil interaction and settlement effects induced by deep excavations. Journal of Geotechnical and Geoenvironmental Engineering, 142(8), 04016034.

Lee, C. J. (2012a). Three-dimensional numerical analyses of the response of a single pile and pile groups to tunnelling in weak weathered rock. Tunnelling and Underground Space Technology, 32(0):132-142.

Lee, C. J. (2012b). Numerical analysis of the interface shear transfer mechanism of a single pile to tunnelling in weathered residual soil. Computers and Geotechnics, 42: 193-203.

Lee, C. J. (2013). Numerical analysis of pile response to open face tunnelling in stiff clay. Computers and Geotechnics, 51, 116-127.

Lee, C. J., and Chiang, K. H. H. (2007). Responses of single piles to tunneling-induced soil movements in sandy ground. Canadian Geotechnical Journal, 44(10):1224-1241.

Lee, C. J., and Jacobsz, S. W. (2006). The influence of tunnelling on adjacent piled foundations. Tunnelling and Underground Space Technology, 21(3-4):430.

Lee, C. J., Jeon, Y. J., Kim, S. H., & Park, I. J. (2016). The influence of tunnelling on the behaviour of pre-existing piled foundations in weathered soil. Geomechanics & engineering, 11(4): p. 553-570.

Lee, K. M., Rowe, R. K., and Lo, K. Y. (1992). Subsidence owing to tunnelling. I. Estimating the gap parameter. Canadian Geotechnical Journal, 29(6):929-940.

Lee, Y.J., and Bassett, R. H. (2007). Influence zones for 2D pile–soil-tunnelling interaction based on model test and numerical analysis. Tunnelling and Underground Space Technology, 22(3):325–342.

Leung, C. F., Ong, C. W., & Yong, K. Y. (2019). Effect of Tunneling on Adjacent Piled Foundation in Clay. Journal of Civil Engineering and Construction, 8(1), 19-24.

Leung, C.F., Chow, Y.K., and Shen, R.F. (2000). Behavior of pile subject to excavation-induced soil movement. Journal of Geotechnical and geoenvironmental engineering, Vol.126 No. 11, pp. 947-954.

Leung, C.F., Lim J.K., and Shen, R.F. (2003). Behavior of pile groups subject to excavation-induced soil movement. Journal of Geotechnical and geoenvironmental engineering, Vol. 129 No. 1, pp. 58-65.

Leung, C.F., Ong, D.E., and Chow, Y.K. (2006). Pile behavior due to excavation-induced soil movement in clay. II: Collapsed wall. Journal of Geotechnical and geoenvironmental engineering, Vol. 132 No. 1, pp. 45-53.

Li, L., Dong, G., Zhang, F., & Yang, M. (2014a). Three-dimensional numerical analyses of pile response due to unstrutted excavation-induced lateral soil movement. Tunneling and Underground Construction, p. 808-817).

Li, L., Hu, X. X., Dong, G. H., & Liu, J. (2014b). Three-Dimensional Numerical Analyses of Pile Response due to Braceded Excavation-Induced Lateral Soil Movement. Applied Mechanics and Materials, Trans Tech Publications Ltd, Vol. 580, pp. 524-531.

Liang, F., Yu, F., & Han, J. (2013). A simplified analytical method for response of an axially loaded pile group subjected to lateral soil movement. KSCE Journal of Civil Engineering, 17(2), 368-376.

Lim, J. K. (2001). Behaviour of piles subject to excavation-induced soil movement. Masters of Engineering Thesis, National University of Singapore.

Liyanapathirana, D., and Nishanthan, R. (2016). Influence of deep excavation induced ground movements on adjacent piles. Tunnelling and Underground Space Technology, Vol. 52, pp. 168-181.

Loganathan, N., and Poulos, H. G. (1998). Analytical prediction for tunneling-induced ground movements in clays. Journal of Geotechnical and Geoenvironmental Engineering, 124(9):846–856.

Loganathan, N., Poulos, H. G., and Stewart, D. (2000). Centrifuge model testing of tunnelling-induced ground and pile deformations. Geotechnique, 50(3): p. 283-294.

Loganathan, N., Poulos, H. G., and Xu, K. (2001). Ground and pile-group responses due to tunnelling. Soils and Foundations, 41(1): p. 57-67.

Madhumathi, R. K., & Ilamparuthi, K. (2018). Laboratory study on response of single pile adjacent to supported cut. Geotechnical and Geological Engineering, 36(5), 3111-3133.

Mair, R. J. (1979). Centrifugal modelling of tunnel construction in soft clay. PhD Thesis, Cambridge University.

Mair, R. J. (1993). Unwin memorial lecture 1992: developments in geotechnical engineering research: application to tunnels and deep excavations. Proceedings of the ICE – Civil Engineering, 97(1):27–41.

Mair, R. J. (1996). Settlement effects of bored tunnels. Session Report, Proc Int Symposium on Geotechnical Ascepts of Underground Construction in Soft Ground, London, Balkema, pp. 43-53.

Mair, R. J., & Taylor, R. N. (1999). Theme lecture: Bored tunnelling in the urban environment. Proceedings of the 14th international conference on soil mechanics and foundation engineering, Balkema, Hamburg, vol 4, 2353–2385.

Mair, R. J., Taylor, R. N., and Bracegirdle, A. (1993). Subsurface settlement profiles above tunnels in clay. Géotechnique, 43(2):315–320.

Mana, A.I., & Clough, G.W. (1981). Prediction of movements for braced cuts in clay. Journal of Geotechnical Engineering, American Society of Civil Engineers, vol. 107, pp. 759-777.

Marshall, A. M. (2009). Tunnelling in sand and its effect on pipelines and piles. PhD Thesis, Cambridge University, p. 250.

Marshall, A. M. (2012). Tunnel-Pile Interaction Analysis Using Cavity Expansion Methods. Journal of Geotechnical and Geoenviromental Engineering, 138(10), 1237–1246.

Marshall, A. M., and Haji, T. (2015). An analytical study of tunnel-pile interaction. Tunnelling and Underground Space Technology, 45: p. 43–51.

Marshall, A. M., and Mair, R. J. (2011). Tunneling beneath driven or jacked end-bearing piles in sand. Canadian Geotechnical Journal, 48(12):1757–1771.

Marshall, A. M., Farrell, R., Klar, A., and Mair, R. J. (2012). Tunnels in sands: the effect of size, depth and volume loss on greenfield displacements. Géotechnique, 62(5):385–399.

Martos, F. (1958). Concerning an approximate equation of the subsidence trough and its time factors. In International Strata Control Congress, pages 191-205.

Mattes, N.S., and Poulos, H. G. (1969). Settlement of single compressible pile. ASCE Journal of the Soil Mechanics and Foundations Division, 95(SM1):189-207.

Mestat, P., Prat, M., Bisch, P., Millard, A., Pijaudier-Cabot, G. (1999). Ouvrages en interaction. Hermes, AFPC-Emploi des Eléments Finis en Génie Civil, Paris, p. 934.

Migliazza, M., Chiorboli, M., Giani, G.P. (2009), "Comparison of analytical method, 3D finite element model with experimental subsidence measurements resulting from extension of the Milan underground", *Computers and Geotechnics*, Vol. 36, pp. 113–124.

Moh, Z. C., Ju, D. H., and Hwang, R. N. (1996). Ground movements around tunnels in soft ground. In Proceedings International Symposium on Geotechnical Aspects of Underground Construction in Soft Ground, Balkema, London, volume 730, pages 725–730.

Morton, J. D., and King, K. H. (1979). Effect of tunneling on the bearing capacity of and settlement of piled foundations. Proc. Tunneling ’79, (ed. M. J. Jones), London: IMM, pp. 57-58.

Mroueh, H., and Shahrour, I. (2002). Three-dimensional finite element analysis of the interaction between tunneling and pile foundations. International Journal for Numerical and Analytical Methods in Geomechanics, 26(3):217-230.

New, B. M., & Bowers, K. (1994). Ground movement model validation at the Heathrow Express trial tunnel. Tunnelling’94: Proceedings of the 7th International Symposium, London, pp. 301-329.

New, B. M., and O’Reilly, M. P. (1991). Tunnelling induced ground movements; predicting their magnitude and effects. In 4th Int. Conf. Ground Movements and Structures, Pentech Press Ltd, Cardiff, pp. 671-697.

Ng, C. W.W., Shakeel, M., Wei, J., & Lin, S. (2021). Performance of existing piled raft and pile group due to adjacent multipropped excavation: 3D centrifuge and numerical modeling. Journal of Geotechnical and Geoenvironmental Engineering, 147(4), 04021012.

Ng, C.W.W., Lu, H., and Peng, S. (2013). Three-dimensional centrifuge modelling of the effects of twin tunnelling on an existing pile. Tunnelling and Underground Space Technology, 35: p. 189-199.

Ng, C.W.W., Wei, J., Poulos, H. G., and Liu, H. (2017). Effects of multipropped excavation on an adjacent floating pile. Journal of Geotechnical and geoenvironmental engineering, Vol. 143 No. 7, pp. 04017021.

Ng, C.W.W., Yau, T. L., Li, J. H., & Tang, W. H. (2001). New failure load criterion for large diameter bored piles in weathered geomaterials. Journal of Geotechnical and geoenvironmental engineering, 127(6): p. 488-498.

Nishanthan, R., Liyanapathirana, D. S., & Leo, C. J. (2017). Shielding effect in pile groups adjacent to deep unbraced and braced excavations. International Journal of Geotechnical Engineering, 11(2), 162-174.

O’Reilly, M. P., and New, B. M. (1982). Settlements above tunnels in the United Kingdom - their magnitude and prediction. Tunnelling’82, Papers Presented at the 3rd International Symposium, London, p. 173-181.

Ong, C. W. (2009). Centrifuge model study of tunnel-soil-pile interaction in soft clay. PhD thesis, National University of Singapore, p. 326.

Ong, C. W., Leung, C. F., Yong, K. Y., & Chow, Y. K. (2007a). Performance of pile due to tunneling-induced soil movements. In : Underground Space-The 4th Dimension of Metropolises, Three Volume Set+ CD-ROM. CRC Press, p. 647-652.

Ong, C. W., Leung, C. F., Yong, K. Y., and Chow, Y. K. (2006b). Pile responses due to tunneling in clay. Proc. of the 6th International Conference on Physical Modelling in Geotechnics, London, p. 1177- 1182.

Ong, D. E. L. (2004). Pile behaviour subject to excavation-induced soil movement in clay. PhD thesis, National University of Singapore.

Ong, D. E. L. (2008). Benchmarking of FEM technique involving deep excavation, pile-soil interaction and embankment construction. Proc of the 12th Inter Conference of Inter Association for Computer Methods and Advanced in Geomechanics (IACMAG), Goa, India, p. 154-162.

Ong, D. E. L., Leung, C. F., & Chow, Y. K. (2003). Time-dependent pile behaviour due to excavation-induced soil movement in clay. In Proceedings of the 12th Pan-American Conference on Soil Mechanics and Geotechnical Engineering, Massachusetts Institute of Technology Boston, USA, Vol. 2, pp. 2035-2040.

Ong, D. E. L., Leung, C. F., and Chow, Y. K. (2006a). Pile behavior due to excavation-induced soil movement in clay. I: Stable wall. Journal of Geotechnical and geoenvironmental engineering, Vol. 132 No. 1, pp. 36-44.

Ong, D. E. L., Leung, C. F., and Chow, Y. K. (2009). Behavior of pile groups subject to excavation-induced soil movement in very soft clay. Journal of Geotechnical and geoenvironmental engineering, Vol. 135 No. 10, pp. 1462-1474.

Ong, D. E. L., Leung, C. F., Chow, Y. K., and Yang, D. Q. (2007b). Effect of horizontal limiting soil pressures on pile behaviour. 16th South-east asian Geotechnical Conference (16SEAGC), Kuala Lumpur, Malaysia, pp. 427-437.

Ou, C. Y. (2006). Deep Excavation: Theory and Practice. Taylor and Francis, Netherlands. p. 551.

Ou, C. Y., and Hsieh, P. G. (2000). Prediction of Ground Surface Settlement Induced by Deep Excavation. Geotechnical Research Report No. GT200008, Department of Construction Engineering, National Taiwan University of Science and Technology.

Ou, C. Y., and Yang, L. L. (2000). Ground Movement Induced by the Construction of Diaphragm Wall. Geotechnical Research Report No. GT200005, Department of Construction Engineering, National Taiwan University of Science and Technology.

Ou, C. Y., Hsieh, P. G., and Duan, S. M. (2005). A Simplified Method to Estimate the Ground Surface Settlement Induced by Deep Excavation. Geotechnical Research Report No. GT200502, Department of Construction Engineering, National Taiwan University of Science and Technology.

Ou, C.Y., Hsieh, P.G., and Chiou, D.C. (1993). Characteristics of ground surface settlement during excavation. Canadian Geotechenical Journal, Vol. 30, No. 5, pp. 758-767.

Pang, C. H., Yong, K. Y., and Chow, Y. K. (2005a). Three-dimensional numerical simulation of tunnel advancement on adjacent pile foundation. Underground Space Use: Analysis of the Past and Lessons for the Future: Proceedings of the 31st World Tunnelling Congress, Istanbul, Turkey, 2:1141-1148.

Pang, C. H., Yong, K. Y., Chow, Y.K., and Wang, J. (2005b). The response of pile foundations subjected to shield tunnelling. Proceedings of the 5th International Symposium on Geotechncial Aspects of Underground Construction in Soft Ground, p. 737-744.

Peck, R. B. (1969). Deep excavation and tunneling in soft ground. In 7th International Conference on Soil Mechanics and Foundation Engineering, State-of-the Art Volume, Mexico City, pp. 225-290.

Poh, T. Y., & Wong, I. H. (1998). Effects of construction of diaphragm wall panels on adjacent ground: Field trial. journal of geotechnical and geoenvironmental engineering, ASCE, 124(8), pp. 749–756.

Poulos, H. G., and Chen, L. T. (1996). Pile response due to unsupported excavation-induced lateral soil movement. Canadian Geotechnical Journal, Vol. 33 No. 4, pp. 670-677.

Poulos, H. G., and Chen, L. T. (1997). Pile response due to excavation-induced lateral soil movement. Journal of Geotechnical and geoenvironmental engineering, Vol. 123 No. 2, pp. 94-99.

Ran, X. (2004). Tunnel pile interaction in clay. Master-Eng thesis, National University of Singapore.

Sagaseta, C. (1987). Analysis of undrained soil deformation due to ground loss. Géotechnique, 37(3): pp 301–320.

Schanz, T., and Vermeer, P. (1998). Special issue on Pre-failure deformation behaviour of geomaterials. Geotechnique,Vol. 48, pp. 383-387.

Schmidt, B. (1969). Settlements and ground movements associated with tunnelling in soil. PhD thesis, University of Illinois, Urbana.

Selemetas, D. (2005). The response of full-scale piles and piled structures to tunnelling. PhD Thesis, Cambridge University, p. 302.

Selemetas, D., Standing, J.R., and Mair, R.J. (2005). The response of full-scale piles to tunnelling. In Proceedings of the 5th International Symposium on Geotechnical Aspects of Underground Construction in Soft Ground, pages 763-769.

Shakeel, M., and Ng, C.W.W. (2018). Settlement and load transfer mechanism of a pile group adjacent to a deep excavation in soft clay. Computers and Geotechnics, Vol. 96, pp. 55-72.

Shakeel, M., Wei, J., & Ng, C. W. W. (2018). Numerical study on the influence of excavation depth to pile length ratio on a pile group adjacent to an excavation. Conference Paper, November 2018.

Sharma, J. S., Bolton, M. D., and Boyle. R. E. (2001). A new technique for simulation of tunnel excavation in a centrifuge. Geotechnical Testing Journal, Vol. 24, No. 4, pp. 343-349.

Shen, R. F. (1999). Pile behaviour due to excavation-induced soil movement. Master of Engineering Thesis, National University of Singapore.

Shi, J., Wei, J., Ng, C.W.W. and Lu, H. (2019). Stress transfer mechanisms and settlement of a floating pile due to adjacent multi-propped deep excavation in dry sand. Computers and Geotechnics, 116, pp. 103-116.

Sohaei, H., Namazi, E., & Marto, A. (2017). Control of pile movements induced by tunnelling using micropiles. International Journal of Physical Modelling in Geotechnics, 18(4), 191-207.

Sohaei, H., Namazi, E., Hajihassani, M., & Marto, A. (2020). A Review on Tunnel–Pile Interaction Applied by Physical Modeling. Geotechnical and Geological Engineering, 38(4), 3341-3362.

Soomro, M. A., Hong, Y., Ng, C. W. W., Lu, H., and Peng, S. (2015). Load transfer mechanism in pile group due to single tunnel advancement in stiff clay. Tunnelling and Underground Space Technology, 45: p. 63–72.

Soomro, M. A., Keerio, M. A., and Bangwar, D. (2017). 3D centrifuge modeling of the effect of twin tunneling to an existing pile group. Engineering, Technology & Applied Science Research, 7(5): p. 2030-2040.

Soomro, M. A., Kumar, M., Xiong, H., Mangnejo, D. A., & Mangi, N. (2020b). Investigation of effects of different construction sequences on settlement and load transfer mechanism of single pile due to twin stacked tunnelling. Tunnelling and Underground Space Technology, 96: p. 103171.

Soomro, M. A., Mangi, N., Cheng, W. C., & Mangnejo, D. A. (2020a). The effects of multi-propped deep excavation-induced ground movements on adjacent high-rise building founded on piled raft in sand. Advances in civil engineering, DOI.ORG/10.1155/2020/8897507, ID 8897507, V. 2020, p. 1-12.

Soomro, M. A., Mangnejo, D. A., and Bhanbhro, R. (2019a). 3D finite element analysis of pile responses to adjacent excavation in soft clay: Effects of different excavation depths systems relative to a floating pile. Tunnelling and Underground Space Technology, Vol. 86, pp. 138-155.

Soomro, M. A., Ng, C. W. W., Memon, N. A., & Bhanbhro, R. (2018a). Lateral behaviour of a pile group due to side-by-side twin tunnelling in dry sand: 3D centrifuge tests and numerical modelling. Computers and Geotechnics, 101: p. 48-64.

Soomro, M. A., Saand, A., Mangi, N., Mangnejo, D. A., Karira, H., and Liu, K. (2019b). Numerical modelling of effects of different multipropped excavation depths on adjacent single piles: comparison between floating and end bearing pile responses. European Journal of Environmental and Civil Engineering, Vol.23 No.1, pp. 1-31.

Soomro, M.A., Brohi, A.S., Soomro, M.A., and Bangwar, D.K. (2018b). 3D numerical modeling of pile group responses to excavation-induced stress release in silty clay. Engineering, Technology & Applied Science Research, Vol. 8 No. 1, pp. 2577-2584.

Standing, J. R., and Selemetas, D. (2013). Greenfield ground response to EPBM tunnelling in London Clay. Geotechnique, 63(12):989-1007.

Surjadinata, J., Hull, T. S., Carter, J. P., and Poulos, H. G. (2006). Combined finite and boundary element analysis of the effects of tunneling on single piles. ASCE International Journal of Geomechanics, 6(5):374-377.

Symons, I. F. (1980). Discussion, Session VII. Proceedings of the 2nd International Conference Ground Movements and Structures, Cardiff, Pentech Press, London, p. 498-954.

Tatsuoka, F., Goto, S., and Sakamoto, M. (1986). Effects of some factorsand strength and deformation characteristics of sand at low pressure. Soils and Foundations, 26(1), 105–114.

Taylor, R. N. (1994). Tunnelling in soft ground in the UK. In Proceedings of the 1st International Symposium on Underground Construction in Soft Ground, New Delhi, India, pages 123-126.

Teh, C., and Wong, K. (1995). Analysis of downdrag on pile groups. Geotechnique, 45(2): p. 191-207.

Terzaghi, K. (1943). Theorical Soil Mechanics. John Wiley & Sons, New York.

The, C., Wong, K. (1995), "Analysis of downdrag on pile groups", *Geotechnique,* Vol. 45 No. 2, pp. 191 207.

Tschebotarioff, G. P. (1973). Foundations, retainings and earth structures , second edition. Mac Graw Hill Book Company, p. 642.

Vorster, T. E. B. (2005). The effects of tunnelling on buried pipes. PhD Thesis, Cambridge University.

Vorster, T. E. B., Klar, A., Soga, K., and Mair, R. J. (2005). Estimating the effects of tunneling on existing pipelines. Journal of Geotechnical and Geoenvironmental Engineering, 131(11):1399–1410.

Wang, J. H., Xu, Z. H., and Wang, W.D. (2010). Wall and ground movements due to deep excavations in Shanghai soft soils. Journal of Geotechnical and Geoenvironmental Engineering, Vol. 136 (7), pp. 985-994.

Williamson, M. G. (2010). The Effects of Tunnelling on Bored Piles. First year report submitted to proceed to the degree of Doctor of Philosophy, Department of Engineering, Cambridge University.

Williamson, M. G. (2014). Tunnelling effects on bored piles in clay. PhD Thesis, Cambridge University.

Xu, K. J., and Poulos, H. G. (2000). General elastic analysis of piles and pile groups. International Journal for Numerical and Analytical Methods in Geomechanics, 24(15):1109–1138.

Xu, K. J., and Poulos, H. G. (2001). 3-D elastic analysis of vertical piles subjected to "passive" loadings. Computers and Geotechnics, 28(5):349–375.

Yang, M., Sun, Q., Li, W. C., & Ma, K. (2011). Three-dimensional finite element analysis on effects of tunnel construction on nearby pile foundation. Journal of Central South University, 18(3), 909-916.

Zapata-Medina, D. G. (2007). Semi-empirical method for designing excavation support systems based on deformation control. MSc Thesis, University of Kentucky, pp. 468.

Zhang, R. J., Zheng, J. J., and Yu, S. (2013). Responses of piles subjected to excavation induced vertical soil movement considering unloading effect and interfacial slip characteristics. Tunnelling and Underground Space Technology, 36:66–79.

Zhang, R. J., Zheng, J. J., Zhang, L. M., and Pu, H. F. (2011a). An analysis method for the influence of tunneling on adjacent loaded pile groups with rigid elevated caps. International Journal for Numerical and Analytical Methods in Geomechanics, 35(18):1949–1971.

Zhang, R., Zhang, W., & Goh, A. T. C. (2021). Numerical investigation of pile responses caused by adjacent braced excavation in soft clays. International Journal of Geotechnical Engineering, 15(7), 783-797.

Zhang, R., Zheng, J., Pu, H., and Zhang, L. (2011b). Analysis of excavation-induced responses of loaded pile foundations considering unloading effect. Tunnelling and Underground Space Technology, 26(2):320–335.

Zhang, Z., Huang, M., Xu, C., Jiang, Y., & Wang, W. (2018). Simplified solution for tunnel-soil-pile interaction in Pasternak's foundation model. Tunnelling and Underground Space Technology. 78: p. 146-158.

Zheng, G., Peng, S.Y., Ng, C.W.W., and Diao, Y. (2012). Excavation effects on pile behaviour and capacity. Canadian Geotechnical Journal, Vol. 49 No. 12, pp. 1347-1356.

Zidan, A. F., and Ramadan, O. M. O. (2015). Three dimensional numerical analysis of the effects of tunnelling near piled structures. KSCE Journal of Civil Engineering, 19(4): p. 917-928.